Terrestrial Fluid

Earthquakes an

The Hiroshi Wak

Edited by
Nemesio M. Pérez
Sergio Gurrieri
Chi-Yu King
Yuri Toran

Terrestrial Fluids, **Earthquakes** and **Volcanoes**: The Hiroshi Wakita Volume II

Edited by
Nemesio M. Pérez
Sergio Gurrieri
Chi-Yu King
Yuri Taran

Editors:
Nemesio M. Pérez
Environmental Research Division
Instituto Tecnológico y de Energias
Renovables
Polígono Industrial de Granadilla s/n
38611 Granadilla, Tenerife
Canary Islands
Spain
e-mail: nperez@iter.es

Chi-Yu King
Earthquake Prediction Research, Inc
381 Hawthorne Ave.
Los Altos, CA 94022
USA
e-mail: Chiyuking@aol.com

Sergio Gurrieri
Istituto Nazionale di Geofisica e
Vulcanologia
Sezione di Palermo
V. Ugo La Malfa, 153
90146 Palermo
Italy
e-mail: peppo@pa.ingv.it

Yuri Taran
Volcanology Department
Institute of Geophysics
UNAM
3000, Av. Universidad
Mexico D.F., 04510
Mexico
e-mail: taran@geofisica.unam.mx

Contents

Hiroshi Wakita was born in Nishinomiya (Hyogo, Japan) on September 29, 1936, and is actually an Emeritus Professor at The University of Tokyo (Japan). He graduated with B.Sc., M.Sc. and Ph.D. from Gakushuin University (Tokyo) in 1962, 1964 and 1968, respectively. He was a Research at the Japan Atomic Energy Research Institution, Tokyo (1964–68), Research Associate at Oregon State University, Corvallis, USA (1968–71), Research Associate at the University of Tokyo (1971–77), Lecture at The University of Tokyo (1977–78), Associate Professor at The University of Tokyo (1978–86), Professor at The University of Tokyo (1986–97), and Professor at the Gakushuin Women's College, Tokyo (1998–2007). He was also the Director of the Laboratory for Earthquake Chemistry at The University of Tokyo (1988–97), Associate Editor of Applied Geochemistry (1992–96), President of the Geochemical Society of Japan (1992–93), and Vice-president of the Geochemistry Research Association (1996). He received the Miyake Prize for his contribution on the field of geochemistry from the Geochemistry Research Association in 1989.

Introduction

Terrestrial Fluids, Earthquakes and Volcanoes: The Hiroshi Wakita Volume II is a special publication to honor Professor Hiroshi Wakita for his scientific contributions to science and to commemorate his 10th anniversary as Emeritus Professor at the University of Tokyo. The volume II consists of 10 original papers written by researchers from Japan, Germany, Italy, Costa Rica, Sweden, El Salvador, Turkey, USA, Greece, and Spain dealing with various aspects of the role of terrestrial fluids in earthquake and volcanic processes which reflect Prof. Wakita's wide scope of research interests. The Pure and Applied Geophysics "*Terrestrial Fluids, Earthquakes and Volcanoes: The Hiroshi Wakita Volume I*" published 17 scientific contributions in May 2006, and the volume III will be published in January 2008. These Pure and Applied Geophysics Hiroshi Wakita volumes should be useful for active researchers in the subject field, and graduate students who wish to become acquainted with them.

Professor Wakita founded the Laboratory for Earthquake Chemistry in April 1978 with the aim of establishing a scientific base for earthquake prediction by means of geochemical studies, and served as its director from 1988 until his retirement from the university in 1997. He has made the laboratory a leading world center for studying earthquakes and volcanic activities by means of geochemical and hydrological methods. Together with his research team and numerous foreign guest researchers that he attracted, he has made many significant contributions in the above-mentioned scientific fields of interest. This achievement is a testimony for not only his scientific talent, but also his enthusiasm, his openmindedness, and his drive in obtaining both human and financial support.

The ten contributions of this volume II are arranged into two groups. The first group of five papers deals with movement and signatures of terrestrial fluids related to earthquakes. The first two papers are related to groundwater-level observations in Japan. The paper by MATSUMOTO *et al*. describes groundwater-level anomalies associated with a hypothetical preslip prior to the anticipated M8 Tokai earthquake, and evaluates the detectability of the anomalies using data from seven groundwater wells. The paper by ITABA and KOIZUMI analyzed groundwater-level data recorded at the Dogo hot spring, one of the oldest and most famous hot springs in Japan, immediately after the 1946 Nankai earthquake and during the period from 1985 to 2006. The following contribution is a paper by FAVARA *et al*. which describes the observed hydro-geochemical changes in warm

springs and cold discharges located in Central-Northern Sicily related to a moderate seismic activity. Poroelastic aquifer contraction, shaking-induced dilatancy theory as well as seismogenetic-induced changes in aquifers' properties have been proposed as possible mechanisms for the observed changes. The paper by PÉREZ *et al.* describes the detection of precursory geochemical signatures of radon degassing from a bubbling CO_2-rich gas spot in the subsurface several months prior to the 2004 seismic crisis in Tenerife, Canary Islands (Spain). The material Failure Forecast Method was applied by the authors on this geochemical observation to forecast the largest seismic event of the crisis. The last earthquake-related contribution of this special volume is a paper by DOGAN *et al.* which describes diffuse H_2 and CO_2 degassing surveys performed along seven active faults and around the aftershock region of the 2000 Tottori-ken Seibu earthquake in Japan.

This earthquake-related paper is then followed by five additional contributions dealing with observations related to volcanic processes. The paper by MELIÁN *et al.* describes the use of diffuse H_2 degassing surveys as a potential geochemical tool for the volcanic surveillance at Poás volcano (Costa Rica, Central America) after evaluating the results of the 2000–2003 monitoring period. The following paper by OLMOS *et al.* presents the observed anomalous SO_2 emission values prior the 2005 eruption of Santa Ana volcano (El Salvador, Central America) which were recorded by a mini-DOAS (miniaturized - Differential Optical Absorption Spectroscopy) in a mobile-terrestrial position. Additional premonitory signatures of the recent eruption of Santa Ana volcano are described by HERNÁNDEZ *et al.*'s paper through thermal infrared images of its summit crater. A significant increase in the extent and intensity of the fumarolic field inside the crater rim and of the surface temperature of the crater's lake was observed prior to the 2005 eruption as well as changes in the estimated energy input. The following paper by GIAMMANCO *et al.* performs a statistical analysis (Cluster Analysis) of major, minor and trace elements in groundwaters from Mt. Etna volcano which were collected in 1994, 1995 and 1997. The observed changes were basically interpreted as a result of the different response of dissolved chemical elements to changes in the aqueous environment and/or in their solubility/mobility in water due to different rates of input of magmatic gases to Etna's aquifers. The last volcano-related contribution of this volume II is written by TESCHNER *et al.*, and they describe the installation and long-term operation of a system for continuous monitoring of fumarolic gases at Nysiros volcano in Greece.

Nemesio M. Pérez
Environmental Research Division
Instituto Tecnológico y de Energías
Renovables (ITER)
Tenerife, Canary Islands
Spain

Sergio Gurrieri
Istituto Nazionale di Geofisica e
Vulcanologia
V. Ugo La Malfa
153 - 90146 Palermo
Italy

Chi-Yu King
Earthquake Prediction Research, Inc.
381 Hawthorne Ave
Los Altos, CA 94022
USA

Yuri Taran
Institute of Geophysics
Universidad Nacional Autónoma
de México (UNAM)
Mexico D.F 04510
Mexico

Groundwater-level Anomalies Associated with a Hypothetical Preslip Prior to the Anticipated Tokai Earthquake: Detectability Using the Groundwater Observation Network of the Geological Survey of Japan, AIST

Norio Matsumoto,[1,2] Yuichi Kitagawa,[1] and Naoji Koizumi[1]

Abstract—We infer the groundwater-level anomalies associated with a hypothetical preslip prior to the anticipated M 8 Tokai earthquake, and evaluate the detectability of the anomalies using data from seven groundwater wells. We evaluate the detectability of the anomalies under the following assumptions: (1) an Mw 5.5–6.5 aseismic preslip event occurs at the plate boundary in and around the hypothetical focal zone of the Tokai earthquake; (2) the total amount of the strain step at each observation associated with the preslip can be calculated by tensile and shear faulting based on the dislocation model; (3) a normalized strain history associated with the preslip is defined from the results of numerical simulations based on rate- and state-dependent friction laws; and (4) the groundwater-level anomaly prior to the earthquake is proportional to the estimated history of the strain change associated with the preslip. We investigate the detection time of the anomaly at seven wells given an Mw 5.5, 6.0, or 6.5 aseismic preslip at one of the 272 grid points in and around the area of the hypothetical focal zone of the Tokai earthquake. As a result, over the time interval between 1 and 48 hours prior to the hypothetical Tokai earthquake, we are able to detect at each of the seven wells a hypothetical Mw 6.5 preslip at 10–86 of the 272 grid points, an Mw 6 preslip at 0–19 grid points, and an Mw 5.5 preslip at 0–5 grid points.

Key words: Tokai earthquake, groundwater level, preslip, strain, earthquake prediction, noise level, central Japan.

1. Introduction

Many studies have reported the occurrence of hydrological anomalies prior to earthquakes in Japan (Wakita, 1981; Kawabe, 1991; Igarashi and Wakita, 1992; Igarashi *et al.*, 1995; Tsunogai and Wakita, 1995; Koizumi *et al.*, 2004). Even if such anomalies are observed in several wells, it is still impossible to estimate the magnitude, epicenter, or timing of an anticipated earthquake in the absence of additional data. The magnitudes and epicenters of large anticipated earthquakes, for which equivalent

---

[1] Geological Survey of Japan, National Institute of Advanced Industrial Science and Technology (AIST), Japan.
[2] AIST Tsukuba Central 7, 1-1-1 Higashi, Tsukuba, Ibaraki 305-8567, Japan.
E-mail: n.matsumoto@aist.go.jp

earthquakes have occurred repeatedly in the past, are commonly inferred from data on past earthquakes, historical documents, and the results from paleoseismic analyses (e.g., SCHOLZ, 1990). In the case of large anticipated earthquakes, it is of vital importance to predict the occurrence of the event. To make such estimates based on groundwater-level data, we need to know reasonable mechanisms to estimate the history of preseismic changes in groundwater levels, and we need to compare the amplitudes of the estimated preseismic changes in groundwater levels with those of normal fluctuations. We can only predict the occurrence time of an anticipated earthquake if the estimated changes in groundwater levels exceed normal fluctuations.

The relationship between pore pressure and strain is described by poroelastic theory (e.g., WANG, 2000). If typical elastic and poroelastic constants are assumed, 10^{-6} contractional volumetric strain can produce a 1 m rise in groundwater level (ROELOFFS, 1996). In this way, it is possible to detect the crustal deformation that occurs prior to a large earthquake using groundwater levels. For example, changes in groundwater levels induced by the intrusion of dikes have been observed leading up to earthquake swarms and/or volcanic eruption (MATSUMOTO *et al.*, 2002; KOIZUMI *et al.*, 2004).

We consider preseismic sliding (hereafter referred to as preslip; KATO and HIRASAWA, 1996, 1999), which is described below, to be a reasonable mechanism of crustal deformation prior to an earthquake. To evaluate the possibility of predicting the anticipated Tokai earthquake using a groundwater observation network, we investigate the detectability of anomalous changes in groundwater levels caused by preslip. In this paper, we assume that the record of groundwater-level anomalies is induced by a hypothetical preslip event leading up to the anticipated Tokai earthquake; we evaluate the detectability of the anomalies in seven observation wells.

2. Anticipated Tokai Earthquake and Current Prediction system

In the past, large earthquakes of M 8 or higher have occurred along the Nankai and Suruga troughs, offshore from central and southwest Japan, at intervals of 100–200 years (ANDO, 1975). These thrust-type earthquakes have resulted from subduction of the Philippine Sea plate beneath the Eurasian plate at these troughs. Recent seismic events along the Nankai and Suruga troughs include the 1944 Tonankai (M 7.9) and 1946 Nankai (M 8.0) earthquakes, which occurred 90–92 years after the 1854 Ansei Tokai (M 8.4) and 1854 Ansei Nankai (M 8.4) earthquakes. Given that the most recent major earthquake to occur along the Suruga trough was recorded in 1854, a large earthquake is anticipated in this area in the near future (ANDO, 1975; ISHIBASHI, 1981; MATSUMURA, 1997). This anticipated earthquake is referred to as the Tokai earthquake, and the Japanese Government has maintained an earthquake prediction program for this earthquake since 1978 (MOGI, 1985).

The Japan Meteorological Agency (JMA), responsible for the prediction of the anticipated Tokai earthquake, has been monitoring crustal deformation in the Tokai

region since 1976 using 16 borehole strainmeters (SUYEHIRO, 1982; NIHEI *et al.*, 1987). To aid in this effort, the Geological Survey of Japan, as part of the National Institute of Advanced Industrial Science and Technology (GSJ, AIST), has been monitoring groundwater levels in the Tokai region since 1978 (KATO *et al.*, 1981; TAKAHASHI, 1993). As of 2007, 15 wells at nine observation sites in the Tokai region are continuously monitored by GSJ, AIST.

KATO and HIRASAWA (1999) presented several cases of significant preslip prior to the anticipated Tokai earthquake based on rate- and state-dependent friction laws and numerical simulations. The authors also inferred histories of the volumetric strain rate at several JMA borehole strainmeter sites, and compared noise levels with those of the strainmeter investigated by KOBAYASHI and MATSUMORI (1999). KATO and HIRASAWA (1999) concluded that it would be possible for borehole strainmeters to detect significant preslip-related crustal deformation anomalies approximately 1 day before the Tokai earthquake.

JMA revised the warning system for the Tokai earthquake in 2003. The revised system is now based on the detection of preslip-related crustal deformation anomalies by the JMA strainmeter network (JMA, 2003; KAMAYA and ITO, 2004; KAMIGAICHI and TSUKADA, 2006). JMA defined the 'noise level' of the strainmeter data as a threshold by which we can only extract the maximum value of normal fluctuations, and defined an 'obvious anomaly' as a value that is 1.5–1.8 times as high as the noise level. In the event that the JMA observes an obvious preslip-related anomaly within strainmeter data, the JMA issues either a "Tokai earthquake report," "Tokai earthquake advisory," or "Tokai earthquake warning" (JMA, 2003; KAMAYA and ITO, 2004; KAMIGAICHI and TSUKADA, 2006).

To predict the anticipated Tokai earthquake using the groundwater observation network, it is first necessary to evaluate the detectability of preslip-related anomalies in terms of the groundwater level.

Using the same noise-level definition as that used for JMA strainmeter data, MATSUMOTO and KITAGAWA (2005) investigated the noise levels of groundwater levels at seven wells located in the Tokai region. The authors also estimated the strain sensitivities of the groundwater levels based on the response of the groundwater level to volumetric strain induced by the Earth tide, and converted the noise levels of the groundwater levels into those for volumetric strain based on the strain sensitivities of the groundwater levels. The authors concluded that the minimum strain-converted noise level of the groundwater level is the same as the noise levels of JMA strainmeters; in addition, the maximum strain-converted noise level for periods with rainfall is five times larger than the noise level of the strainmeters, which is itself several times larger than the noise level during periods without rainfall (KOBAYASHI and MATSUMORI, 1999).

In the present paper, we employ the following steps in evaluating the detectability of preslip in the seven AIST groundwater observation wells. First, based on the results of KATO and HIRASAWA (1999), we assume a normalized strain history following the occurrence of a preslip event. Second, the histories of groundwater levels in the seven

wells are inferred for the cases of preslips with magnitudes of Mw 5.5, 6.0, and 6.5 at arbitrary grid points in and around the hypothetical focal zone of the Tokai earthquake. We then evaluate the detectability at the seven wells of the corrected water-level anomalies associated with the preslip event by comparing the absolute change in inferred water level with the noise level of the groundwater level at the seven wells, as determined by MATSUMOTO and KITAGAWA (2005).

3. Groundwater-level Observations and Noise Level

Here, we evaluate the detectability of groundwater-level anomalies in the KNG, HAI, HMO, OGS, DIT, TYH1, and TYH2 wells (Fig. 1) located in and around the hypothetical focal zone of the anticipated Tokai earthquake (CENTRAL DISASTER PREVENTION COUNCIL, 2001). Table 1 lists the location, depths, screened depths, and geology of the screened depths of the seven wells. The accuracy and resolution of the groundwater-level measurements are 1 and 0.1 mm, respectively. At the well sites, we also measured atmospheric pressure and rainfall with accuracies of 0.15–0.2 hPa and 0.5 mm, respectively. The data were recorded every 2 minutes and sent to AIST every 30 minutes
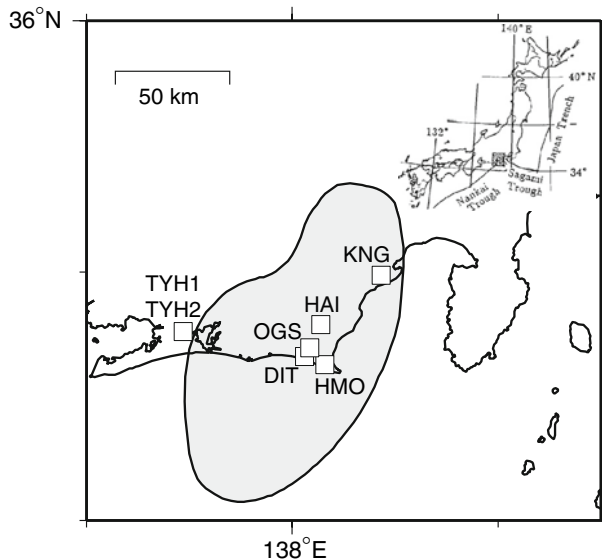
Figure 1
Locations of the seven observation wells. The gray area represents the hypothetical rupture zone of the anticipated Tokai earthquake (CENTRAL DISASTER PREVENTION COUNCIL, 2001).

Table 1

Descriptions of the seven observation wells (MATSUMOTO and KITAGAWA, 2005)

Well name	Location of well			Well depth (m)	Screened depth (m)	Geology
	Lat. (deg.)	Lon. (m)	alt. (m)			
DIT	34.663	138.059	9	260	145–167	Ts
					210–222	
KNG	34.987	138.433	21	250	235–246	Qs
HAI	34.790	138.139	58	171	71–154	Ts
HMO	34.630	139.159	37	270	154–265	Ts
OGS	34.696	138.085	8	150	128–145	Ts
TYH1	34.763	137.470	71	245	182–198	PTs
TYH2	34.763	137.470	71	150	135–150	PTs

Qs: Quaternary sedimentary rocks, Ts: Tertiary sedimentary rocks, PTs: Pre- Tertiary sedimentary rocks

Table 2

Noise levels of the 24-hour difference in the corrected water levels, strain sensitivities inferred from theoretical tidal strain and the response of water level to the tidal strain, and strain-converted noise level of the 24-hour difference in the water level at the seven wells (MATSUMOTO and KITAGAWA, 2005)

	DIT	KNG	HAI	HMO	OGS	TYH1	TYH2
Noise level (mm)	72	15	11.5	19.1	7.6	38.6	153.5
Strain sensitivity (mm/10^{-8})	5.2	4.0	2.5	0.39	0.42	2.4	13.1
Strain-converted Noise level (10^{-8})	13.9	3.8	4.6	49.0	18.1	16.2	11.7

from KNG, HAI, HMO, TYH1 and TYH2, and sent twice a day from OGS and DIT (MATSUMOTO and KITAGAWA, 2005).

Table 2 lists the strain sensitivities of the groundwater levels at the seven wells (MATSUMOTO and KITAGAWA, 2005). The strain sensitivity data are inferred from the responses of the groundwater levels to the M_2 and/or O_1 tidal constituents divided by the theoretical amplitudes of M_2 and/or O_1 tidal strain. In the case that the response of the groundwater level to the M_2 tidal strain was almost the same as that to the O_1 tidal strain, MATSUMOTO and KITAGAWA (2005) took the average of the responses to M_2 and O_1 tidal strain as the strain sensitivity of the groundwater level. When the two responses were dissimilar, however, the authors chose the smaller response as the strain sensitivity.

The corrected groundwater level is calculated by removing the atmospheric, tidal, and rainfall responses to the groundwater level from the observed groundwater level, as per the following procedure: (i) The coefficients of hourly resampled groundwater level to volumetric strain in 12 tidal constituents are determined using the computer program BAYTAP-G (TAMURA et al., 1991); (ii) atmospheric and rain coefficients are determined using the computer program developed by KITAGAWA and MATSUMOTO (1996); and (iii) the corrected groundwater level is calculated by applying the estimated atmospheric, tidal,
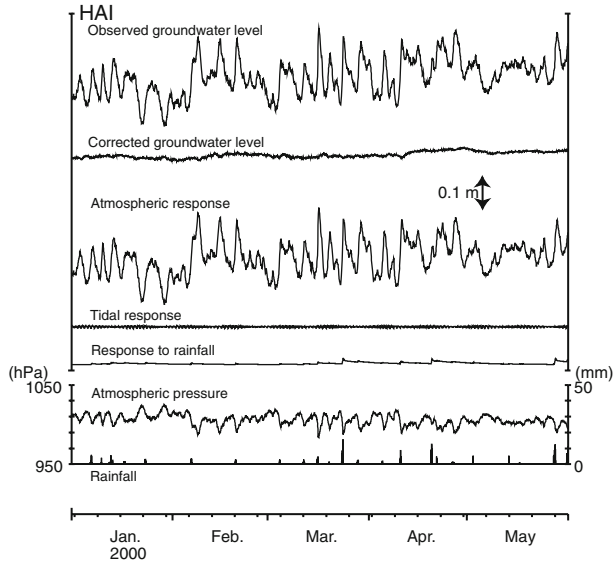
Figure 2

Observed groundwater level and the corrected water level used to investigate the timing of preslip detection, along with atmospheric pressure, rainfall, and atmospheric, tidal and rainfall responses, at HAI during the period from January to May 2000. To obtain the corrected groundwater level, we applied the data-processing method described in Section 3.

and rain coefficients to the computer program developed by MATSUMOTO (1992). In the present paper, we use the corrected groundwater level (Fig. 2) in evaluating the detectability of preslip prior to the Tokai earthquake. We select the noise level as a slightly larger value than the second-largest absolute value of the 24-hour difference in the corrected water level after removing obvious natural and artificial anomalies in the corrected water level (e.g., coseismic and postseismic changes in water level). We define the term "24-hour difference in the corrected water level" as the value obtained by subtracting the corrected water level calculated 24 hours before a given time from the corrected water level at the given time.

Table 2 also shows the noise levels and strain-converted noise levels of the 24-hour differences in the corrected groundwater levels in the seven wells. MATSUMOTO and KITAGAWA (2005) concluded that the strain-converted noise levels of water levels in KNG and HAI are slightly higher than the noise levels of JMA strainmeters during periods without rainfall. The authors also showed that the strain-converted noise levels recorded in TYH2 exceeded the noise level of the JMA strainmeter during rainfall periods by a factor of one, while the noise levels in DIT, OGS, and TYH1 exceeded the JMA value by a factor of two, and the level in HMO exceeded the JMA value by factor of five (Fig. 3).
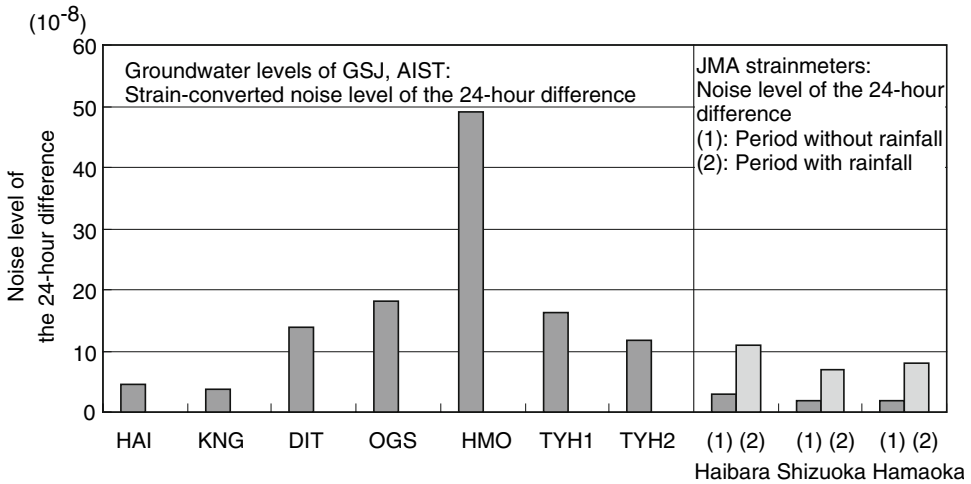
Figure 3

Strain-converted noise levels of the 24-hour difference in the corrected water levels at the seven studied wells (MATSUMOTO and KITAGAWA, 2005) and the noise levels of the 24-hour difference in the JMA strainmeter during periods with and without rainfall (KOBAYASHI and MATSUMORI, 1999).

4. Definition of Preslip and Estimation of Water-level Anomalies

In this paper, we make the following assumptions regarding the fault parameters of the preslip event prior to the anticipated Tokai earthquake and the history of the water-level anomaly associated with the preslip.

 (i) The preslip occurs in and/or around the hypothetical focal zone of the anticipated Tokai earthquake at the depth of the boundary between the Philippine Sea plate and the Eurasian plate. The preslip slides against the direction of subduction of the Philippine Sea plate.

 (ii) We establish a grid that covers the hypothetical focal zone of the anticipated Tokai earthquake, ranging from 33.9 to 35.5° N and from 137.1 to 138.6° E, with an increment of 0.1° (see Fig. 4). The total number of grid points is 272.

(iii) At one of the 272 grid points, we assume the occurrence of an Mw 5.5, 6.0, or 6.5 preslip event. Table 3 shows the parameters of the hypothetical fault models of the Mw 5.5, 6.0, and 6.5 preslip events. The rake angle of the preslip at the chosen grid point is assumed to be opposite to the subduction direction of the Philippine Sea plate inferred by HARADA *et al.* (1998). The depth of the preslip at the selected grid point is assumed to be the depth of the boundary between the Philippine Sea plate and the Eurasian plate, as calculated using the boundary geometry inferred by

HARADA *et al.* (1998) (Fig. 4). For the seven observation sites, the final values of the volumetric strain histories associated with the preslip just before the mainshock are chosen as the calculation results of the strain at the seven sites obtained using the fault model of the preslip at one of the grid points.

(iv) The strain-rate history associated with the preslip follows that described by Case 1 in Figure 9 of KATO and HIRASAWA (1999), which is their reference case and which was obtained by adopting the slowness version of the rate- and state-dependent friction law. We assume a normalized history of the volumetric strain induced by the preslip, using KATO and HIRASAWA's (1999) strain-rate history (see Fig. 5). The history of volumetric strain at each observation well is obtained by multiplying the history of the normalized strain change by the final value of the volumetric strain change associated with the preslip based on the dislocation model, which is already calculated in (iii).

(v) The histories of groundwater-level changes associated with the preslip at the seven wells are obtained by multiplying the histories of volumetric strain changes associated with the preslip, as determined in (iv), by the sensitivities of groundwater levels to the volumetric strain in the seven observation wells (see Table 2). We identify a groundwater-level anomaly relevant to the preslip when the absolute value
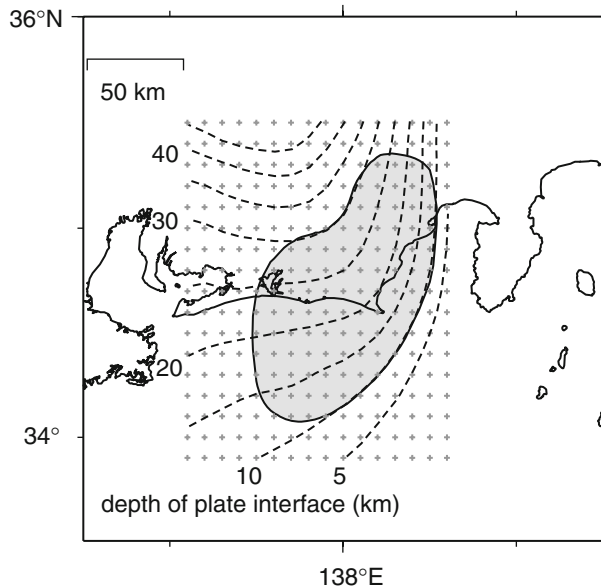
Figure 4

Map showing the locations of the 272 grid points and the depth of the interface between the Philippine Sea plate and the Eurasian plate (dashed contour lines; HARADA *et al.*, 1998) in and around the hypothetical focal zone of the anticipated Tokai earthquake (gray area; CENTRAL DISASTER PREVENTION COUNCIL, 2001). In this paper, a Mw 5.5, 6.0 or 6.5 preslip is assumed to occur at each grid point.

Table 3

Assumed lengths, widths and rupture displacements of the Mw 5.5, 6.0 and 6.5 preslips. The rake angle of the preslip is assumed to be opposite to the subduction direction of the Philippine Sea plate, and the depth of the preslip is assumed to be the depth of the boundary between the Philippine Sea plate and Eurasian plate (HARADA et al., 1998)

	Length (km)	Width (km)	Displacement (m)
Mw 6.5 preslip	24.6	12.3	0.78
Mw 6 preslip	13.8	6.9	0.44
Mw 5.5 preslip	7.8	3.9	0.25
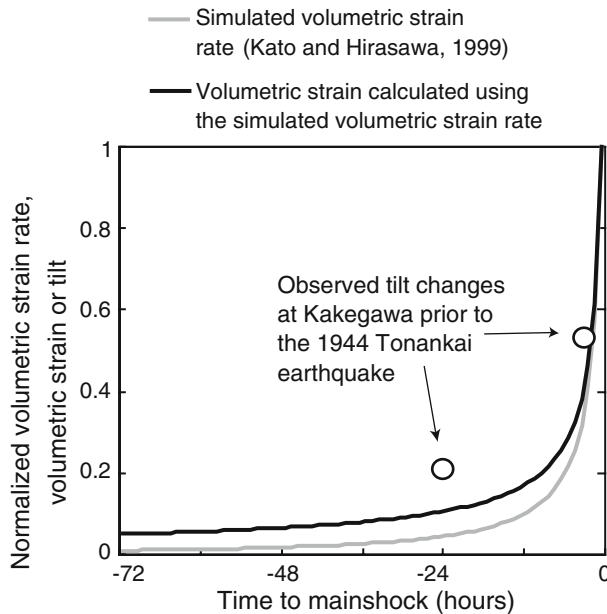
Figure 5

History of normalized strain rate induced by the hypothetical preslip (KATO and HIRASAWA, 1999) and inferred normalized strain history based on the normalized strain rate prior to the anticipated Tokai earthquake. Open circles show the normalized observed tilt changes prior to the 1944 Tonankai earthquake, as determined by MOGI (1984) and NAGOYA UNIV. (2003).

of the 24-hour difference in the estimated water-level history exceeds the noise level of the 24-hour difference in the corrected water level at the observation well (Table 2). We investigate the timing of the anomaly at the seven wells for cases in which the Mw 5.5, 6.0, and 6.5 preslip events occur at each of the 272 grid points.

We use the computer program developed by NAKAMURA and TAKENAKA (2004) to estimate the volumetric strain associated with interplate slip in the Tokai region. The program
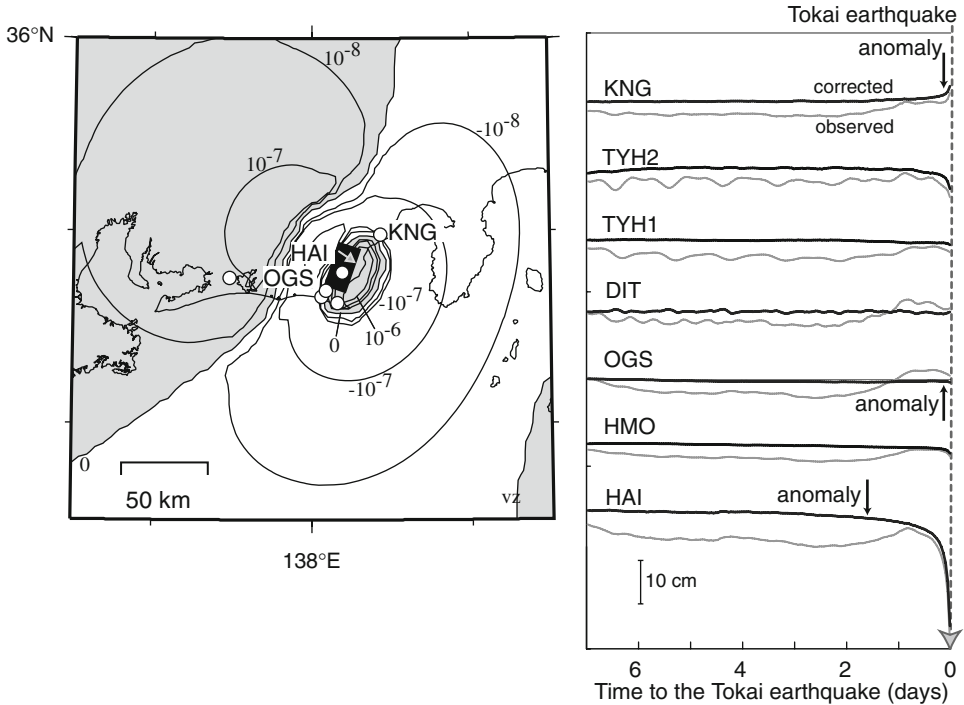
Figure 6

Estimated volumetric strain distribution in the Tokai region induced by a hypothetical Mw 6.5 aseismic preslip at the grid point of 138.2° E, 34.8° N and 21-km depth immediately before the mainshock. The gray and white areas denote extensional and contractional strain induced by the preslip, respectively. Also shown are 7-day histories of the estimated groundwater levels in the seven wells. The estimated groundwater levels were obtained by adding the estimated water-level histories induced by the Mw 6.5 preslip to measured data. The arrows indicate the times when the 24-hour differences in the corrected water level exceeded the noise levels (i.e., detected anomalies) at KNG, OGS, and HAI prior to the mainshock.

makes use of Okada's calculation code (OKADA, 1992), which uses the dislocation model to calculate crustal deformation arising from tensile and shear faulting.

Figure 6 shows an example of the volumetric strain distribution in the Tokai region for an Mw 6.5 aseismic preslip event at the grid point at 138.2° E, 34.8° N and 21 km depth. The volumetric extension of 2.08×10^{-6} strain is estimated at HAI as the final value of the volumetric strain change associated with the preslip. Figure 6 also shows 7-day histories of the estimated water levels in the seven wells prior to the Tokai earthquake, as calculated using the procedure described above. The estimated changes in groundwater levels at HAI, KNG, and OGS exceed the noise levels at 38, 3, and 3 hours prior to the Tokai earthquake, respectively. Hereafter, we refer to the time at which the estimated water level associated with the preslip exceeds the noise level at the observation well as the "timing of anomaly detection" in terms of the number of hours prior to the mainshock.

5. Results

This section details the timing of anomalies detected at the seven observation wells relative to the mainshock associated with the hypothetical Mw 5.5, 6.0, and 6.5 preslip events that occurred at each grid point prior to the anticipated Tokai earthquake.

5.1. Detectability of Mw 6.5 Preslip

Figure 7 shows the timing of anomalies detected at the seven wells in association with a hypothetical Mw 6.5 preslip that occurred at each grid point prior to the Tokai earthquake.

In several cases, anomalous water levels were detected at KNG and HAI more than 48 hours prior to the mainshock (black areas in Fig. 7). Anomalies were detected more than 1 hour in advance of the mainshock at KNG and HAI in response to preslips at 77 and 86 grid points, respectively. The detectability of preslip-related water-level anomalies is highest at KNG and HAI among the seven wells. This is because the strain-converted noise levels in the 24-hour difference at the two wells are almost as small as the noise levels of the three volumetric strainmeters installed by JMA around the two wells during the period without rainfall (Fig. 3). The relatively shallow depth of the subduction interface at KNG and HAI (Fig. 4) also contributes to improved detection relative to the other five wells, as a greater strain change is expected if the preslip occurs at shallow depths.

At DIT, OGS, TYH1, and TYH2, water-level anomalies were detected up to 12–19 hours prior to the hypothetical earthquake. For these four wells, preslip-related anomalies were detected more than 1 hour prior to the mainshock at 19–29 grid points. The anomalies associated with the Mw 6.5 preslip are less detectable at these four wells because the strain-converted noise levels of the groundwater levels are several times larger than the noise levels at KNG and HAI (Fig. 3; Table 3); however, during rainfall periods the Mw 6.5 preslip is just as easily detected in the water levels at the four wells as in the JMA strainmeters because the noise levels of the 24-hour difference in the JMA strainmeters with rainfall are as large as the strain-converted noise levels of the 24-hour difference in the corrected water level at the four wells (see Fig. 3).

For HMO, we were able to detect groundwater-level anomalies associated with the Mw 6.5 preslip at 10 grid points at times of 1–6 hours prior to the hypothetical earthquake. This result was achieved because the strain-converted noise level of the groundwater level at HMO is the highest among the different wells, being approximately 10 times higher than the noise levels at KNG and HAI (Fig. 3; Table 3).

The detected anomalies associated with the Mw 6.5 preslip are considered to be more reliable when identified at two or more wells. Water-level anomalies detected at any two wells associated with the Mw 6.5 preslip are recognized at 92 grid points at times of 1–17 hours prior to the Tokai earthquake (Fig. 8). While few preslips are detectable in areas offshore of the hypothetical focal zone, many Mw 6.5 preslips are detectable on the landward side and within Suruga Bay.
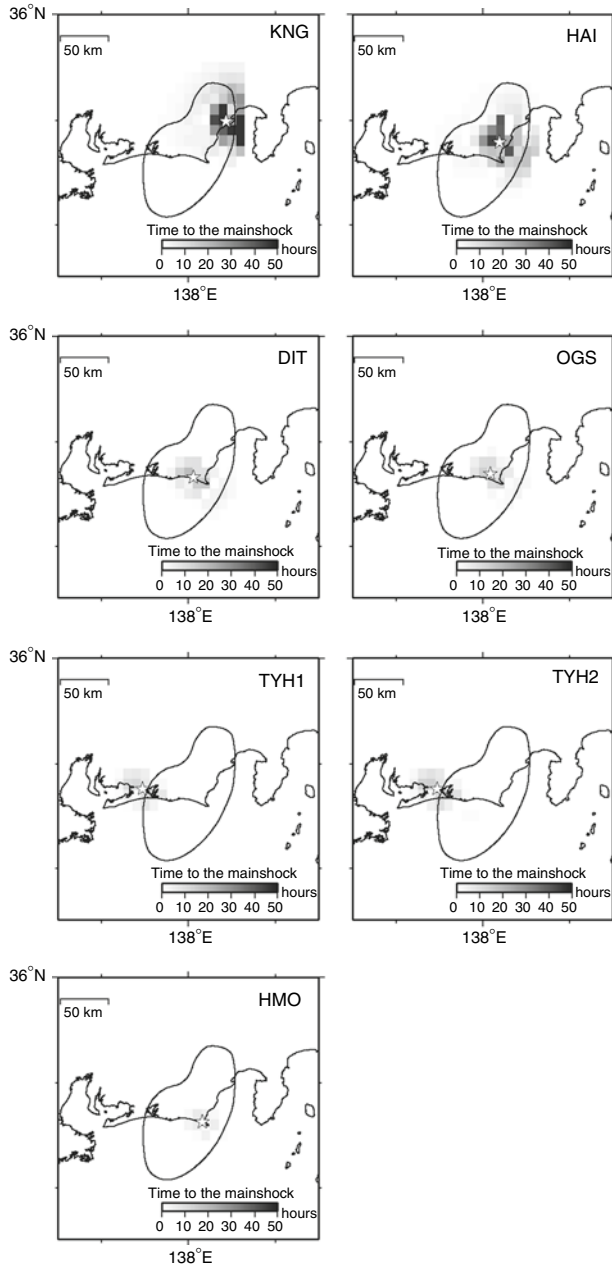
Figure 7

Spatial distributions of the timing of anomaly detection prior to the Tokai earthquake at KNG, HAI, DIT, OGS, TYH1, TYH2, and HMO for an assumed Mw 6.5 preslip event at each grid point. The star represents the location of the well. The black outline represents the hypothetical rupture zone of the anticipated Tokai earthquake (CENTRAL DISASTER PREVENTION COUNCIL, 2001).

Figure 8

Spatial distribution of the timing of anomalies detected at any two of the seven wells (open circles) for an assumed Mw 6.5 preslip event at each grid point.

5.2. Detectability of Mw 6 Preslip

Figure 9 shows the timing of anomalies detected at KNG, HAI, DIT, OGS, TYH1 and TYH2 wells in association with the hypothetical Mw 6 preslip for each grid point prior to the anticipated Tokai earthquake.

The Mw 6 preslips at 19 grid points are detectable at KNG and HAI over periods of 1–36 and 1–12 hours prior to the Tokai earthquake, respectively. At DIT, OGS, TYH1, and TYH2, water-level anomalies associated with the Mw 6 preslip are detectable at only 3–7 grid points at times of 1–4 hours prior to the earthquake. We were unable to detect any water-level anomalies in HMO associated with the Mw 6 preslip, regardless of the grid points selected as the focus area. Water-level anomalies at any two wells associated with the Mw 6 preslip at 10 grid points can be detected 1–4 hours prior to the earthquake (Fig. 10).

We conclude that over a limited area, water-level anomalies can be used to detect hypothetical Mw 6 preslip at the seven observation wells.

5.3. Detectability of Mw 5.5 Preslip

Figure 11 shows the timing of anomalies detected at KNG and HAI in association with a hypothetical Mw 5.5 preslip for each grid point prior to the anticipated Tokai earthquake.

Figure 9
Spatial distributions of the timing of anomalies detected at KNG, HAI, DIT, OGS, TYH1 and TYH2 for an
assumed Mw 6 preslip event at each grid point.

For HAI and KNG, the Mw 5.5 preslips at 3 and 5 grid points, respectively, are detectable using groundwater levels at periods 1–14 hours prior to the Tokai earthquake. These detectable preslips are located immediately below the observation wells. At HAI, the Mw 5.5 preslip is the minimum magnitude at which we can detect anomalies during periods at least 1 hour prior to the mainshock. For all 272 grid points, we were unable to detect water-level anomalies at DIT, HMO, OGS, TYH1, or TYH2.

At KNG, the minimum preslip for which we can detect anomalies 1 hour prior to the anticipated earthquake is Mw 5.0 preslip located at 138.4° E, 35.0° N.
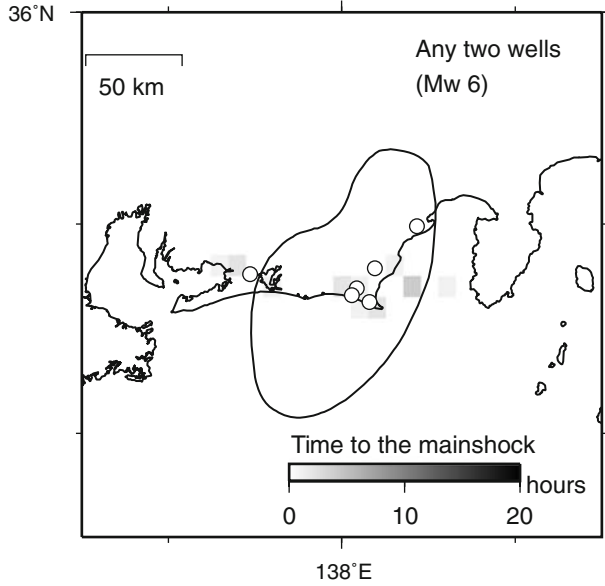
Figure 10
Spatial distribution of the timing of anomalies detected at any two of the seven wells (open circles) for an assumed Mw 6 preslip event at each grid point.
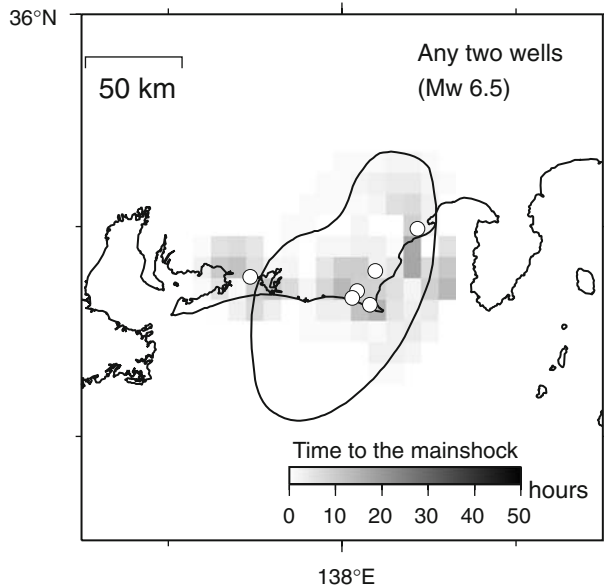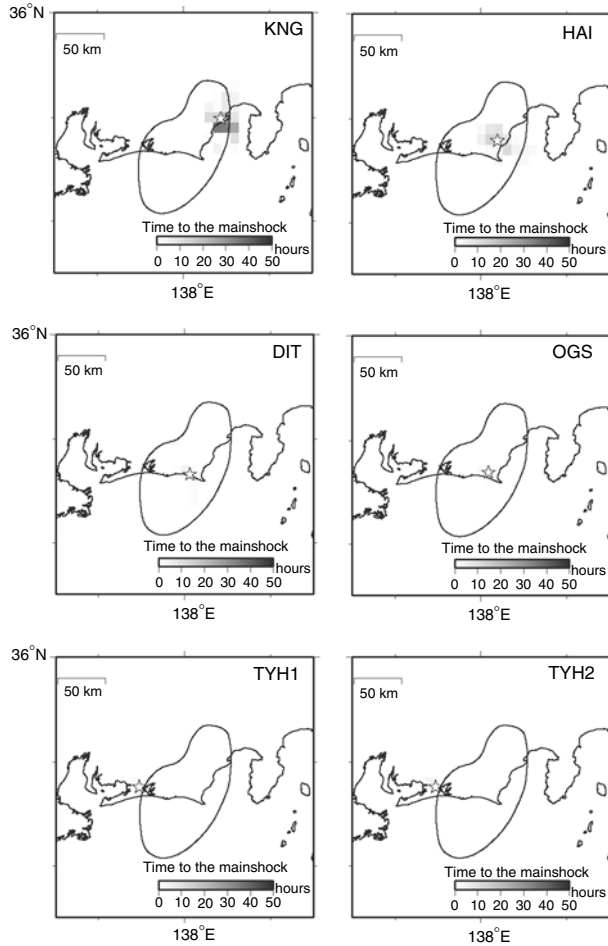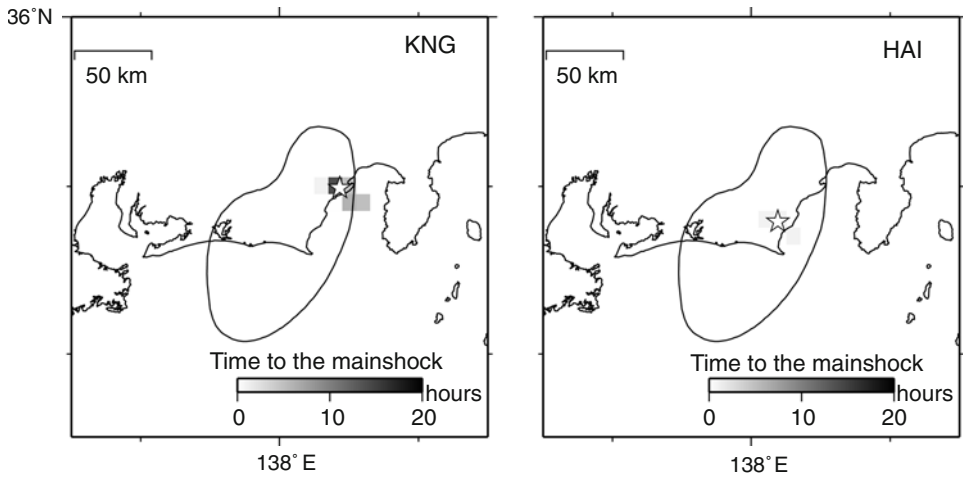

Figure 11
Spatial distributions of the timing of anomalies detected at KNG and HAI for an assumed Mw 5.5 preslip event at each grid point. No anomalies were detected at the other five wells for an Mw 5.5 preslip.

6. Discussion

MOGI (1984) and NAGOYA UNIV. (2003) calculated anomalous changes in ground tilting from precise leveling observations around Kakegawa at times of 24 hours, 3 hours, and 10 minutes prior to the 1944 Tonankai earthquake. The Kakegawa area is located close to the center of the hypothetical focal zone of the anticipated Tokai earthquake, and several tens of kilometers from the focal zone of the 1944 Tonankai earthquake (MOGI, 1984). Normalized tilt changes leading up to the 1944 Tonankai earthquake are calculated by taking the observed tilt change 10 minutes prior to the earthquake to be the maximum change in tilt prior to the earthquake. The hypothetical history of the normalized volumetric strain is considered to be plausible because it is similar to the normalized changes in observed tilt at Kakegawa, as shown by open circles in Figure 5.

The strain-rate history applied in the present study is the plausible example as mentioned above; however, the actual strain-rate history prior to the earthquake may differ from this. For example, the strain-rate history showed in Case 4 in Figure 9 of KATO and HIRASAWA (1999) changes much earlier than the history curve applied in the present study. If the actual history of the change in volumetric strain differs from the hypothetical history of the normalized volumetric strain, the actual time from anomaly detection to the mainshock will differ from the estimated time to the mainshock.

Short-term slow slip events (SSEs) are recursively observed every six months at a northwest adjacent area of the hypothetical focal zone of the Tokai earthquake (HIROSE and OBARA, 2006; KOBAYASHI *et al.*, 2006). The corresponding magnitude and duration of the events are Mw 5.7–5.9 and 2–3 days, respectively, and the events finish with decay in the observed tilt or strain (HIROSE and OBARA, 2006). The occurrence of the SSEs is the reason why, in the previous section, we presumed that the corresponding magnitude of the preslip is Mw 5.5–6.5. KAMIGAICHI and TSUKADA (2006) listed the following criteria to be satisfied in identifying a preslip associated with the Tokai earthquake: (1) Observed anomalies must be explained by an aseismic slip of thrust fault at the depth of plate boundary; (2) the observed anomalies in more than two observation wells must be synchronized, and histories of the anomalies must be similar; (3) the observed anomalies must accelerate over time. We can correctly distinguish a preslip event from SSEs and observation noise using these criteria.

Many previous studies have demonstrated that observed coseismic changes in groundwater levels do not match the coseismic volumetric strain steps (IGARASHI and WAKITA, 1991; ROELOFFS, 1998; MATSUMOTO *et al.*, 2003; BRODSKY *et al.*, 2003). In some of these previous works, the major cause of the coseismic changes in water level was ground motion (MATSUMOTO *et al.*, 2003; BRODSKY *et al.*, 2003); however, the preslip expected prior to the Tokai earthquake is aseismic, meaning that we do not need to take into account changes in groundwater level associated with ground motion. For this reason, we can expect that a groundwater-level anomaly prior to the anticipated Tokai earthquake will be proportional to the volumetric strain produced by the preslip.

Previous studies have inferred the history of strain changes at the JMA volumetric strainmeter installed at Haibara, 150 m south of HAI, associated with the hypothetical Mw 6.5 preslip at 138.2° E, 34.8° N (the same location as that shown in Fig. 6) (JMA, 2003; KAMIGAICHI and TSUKADA, 2006). These studies report that the strain change exceeded the noise level of the Haibara strainmeter 52 hours prior to the mainshock, whereas the groundwater level at HAI exceeded the noise level at HAI 38 hours prior to the mainshock, as mentioned in the previous section. Therefore, there is a difference in the timing of anomaly detection between the strainmeter and water level. The reason for this discrepancy is that the noise level of the 24-hour difference in the Haibara strainmeter during the period with no rainfall, 3×10^{-8}, is slightly lower than the strain-converted noise level of the 24-hour difference in the corrected water level at HAI, 4.6×10^{-8}. The strain-converted noise level of the 24-hour difference in the water level at KNG is also small (3.75×10^{-8}; see Table 2). Therefore, the corrected groundwater levels at KNG and HAI, as well as the JMA strainmeters, are sufficient in detecting the preslip that occurs prior to the anticipated Tokai earthquake.

The degree of detectability of a preslip using groundwater observation wells will be improved if we can find existing wells for which the water levels have a small strain-converted noise level (i.e., having both a small noise level of the corrected water level and a large response of the observed groundwater level to crustal strain), and if we add such wells to improve the coverage of observation wells. Given the large number of existing wells in the Tokai region, it is necessary to survey existing wells and initiate groundwater-level observations at these wells to improve the preslip detectability of the AIST groundwater observation network.

7. Conclusions

We evaluated the detectability of inferred groundwater-level anomalies at seven wells, as induced by a hypothetical Mw 5.5–6.5 aseismic preslip prior to the anticipated Tokai earthquake. The assumed corresponding magnitude and time history of groundwater levels associated with the preslip are plausible because they are based on a numerical simulation, past observations of pre-seismic tilting, and recent observations of short-term slow slip events located adjacent to the anticipated focal area of the Tokai earthquake. The groundwater-level anomalies at each of the seven wells associated with a hypothetical Mw 6.5 preslip located at 10–86 of the 272 grid points are expected to be detected 1–48 hours prior to the Tokai earthquake. The hypothetical M 6.5 preslip can be detected at 92 grid points based on anomalies at any two of the seven wells 1–17 hours prior to the Tokai earthquake, with most of the points being located on land and beneath Suruga Bay. Hypothetical Mw 6 and Mw 5.5 preslips located at 3–19 and 3–5 grid points are detectable from groundwater-level anomalies at six and two wells during periods of 1–36 and 1–14 hours prior to the Tokai earthquake, respectively. The groundwater-level anomalies associated with the

Mw 6 preslip at any two of the seven wells can be detected at 10 grid points 1–4 hours prior to the earthquake.

This evaluation of preslip detectability is only one of many possible examples because the magnitude and time history of the actual groundwater-level anomalies may differ from our estimates. It would be beneficial to increase the number of observation wells to improve the detectability of groundwater-level anomalies associated with preslip events.

Acknowledgements

REFERENCES

ANDO, M. (1975), *Source mechanisms and tectonic significance of historical earthquakes along the Nankai trough, Japan*, Tectonophysics *27*, 119–140.

BRODSKY, E.E., E. ROELOFFS, D. WOODCOCK, I. GALL, and M. MANGA (2003), *A mechanism for sustained water pressure changes induced by distant earthquakes*, J. Geophys. Res. *108*, doi:10.1029/2002JB002321.

CENTRAL DISASTER PREVENTION COUNCIL (2001) Report of the Expert Committee of the Tokai Earthquake, the Central Disaster Prevention Council, Document No. 2-2 (http://www.bousai.go.jp/jishin/chubou/20011218/siryou2-2.pdf, in Japanese).

HARADA, S., A. YOSHIDA and T. AKETAGAWA (1998), *Configuration of the Philippine Sea slab and seismic activity in the Tokai region*, Bull. Earthq. Res. Inst. *73*, 291–304 (in Japanese with English abstract).

HIROSE, H. and K. OBARA (2006), *Short-tem slow slip and correlated tremor episodes in the Tokai region, central Japan*, Geophys. Res. Lett. *33*, 10.1029/2006GL026579.

IGARASHI, G. and H. WAKITA (1991), *Tidal responses and earthquake-related changes in the water level of deep wells*, J. Geophys. Res. *96*, 4269–4278.

IGARASHI, G. and H. WAKITA (1992), *Precursory and coseismic anomalies in well water levels observed for the February 2, 1992 Tokyo Bay earthquake*, Geophys. Res. Lett. *19*, 1583–1586.

IGARASHI, G., S. SAEKI, N. TAKAHATA, K. SUMIKAWA, S. TASAKA, Y. SASAKI, M. TAKAHASHI, and Y. SANO (1995), *Groundwater radon anomaly before the Kobe earthquake in Japan*. Science 269, 60–61.

ISHIBASHI, K., *Specification of a soon-to-occur seismic faulting in the Tokai district, central Japan*. In *Earthquake Prediction: An International Review*, Maurice Ewing Series 4, 297–332, (eds. Simpson, D.W. and Richards, P. G.), (AGU, Washington D.C., 1981).

JAPAN METEOROLOGICAL AGENCY (2003), *Announcement of new information about the Tokai earthquake*, Press release on 28 July 2003, 17 pp. (http://www.seisvol.kishou.go.jp/eq/tokai/20030728tokai.pdf, in Japanese).

KAMAYA N. and H. ITO (2004), *New system of information about the Tokai earthquake based on pre-slip models*, Abst. 5th U.S.-Japan Natural Resources Meeting, p. 50, U.S.Geological Survey.

KAMIGAICHI, O. and S. TSUKADA (2006), *JMA's strategy for short-term prediction of the great Tokai earthquake and the new information framework*, Zisin II, *59*, 61–67 (in Japanese with English abstract).

KATO, K., K. IKEDA, N. TONO, T. KAKIMI and M. INO (1981), *The observation system of the groundwater for earthquake prediction in the eastern part of the Tokai District -outline of observation wells and observation instruments*, Bull. Geol.. Surv. Japan *32*, 45–55.

KATO, N. and T. HIRASAWA (1996), *Effect of strain rate and strength nonuniformity on the slip nucleation process: a numerical experiment*, Tectonophysics *265*, 299–311.

KATO, N. and T. HIRASAWA (1999), *A model for possible crustal deformation prior to a coming large interplate earthquake in the Tokai district, central Japan*, Bull. Seismol. Soc. Am. *89*, 1401–1417.

KAWABE, I. (1991). *Hydro-geochemical anomalies associated with earthquakes*, Zisin *II*, 44, Special Issue, 341–364 (in Japanese with English abstract).

KITAGAWA, G. and N. MATSUMOTO (1996), *Detection of coseismic changes of underground water level*. J. Am. Stat. Assoc. *434*, 521–528.

KOBAYASHI, A. and T. MATSUMORI (1999), *An investigation of noise levels for the data of bore-hole type volumetric strain-meters and process for detecting abnormal changes*, Q. J. Seismol. *62*, 17–41 (in Japanese).

KOBAYASHI, A., T. YAMAMOTO, K. NAKAMURA, and K. KIMURA (2006), *Short-tem slow slip events detected by the strainmeters in Tokai region in the period from 1984 to 2005*, Zisin *II*, 59, 19–27 (in Japanese with English abstract).

KOIZUMI, N., Y. KITAGAWA, N. MATSUMOTO, M. TAKAHASHI, T. SATO, O. KAMIGAICHI and K. NAKAMURA (2004), *Preseismic groundwater level changes induced by crustal deformations related to earthquake swarms off the east coast of Izu Peninsula, Japan*, Geophys. Res. Lett. *31*, 19.1928/2994GL019557.

MATSUMOTO, K., T. SATO, T. TAKANEZAWA, and M. OOE (2001), *GOTIC2: A program for computation of oceanic tidal loading effect*, J. Geod. Soc. Japan, *47*, 243–248.

MATSUMOTO, N. (1992), *Regression analysis for anomalous changes of ground water level due to earthquakes*, Geophys. Res. Lett. *19*, 1193–1196.

MATSUMOTO, N., T. SATO, N. MATSUSHIMA, F. AKITA, T. SHIBATA and A. SUZUKI (2002), *Hydrological anomalies associated with crustal deformation before the 2000 eruption of Usu volcano, Japan*, Geophys. Res. Lett. *29*, 10.1029/2001GL013968.

MATSUMOTO, N., G. KITAGAWA and E. A. ROELOFFS (2003), *Hydrologic response to earthquakes in the Haibara well, central Japan: I. Groundwater-level changes revealed using state space decomposition of atmospheric pressure, rainfall, and tidal responses*, Geophys. J. Int. *155*, 885–898.

MATSUMOTO, N. and Y. KITAGAWA (2005), *Strain sensitivity and noise level in groundwater level at observation wells in and around the rupture zone of the future Tokai earthquake*, J. Geod. Soc. Japan *51*, 131–145 (in Japanese with English abstract).

MATSUMURA, S. (1997), *Focal zone of a future Tokai earthquake inferred from the seismicity pattern around the plate interface*, Tectonophysics *273*, 271–291.

MOGI, K. (1984), *Temporal variation of crustal deformation during the days preceding a thrust-type great earthquake- the 1944 Tonankai earthquake of magnitude 8.1, Japan*, Pure Appl. Geophys. *122*, 765–780.

MOGI, K. *Earthquake Prediction*, (Academic Press, Tokyo 1985).

NAGOYA UNIV. (2003), *Pre-slip model estimated from the leveling survey immediately before 1944 Tonankai earthquake*, Report of the Coordinating Committee for Earthquake Prediction *73*, 201–203 (in Japanese).

NAKAMURA, K. and J. TAKENAKA (2004), *The support software for estimation of interplate slip*, Q. J. Seismol. *68*, 25–35 (in Japanese).

NIHEI, S., O. KAMIGAICHI, and K. SATO (1987), *Observation of volume strainmeter, based on the data of 1876 to 1986; Part 1*, Q. J. Seismol. *50*, 65–88 (in Japanese).

OKADA, Y. (1992), *Internal deformation due to shear and tensile faults in a half-space*, Bull. Seismol. Soc. Am. *82*, 1018–1040.

ROELOFFS, E. A. (1988), *Hydrological precursors to earthquakes: A review*, Pure Appl. Geophys. *126*, 177–206.

ROELOFFS, E. A. (1996), *Poroelastic techniques in the study of earthquake-related hydrologic phenomena*. In *Advances in Geophysics*, *37*, 135–195, (ed. Dmowska, R.) (Academic Press, San Diego, Calif, 1996).

ROELOFFS, E.A. (1998), *Persistent water level changes in a well near Parkfield, California, due to local and distant earthquakes*, J. Geophys. Res. *103*, 869–889.

SCHOLZ, C. H. (1990) *The mechanics of earthquakes and faulting* Cambridge University Press, 1990) 439 pp.

SUYEHIRO, S. (1982), *Continuous observation of crustal movement*, In *Earthquake Prediction Techniques* pp.117–145, (ed. Asada, T.) (Univ. Tokyo Press, Tokyo 1982) (in Japanese).

TAKAHASHI, M. (1993), *Groundwater telemetering system for earthquake prediction*, Chigaku Zasshi (J. Geography) *102*, 241–251 (in Japanese with English abstract).

TAMURA, Y., T. Sato, M. Ooe and M. Ishiguro (1991), *A procedure for tidal analysis with a Bayesian information criterion*, Geophys. J. Inter. *104*, 507–516.

TSUNOGAI, U. and H. Wakita (1995), *Precursory chemical changes in ground water: Kobe earthquake, Japan*, Science *269*, 61–63.

WAKITA, H. *Precursory changes in groundwater prior to the 1978 Izu-Oshima-Kinkai earthquake*, In *Earthquake Prediction -An International Review*, Maurice Ewing Series *4*, 527–532. (eds. D. W. Simpson and P.G. Richard) (AGU, Washington D.C. 1981).

WANG, H. F. *Theory of linear poroelasticity with applications to geomechanics and hydrogeology*, (Princeton University Press, Princeton, NJ, 2000).

WESSEL, P. and W. H. F. SMITH (1998). *New, improved version of the Generic Mapping Tools released*, EOS Trans. AGU *79*, 579.

To access this journal online:
www.birkhauser.ch/pageoph

█ Pure and Applied Geophysics

Earthquake-related Changes in Groundwater Levels at the Dogo Hot Spring, Japan

SATOSHI ITABA and NAOJI KOIZUMI

Abstract—The Dogo hot spring, situated in Matsuyama City, Ehime Prefecture, Japan, is one of the oldest and most famous hot springs in Japan. The groundwater level or discharge at the spring decreased four times during the past eight or nine Nankai earthquakes. These are large interplate earthquakes that have occurred repeatedly in the western part of the Nankai Trough at intervals of 100–200 years since A.D. 684. To clarify the mechanism of these earthquake-related changes in the water level at the spring, we analyzed groundwater-level data recorded at the spring immediately after the 1946 Nankai earthquake and over the period from 1985 to 2006. We detected the other nine postseismic increases in groundwater level and no decreases, except for a large decrease of 11.4 m related to the 1946 Nankai earthquake. The increases were probably caused by ground-shaking, while the decrease was caused by a change in coseismic volumetric strain. These results lead to the following explanation of the recorded earthquake-related changes in the groundwater level at the Dogo hot spring. Both coseismic changes in volumetric strain and ground-shaking can lead to postseismic changes in groundwater pressure. The increase in groundwater pressure arising from ground-shaking is generally greater than the change in pressure associated with changes in coseismic volumetric strain; however, at the time of the Nankai earthquakes, the spring experiences a large increase in coseismic volumetric strain, leading to a considerably larger decrease in the groundwater level than the increase associated with ground-shaking. Therefore, the groundwater level at the Dogo hot spring usually increases at times of relatively large earthquakes, although the groundwater level or discharge decreases in the case of the Nankai earthquakes.

Key words: Earthquake prediction, hot spring, groundwater, Nankai earthquake, strain, stability of groundwater.

1. Introduction

The Dogo hot spring, situated in Matsuyama City, Ehime Prefecture, Japan (Fig. 1), is one of the oldest and most famous in Japan; it is said that the spring was in use more than 1,400 years ago. The hot spring is also known for earthquake-related changes in groundwater level or discharge, especially decreases in groundwater level or discharge associated with earthquakes located within the western Nankai Trough (hereafter referred to as Nankai earthquakes). The groundwater level or discharge at the spring has decreased four times during the past eight or nine Nankai earthquakes (Fig. 2; USAMI, 2003). During

Geological Survey of Japan, AIST, Site C-7, 1-1-1 Higashi, Tsukuba 305-8567, Japan.
E-mail: koizumi-n@aist.go.jp
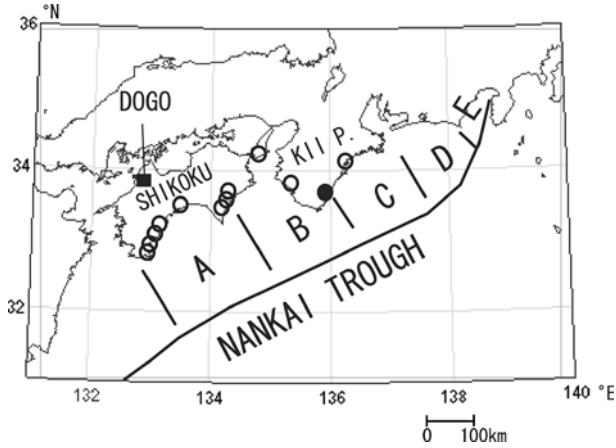
Figure 1

Map of Southwest Japan, showing the Nankai and Suruga Troughs. The Nankai Trough is divided into four areas (A–D; ANDO, 1975); area E is the Suruga Trough. The location of the Dogo hot spring is also shown. Kii P. represents the Kii Peninsula. The 11 open circles represent areas where groundwater levels fell several days before the 1946 Nankai earthquake, while the solid circle indicates an area that recorded a decrease in hot-spring discharge prior to the earthquake (HYDROGRAPHIC BUREAU, 1948).
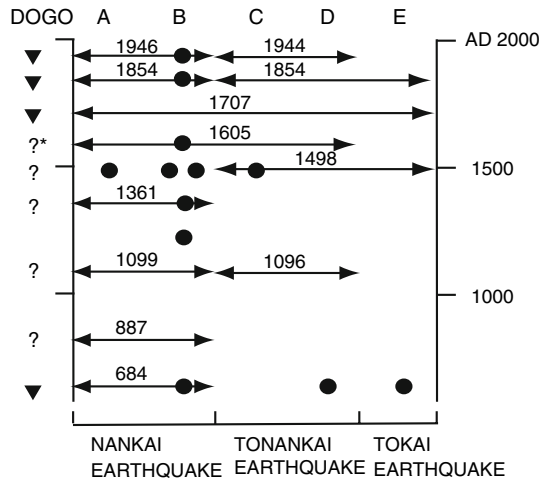
Figure 2

Space-time distribution of large-scale earthquakes along the Nankai (A–D) and Suruga (E) Troughs, as modified from SANGAWA (1992). The numbers in the figure indicate the years in which earthquakes occurred. Solid lines and circles indicate dates determined from historical documents and archaeological data, respectively. Solid triangles to the left of the figure indicate a decrease in groundwater level or cessation of discharge at the Dogo hot spring. (*: '?' means that it is unknown whether there were any earthquake-related changes in the groundwater or not.) The earthquakes located within the eastern Nankai Trough (C–D) are referred to as Tonankai earthquakes and the earthquake within the Suruga Trough is referred to as Tokai earthquake in this paper.

the 684, 1707, and 1854 earthquakes, when there was only one flowing artesian well at the spring (No. 1 well in Fig. 3), discharge stopped completely. During the 1946 event, discharge ceased at the No. 1 well, and the groundwater level showed a marked reduction at Nos. 2–4 (Fig. 3). A lack of historical records means that it is unknown whether earthquake-related changes in groundwater discharge occurred during other Nankai earthquakes (Fig. 2).

Nankai earthquakes are large interplate earthquakes that have occurred repeatedly in the western part of the Nankai Trough (Fig. 1) at intervals of 100–200 years since A.D. 684 (ANDO, 1975; SANGAWA, 1992). The Nankai Trough is divided into four parts (A–D; ANDO, 1975), with large earthquakes that occur in parts A and B being referred to as Nankai earthquakes (Fig. 2). Historical records spanning the past 1,300 years indicate that Nankai earthquakes have occurred 8 or 9 times since A.D. 684 (Fig. 2), making Nankai earthquakes one of the most well-known large interplate earthquakes in the world.

The most recent event, with a magnitude of 8.0, occurred on December 21, 1946, and is referred to as the 1946 Nankai earthquake. The groundwater level at the Dogo hot
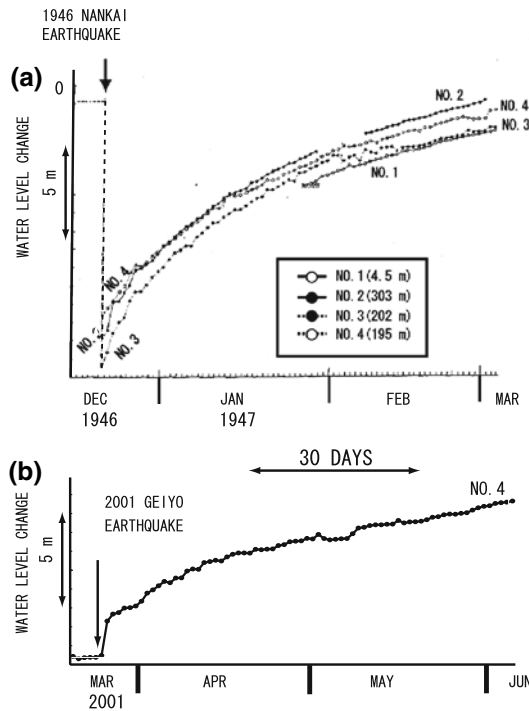
Figure 3

(a) Changes in water level within four wells at Dogo hot spring associated with the 1946 Nankai earthquake. Numbers in parentheses indicate the depths of the wells. This figure is modified from KAWABE (1991). The groundwater levels at the four wells immediately prior to the 1946 Nankai earthquake, which are all set at 0 m in this figure, were probably inferred from data measured prior to December 16, 1946. (b) Daily changes in water level within the No. 4 well at Dogo hot spring associated with the 2001 Geiyo earthquake.

spring dropped more than 10 m at the time of this event, although it is not clear whether these changes began prior to the earthquake (Fig. 3). For the same seismic event, the HYDROGRAPHIC BUREAU (1948) reported 11 shallow preseismic drops in groundwater level and one decrease in discharge from a hot spring near the coastal regions of Shikoku and Kii Peninsula (Fig. 1).

It is therefore important to clarify the mechanism of earthquake-related changes in the groundwater level or discharge at the Dogo hot spring for the purpose of earthquake prediction and the evaluation of long-term changes in groundwater levels. In this paper, we focus on recent records of groundwater levels at the Dogo hot spring and evaluate these records in terms of seismic ground motion and changes in volumetric strain.

2. Observation and Methods

Continuous observations of water levels at the Dogo hot spring had not been established at the time of the 1946 Nankai earthquake, when water levels within the four wells at the spring dropped more than 10 m (RIKITAKE, 1947; KAWABE, 1991). These changes prompted observations of the water levels until March 1947, by which time the groundwater had recovered to its pre-earthquake level (Fig. 3a). Over the period from March 1947 to 1984, no records were kept of groundwater levels at the Dogo hot spring, although the Matsuyama City Government, which has been managing the spring since 1944, reports that the groundwater levels have never fallen by more than 10 m since the 1946 Nankai earthquake. At the No. 4 well, within which the water level fell during the 1946 Nankai earthquake (Fig. 3a), pumping was discontinued prior to 1985. Since this time, the well has been used for monitoring the groundwater level at the spring. Between February 1, 1985 and June 9, 2003, the Matsuyama City Government took daily measurements at about 10:00 am. From the afternoon of June 9, 2003, the Geological Survey of Japan, AIST, in cooperation with the Matsuyama City Government, began continuous monitoring (10-min. sampling intervals) of the water level within the Dogo No. 4 well (Table 1).

Rainfall, atmospheric pressure, and seismic intensity have been observed at the Matsuyama Local Meteorological Observatory, located about 1 km from the Dogo hot

Table 1

Records of groundwater levels within the No. 4 well at the Dogo hot spring

Period	Sampling Interval	Resolution	Observation method
12/22/1946–3/3/1947*	1 day	several cm	manual
2/1/1985–6/9/2003	1 day	several cm	manual
6/9/2003–	10 min	1 mm	automatic

* Observations began just after the 1946 Nankai earthquake.

spring, since its establishment in 1890. Given the close proximity of the two sites, we treat the data collected at the observatory as being representative of the conditions at the spring. In this paper, seismic intensity is expressed using the scale proposed by the JAPAN METEOROLOGICAL AGENCY (1996).

3. Results

Figure 4 shows the daily groundwater level recorded at the No. 4 well during the period from 1985 to 2006. The records show seasonal variations of 2–3 m, with the groundwater level being lowest around April and highest around October. This variation is considered to reflect seasonal changes in rainfall at Matsuyama City. A large drop in the water level recorded in April 2000 was related to one-off pumping up in the other wells of the spring. A marked increase in water level was recorded following the 2001 Geiyo earthquake on March 24, 2001 (M 6.7). About five months after the earthquake, the water level was approximately 10 m higher than the preseismic level (Fig. 4). The seismic intensity of the 2001 Geiyo earthquake at the Dogo hot spring was "5 Upper" on the scale of the Japan Meteorological Agency (JMA), making it the largest event over the
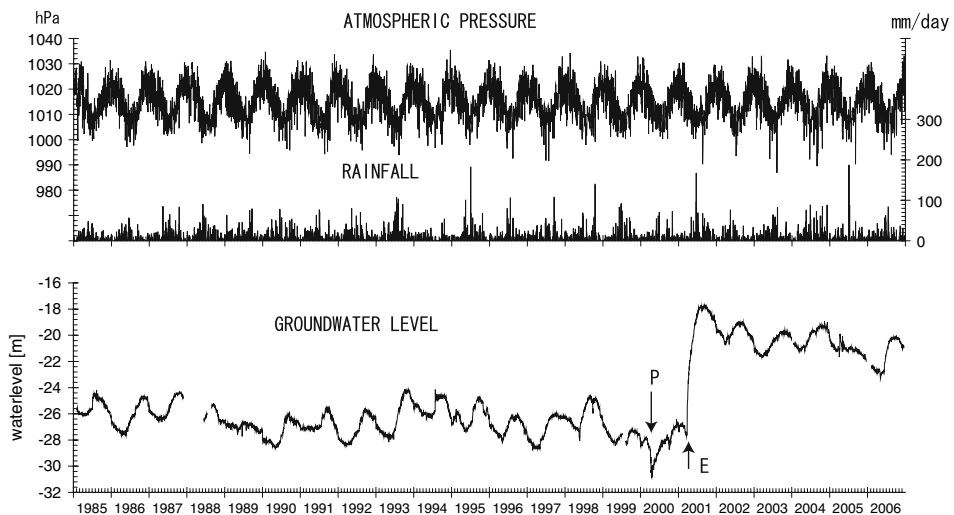
Figure 4

Daily changes in water level within the No. 4 well during the period from February 1985 to December 2006. The level of the surface is set at 0 m. Recording time was about 10:00 a.m. from 1985 to June 9, 2003, and 6:00 a.m. from June 10, 2003. Atmospheric pressure and rainfall were observed at the Matsuyama Local Meteorological Observatory, which is located about 1 km from the Dogo hot spring. "P" indicates a one-off pumping up in the wells (excluding the No. 4 well) of the Dogo hot spring, while "E" indicates the timing of the 2001 Geiyo earthquake.
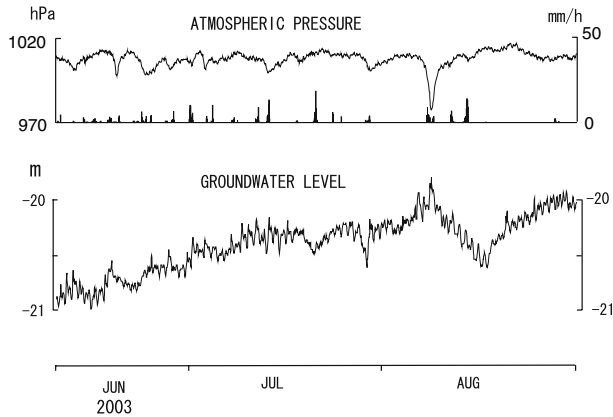
Figure 5

Hourly changes in atmospheric pressure, rainfall and water level within the No. 4 well during the period from June 9 to August 31, 2003. The data show diurnal and semi-diurnal tidal-related changes in water level. Weekly changes and a large decrease in the middle of August reflect pumping up in other wells at the spring.

period from 1946 to 2006. In the case of the 1946 Nankai earthquake, the water level dropped immediately and recovered three months later (Fig. 3); however, in the case of the 2001 Geiyo earthquake, the water level showed a gradual increase over a period of five months following the event, and did not recover to preseismic levels until December 2006 (Figs. 3 and 4).

Hourly groundwater-level data show tidal variations and changes induced by rainfall and atmospheric loading (Fig. 5). Figure 5 also reveals weekly changes related to large-scale pumping up in the other wells during the weekend, when many people visit the spring. The groundwater level shows a clear pumping-related decrease during the middle of August, which is a main holiday season in Japan (Fig. 5).

The tidal components of the groundwater level at the No. 4 well, as calculated using the tidal analysis program BAYTAP-G (TAMURA et al., 1991), are 27.2 and 20.5 mm for M_2 and O_1, respectively (Table 2). Theoretical tidal volumetric strain at the Dogo hot spring, including the contribution from earth and ocean tides, is 12.0 and 4.05 nstrain (10^{-9} strain) for M_2 and O_1, respectively, as calculated using the program GOTIC (SATO and HANADA, 1984). Therefore, the volumetric strain sensitivity of the water level is $-$ 2.26 mm/nstrain or -2.26 m/ppm (Table 2) if we adopt the value for the M_2 component, which is more accurate than the estimates of O_1. The minus sign represents the phase shift between changes in the water level of the well and changes in volumetric strain, as they differ by 180 degrees. The sensitivity of -2.26 m/ppm is very large, thereby indicating that the groundwater level at the No. 4 well is highly sensitive to changes in volumetric strain.

Table 2

Sensitivity of the groundwater level within the No. 4 well to changes in tidal volumetric strain[1]

	Well water level		Theoretical tidal volumetric strain		Strain sensitivity a/c	Phase shift b–d
	a. Amp[2] mm	b. Phase degree	c. Amp nstrain	d. Phase degree	nstrain	degree
O_1[3]	20.51 (6.17)	167.0 (22.0)	4.05	−3.5	5.06 (1.52)	170.5 (22.0)
M_2[3]	27.15 (2.99)	154.0 (10.6)	12.00	−46.9	2.26 (0.25)	200.9 (10.6)

[1]First, the tidal components of the groundwater level were calculated every 31 days over the period from June 2003 to December 2006. The average values and standard deviations, as shown in parentheses, were then calculated for the calculated tidal components.
[2]Amp: amplitude.
[3]The periods for O_1 and M_2 are 25.8 and 12.4 hours, respectively.

4. Discussion

MONTGOMERY and MANGA (2003) stated that changes in strain or stress and ground-shaking are the two main factors in generating earthquake-related changes in groundwater levels (ROJSTACZER and WOLF, 1992; ROELOFFS, 1996; KOIZUMI et al., 2004). During the 1946 Nankai and 2001 Geiyo earthquakes, the seismic intensities at the Dogo hot spring (as measured at the Matsuyama Local Meteorological Observatory) were 4 and 5 upper, respectively. The coseismic change in volumetric strain at the Dogo hot spring during the 1946 Nankai earthquake is estimated to have been 5300–6000 nstrain, as calculated using the fault models of SAGIYA and THATCHER (1999) and TANIOKA and SATAKE (2001) and the programs developed by OKADA (1992) and NAITO and YOSHIKAWA (1999). The equivalent value estimated for the 2001 Geiyo earthquake is −400 nstrain, as calculated using the model of the GEOGRAPHICAL SURVEY INSTITUTE (2001b).

To investigate the mechanism of earthquake-related changes in the groundwater level at the Dogo hot spring, we chose to analyze the 1946 Nankai earthquake and 14 other earthquakes with seismic intensities of 3 or greater at the spring (Table 3; Fig. 6) during the observation period (12/22/1946–3/3/1947, 2/1/1985–12/31/2006) shown in Table 1. We also checked for earthquake-related changes in water level associated with these 15 earthquakes, and estimated the coseismic and postseismic changes in the water level. Using the obtained strain sensitivity of 2.26 m/ppm (Table 2), we also calculated the changes in the groundwater level expected from the obtained coseismic changes in volumetric strain. In calculating the change in strain, we used the fault model of HASHIMOTO et al., (1996) for earthquake No. 6 (see Table 3) and that of GEOGRAPHICAL SURVEY INSTITUTE (2001a) for earthquake No. 10. Fault models were only available for four earthquakes: Nos. 1 (1946 Nankai earthquake), 6, 10, and 11 (2001 Geiyo earthquake); therefore, we used the point source model of the UNITED STATES GEOLOGICAL SURVEY (2007) for earthquake No. 2, the models of the JAPAN METEOROLOGICAL AGENCY

Table 3

Earthquakes with seismic intensities at the Dogo hot spring of 3 or greater during the observation period shown in Table 1

No.	Date	Time	Hypocenter Lat.	Long.	Depth (km)	M[*1]	SI[*2]	Observed changes COWL[*3] (cm)	POWL[*4] (cm)	ECVS[*5] nstrain	EWL[*6] cm	Remarks
1	12/21/1946	04:19	32°56.1'N	135°50.9'E	24	8.0	4	−1140	−1140	5,300–6,000	−1200 to −1360	1946 Nankai earthquake
2	5/13/1985	19:41	32°59.9'N	132°35.0'E	39	6.0	3	NO[*7]	NO[*7]	0.12	−0.03	No record of groundwater level
3	7/29/1988	18:59	33°40.9'N	132°30.3'E	53	5.1	3	–	–	−0.02	–[*8]	
4	1/4/1991	03:36	33°32.9'N	132°19.1'E	58	5.3	3	NO	NO	unknown	–	No fault model
5	8/31/1993	00:08	33°36.2'N	132°28.1'E	62	5.1	3	16	16–53[*9]	–[*10]	–	
6	1/17/1995	05:46	34°35.9'N	135°2.1'E	16	7.3	3	13	43	5.98	−1.35	1995 Kobe earthquake
7	6/25/1997	18:50	34°26.4'N	131°39.9'E	8	6.6	3	14	30	0.45	−0.10	
8	5/23/1998	04:49	33°42.2'N	131°50.5'E	86	5.4	3	5	127–142[*9]	0.042	−0.01	
9	10/6/2000	13:30	35°16.4'N	133°20.9'E	9	7.3	4	−7	36	−13.1	2.96	2000 Tottoriken-Seibu earthquake
10	1/9/2001	13:37	33°35.3'N	132°21.4'E	46	4.7	3	4	39	0.049	−0.01	
11	3/24/2001	15:27	34°7.9'N	132°41.6'E	46	6.7	5U[*11]	10	983	−400	90.40	2001 Geiyo earthquake
12	3/26/2001	05:40	34°7.0'N	132°42.5'E	46	5.2	3	NO	NO	0.14	−0.03	Aftershock of the 2001 Geiyo earthquake
13	3/25/2002	22:58	33°49.4'N	132°36.9'E	46	4.7	3	12	25	−0.064	0.01	
14	6/12/2006	05:01	33°8.1'N	131°26.1'E	145	6.2	4	14	73	−0.19	0.04	
15	9/26/2006	07:03	33°30.3'N	131°53.0'E	70	5.3	3	NO	NO	−0.027	0.01	

[*1] M: Seismic magnitude reported by the Japan Meteorological Agency.
[*2] SI: Seismic intensity.
[*3] COWL: Coseismic change in groundwater level recorded within the No. 4 well.
[*4] POWL: Postseismic change in groundwater level recorded within the No. 4 well.
[*5] ECVS: Estimated coseismic change in volumetric strain.
[*6] EWL: Expected change in groundwater level associated with ECVS.
[*7] NO: No earthquake-related changes in groundwater level.
[*8] "–": The amplitude of EWL is less than 0.01 cm.
[*9] Rainfall immediately before or after the earthquake made it difficult to estimate the precise magnitude of the postseismic change.
[*10] Absolute value of ECVS is less than 0.01 nstrain.
[*11] 5U: 5 Upper.
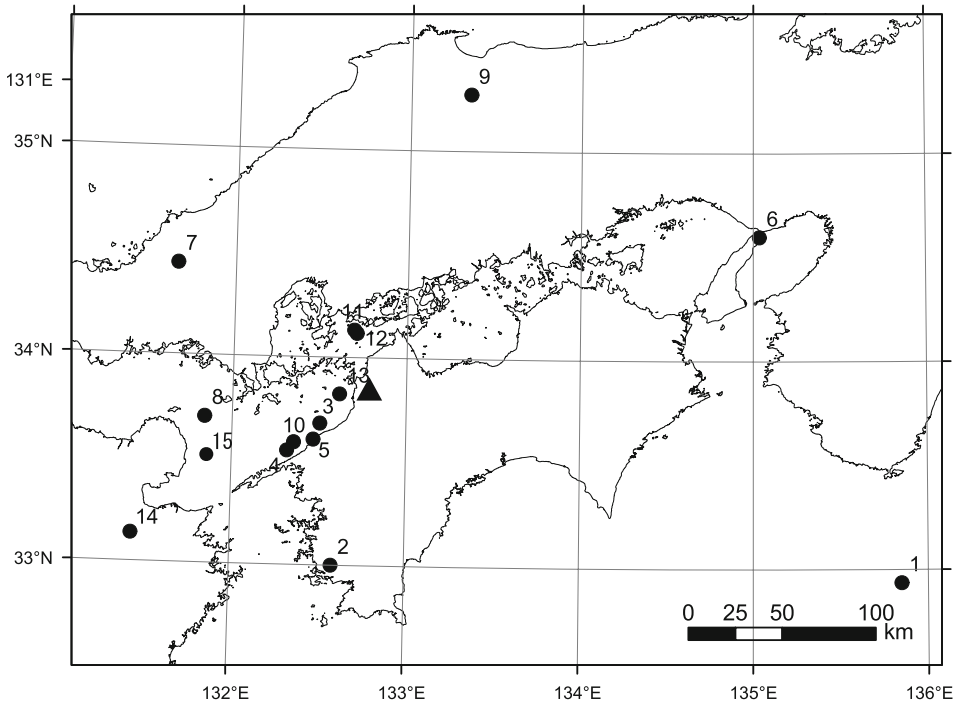
Figure 6

Map of Southwest Japan showing the locations of the epicenters of the earthquakes shown in Table 3 (solid circles). The solid triangle represents the location of Dogo hot spring.

(1989, 1994) for earthquakes Nos. 3 and 5, and those of NATIONAL RESEARCH INSTITUTE FOR EARTH SCIENCE AND DISASTER PREVENTION (2007) for earthquakes No. 7–9 and 12–15. The lack of both a fault model and point source model for earthquake No. 4 (Table 3) meant that we were unable to calculate the change in coseismic volumetric strain for this event.

The coseismic and postseismic changes in water level were estimated as follows. The coseismic change in the water level was calculated from records collected immediately before and 1 day after the earthquake. The postseismic change in water level was calculated from the record collected immediately before the earthquake and the first local maximum or minimum value following the quake. The calculations used daily data for the period from 1985 to 2006; examples are shown in Figures 7 and 8. In the case of the 1946 Nankai earthquake, which occurred at 4:19 a.m. on December 21, 1946, both the coseismic and postseismic changes in groundwater level are considered to be −11.4 m, although there are no records for the period between December 16 and 21, 1946 (Fig. 3; Table 1). The results of the calculations are shown in Table 3.

The standard deviation of the daily differences in groundwater level data for the period from February 1985 to December 2006 is 9 cm, and tidal changes have an amplitude of about 10 cm (Figs. 5 and 8). Therefore, any changes in the daily
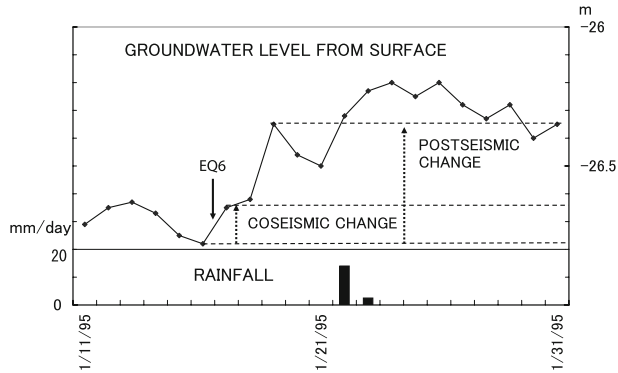
Figure 7
Estimation of coseismic and postseismic changes in water level associated with earthquake No. 6 (EQ6) in
Table 3.
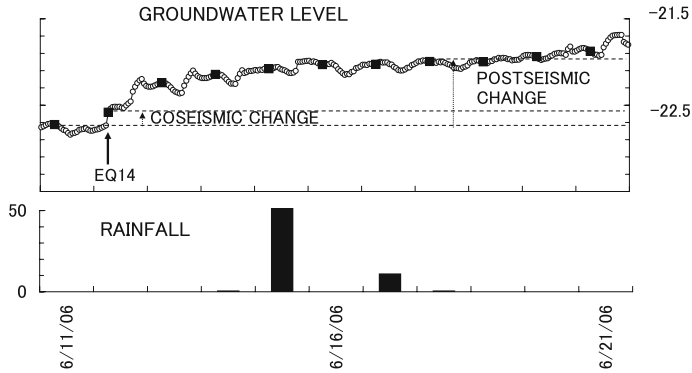
Figure 8
Estimation of coseismic and postseismic changes in water level associated with earthquake No. 14 (EQ14) in
Table 3. The open circles and solid squares represent hourly and daily values, respectively, of the groundwater
level within the No. 4 well at the Dogo hot spring.

groundwater-level records of <9 cm immediately following one of the analyzed
earthquakes were not considered as evidence of coseismic change (Table 3); the same
approach was taken in identifying postseismic change. As a result, we detected ten events
involving coseismic and postseismic changes in the groundwater level (Table 3);
however, all of the recognized coseismic changes (with the exception of the 1946 Nankai
earthquake) were smaller than 18 cm (i.e., twice the standard deviation). Therefore, these
coseismic changes are relatively imprecise. In contrast, the postseismic changes are all
greater than 25 cm, and are therefore considered to be more reliable. On this basis, we
evaluated the ten postseismic changes listed in Table 3.

Figure 9

Relationships among postseismic change in groundwater level, coseismic change in volumetric strain, and seismic intensity at the Dogo hot spring. ΔH indicates postseismic change in groundwater level, while '5L' and '5U' represent the seismic intensities of '5 Lower' and '5 Upper', respectively (JAPAN METEOROLOGICAL AGENCY, 1996). Numbers next to symbols correspond to the earthquakes listed in Table 3. The open triangle indicates that both the amplitude and sense of the postseismic change in groundwater level can be explained by coseismic change in volumetric strain at the spring. Solid triangles indicate that neither the amplitude nor sense of it can be explained by the coseismic change in volumetric strain. The gray triangle means that only the sense of the postseismic change in groundwater level can be explained by the coseismic change in volumetric strain. Earthquakes Nos. 3, 4, and 5 in Table 3 are not shown in this figure.

Figure 9 shows the relationships among coseismic change in volumetric strain, seismic intensity, and postseismic change in groundwater level. The groundwater level within the No. 4 well generally shows a postseismic increase for events with a seismic intensity of 3 or greater at the spring. Given that these increases cannot be explained by the recorded coseismic changes in volumetric strain, they are considered largely reflective of the effects of ground-shaking at the spring. The one example of a large decrease in groundwater level, which occurred in response to the 1946 Nankai earthquake, can be quantitatively explained by a coseismic increase in volumetric strain.

The above results lead to the following explanation of earthquake-related changes in water level at the Dogo hot spring. Both coseismic changes in volumetric strain and ground-shaking lead to postseismic changes in groundwater pressure. The increase in groundwater pressure arising from ground-shaking is generally larger than the change in pressure arising from changes in coseismic volumetric strain; however, Nankai earthquakes lead to a large increase in coseismic volumetric strain at the spring; meaning that the decrease in the groundwater level exceeds the increase associated with ground-shaking. Therefore, the groundwater level at the Dogo hot spring usually increases with relatively large earthquakes, although the groundwater level or discharge

decreases in the case of Nankai earthquakes. Given this scenario, we consider that the three other postseismic decreases related to past Nankai earthquakes (see Fig. 2) arose from coseismic increases in volumetric strain. In other words, the three pre-1946 postseismic decreases in groundwater level or discharge at Dogo hot spring appear to represent coseismic increases in volumetric strain at the spring.

In terms of postseismic recovery, for most of the seismic events the groundwater had recovered to pre-seismic levels within a month of the event. The large drop in water level of 11.4 m caused by the 1946 Nankai earthquake recovered within three months. Only in the case of the 2001 Geiyo earthquake did the postseismic changes take a long time; in this case the levels did not fully recover until December 2006. It is thought that the strong ground-shaking of '5 Upper' that accompanied the Geiyo earthquake had a pronounced effect on the hydrogeological system of the Dogo hot spring. This means that the effect of strong ground-shaking on groundwater levels is more important than changes in volumetric strain when evaluating groundwater stability.

5. Conclusion

We analyzed groundwater level data at the No. 4 well at Dogo hot spring at the observation periods shown in Table 1, and evaluated the relationships among 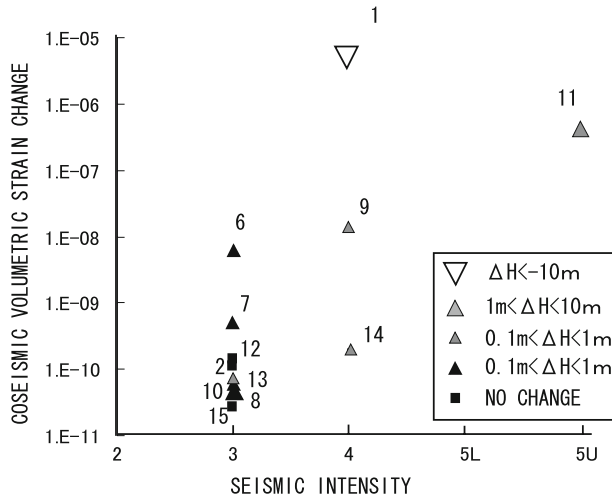postseismic change in groundwater levels, coseismic change in volumetric strain, and ground-shaking or seismic intensity. The conclusions of this study are as follows.

1. The groundwater level at the spring is highly sensitive to changes in volumetric strain.
2. The groundwater level tends to increase postseismically for earthquakes accompanied by pronounced ground-shaking at the spring. This increase is considered to be caused by ground-shaking.
3. Only one postseismic decrease in groundwater level was recorded at the spring; this was larger than 10 m and occurred following the 1946 Nankai earthquake. This decrease can be quantitatively explained by coseismic changes in volumetric strain.
4. Both coseismic change in volumetric strain and ground-shaking can lead to postseismic changes in groundwater pressure at the spring. The increase in groundwater pressure generated by ground-shaking is generally larger than the change in groundwater pressure associated with coseismic changes in volumetric strain. However, for the Nankai earthquakes, a large coseismic increase in volumetric strain is recorded at the spring, meaning that the decrease in groundwater level exceeds the increase associated with ground-shaking.
5. These postseismic changes in groundwater level usually recover to preseismic levels within several months; however, in the case of the 2001 Geiyo earthquake, which caused the strongest ground-shaking of any seismic event over the past 60 years, the postseismic changes did not recover until December 2006.

Acknowledgement

We are grateful to the Matsuyama Local Government for their cooperation in this research.

REFERENCES

ANDO, M. (1975), *Source mechanisms and tectonic significance of historical earthquakes along the Nankai trough, Japan*, Tectonophysics *27*, 119–140.

GEOGRAPHICAL SURVEY INSTITUTE (2001a), *Crustal movements in the Chugoku District*, Rep. Coord. Comm. Earthq. Pred. *65*, 592–618 (in Japanese).

GEOGRAPHICAL SURVEY INSTITUTE (2001b), *Crustal movements in the Chugoku, Shikoku and Kyushu Districts*, Rep. Coord. Comm. Earthq. Pred. *66*, 486–512 (In Japanese).

HASHIMOTO, M., SAGIYA T., TSUJI H., HATANAKA Y. and TADA T. (1996), *Co-seismic displacements of the 1995 Hyogo-ken Nanbu Earthquake*, J. Phys. Earth *44*, 255–280.

HYDROGRAPHIC BUREAU (1948), *Report on the Nankai earthquake in 1946 (change of the land surface and damage)*, Hydrographic Bull. (special number), 192 pp. (In Japanese).

JAPAN METEOROLOGICAL AGENCY (1989), *On the earthquake in Iyo-Nada, July 29, 1988*, Report of the Coordinating Committee for Earthquake Prediction *41*, 436–441 (in Japanese).

JAPAN METEOROLOGICAL AGENCY (1994), *The Seismological Bulletin of the Japan Meteorological Agency for August 1993*, 202.

JAPAN METEOROLOGICAL AGENCY (1996), *JMA Seismic Intensity Scale*, http://www.jma.go.jp/jma/kishou/know/ shindo/shindokai.html.

KAWABE, I. (1991), *Hydro-geochemical anomalies associated with earthquakes*, J. Seismol. Soc. Jpn. *44*, 341–364 (In Japanese).

KOIZUMI, N., KITAGAWA, Y., MATSUMOTO, N., TAKAHASHI, M., SATO, T., KAMIGAICHI, O., and NAKAMURA K. (2004), *Preseismic groundwater level changes induced by crustal deformations related to earthquake swarms off the east coast of Izu Peninsula, Japan*, Geophys. Res. Lett. *31*, L10606, doi:10.1029/2004GL019557.

MONTGOMERY, R. and MANGA, M. (2003), *Streamflow and water well responses to earthquakes*, Science, *300*, 2047–2049.

NAITO, H., and YOSHIKAWA, S. (1999), *A program to assist crustal deformation analysis*, J. Seismol. Soc. Jpn. *52*, 101–103 (in Japanese).

NATIONAL RESEARCH INSTITUTE FOR EARTH SCIENCE AND DISASTER PREVENTION (2007), *Earthquake mechanism information*, http://www.fnet.bosai.go.jp/freesia/event/hypo/old.html.

OKADA, Y. (1992), *Internal deformation due to shear and tensile faults in a half-space*, Bull. Seismol. Soc. Am. *82*, 1018–1040.

RIKITAKE, T. (1947), *Groundwater changes at the Dogo hot spring related to the Nankai earthquake*, Bull. Earthq. Res. Inst. *5*, 189 –194 (In Japanese).

ROELOFFS, E., *Poroelastic methods in the study of earthquake-related hydrologic phenomena*, In *Advances in geophysics* (Dmowska, R., ed.), (San Diego, California, Academic Press, 1996) 135–195.

ROJSTACZER, S. and WOLF, S. (1992), *Permeability changes associated with large earthquakes: An example from the Loma Prieta*, California, Geology *20*, 211–214.

SAGIYA, T. and THATCHER W. (1999), *Coseismic slip resolution along a plate boundary megathrust: The Nankai trough, southwest Japan*, J. Geophys. Res. *104*, 1111–1129.

SANGAWA, A. (1992), *Jishin-Kokogaku (Earthquake Archaeology)*, Chuokoron-sha, Tokyo, 251 pp (in Japanese).

SATO, T. and H. HANADA (1984), *A program for the computation of oceanic tidal loading effects ' GOTIC'*, Publ. Int. Latitu. Mizusawa *18*, 63–82.

TAMURA, Y., SATO, T., OOE M., and ISHIGURO, M. (1991), *A procedure for tidal analysis with a Bayesian information criterion*, Geophys. J. Int. *104*, 507–516.

TANIOKA, Y. and SATAKE, K. (2001), *Coseismic slip distribution of the 1946 Nankai earthquake and aseismic slips caused by the earthquake*, Earth Planets Space, *53*, 235–241.

UNITED STATES GEOLOGICAL SURVEY (2007), *Moment Tensor and Broadband Source Parameter Search*, http://
  neic.usgs.gov/neis/sopar/.
USAMI, T., *Materials for comprehensive list of destructive earthquakes in Japan, (416)-2001* (University Tokyo
  Press 2003), 605 pp (in Japanese).

To access this journal online:
www.birkhauser.ch/pageoph

█Pure and Applied Geophysics

Flow Changes and Geochemical Anomalies in Warm and Cold Springs Associated with the 1992–1994 Seismic Sequence at Pollina, Central Sicily, Italy

Rocco Favara,[1] Fausto Grassa,[1] Paolo Madonia,[1] and Mariano Valenza[2]

Abstract—During a three-year discontinuous geochemical monitoring of some warm springs and cold discharges located in central-northern Sicily, some hydro-geochemical changes were observed. Excluding a possible related to a moderate seismic activity were accidentally identified. The observed anomalies showed amplitudes that were modulated by the different geometries and volumes of the feeding aquifers. A poroelastic aquifer contraction, a shaking-induced dilatancy theory as well as seismogenetic-induced changes in the properties of the aquifers have been proposed as possible mechanisms for the water flow and hydro-geochemical changes. These preliminary results could be used to design a monitoring network aimed at surveilling the seismic activity of the studied area from a geochemical standpoint.

1. Introduction

In the last decades, several researches in Japan, China, the USA and Europe, have been focused on the understanding of the seismogenetic processes for earthquake prediction purposes. In particular, researchers have directed their attention towards two main features of the seismogenetic process:

1) The role played by the fluids during seismogenesis (Dworkin, 1999; Sornette, 1999 and literature therein);
2) Theoretical modeling of the physical processes responsible for the hydrological, chemical and isotope changes in crustal fluids, such as gases and groundwaters, induced by increasing crustal strain. (Rikitake, 1976; Wakita, 1977, 1982; Carapezza et al., 1980; Cai et al., 1984; Barsukov et al., 1985; Thomas, 1988; Valenza and Nuccio, 1993; Favara et al., 2001a b and references there cited).

In order to recognize the geochemical anomalies related to earthquake preparation and to use them as practical tools in earthquake prediction, each natural system needs to be

---

[1] Istituto Nazionale di Geofisica e Vulcanologia- Section of Palermo, Via Ugo La Malfa 153, 90146 Palermo, Italy. E-mail: favara@pa.ingv.it
[2] Dipartimento CFTA, University of Palermo, Via Archirafi, 36, 90123 Palermo, Italy.

investigated in detail. For each studied area, basic information regarding the geological and structural setting, the origin of the fluids and model of their circulation, as well as the definition of the geochemical background (including natural and non-natural variations) is crucial to the formulation of a valid geochemical model able to explain the recognized anomalies and their relationships to increasing crustal strain (FAVARA *et al.*, 2001a).

A seismically active area located in the northern part of Sicily (Pollina area, Fig. 1) was affected by a long seismic sequence. It started in September 1992, during which more than 500 seismic shocks, at a depth ranging between 3 and 5 km, were recorded. The seismic swarm culminated with the strongest event that took place on June 26, 1993, and that had a magnitude of 4.4 (Fig. 2).

Some significant geochemical variations in both the output and in the chemical composition of He, CO_2, Rn and Ne, were observed during the strongest event of the recorded seismic swarm. This was ascertained by comparing the data collected during three soil gas investigations (DE GREGORIO *et al.*, 1996).

During the same period, groundwaters from seven springs and one well (PC), representative of different aquifers present in this area and discontinuously monitored every three months for a more ample hydrogeological study, showed both hydrological and geochemical anomalies.

2. Geology and Hydrogeology

The studied area is located in the eastern part of the Madonie Mountains in north-central Sicily (Italy). The Madonie Mountains extend for an area of about 220 km^2 (Fig. 1). Several cold springs, giving a total flow discharge of about 3500 l/s (FAVARA *et al.*, 1984), lie in this region, and represent one of the most important hydrogeological domain in Sicily. The main springs are located both within the area of the Madonie Mountains and along the northern coast of Sicily, near the town of Cefalù.

The stratigraphic sequence of this area consists only of sedimentary terrains: No crystalline or metamorphic rocks outcrop, neither have any been found during drillings. This sequence includes Triassic-Miocene limestones, siliceous-limestones (Imerese Basin) and Triassic-Eocene limestones and dolostones (Panormide Platform). Shales and quartz-sandstones of the Upper Oligocene Numidian Flysch outcrop on the borders of the studied area. Clays and sandstones deriving from the erosion of the Sicilide Domain deposits, Upper Cretaceous in age, outcrop near the coast. Post-orogenic deposits including clays, sandstones and evaporite deposits of Upper Tortonian to Pleistocene age complete the stratigraphic succession. In particular, the evaporitic sequence is present only in the southern part of the Madonie Mountains, as it had already emerged during the deposition of the Messinian gypsum-dominant series. Fluvial and marine deposits of Quaternary age are also present on the coast and in fluvial valleys.

Tectonics resulted from several compressive and distensive episodes from Miocene to Upper Pliocene (ABATE *et al.*, 1982). The main fault systems are characterized by N-S and
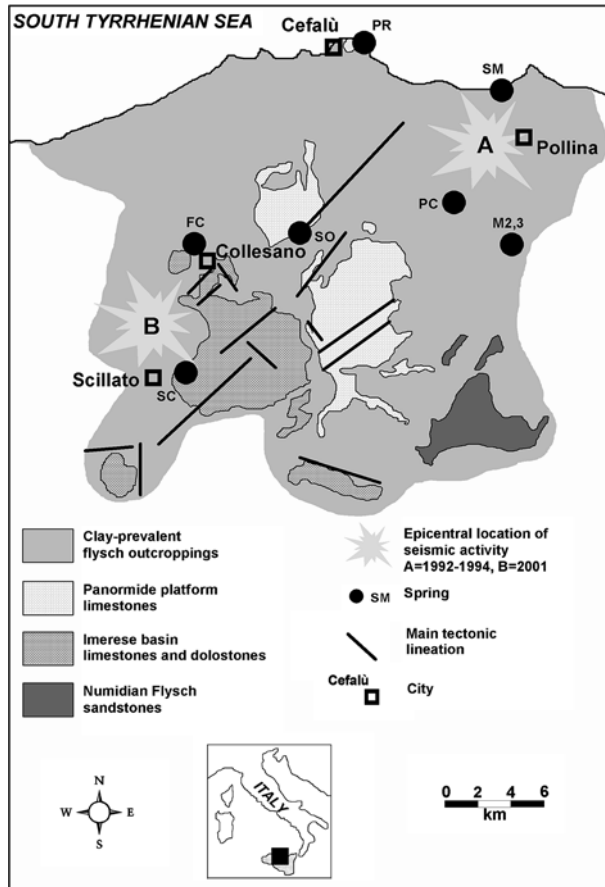
Figure 1
Location map of the study area. Main geological features, location of the sampling sites and the epicenters of the recent local seismic activity (1992–1994 and 2001) are also reported.

NE-SW directions. These different tectonic phases created a building with vertical recurrences of platform and basin limestones and dolostones, overthrusted with their cover of alternating sandstones and clays (Numidian Flysch).

As stated in previous studies (CUSIMANO, 1989; CUSIMANO et al., 1992; MADONIA, 1993; GRASSA et al., 2002), the main aquifers are of mixed type, with a main contribution from the carbonate sequences and a minor component to be referred to underground circulation into the permeable portion of the Numidian Flysch. The carbonate aquifers are of two different sub-types: In the NE portion karst is predominant, related to the platform limestone sequences of the Panormide domain; in the SW portion fractured rocks related to the deep sea sequences of the Imerese basin
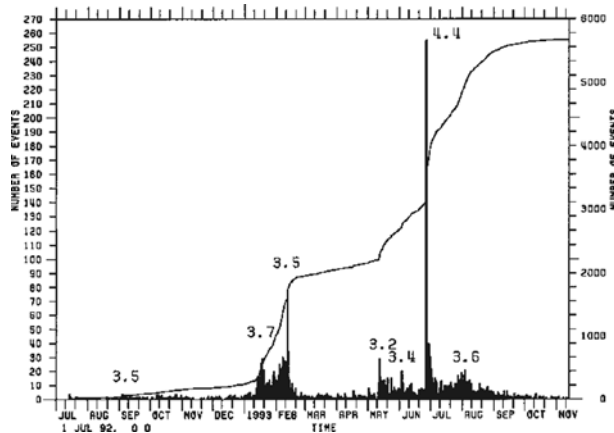
Figure 2
Plot of earthquake distribution during the Pollina seismic sequence from July 1992 to November 1993. Histogram (left scale), cumulative frequency (right scale) and shocks with M > 3.0 are reported (from Azzara *et al.*, unpublished data).

domain prevail. The two hydro-structures are probably in lateral hydraulic continuity (Madonia, 1993) and, as the higher portion of the Panormide aquifer is located at higher altitudes than those of the Imerese hydro-structure, underground waters may flow from the previous to the latter.

From a hydro-geochemical point of view (Cusimano *et al.*, 1992; Madonia, 1993), the prevailing carbonate species are modulated by its different mixings with waters circulating into the permeable portions of the Numidian Flysch. These latter are characterized by higher concentrations of ions derived from the interaction with sulphur minerals and H_2S, as better specified in section 4.

Sandstone-hosted aquifers became dominant only in the south-east portion of the Madonie area, while marine, fluvial and alluvial deposits of the northern Imera and Pollina Rivers form lateral aquifers of minor importance. The total water storage capability was estimated at about 1.1×10^8 m^3 (Cusimano, 1989).

3. Analytical Methods

Electrical conductivity, pH and water temperature were measured directly in the field. Conductivity was measured using a Crison 524 conductimeter (accuracy $\pm$ 3%); pH by using an Orion 250 pH meter (accuracy $\pm$ 0.01 pH unit) and water temperatures by means of a mercury thermometer (accuracy $\pm$ 0.1°C). HCO_3 was determined by volumetric titration with 0.1 N HCl Suprapur. Major and minor constituents were determined by a Dionex 2000i ion chromatograph (reproducibility

within ±2%). A Dionex AS4A-SC column was used for anion determinations (F, Cl, NO_3, Br, SO_4), whereas a Dionex CS-12 column was used for the cations (Li, Na, K, Mg, Ca).

4. Water Geochemistry

Chemical composition of collected waters together with physico-chemical parameters are reported in Table 1.

Water temperature, electrical conductivity and pH range between 13.2°C and 28.6°C, 342 and 2869 μS/cm and 6.74 and 7.87, respectively. A first classification of the sampled waters was obtained by using a Langelier-Ludwig diagram (Fig. 3):

– The Scillato (SC) and Favara di Collesano (FC) springs fall within the bicarbonate alkaline-earth field (group A). They are characterized by low salinity (TDS < 400 mg/l) and their chemistry is dominated both by HCO_3 and by alkaline-earth metals (Ca and Mg). The Scillato spring is located at an altitude of 380 m a.s.l., on the western flank of the Madonie Mountains and has a flow rate of several hundreds of l/s. Due to its location along the lateral contact between the Imerese and Flysch series and to the fact that the amount of discharged water represents more than 50% of the whole calculated recharge of the Imerese structure, it can be considered as being the main basal discharge of the Imerese domain (MADONIA, 1993). The Favara di Collesano spring is located at a slightly higher altitude (i.e., 450 m a.s.l.), and has a flow rate of only a few tenths of a l/s. It is a secondary discharge of the Imerese aquifer and is linked to the contact between two different carbonate thrusts with an interposed Numidian Flysch layer. These springs reach full chemical equilibrium with the carbonate rocks, as suggested by the saturation indexes of calcite and dolomite that close to zero.

– The Marcatagliastro springs (M2 and M3) fall within the chloride-sulphate alkaline-earth field (group B). They belong to groundwaters circulating within the Numidian Flysch formation. There, the observed sulphate-enrichment could probably be related to two different mechanisms: the weathering of sulphides and sulfate-rich minerals and the oxidation of H_2S minerals, such as Pyrite (Fe_2S), Natrojarosite ($NaFe_3(SO_4)_2(OH)_6$) and Thenardite (Na_2SO_4), which were found in the clay interlayers of the Numidian Flysch (ALAIMO and FERLA, 1975). Moreover, the potential high redox values measured in the aquifers allow for the oxidation of S-rich fluids, both of deep origin and derived from the alteration, in anoxic conditions, of the organic matter of the Numidian Flysch clays.

All the other water samples but PC sample are distributed within a triangle, the corners of which represent three end members, suggesting the existence of mixing processes between sea water (SW), groups A and B waters:

Table 1

Chemical analyses of waters from the Madonie Mountains

Sample	Date	Flow rate	pH	EC	T	Na	K	Ca	Mg	Cl	SO₄	HCO₃	TDS
Sm[a]	13/6/91	0.04	7.36	1960	16.8	178	16	141	59	189	370	476	1431
	30/9/91	0.05	7.47	1970	18.6	211	18	143	63	201	384	470	1491
	30/1/92	0.05	7.72	1920	15.8	194	17	136	64	209	393	464	1479
	26/3/92	0.05	7.63	1930	15.4	209	15	140	49	202	376	458	1451
	12/7/92	n.m.	7.28	2000	17.8	211	13	136	60	203	389	458	1475
	30/9/92	0.05	7.26	1941	19.0	197	15	121	54	195	405	384	1373
	15/1/93	0.05	7.78	1860	15.9	184	13	140	58	175	361	439	1373
	6/7/93	0.25	7.18	1880	17.0	229	17	159	65	213	475	476	1635
	3/8/93	0.50	7.26	1860	17.4	210	18	146	65	211	430	415	1496
	10/8/93	n.m.	n.m.	n.m.	n.m.	210	18	144	61	203	408	409	1457
	17/8/93	n.m.	n.m.	n.m.	n.m.	212	18	143	61	200	402	415	1453
	24/8/93	n.m.	n.m.	n.m.	n.m.	209	18	146	61	198	399	427	1461
	31/8/93	n.m.	n.m.	n.m.	n.m.	213	19	144	61	198	399	415	1452
	10/9/93	n.m.	7.23	1991	17.8	211	17	152	60	194	400	488	1525
	7/10/93	0.07	7.10	1910	17.6	205	19	144	61	194	377	427	1432
	30/11/93	0.07	7.16	1375	16.1	206	19	143	60	193	368	427	1420
	21/1/94	0.07	7.25	1675	16.7	200	18	144	64	192	362	464	1448
	18/2/94	0.08	7.44	1816	16.5	197	17	137	61	168	342	476	1404
	25/2/94	0.05	7.37	1824	16.5	197	18	137	59	157	330	476	1378
	26/2/94	n.m.	n.m.	n.m.	n.m.	189	17	124	63	169	341	476	1382
	27/2/94	n.m.	n.m.	n.m.	n.m.	188	17	124	63	169	346	464	1373
	28/2/94	n.m.	n.m.	n.m.	n.m.	189	17	124	64	168	344	476	1385
	1/3/94	n.m.	n.m.	n.m.	n.m.	191	17	119	64	167	343	470	1377
	2/3/94	n.m.	n.m.	n.m.	n.m.	192	17	122	64	165	346	476	1389
	3/3/94	n.m.	n.m.	n.m.	n.m.	188	17	126	63	172	342	470	1386
	4/3/94	n.m.	n.m.	n.m.	n.m.	191	17	126	63	174	349	476	1399
	5/3/94	n.m.	n.m.	n.m.	n.m.	192	17	126	63	170	346	476	1392
	6/3/94	n.m.	n.m.	n.m.	n.m.	191	17	122	64	169	344	464	1373
	7/3/94	n.m.	7.20	1798	16.5	190	17	124	63	168	344	470	1379
	8/3/94	n.m.	n.m.	n.m.	n.m.	188	17	124	63	168	344	476	1383
	9/3/94	n.m.	n.m.	n.m.	n.m.	188	17	124	63	169	343	476	1383
	10/3/94	n.m.	7.32	1760	16.5	192	17	124	63	168	342	476	1384
	25/3/94	0.06	7.12	1780	16.5	188	14	127	54	162	344	476	1368
	26/4/94	0.03	7.37	1805	16.6	187	14	130	55	155	340	476	1358
	26/5/94	0.04	7.41	1750	17.0	180	14	131	56	154	336	488	1359
M2[a]	30/11/93	0.13	7.28	1562	17.9	94	13	207	66	97	550	306	1335
M3[a]	30/11/93	0.42	6.74	1635	20.6	92	12	203	66	95	492	392	1356
PC[b]	18/2/94	n.m.	7.40	2563	28.6	638	12	6	2	172	10	1484	2328
SO[a]	13/6/91	n.m.	6.95	696	13.1	31	1	122	21	21	129	403	729
	30/9/91	0.06	7.16	726	14.6	39	2	133	24	23	134	421	776
	30/1/92	0.40	7.28	728	13.1	36	1	136	24	25	164	403	792
	26/3/92	0.40	7.61	700	12.4	35	1	141	21	25	144	397	765
	12/7/92	n.m.	n.m.	790	13.3	34	1	141	21	25	141	403	766
	30/9/92	0.08	7.33	696	14.4	36	1	132	20	20	130	345	686
	16/1/93	0.50	7.20	709	12.9	43	1	152	24	22	127	384	758
	1/4/93	0.75	7.13	744	12.1	33	2	134	20	23	113	397	726
	8/7/93	1.50	7.11	666	13.7	38	1	134	22	23	130	415	766
	1/5/94	n.m.	7.04	802	12.7	31	1	125	20	18	109	397	707
	1/6/94	0.50	6.93	800	12.7	32	1	130	21	19	112	409	729

Table 1

(Contd.)

Sample	Date	Flow rate	pH	EC	T	Na	K	Ca	Mg	Cl	SO4	HCO3	TDS
SC[a]	13/6/91	432	7.69	342	14.2	8	1	50	18	9	16	207	310
	1/7/91	n.m.	7.63	439	12.2	8	1	44	19	10	15	203	301
	1/8/91	n.m.	7.74	425	14.1	7	1	50	17	9	17	207	309
	30/9/91	410	7.20	314	14.6	6	1	49	17	9	17	201	301
	1/10/91	n.m.	n.m.	382	13.8	7	1	51	16	9	16	207	309
	1/11/91	n.m.	n.m.	405	13.7	7	1	50	16	9	17	214	314
	30/1/92	452	7.77	315	13.4	7	1	50	17	9	17	214	316
	26/3/92	447	7.61	306	13.8	7	1	51	16	10	16	214	315
	12/7/92	419	7.42	312	14.3	7	1	48	15	10	17	201	299
	30/9/92	380	7.64	303	14.5	7	1	49	15	8	15	210	306
	13/1/93	380	7.87	296	12.3	7	1	51	14	7	15	214	309
	2/4/93	550	7.77	293	13.1	7	1	52	15	8	15	214	313
	7/7/93	500	7.63	315	14.5	7	1	50	16	10	16	210	312
PR[a]	13/6/91	759	7.18	2745	15.4	507	21	134	63	910	126	275	2041
	1/7/91	n.m.	7.23	3891	15.5	548	20	125	62	892	127	276	2056
	1/8/91	n.m.	7.25	3720	15.3	534	19	127	60	863	120	275	2003
	30/9/91	651	7.17	2497	15.5	465	19	117	60	862	116	275	1916
	1/10/91	n.m.	n.m.	3292	15.5	471	16	121	56	809	126	275	1880
	1/11/91	n.m.	n.m.	3270	15.5	458	16	113	56	753	116	275	1794
	30/1/92	941	7.29	2431	15.5	436	13	106	51	807	122	275	1812
	26/3/92	588	7.36	2465	15.5	436	13	106	51	807	122	275	1812
	12/7/92	624	7.12	2662	15.4	482	13	123	56	887	114	281	1963
	30/9/92	619	7.42	2310	15.7	442	16	100	47	796	115	275	1796
	15/1/93	655	7.48	2594	15.4	465	20	118	63	808	108	275	1867
	1/4/93	403	7.41	2592	15.1	459	23	137	58	864	105	275	1942
	8/7/93	811	7.47	2610	15.5	520	20	129	58	917	129	275	2052
	25/3/94	n.m.	7.33	3080	15.6	535	11	126	56	938	116	275	2064
	26/4/94	n.m.	n.m.	n.m.	n.m.	425	14	106	51	740	97	275	1715
FC[a]	13-giu-91	26.40	7.39	442	16.5	13	1	59	26	15	27	253	399
	1-lug-91	n.m.	7.47	546	16.5	12	1	55	28	16	28	258	402
	1-ago-91	n.m.	7.46	546	16.5	12	2	58	27	29	27	256	414
	30-Set-91	16.50	7.15	425	16.8	12	2	54	28	15	28	256	396
	1-Ott-91	n.m.	7.44	524	16.5	13	1	56	27	15	28	275	416
	1-nov-91	n.m.	n.m.	527	16.2	13	1	57	28	14	29	275	418
	30-gen-92	11.50	7.47	430	16.2	13	1	58	29	15	30	275	423
	26-mar-92	13.10	7.32	432	16.2	12	2	58	28	17	29	275	422
	12-lug-92	4.56	7.26	416	16.7	11	2	54	27	15	29	268	409
	30-set-92	5.28	7.20	428	17.1	11	1	56	26	13	28	271	410
	13-gen-93	1.94	7.83	398	14.9	10	2	51	27	13	26	268	400
	2-apr-93	7.59	7.57	477	15.9	14	2	62	28	18	32	287	449
	1-mag-94	3.00	7.44	450	17.0	12	1	58	25	14	24	268	405

Flow rates are expressed in l/s, pH in pH unit, EC = electrical conductivity at 20°C is expressed in mS/cm, T = water temperature in °C. Concentrations and TDS are expressed in mg/l.; a = spring; b = well. n.m. not measured. Saturation indexes with respect to calcite (SI_{Calc}) and dolomite (SI_{Dolom}) are also reported

– The Presidiana (PR) spring lies in the chloride-sulphate-alkaline field. It is located at sea level, it has the greatest flow rate in the Madonie area (up to 1000 l/s), and is the main northern discharge point of the basal aquifer that is hosted within the Panormide
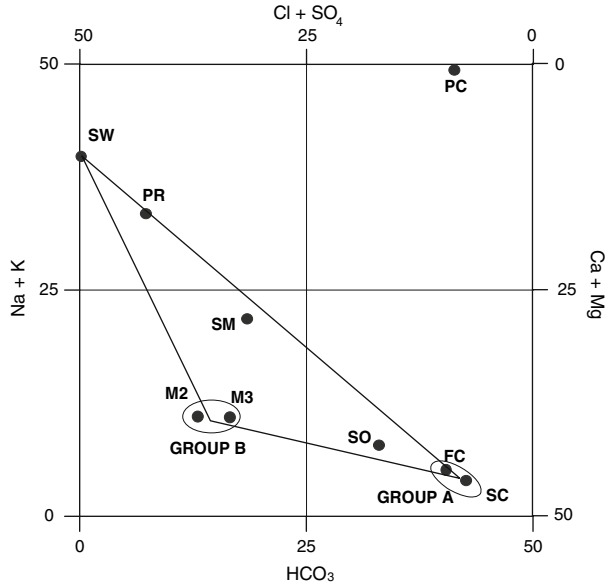
Figure 3

Langelier-Ludwig classification diagram. Three main groups have been distinguished: bicarbonate alkaline-earth waters (group A), chloride-sulphate alkaline-earth waters (group B) and bicarbonate alkaline waters (PC well). SW = seawater.

  domain (CUSIMANO *et al.*, 1992). Its chemistry reflects seawater contamination (up to 3%).
– The waters of the S. Maria (SM) spring are chloride-sulphate alkaline-earth. Its flow rate is of the order of a few decimals of a l/s, and is fairly constant during the entire hydrological cycle. It is not affected by seawater mixing, as indicated by the chloride/sulphate ratio (Fig. 4). Its related aquifer develops entirely within the Numidian Flysch deposits, whereas the carbonate ions may derive from the dissolution of the calcite cement of sandstones and/or from carbonate olystolithes present in the Numidian sequences.

The Sonno spring (SO) is a transitional term between bicarbonate-alkaline earth and chloride-sulphate-alkaline waters, and its maximum flow rates are 1–1.5 l/s. It lies along a very important tectonic discontinuity, marked by the deep Isnello Valley, and its chemistry is the result of the mixing of Panormide and Numidian aquifers.

    The Pozzo Casalo sample (PC) lies in the bicarbonate alkaline field and shows relatively high salinity (about 2500 mg/l). Na and HCO_3 are the dominant chemical constituents as the sum of the two is greater than 90% of the total dissolved ions (in meq/l).

    These unusual chemical features suggest a two-step geochemical process. First, the dissolution of carbonate minerals (both calcite and dolomite) by CO_2 enriched waters
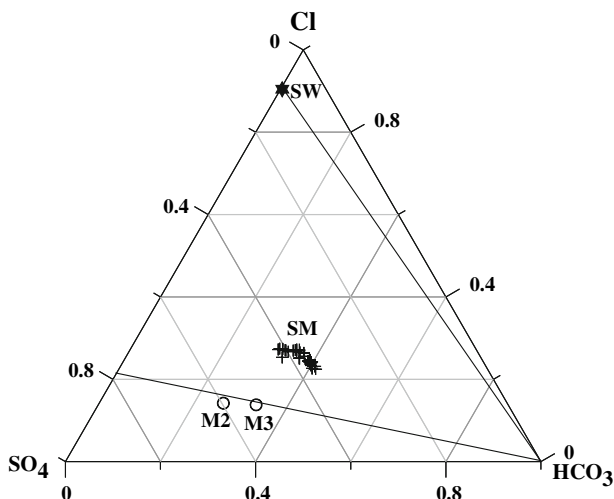
Figure 4

Triangular plot for anions. The SO_4/Cl ratio at the SM spring is costant with time and closer to that of the chloride-sulphate alkaline-earth end-member (M2 and M3 springs) rather than to that of seawater.

accounts for most of the solute content. In a second time, the ion-exchange reactions between groundwater and clay minerals, probably modify pristine ion ratios, causing an increase in Na and a consequent removal of Ca and Mg from the solution. The latter can be described by an equilibrium constant (APPELO and POSTMA, 1993) as follows:

$$Na-X + 0.5\ Ca^{2+} \leftrightarrow Na^{+} + 0.5\ Ca-X_2 \tag{1}$$

and

$$Na-X\ +\ 0.5\ Mg^{2+} \leftrightarrow Na^{+} + 0.5\ Mg-X_2, \tag{2}$$
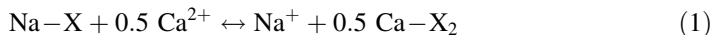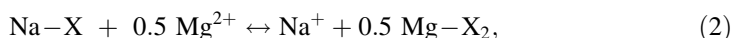
where X indicates the clay exchanger.

In order to verify the hydrogeochemical processes inferred above, the computer program NETPATH (PLUMMER et al., 1991) was used to calculate the mass balance of the chemical reactions. The geochemical evolution during flow path was simulated starting from groundwater similar to that of the SC spring (the most representative carbonate groundwater). Taking into account the local geological setting, one of the most plausible reactions can be written as follows:

$$SC_{water} + 7.7\ CO_2 + 11.7\ Ca_{0.85}Mg_{0.15}CO_3 + 2.3\ Mg^{+2} + 11\ Ca^{+2}$$
$$+\ 13.3\ NaEx < = > PC_{water}.$$
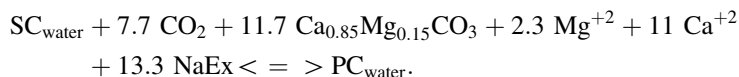
Another process that could produce $Na-HCO_3$ waters is the alteration of albite-rich rocks to form Na-montmorillonite enhanced by the dissolution of carbon dioxide. However, this

hypothesis can be ruled out because of the lack of crystalline rocks in this area. As can be noted, both these reactions imply the presence of a CO_2-rich phase interacting with groundwaters.

This agrees with the soil gas measurements carried out during the three surveys effected in the studied area (DE GREGORIO *et al.*, 1996). Field investigations have revealed the presence of high CO_2 flux, with the highest values being about $3 * 10^{-4}$ cm/sec. The results of carbon isotope measurements ($\delta^{13}C_{CO_2}$) performed at only two sites having high CO_2 concentration (1–2% vol.) are close to -25 δ‰, vs. V-PDB, thus indicating that this gas derives from the oxidation of organic matter.

5. Temporal Variations

Although the sampling rate was neither high nor constant, some physico-chemical changes were observed in some of the studied springs.

During the period June 1991–January 1993, the flow rate values at SM spring remained almost constant, showing only a seasonal trend at SO spring that resulted in lower values during the dry season, which in Mediterranean areas corresponds to late spring – beginning of autumn. In proximity of the 26th June event, the flow rate at SO and SM springs increased up to 10 times (Fig. 5).

If we analyze the entire sampling period more in detail, we will ascertain that some geochemical changes were also observed at the SM, FC and SC springs. FC and SM springs showed anomalies in the TDS content and SC spring displayed a marked change in Mg concentration.

First of all, our attention will be focused on TDS (Fig. 6). Unfortunately, due to some sampling problems, we have no data either for the FC spring immediately after the
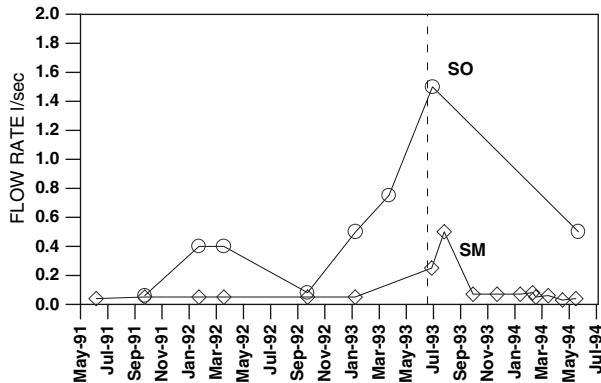
Figure 5

Temporal variation of flow rate at the SM (diamonds) and SO (circles) springs. Dashed line indicates the occurrence of the strongest earthquake (June 26, 1993, M = 4.4).
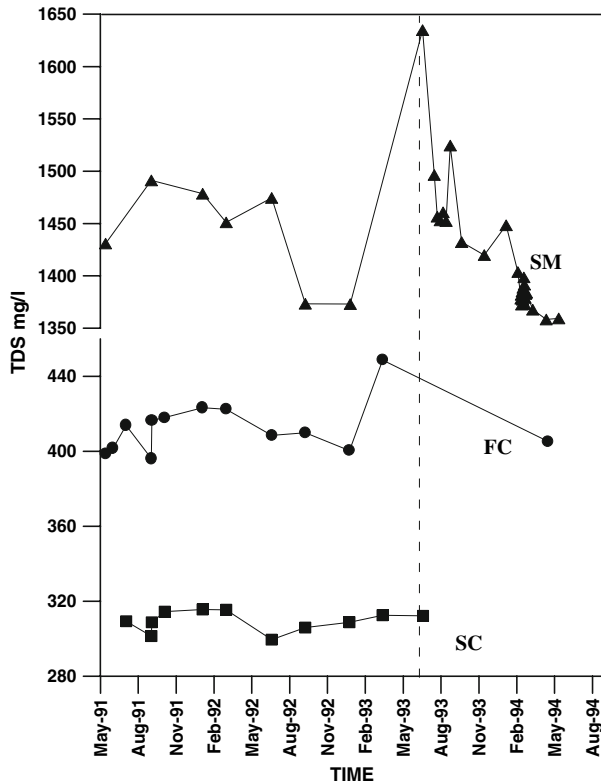
Figure 6

Changes in TDS values at the SM (triangles), FC (circles) and SC (squares) springs. The 26th June event (M = 4.4) is also highlighted (dashed line). The amplitude of the observed anomalies is inversely proportional to the extent of the aquifer, as such modifications are more evident at the SM spring that has a smaller reservoir.

strongest earthquake or for the SM spring immediately before it. In spite of this lack of data for both these springs a common trend is evident. This consists of a relative minimum in January 1993 with TDS values of 1400 and 400 mg/l at SM and FC springs, respectively. Subsequently, the values rose up to 1600 mg/l (SM spring) and 450 mg/l (at FC spring), falling outside their respective average values for the previous period.

The increases in TDS values are explained by a general increase in the salinity of water rather than by the increase of only one chemical component. However, both at SM and FC springs and also at SC and PR springs, where TDS values remain within their respective background values, sulphate concentration changes with time (Fig. 7).

In these four springs, it is possible to observe a homogeneous style of variation although the amplitude of the anomalies in the SO_4 content is quite different. All the discharges showed a decreasing before the earthquake of 26th June 1993 and subsequently an increase. This behavior is particularly marked at the SM spring where
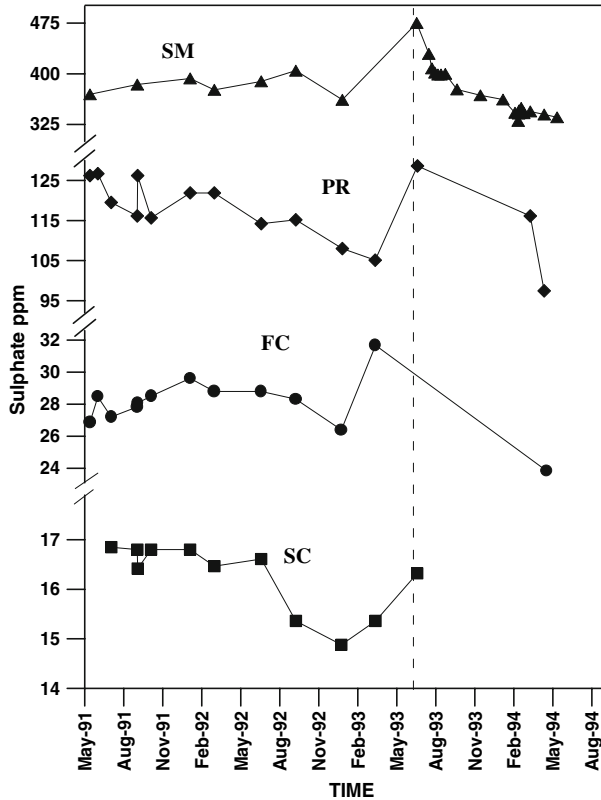
Figure 7

Changes in SO$_4$ contens at the SM (triangles), PR (diamonds), FC (circles) and SC (squares) springs. All these springs show a decrease before the main earthquake (June 26, 1993, M = 4.4, dashed line) and subsequently an increase. Although the amplitude of the anomalies is quite different, a homogeneous style of variation can be identified. This behavior is particularly enhanced at the SM spring which is fed by a small aquifer, while the SC, PR and SC springs showed lower variations due to the huge volume of their respective feeding aquifers.

the largest anomalies were recorded, while it is slightly evident at the SC spring where the changes in sulphate concentration are less than 3 ppm.

In this discharge, during a nonseismic period between June 1991 and August 1992, the average sulphate was 386 (1σ = 12 ppm). Before the earthquake of June 26th, 1993, the SO$_4$ content decreased to below the background, while a few days after it, the SO$_4$ concentration reached 475 ppm, thus increasing by 25% with respect to the mean values previously recorded.

At the FC spring, during the same nonseismic period, the average SO$_4$ content generally showed almost constant values ranging within 28.1 $\pm$ 0.8 ppm (1σ). An
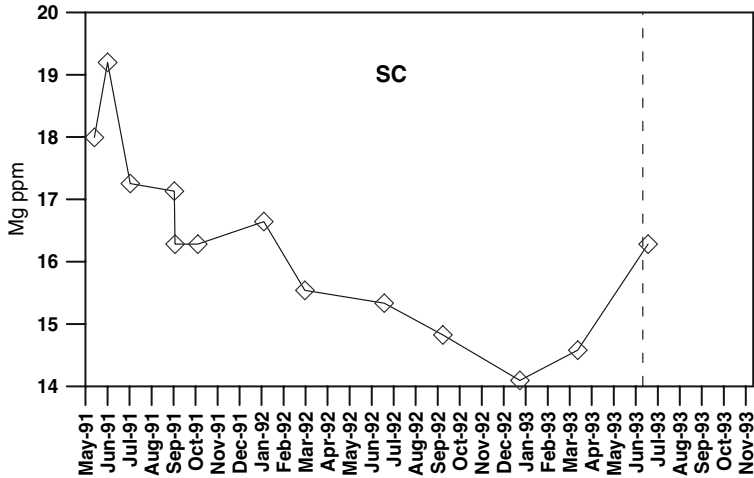
Figure 8

Plot of temporal variations of magnesium content at SC spring. Dashed line indicates the earthquake of June 26th, 1993, M = 4.4. The lowering of the magnesium content before this event may be due to relative variations of the permeability between limestones and dolostones caused by a modification of local crustal stress.

increase by about 13% with respect to the mean sulphate concentration was recorded just before the 26th June event.

Finally, the SC spring showed also a decreasing trend in the Magnesium content (Fig. 8). At the beginning of this survey (July, 1991) Mg concentration was 19.5 ppm and it reached its minimum in January 1993 with only 14 ppm showing a decreasing of about 30% with respect to the initial value.

6. Discussion

In order to identify the possible causes responsible for the observed temporal variations the hydrogeological and geochemical data have been compared both to the local rainfall data and to earthquake distribution during the Pollina seismic sequence (Figs. 9–12). Precipitation values were collected during the 1991–1994 period at the rain-gauges of Isnello, Castelbuono, Scillato and Collesano, the nearest stations to SO, SM, SC and FC and springs, respectively. Seismic data were recorded from the ING network during the period from July 1992 to November 1993 (Azzara *et al*., unpublished data). It clearly appears that the observed anomalies in flow rate at SO and SM springs are not linked to a larger meteoric recharge because they were not preceded by any anomalous rain events. Moreover, if the increase in flow rate is due to anomalous meteoric recharge events, the expected modifications in the geochemical parameters are not compatible with the geochemical variations really observed. In fact, the marked increase of a meteoric

Figure 9

Plots of temporal variations of earthquake distribution, rainfall, geochemical parameter and flow rate at SM spring. Dashed line indicates the earthquake of June 26th, 1993, M = 4.4. Earthquakes distribution from the ING network (Azzara et al., unpublished data). Rainfall are relative to the Castelbuono station.

component should have produced an evident dilution in the total amount of dissolved salts (TDS values) while a strong increase and almost constant values were observed at SM and SO spring, respectively.

On the contrary, the anomalies in the flow rate seem to occur as a consequence of releasing of the major energy (June, 1993) and for this reason, we think that the increasing in flow rate at SO and SM could be related to the local seismic activity.

An increase in the transmissivity of the aquifer, probably as a consequence of a shaking-induced dilatancy (BOWER and HEATON, 1978) could be responsible for the increase of flow rate in both these springs. Unfortunately, due to the small amount of data
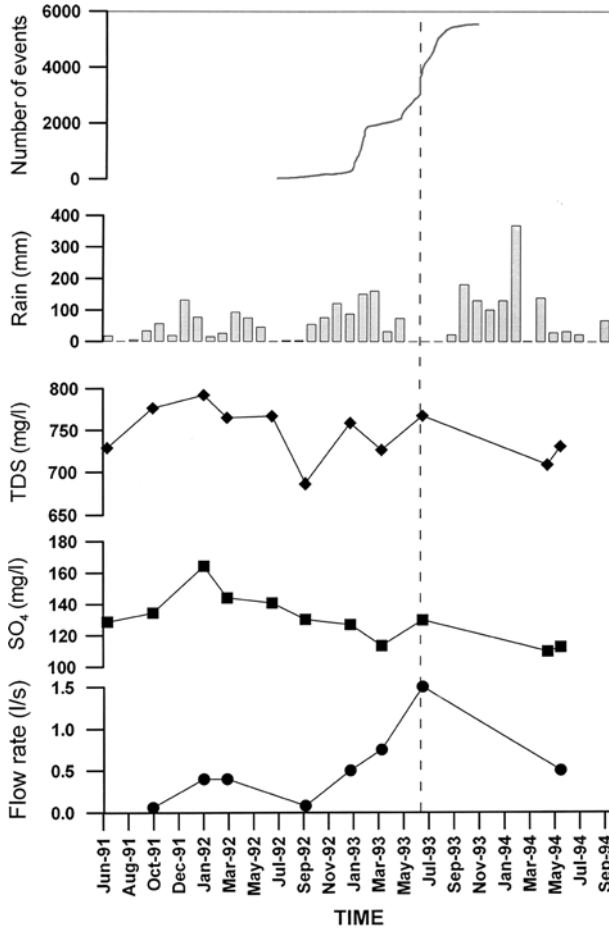
Figure 10

Plots of temporal variations of earthquake distribution, rainfall, geochemical parameter and flow rate at SO spring. Dashed line indicates the earthquake of June 26th, 1993, M = 4.4. Earthquakes distribution from the ING network (AZZARA et al., unpublished data). Rainfall are relative to the Isnello station.

available, it was not possible to constrain the temporal relationships to the observed increases and the strongest earthquake.

Because the increase in TDS results from a global increase of many dissolved chemical constituents, in our opinion, one of the possible mechanisms could be the progressive rock-fracturing provoked by the release of accumulated crustal stress. This process exposes fresh surfaces to water-rock interaction and hence enhances the dissolution of minerals. Confirmation of this is given by similar anomalies in the TDS trend that were observed at the FC spring (GRASSA et al., 2002) in coincidence with an M 4.0 earthquake that occurred on November 25, 2001. This was located by the Italian
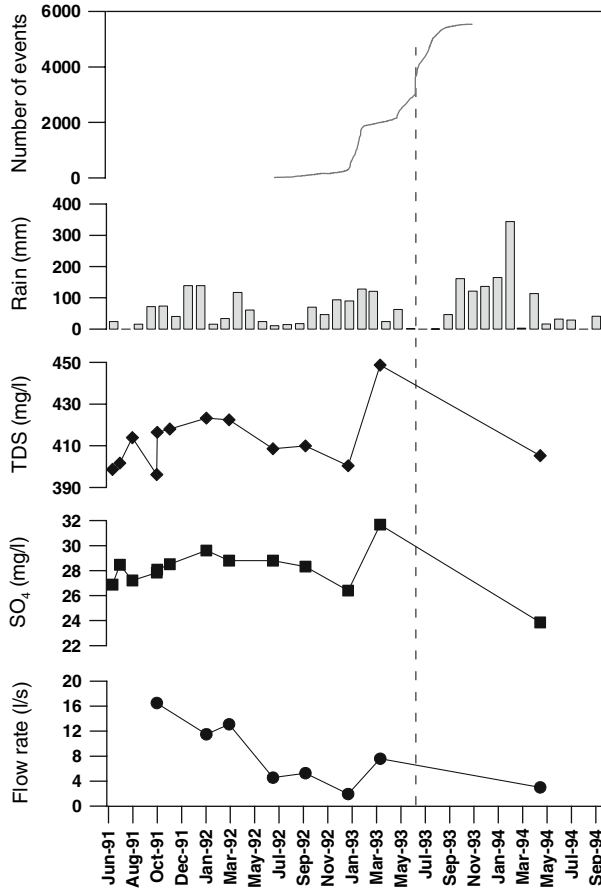
Figure 11

Plots of temporal variations of earthquake distribution, rainfall, geochemical parameter and flow rate at FCM spring. Dashed line indicates the earthquake of June 26th, 1993, M = 4.4. Earthquakes distribution from the ING network (Azzara *et al*., unpublished data). Rainfall are relative to the Collesano station.

national seismic network in the area between the small towns of Scillato and Collesano (Fig. 1), which are very near to this spring. Also at that time the TDS values progressively increased with respect to a minimum value, which however remains "*unknown*" due to the absence of pre-event samples.

A different explanation can be invoked for the temporal variation in the Mg content at the SC spring. As already argued, magnesium can be considered a geochemical tracer of groundwater flowing within the dolomitic portion of the feeding aquifer mainly belonging to the Imerese basin domain. This part of the aquifer is characterized by lower permeability values and very reduced volumes than the limestones that constitute the
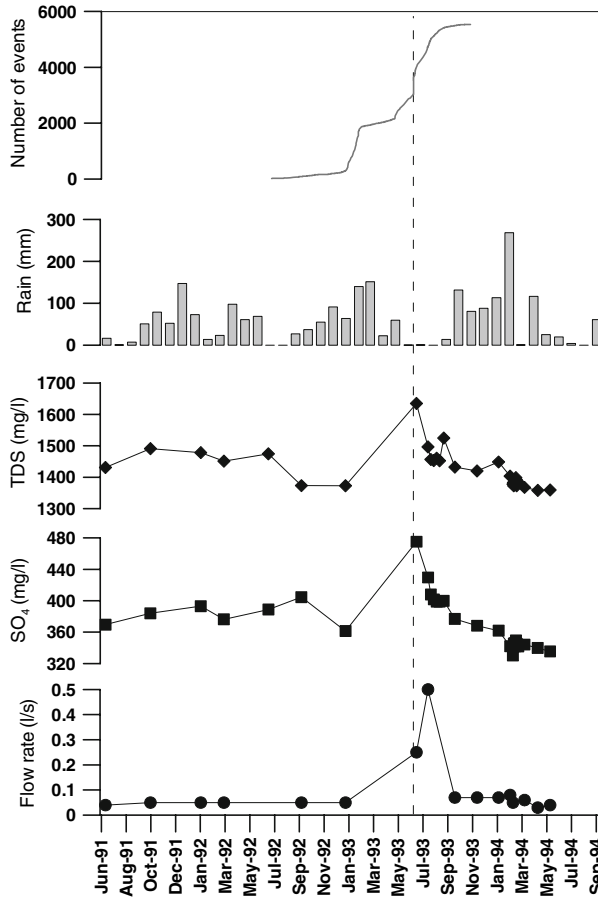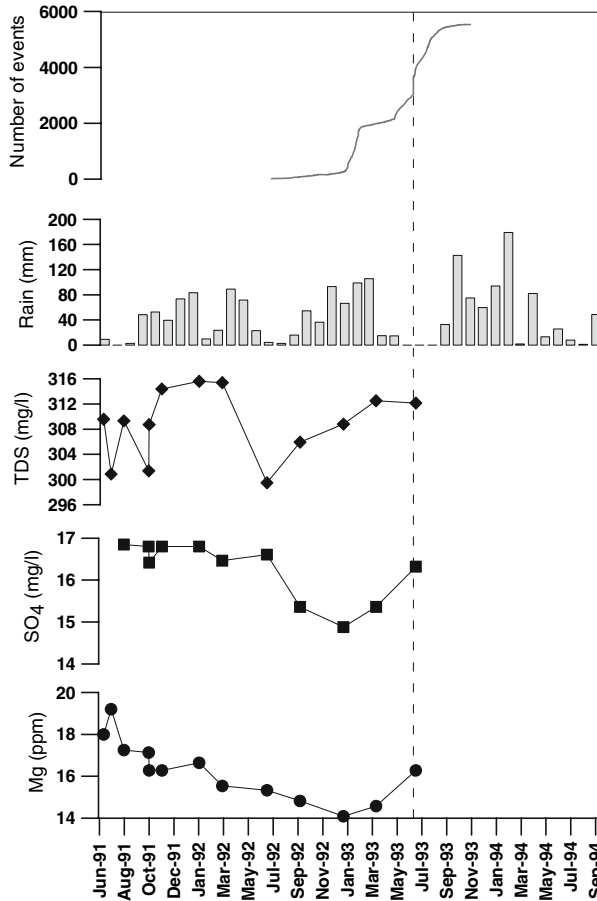
Figure 12

Plots of temporal variations of earthquake distribution, rainfall, geochemical parameter and flow rate at the SC spring. Dashed line indicates the earthquake of June 26th, 1993, M = 4.4. Earthquakes distribution from the ING network (AZZARA *et al.*, unpublished data). Rainfall are relative to the Scillato station.

prevailing lithology of the hydrogeologic structure feeding the SC spring. The lowering of the magnesium content before the strongest earthquake might be due to relative variations of the permeability between the limestones and dolostones, caused by a modification of the local crustal stress. However, the circulation of groundwater in the dolostones is to be referred to fracture-related permeability, which in the case of limestone karst phenomena assumes with a greater importance. This results in a different degree of water-bearing discontinuities: they are greater in limestones and smaller in dolostones, and this is the reason why crustal stress accumulation is reflected more in the latter than in the former. However, seismic-induced permeability variations do not represent the only possible model capable of explaining the observed anomalies.

As regards the change in sulphate concentrations at SO, SM, FC and SC springs it can be explained by a modification of the relative proportions of a simple two-component mixing process or by a mobilization of fluids from depth towards a shallower part to be referred to elastic compression actions. Both these processes can be the result of the stress-state modifications in the studied area.

During the initial perturbation phase of a steady state due to changes in the stress field, a decrease in the near-surface permeability could have happened. On the contrary, when rupture limit conditions have been reached, at the time of the 26th June event, there could be an opposite effect (increasing of permeability) probably generated by micro-fracturing of hosting rocks.

The positive transient of the SO_4 content could also be explained by the release of a greater amount of deep component, such as S-rich fluids, that are mobilized by increasing compression actions. It is also possible that both the proposed mechanisms (i.e., change in crustal permeability and elastic compression) acted at the same time, thus producing a combined effect.

As already discussed, the widest anomalies were recorded at the SM spring while very small changes were observed at PR and SC springs. A relationship between the width of the observed hydrogeological and geochemical changes and the volumes and geometry of the aquifers, as well as their relative proximity to the tectonic structures involved in the seismogenetic process, can be recognized.

The width of the geochemical anomalies is inversely proportional to the size of the aquifer. At the same way, the lesser the distance between the spring and the epicentral area, the wider geochemical variations.

SM spring is the nearest spring to the seismogenetic structure of the 26th June, 1993 event, and moreover it is fed by a very small aquifer. Its low flow rate ($Q_{mean} = 0.05$ l/s) and the moderate capacity of its aquifer, seems to make the SM spring one of the most sensitive sites to modifications in the local crustal stress. On the contrary, because of their huge volume of the feeding aquifers, PR and SC springs showed the same style of variation but narrower than those observed at SM spring.

7. *Concluding Remarks*

The present study has highlighted the main geochemical processes that affect the chemistry of the groundwater in the Polling area (i.e., Moonie Mountains). In particular, water-rock interaction involving carbonate dissolution and ion-exchange processes are the main sources of major dissolved ions (Ca, Mg, Na, HCO_3). Dissolution of S-bearing minerals (sulphides and/or sulphates) and oxidation of H_2S-rich fluids represent possible sources of SO_4^- in the studied groundwaters. Only the Presidiana spring (PR) receives a minor contribution of seawater (up to 3%).

During the 1992–1994 period, an intense crustal stress field, generated by compressive actions, seems to have been responsible for the perturbation of the

steadystate of the aquifers. This modification has probably caused changes in the water chemistry and in the flow rate in some of the studied springs. The recorded geochemical anomalies are quite similar to many hydrologic and physico-chemical changes reported in previous scientific papers worldwide in other active seismic regions.

On the basis of the observations we have proposed at least three possible physical mechanisms to explain the hydrogeochemical and geochemical changes in some local groundwater. They are briefly reported here below:

– Shaking-induced dilatancy;
– Poroelastic aquifer contraction;
– Seismogenetic-induced permanent or temporary changes in the mechanical properties of the aquifers.

In the studied area flow rate, magnesium, sulphate and TDS contents seem to be the most sensitive physico-chemical parameters to seismogenetic process. Geochemical surveillance of these parameters, by means of continuous measurements, could be used to reveal local anomalous crustal stress.

REFERENCES

ABATE, B., CATALANO, R., D'ARGENIO, B., DI STEFANO, E., DI STEFANO, P., LO CICERO, G., MONTANARI, L., PECORARO, C., and RENDA, P. (1982), *Evoluzione tra le zone di cerniera tra Piattaforme carbonatiche e bacini nel Mesozoico e nel Palogene della Sicilia Occidentale*. In *Guida alla geologia della Sicilia occidentale*, Soc. Geol. Ital., 53–81.

ALAIMO, R. and FERLA, P. (1975), *Natrojarosite e Thenardite, solfati idrotermali ricchi in Sodio, nelle argille variegate con Dickite di Scillato-Caltavuturo*, Per. Min. Rom., *2–3*, 227–243.

APPELO, C.A.J. and POSTMA, D. (1993), *Geochemistry, Groundwater and Pollution*. (Balkema, Rotterdam 1993).

BARSUKOV, V.L., VARSHAL, G.M., and ZAMOKINA, N.S. (1985), *Recent results of hydro-geochemical studies for earthquake prediction in USSR*. Pure Appl. Geophys. *122*, 143–156.

BOWER, D.R. and HEATON, K.C. (1978), *Response of an aquifer near Ottawa to tidal forcing and the Alaskan earthquake of 1964*, Can. J. Earth Sci. *15*, 331.

CAI, Z., SHI, H., ZHANG, W., LUO, G.E.X., SHI, X., and YANG, H. (1984), *Some applications of fluid-geochemical methods to earthquake prediction in China*, Proceed. Internat. Syp. Continental Seismol. Earthq. Predic., 384–395.

CARAPEZZA, M., NUCCIO, P.M., and VALENZA, M. (1980), *Geochemical precursor of earthquake*. In *High Pressure Science and Technology*, eds. Vodar and Marteau (Pergamon, Oxford 1980) pp. 90–103.

CUSIMANO, G. (1989), *Risorse idriche del settore Settentrionale della provincia di Palermo nel quadro idrogeologico della Sicilia Nord-Occidentale*. Proc of Sicilia e Terzo Mondo-Risorse Idriche e Difesa del Suolo Meeting, 25–65.

Cusimano, G., Favara, R., Francofonte, S., Madonia, P., and Valenza, M. (1992), *Lineamenti idrogeologici e idrogechimici del gruppo montuoso carbonatico delle Madonie (Sicilia)*, Proc. Alpin Caves and Alpine Karst System and their Environmental Context Workshop, 189–192.

De Gregorio, S., Gurrieri, S., La Manna, C.S., and Valenza, M. (1996), *Soil gases and seismic events occurred during 1992–95: Geochemical investigations*, Proc 3rd Internat. Conf. on Rare Gas Geochem., 200–210.

Dworkin, S.I. (1999), *Geochemical constrains on the origin of thrust fault fluids*, Geophys Res. Lett. *26*, 3665–3668.

Favara, R., Dongarrà, G., Hauser, S., and Longinelli, A. (1984), *Studio geochimico isotopico di una serie di sorgenti nell'area di Scillato (PA)*, Soc. It. Min. Petr. *39*, 421–427.

Favara, R., Grassa, F., Inguaggiato, S., and Valenza, M. (2001a), *Hydrogeochemistry and stable isotopes of thermal springs: Earthquake-related chemical changes along Belice fault (Western Sicily)*, Appl. Geochem. *16*, 1–17.

Favara, R., Italiano, F., and Martinelli, G. (2001b), *Earthquake-induced chemical changes in the thermal waters of the Umbria region during the 1997–1998 seismic swarm,* Terra Nova *13*, 227–233.

Grassa, F., Favara, R., and Madonia, P. (2002), *Chemical variations in some springs of the Madonie Mounts area (Sicily) due to local earthquakes*, Proc. XXVII General EGS Assembly, 85.

Madonia, P. (1993), *Studio idrogeochimico dell'area montuosa delle Madonie*, Ph.D. Thesis, University of Palermo, 148 pp, unpublished.

Plummer, L.N., Prestemon, E.C., and Parkhurst, D.L. (1991), *An Interactive code (NETPATH) for modeling NET geochemical reactions along a flow PATH*, USGS Water Res. Invest. Rep. *91*, 4078.

Rikitake, T. (1976), *Earthquake prediction*. (Elsevier, Amsterdam 1976).

Sornette, D. (1999), *Earthquakes: From chemical alteration to mechanical rupture*, Physics Report *313*, 237–291.

Thomas, D. (1988), *Geochemical precursor to seismic activity*, Pure Appl. Geophys. *126*, 241–266.

Valenza, M. and Nuccio, P.M. (1993), *Geochemical precursors of earthquakes. Some experiences in Italy*. In *Isotopic and Geochemical Precursors of Earthquakes and Volcanic Eruptions* (IAEA, Wien 1993) pp. 44–47.

Wakita, H. (1977), *Geochemistry as a tool for earthquake prediction*, J. Phys. Earth. *25*, 175–183.

Wakita, H. (1982), *Changes in groundwater level and chemical composition*. In *Earthquake Prediction Techniques* (University of Tokyo, Tokyo, 1982), pp. 171–216.

To access this journal online:
www.birkhauser.ch/pageoph

▐ Pure and Applied Geophysics

Precursory Subsurface ^{222}Rn and ^{220}Rn Degassing Signatures of the 2004 Seismic Crisis at Tenerife, Canary Islands

NEMESIO M. PÉREZ, PEDRO A. HERNÁNDEZ, ELEAZAR PADRÓN, GLADYS MELIÁN,
RAYCO MARRERO, GERMÁN PADILLA, JOSÉ BARRANCOS, and DÁCIL NOLASCO

Abstract—Precursory geochemical signatures of radon degassing in the subsurface of the Tenerife Island were observed several months prior to the recent 2004 seismic-volcanic crisis. These premonitory signatures were detected by means of a continuous monitoring of ^{222}Rn and ^{220}Rn activity from a bubbling CO_2-rich gas spot located at 2.850 m depth inside a horizontal gallery for groundwater exploitation at Tenerife. Multivariate Regression Analysis (MRA) on time series of the radon activity was applied to eliminate the radon activity fluctuation due to external variables such as barometric pressure, temperature and relative humidity as well as power supply. Material Failure Forecast Method (FFM) was successfully applied to forecast the anomalous seismicity registered in Tenerife Island in 2004. The changes in the ^{222}Rn/^{220}Rn ratio observed after the period of anomalous seismicity might suggest a higher gas flow rate and/or changes in the vertical permeability induced by seismic activity.

Key words: Radon, thoron, Tenerife Island, geochemical precursor.

1. Introduction

Radon, ^{222}Rn, is a naturally occurring radioactive noble gas originating from the decay of radium, ^{226}Ra, which in turn is derived from the decay of uranium, ^{238}U, in rocks and minerals (HOPKE, 1987). Its movement is limited by its short half-life, which is 3.8 days. Thoron, ^{220}Rn, a radon isotope decayed from ^{232}Th, however, has a shorter half-life of only 55.6 s, which makes this gas difficult to study in geochemical investigations (LABRECQUE, 2002). The parent isotopes of these two elements are often transported in groundwater and their concentrations depends on several factors such as oxidation/reduction potentials, water pH and chemistry (SMITH *et al.*, 1976). They can also be brought to the surface by fluid convection caused by high geothermal gradients, and their transport therefore occurs efficiently in areas of high permeability by fracturing (WILLIAMS, 1985). ^{220}Rn/^{222}Rn ratio is an important parameter to monitor since provides information about the source of the radon (GIAMMANCO *et al.*, 2007). This ratio varies as a result of the ^{226}Ra-^{222}Rn and

Enviromental Research Division, Instituto Tecnológico y de Energías Renovables (ITER), 38611 Granadilla, S/C de Tenerife, Spain. E-mail: nperez@iter.es

^{224}Ra-^{220}Rn reactions, time periods to reach equilibrium and changes in the ^{220}Rn/^{222}Rn ratio generally are related to changes in the underground structure, change in the speed of the gas carrier and variations in the distance from the source (YOSHIKAWA *et al*., 2006).

Monitoring of radon ^{222}Rn and ^{220}Rn in terrestrial fluids has become in the last decades an important tool to forecast earthquakes and volcanic eruptions (CHIRKOV, 1975; KING, 1986; FLEROV *et al*., 1986; HIROTAKA *et al*., 1988; IGARASHI and WAKITA, 1990; IGARASHI *et al*., 1995; HEILIGMANN *et al*., 1997; TOUTAIN and BAUBRON, 1999; VIRK, 1986; VIRK *et al*., 2001; RICHON *et al*., 2003; ZMAZEK *et al*., 2005; IMMÈ *et al*., 2006; NERI *et al*., 2006; GIAMMANCO *et al*., 2007). These studies support the hypothesis of radon as a precursor of seismic activity even though the mechanism relating distant seismic events and the ^{222}Rn activity variation in soil-gas or groundwater remains controversial (TOUTAIN and BAUBRON, 1999; RICHON *et al*., 2003).

Radon degassing surveys carried out at the surface environment of the earth's crust suggest that radon ascends towards the surface mainly through cracks or faults (GUERRA and LOMBARDI, 2001; BAUBRON *et al*., 2002; ETIOPE and MARTINELLI, 2002; WALIA *et al*., 2005; YANG *et al*., 2005). As suggested by ETIOPE and MARTINELLI (2002), the gas migration in the short scale (few meters) occurs via diffusion, driven by radon concentration gradients and following the Fick's law, whereas in the large scale, ten to hundreds of meters is supported by advection (pressure changes), driven by pore fluids (water, carbon dioxide, etc.) pressure gradients and following the Darcy's law. Both mechanisms are dependent on both soil porosity and permeability, which in turn vary as a function of the stress field (KING, 1978; HOLUB and BRADY, 1981). Finally, variations in temperature, rainfall, wind, barometric pressure, mechanical stresses, chemical reactions and the precipitation of secondary minerals change the physical characteristics of the host-rocks, thus modifying the rate of radon transport and, consequently, masking eventual variations induced by deeper processes.

At the end of 2002, an automatic station was installed at the entrance of the horizontal drilling "Fuente del Valle" (TFE02 station), Arona, Tenerife, Spain, to measure the activities of ^{222}Rn and ^{220}Rn in the gas discharged from the water and to test its usefulness to detecting early warnings of unusual seismic and/or volcanic activity. The last few years, several studies of ^{222}Rn and ^{220}Rn have been carried out in Tenerife Island, mainly focused on the fumaroles of Teide volcano (PÉREZ *et al*., 1996), on the soil-atmosphere of Las Cañadas caldera (HERNÁNDEZ *et al*., 2004), and the inner atmosphere of the galleries (EFF-DARWICH *et al*., 2002). PÉREZ *et al*. (1996) observed secular variations of ^{222}Rn and ^{220}Rn/^{222}Rn ratios in the fumarolic gas, just few hours before the occurrence of a seismic event (M = 1.8) close to Teidés volcanic system. HERNÁNDEZ *et al*. (2004) studied soil gas ^{222}Rn and ^{220}Rn/^{222}Rn distribution in and around Las Cañadas caldera. They detected an important fracture near Roques de García and suggested a close relationship between gas emissions and volcanic-tectonic features of Las Cañadas caldera. EFF-DARWICH *et al*. (2002) proposed a theoretical model for the radon exhalation at three subsurface monitoring sites of Tenerife and concluded that the radon exhalation was induced by atmospheric pressure changes.

Here we report the observed temporal variations of ^{222}Rn and ^{220}Rn activities at TF02 station and their relationship with the 2004 seismic-volcanic crisis which occurred in Tenerife.

2. Geological and Tectonic Settings of the Studied Area

Tenerife is the largest island of the Canarian archipelago (Fig. 1) and several volcanic eruptions have occurred in the last 500 yr., the last one in 1909. The main volcano-tectonic features of Tenerife Island are three main volcano-tectonic rifts trending N-E, N-W and N-S and, at the interception center of these three volcano-tectonic axes, the Las Cañadas caldera and stratovolcanoes Teide-Pico Viejo. The constructive episodes of Tenerife occurred during the period between 12 and 3.3 Ma when mantle-derived basaltic magmas generated a subaerial shield edifice (ANCOECHEA et al., 1990). During the last episodes of this constructive basaltic period, the emission of more differentiated magmas started the construction of Las Cañadas edifice at the center of the island (MARTÍ et al., 1994). Constructive episodes of the Las Cañadas edifice were interrupted by the formation of the Las Cañadas caldera due to a series of vertical collapses (MARTÍ and GUDMUNSSON, 2000) that originated from an elliptical depression of 16 km × 9 km. On the northern border of Las Cañadas caldera, Teide-Pico Viejo stratovolcanoes were formed over the last 0.18 Ma and have shown a series of basaltic to phonolitic lava flows and domes, also including some explosive events (ABLAY and MARTÍ, 2000). The recent activity of the N-E and N-W rifts, and the Teide-Pico Viejo stratovolcano is actually evidenced because of the existence of historic eruptions (ROMERO, 1991). Present-day visible gas emission is only observed at the summit of Teide where low temperature ($\sim 86°C$) fumarolic activity occurs. Other nonvisible gas emission includes diffuse gas emission through the Teide volcano and Las Cañadas Caldera (HERNÁNDEZ et al., 1998, 2000) and at the volcano-tectonic rift of the islands (GALINDO, 2005), where anomalies of CO_2, H_2, He and ^{222}Rn have been measured.

Due to the thousands of drilled wells and water galleries (1650 km) drilled during the last 150 years tapping the island's volcanic aquifer at different depths (Fig. 1), Tenerife is a unique natural-scale laboratory for hydrological studies in oceanic volcanic islands. Ground waters are mainly Na^+-HCO_3^- water type, mainly due to the continuous volcanic CO_2 supply from the volcanic-hydrothermal system. A significant number of these galleries show a CO_2-rich inner atmosphere, and gas bubbling has also been detected inside some galleries.

3. Tenerife 2004 Seismic Unrest

Since the beginning of seismic monitoring at the Canary Islands, moderate-to-low seismic activity has been recorded as a consequence of regional tectonic stresses
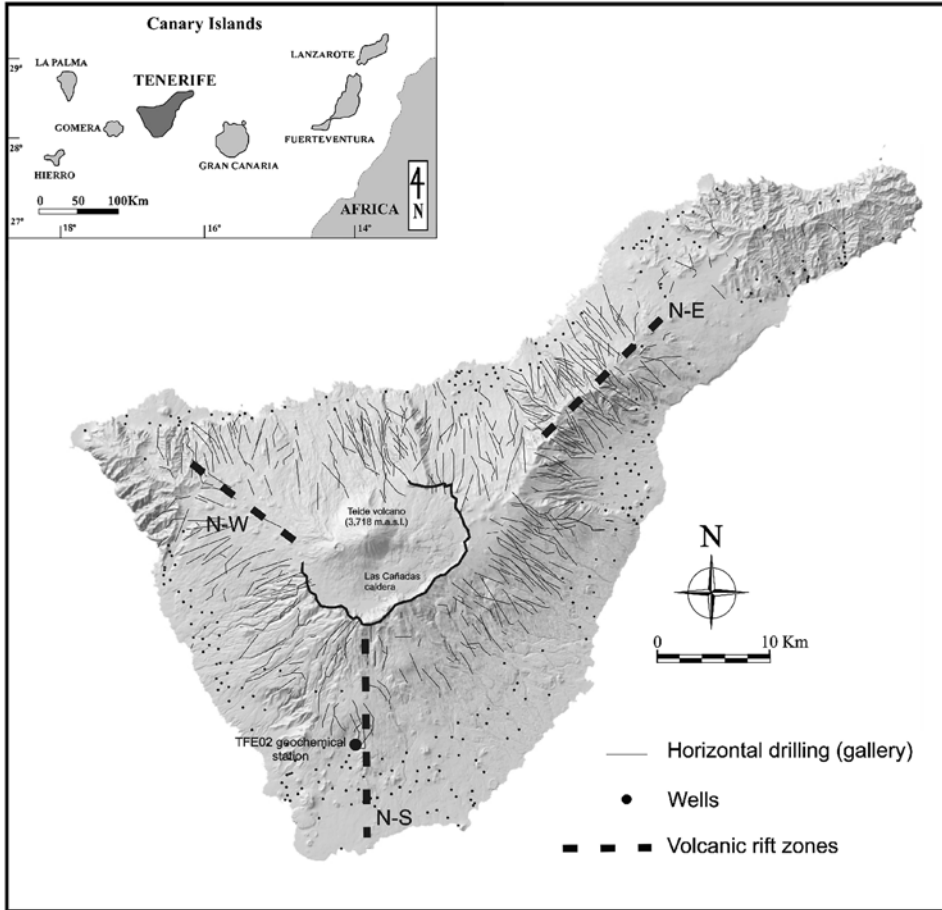
Figure 1
Geographic location of Tenerife Island, Canary Islands and horizontal drillings and wells in Tenerife Island.
Location of the geochemical station TFE02 station is also shown.

(MEZCUA *et al.*, 1992; CAÑAS *et al.*, 1998). Most of the earthquake's epicenters have been clustered in an offshore area southeast of Tenerife and very few earthquakes have occurred in other areas, including Teide volcano. However, since April 2004, a significant increase of the number of earthquakes was reported by IGN (National Geographic Institute) seismic network (LÓPEZ *et al.*, 2006), and some of them were felt by the inhabitants ($M \geq 2.5$). Figure 2 shows the evolution of the seismicity since 2000. The number of earthquakes increased significantly and their epicenters mainly clustered along the N-W rift zone of the island.

The seismic-volcanic unrest was preceded by geochemical and geophysical precursors such as an increase in seismicity at the end of 2001, a significant pulse on the total CO_2 emission from the summit of Teide volcano in the same year, as well as a
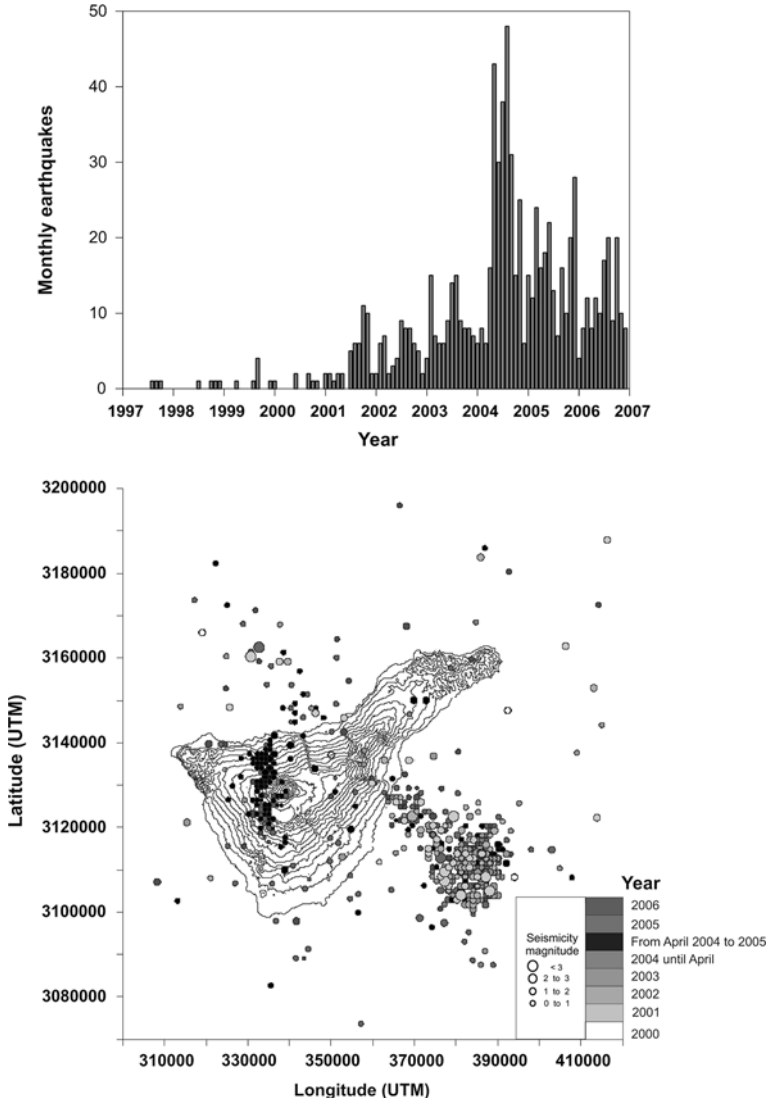
Figure 2
(a) Histogram of the number of earthquakes per month in the Tenerife area during the period 1997–2006, provided by IGN. (b) Seismic activity pattern at Tenerife Island; epicenters (dots) provided by IGN for the period 2000–2006. Colors and sizes of the dots are related to earthquake origin times and magnitudes, respectively.

clear increase in the continuous record of diffuse CO_2 efflux in a geochemical station located at the summit of Teide volcano (PÉREZ et al., 2004, 2005; HERNÁNDEZ et al., 2006a). Physical-chemical hydrological changes related to the volcanic unrest at Tenerife were also reported (MARRERO et al., 2005, submitted to JVGR).

ALMENDROS *et al.* (2006) reported that the seismic unrest was produced by a deep magma injection under the northwestern portion of Teide volcano. They proposed that stress changes associated to the magma injection permitted an enhanced transfer of magmatic gases toward the surface, lubricating the pre-existing fractures, and triggering volcano-tectonic earthquakes. Volcanic tremor and LP events were also generated when the gas flow reached the shallow aquifer under Las Cañadas caldera. In addition, GOTTSMANN *et al.* (2006) observed a gravity increase at the NW rift zone of Tenerife between May 2004 and April 2005 and suggested that the observed changes could be related to: (1) A magma injection into a conjugated fault system beneath the northwest rift zone which acts as a trigger for the reawakening of the volcanic complex, (2) a fluid migration through the central volcanic complex of Tenerife, and (3), a hybrid of both. The seismic unrest started to decline from late 2004, with a progressive decreasing on the number of earthquakes until present.

4. Sampling and Analytical Processes

At the end of 2002, a ^{222}Rn and ^{220}Rn sensor (SARAD RTM 2010) was installed at the entrance of the horizontal drilling "Fuente del Valle," Arona (N28°5′58.8″: W16°39), Tenerife, for the continuous monitoring of the gas discharge from the water (Fig. 3). This geochemical station (TFE02) is located in the S rift of Tenerife. GALINDO (2005) reported important hydrogen anomalies in this zone related to important thermal anomalies in the subsurface. The sampling site of the gas is located 2.85 km inside the horizontal well, where evident gas bubbling occurs. The gas, collected by means of an inverted funnel, is pumped (3 l min^{-1}) towards the gallery entrance, where the instrumentation is located (Fig. 3), through a polyamide pipe. Several water traps are placed to avoid water condensation at the entrance of water into the sampling device. The choice of this site
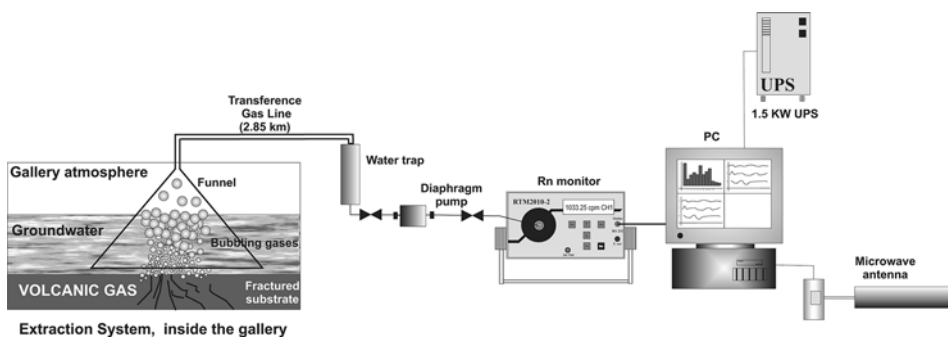
Figure 3
Scheme of the TFE02 geochemical station for the continuous monitoring of the radon activity. The data are sent to ITER via microwave link.

was driven by the peculiar chemical composition of the gas ($CO_2 \sim 85\%$, He ~ 10 ppm, ^{222}Rn ~ 100 kBq m^{-3}; HERNÁNDEZ *et al.*, 2006b) and thermal anomalies registered inside the horizontal drilling. TFE02 has an air conditioning system to maintain a constant sampling temperature, a UPS and an auxiliary engine to provide electrical power supply when failures in the electrical provision occur.

Several analytical methods have been historically used to measure radon and thoron activities: Lucas cells, alpha track films, scintillation method and ionization chamber. Currently it is possible to measure ^{222}Rn and ^{220}Rn in high frequency sampling devices based on electrostatic techniques (one measurement per hour or less) (LaBrecque, 2002; Harley *et al.*, 2005) in which an electrostatic potential gradient sweeps the products derived from the decay of the ^{220}Rn and ^{222}Rn in the chamber. The ^{220}Rn and ^{222}Rn activities are determined by high-resolution alpha spectroscopy of the deposited decay products. The ^{222}Rn activity is obtained from the recorded number of ^{218}Po alpha decays, and the ^{220}Rn activity from the recorded number of ^{216}Po alpha decays. This device has a short sampling cycle and responds rapidly to changes in the gas concentration. The accuracy of measurements depends on two factors: Gas concentration and integration time. The integration time used is 1 hour to reduce the error in the sampling method. The sampling device also has a temperature and humidity sensor since these two parameters affect the measuring process. Another parameter monitored together with the ^{220}Rn and ^{222}Rn time series is barometric pressure due to potential influence in the discharge process (PINAULT and BAUBRON, 1996). Barometric pressure data were obtained from a station belonging to INM network (Meteorological National Institute) located at "Reina Sofia" airport (5 km distant from TFE02).

5. *Results and Discussion*

Time series of ^{222}Rn and ^{220}Rn showed variations between 66–260 kBqm^{-3} and 1.2–10 kBqm^{-3}, respectively, during the entire period of study. The observed values suggest the contribution of a deeper component to this water and gas discharge. Figure 4 shows the time series of ^{222}Rn and ^{220}Rn together with relative humidity and temperature measured at TFE02. Barometric pressure values were measured every three hours.

To gain a better understanding of the behavior of ^{222}Rn and ^{220}Rn time series we applied a frequency analysis to the data recorded on an hourly basis. This analysis allowed us to investigate the presence of periodic components in the ^{222}Rn and ^{220}Rn time series. Power spectral analysis of ^{222}Rn showed and clear power law in log-log scale (Fig. 5), with a value of beta ($\beta = 1.56$), displaying a clear reddened noise behavior and mean persistence times (high values in the time series would be leed by high values in the future and vice versa). Power spectral analysis showed diurnal and semidiurnal cycles, with the existence of higher frequencies at 8-h and 6-h. These cycles can be explained in terms of changes in air temperature and barometric pressure and are observed in many
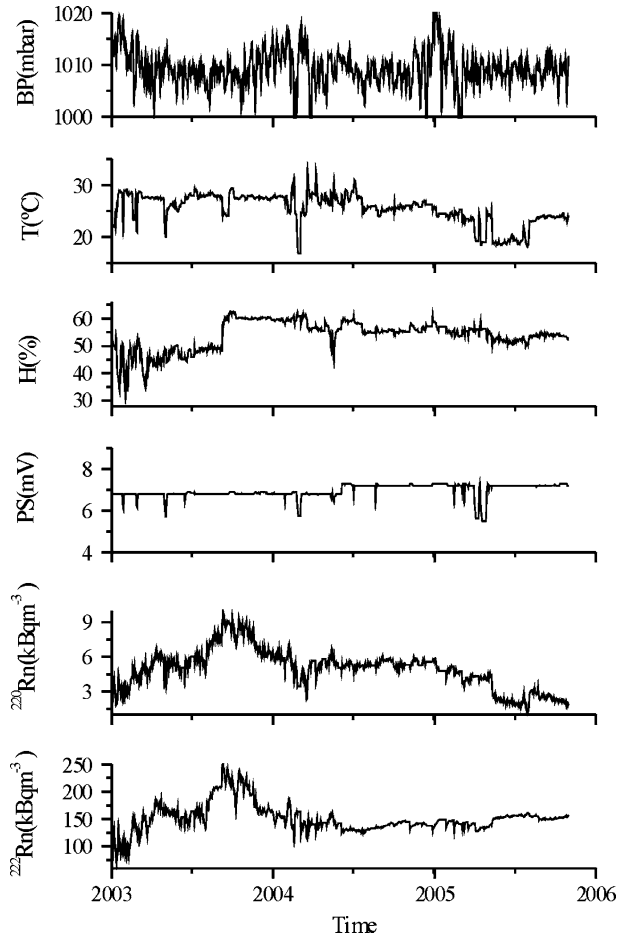
Figure 4
Temporal evolution of ^{222}Rn, ^{220}Rn, gas temperature and relative humidity, power supply of the RTM 2010–2 measured at TFE02 station, and barometric pressure at Tenerife South airport (source Meteorological National Institute, INM).

natural time series. Power spectral analysis of ^{220}Rn displayed a different behavior with a crossover near 1 day. High frequencies (higher than 1 day) presented a white noise-like mode ($\beta_1 = 0.00$) and low frequencies (lower than 1 day) a red noise-like mode ($\beta_2 = 1.00$). According to the observed values of β and β_2, we can conclude that ^{222}Rn showed a higher persistent behavior than ^{220}Rn. Due to the white noise-like mode in the high frequencies, a peak of 1 day modulation is visible, and we suggest that this behavior is due to the own nature of ^{220}Rn. To compare all available data (^{222}Rn, ^{220}Rn, barometric pressure, humidity and temperature) we calculated the daily average. The spectral coherences between barometric pressure and ^{222}Rn as well as ^{220}Rn time series were

computed. Cross-spectral analysis to ^{222}Rn revealed a shared variance between both sets of time series occurring at 4.5, 9-day cycles. In the case of ^{220}Rn only a 9 day cycle was observed.

To delineate the relations between ^{222}Rn and ^{220}Rn time series and external factors and then use these relations to filter out the effects of these factors on the measured time series, a Multiple Regression Analysis (MRA) was performed to obtain a residual free of the influence of the measured external variables. The results of the MRA indicated that only about 7% of total variance in the ^{222}Rn time series was explained using our independent variables (barometric pressure, temperature and humidity of the gas, power supply). However, MRA applied to the ^{220}Rn time series showed that 45% of the total variance was explained with our independent variables, with gas temperature the variable showing the highest contribution. Barometric pressure showed an inverse correlation with ^{222}Rn and ^{220}Rn: A decrease in barometric pressure favors the release of the gas. Other factors which have not been considered in the MRA might have a strong influence in the transport of ^{222}Rn and ^{220}Rn to the surface. Several authors have observed that ^{222}Rn and ^{220}Rn transport in volcanic and geothermal fluids is dominated by the "carrier effect" of other gases like CO_2. According to Etiope (2002), both diffusive and advective transport mechanisms must be considered since variations in the gas pressure due to strain/stress changes of the volcanic-hydrothermal system can strongly affect the transport of gases to the surface.

If the contribution of the independent variables is removed, a clear peak of ^{222}Rn and ^{220}Rn time series is observed in the middle of 2003 (Fig. 6). Since summer 2001, the IGN reported an increasing on the seismic activity pattern in and around Tenerife Island, with the main peak on April 2004, and with the occurrence of an earthquake of magnitude 3.0 felt by the inhabitants of the island. The reported increase in seismicity suggested the initial stage of the volcanic unrest. The anomalous seismicity inside Tenerife was registered one year after the increase on the ^{222}Rn and ^{220}Rn activities at TFE02. This increase in the activity of random can be explained due to a major endogenous contribution to the gas discharged at the sampling site. Alparone et al. (2005) explained that the peaks in ^{222}Rn activity before the paroxysmal summit activity at Mt Etna were due to temporary increases in gas pressure within the shallow plumbing system of the volcano, leading to increased gas leakage through fracture systems intersecting the conduit. However, Neri et al. (2006) observed an increase by several orders of magnitude in radon activity shortly before the phase of eruptive activity of Mount Etna volcano in July 2006 due to micro-fracturing of uranium-bearing rocks, induced by the geodynamic stress of the volcanic-hydrothermal system. This last mechanism seems a plausible explanation of the observed increase in the ^{222}Rn and ^{220}Rn activities at TFE02, since dramatic changes in the nature of the field area were not observed.

Figure 6 shows the time evolution of the ^{222}Rn/^{220}Rn ratio, and ^{222}Rn and ^{220}Rn activities. In the time series of ^{222}Rn /^{220}Rn ratio, three different trends can be distinguished according to the labels A, B and C. Giammanco et al. (2007), categorize three different sources of radon for Mt. Etna, Italy: (1) Deep magmatic degassing,
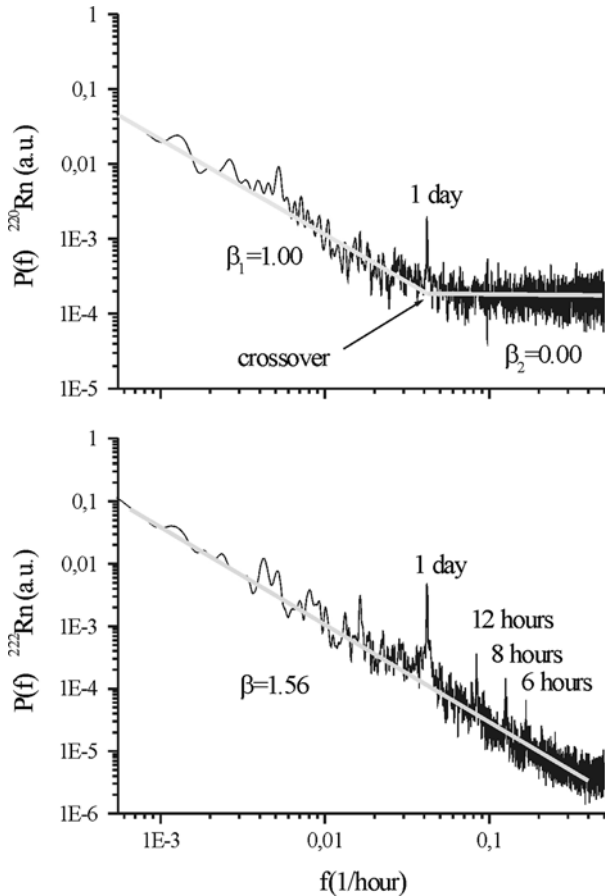
Figure 5
Spectral analysis: Power spectral density (PSD) of ^{222}Rn and ^{220}Rn.

meaning that radon in the gas is coming mainly from the magma, (2) shallow soil degassing, in which radon is originates from shallow surficial volcanic rocks and minerals carried upward along fractures and faults and (3) a mixing of deep magmatic gases with gases equilibrated in shallower porous soils. During the trend A, ^{222}Rn/^{220}Rn ratio remains constant and low, suggesting a shallow degassing source of thoron. During this period of observation, seismic activity was already anomalous (increase in seismicity around Tenerife started at the end of 2001, see Fig. 2), probably inducing geodynamic stress to the volcanic-hydrothermal system and producing micro-fracturing of uranium-bearing rocks at shallower levels, as has been observed in other volcanic and seismically active areas (YANG *et al.*, 2005; GIAMMANCO *et al.*, 2007). However, from February 2004, an increase in the ^{222}Rn /^{220}Rn ratio is observed, coinciding with a sharp increase in the seismic activity. Strain/stress changes in the subsurface related to a magma intrusion
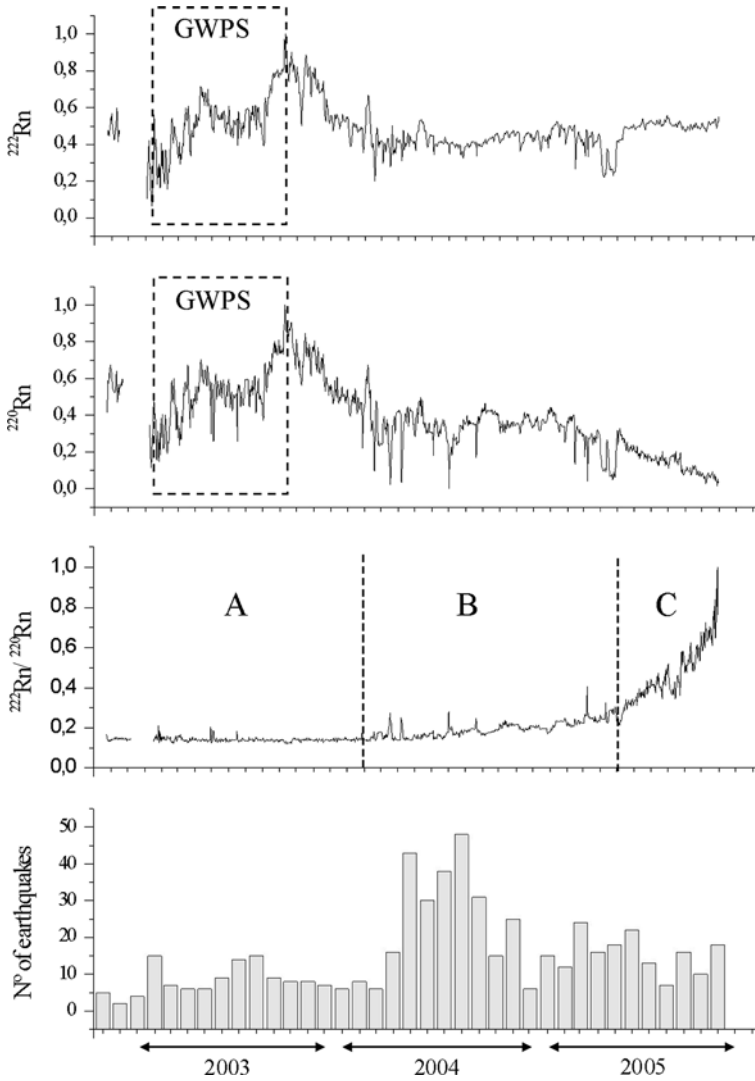
Figure 6

Residuals of the ^{222}Rn, ^{220}Rn and ^{222}Rn/^{220}Rn ratio time series after MRA. Independent variables were barometric pressure, power supply and sampling temperature and humidity. Histogram of the number of earthquakes per month which occurred in and around Tenerife (source IGN) is also shown. Dashed lines divided the tree periods when different behavior of ^{222}Rn was observed.

14-km deep between the NW ridge and the NW side of the T-PV volcanic complex in April 2004 (ALMENDROS *et al*., 2007), seem to be responsible for this sharp increase in the seismicity, disturbing the deep volcanic hydrothermal system and generating an increase on the magmatic gas emissions, mainly CO_2 and sulphur gases (MARRERO *et al*., 2007). Evidences of this hypothesis are the increase of the pCO_2 in the western end of Las

Cañadas aquifer during the period 2001–2004 and, at the same time, an increase in the SO_4/Cl ratio in the groundwater of the "Hoya de la leña" in April of 2004, another gallery for groundwater exploitation. MARRERO *et al.* (2007) report that the levels of pCO_2 in the groundwater during the period 2004–2006 were still over the prior levels in 2001, probably as a result of the increase of vertical permeability. Assuming an increasing flux of magmatic CO_2 into the system during and after the magmatic intrusion and the behavior of CO_2 and radon gases during their transport to the surface (carrier effect), a increase in the $^{222}Rn/^{220}Rn$ ratio is expected, since the magmatic gas is entirely dominated by ^{222}Rn and the $^{222}Rn/^{220}Rn$ ratio will tend to infinite (GIAMMANCO *et al.*, 2007).

The linear correlation between ^{222}Rn and ^{220}Rn has also been verified. Figure 7 shows three different behaviors in the linear correlation between these two gases. From January 2003 to February 2004 (period A in Fig. 7), a positive correlation is found ($R^2 = 0.90$), which suggests that both gases are brought to the surface by other carrier gas from a shallower source. However, from February 2004 to May 2005, (period B in Fig. 6), no correlation appears between these two gases, During this period, an important deep perturbation (magmatic intrusion) originated the anomalous seismic activity, principally located between May 2004 and October 2004. Finally, the last period (period C in Fig. 6) presented a good inverse linear correlation ($R^2 = 0.71$), indicating in this case that both gases are brought to the surface by other carrier gas from a deeper source (YANG *et al.*, 2005).

5.1. Materials Failure Forecast Method

With the aim of investigate the relationship of the observed temporal variations in ^{222}Rn and ^{222}Rn activities and the seismicity occurred in Tenerife during the 2004 seismic-volcanic crisis, spike-like anomalous peaks of ^{222}Rn were tested following the Material Failure Forecast Method (FFM). The FFM was proposed by VOIGHT (1988), after his experience with the eruption of St. Helens volcano. He proposed a law governing accelerating creep to characterize precursory phenomena. VOIGHT (1988) demonstrated that this technique, which generally describes terminal failure of metals, rocks, soils…, is applicable in different volcanic scenarios. During the last years FMM was applied in different volcanoes: Redoubt volcano (CORNELIUS and VOIGHT, 1994) and Pinatubo volcano (CORNELIUS and VOIGHT, 1995); YAMAOKA (1993) was able to forecast the Izu-Oshima (Japan) 1987 eruption, and ORTÍZ *et al.* (2003) forecasted explosions related to the opening of the principal conduit in Villarica volcano in September and December 2000. This method has also been used with different type of volcanological data such as RSAM, SSAM, tilt, etc. We argued that this methodology can be also applied to forecast natural phenomena such as earthquakes and volcanic eruptions by using ^{222}Rn and ^{220}Rn data due to the well known close relationship between observed changes in gas emission and physical processes such as changes in stress/strain prior to the occurrence of a eruption or a earthquake.
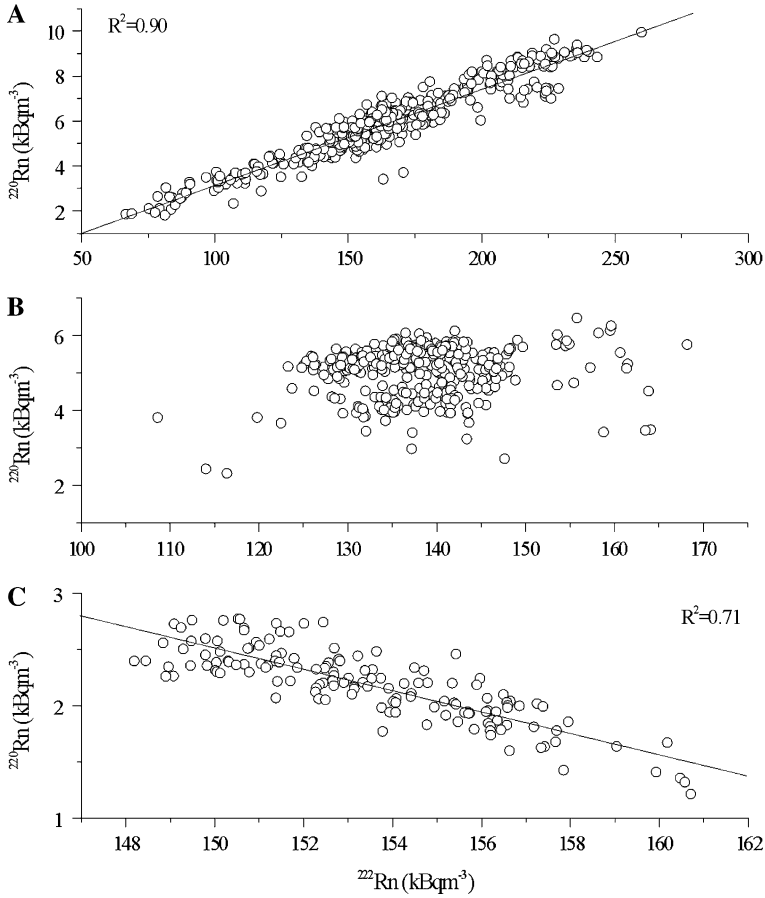
Figure 7
Correlations between ^{222}Rn and ^{220}Rn in the different segments (A, B, C) shown in Figure 6.

Empirical model of material failure is described using the following equation:

$$\ddot{\Omega} = A\dot{\Omega}^{\alpha}, \tag{1}$$

where Ω is any measured parameter, $\dot{\Omega}$ and $\ddot{\Omega}$ are the rate and acceleration of the studied system, and A and α are two parameters. When a time series of a volcanic parameter can be expressed as a solution of a previous differential equation, FFM can be applied. The graphical technique proposed by VOIGHT (1988) is based on a plot of the inverse rate versus time. Inverse rate plots are particularly sensitive to small precursory changes at an early stage of development and the time of singularity, i.e., the occurrence of an infinite rate is found by extending the inverse rate data toward the time axis (CORNELIUS and VOIGHT, 1995). This procedure is straightforward if α is close to 2, doing the inverse rate close to linearity, and we can use linearized least-squares technique to extrapolate and found the

time of singularity ($\dot{\Omega} \to \infty$). An attempt to use ^{222}Rn and ^{220}Rn time series to forecast the seismic activity in and around Tenerife Island by means of the FFM method was done. We selected a Geochemical Window Precursory Signal (GWPS) of data between February and September 2003, when the anomalous increase occurred. First, the α parameter on equation (1) was calculated using a log-log transformation of the equation. A value of α ≈ 2 was obtained, which justify the use of a linear extrapolation. Figure 8 shows the inverse of ^{222}Rn, ^{220}Rn rate and the number of earthquakes per month which have occurred in and around Tenerife since 2003. The interception of the linear fit of the data with the time axis indicates the theoretical moment when earthquakes are most lekely to occur. Thus, this interception in the middle of 2004 shows an excellent correlation with the height of the seismic activity registered on Tenerife Island during 2004.

6. Conclusions

A time series of ^{222}Rn and ^{220}Rn was registered at the TFE02 geochemical station, Tenerife, showing a precursory anomalous increase several months before the seismic unrest registered on the island in 2004. Power spectral analysis of ^{222}Rn ($\beta = 1.56$) and ^{220}Rn ($\beta_2 = 1.00$) showed a clear power law in log-log scale and persistent behavior, and ^{220}Rn presented a crossover around 1 day cycles. An important peak in the ^{222}Rn and ^{220}Rn time series appeared between February and September 2003, about one year before anomalous seismic activity was registered in and around Tenerife. After eliminating the contribution of external variables (barometric pressure, temperature and humidity gas sampling, power supply) the observed increases in the ^{222}Rn and ^{220}Rn time series existed in the denoising signal.

From beginning 2003 to April 2004, ^{222}Rn/^{220}Rn ratios remained constant and low, suggesting a shallow degassing source of thoron, probably induced by geodynamic stress of the volcanic-hydrothermal system and producing micro-fracturing of uranium-bearing rocks at shallower levels. Both gases showed a positive correlation, supporting the hypothesis that both gases are brought to the surface by some other carrier gas from a shallower source. From February 2004 to May 2005, an increase in the ^{222}Rn $/^{220}$Rn ratio is observed, coinciding with a sharp increase in the seismic activity due to the magmatic intrusion occurred between the NW ridge and the NW side of the T-PV volcanic complex in April 2004. Strain/stress changes in the subsurface related this magma intrusion which seem to be the responsible of this observed increase in the ^{222}Rn $/^{220}$Rn ratios. During this period, no correlation between these two gases is observed, Finally, after May 2005, and assuming an increasing flux of magmatic CO_2 into the system, a sharp increase in the ^{222}Rn/^{220}Rn ratio and a good inverse linear correlation between both gases are observed, indicating that the magmatic gas is entirely dominated by ^{222}Rn and that both gases are brought to the surface by other carrier gas (CO_2) from a deeper source. Thus, if the geochemical monitoring site is
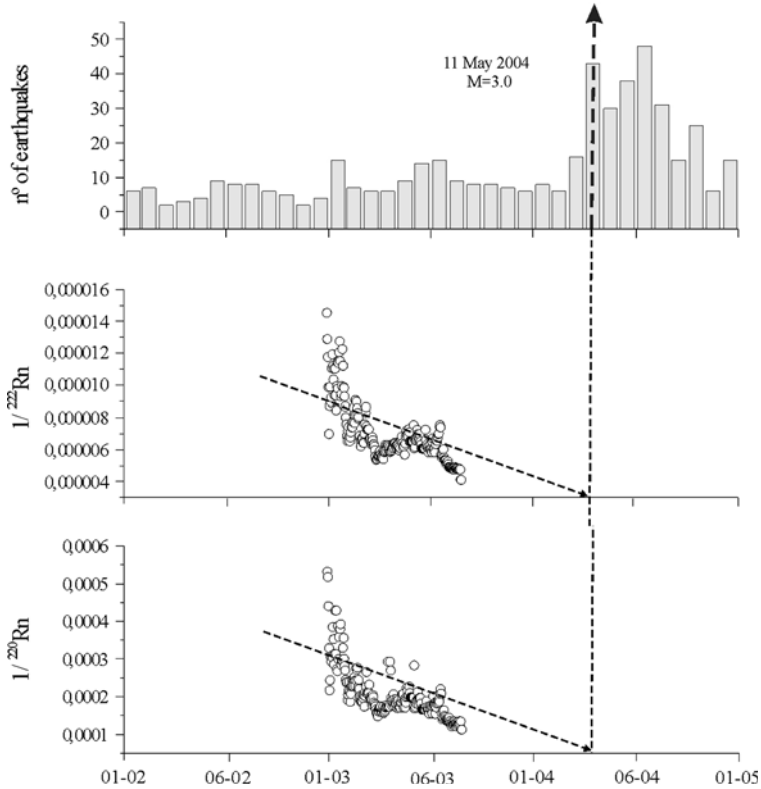
Figure 8

Number of earthquakes registered in and around Tenerife by the seismic network of the Geographic National Institute (IGN) per month and FMM applied to ^{222}Rn, ^{220}Rn in the Geochemical Window Precursory Signal (GWPS) between February and September 2003. The interception of the linear fit with the time axis indicates a successful forecast to the April 2004 seismic unrest.

sensitive to changes in the permeability related to changes of strain/stress, precursory geochemical signals of seismic activity are expected to occur.

Using Material Failure Forecast Method (FFM) in a selected Geochemical Window Precursory Signal (GWPS), the 2004 seismic unrest in the middle 2004 was successfully forecasted. Therefore, TFE02 have demonstrated to be a sensitive site to detect changes in stress/strain processes in Tenerife Island.

Acknowledgements

REFERENCES

ABLAY, G.J. and MARTÍ, J. (2000), *Stratigraphy, structure, and volcanic evolution of the Pico Teide-Pico Viejo formation, Tenerife, Canary Islands*, J. Volcan. Geotherm. Res. *103*, 175–208.

ALPARONE, S., BEHNCKE, B., GIAMMANCO, S., NERI, M., and PRIVITERA, E. (2005), *Paroxysmal summit activity at Mt. Etna monitored through continuous soil radon measurements*, Geophys. Res. Lett. *32*, L16307, doi: 10.1029/2005GL023352.

ANCOECHEA, E., FÚSTER, J.M., IBARROLA, E., CENDRERO, A., COELLO, J., HERNÁN, F., CANTAGREL, J.M., and JAMOND, C. (1990), *Volcanic evolution of the island of Tenerife (Canary Islands) in the light of new K-Ar data*, J. Volcanol. Geotherm. Res. *44*, 231–249.

ALMENDROS, J., IBÁÑEZ, J.M., CARMONA, E., and ZANDOMENEGHI, D. (2006), *Array analyses of volcanic earthquakes and tremor recorded at Las Cañadas caldera (Tenerife Island, Spain) during the 2004 seismic activation of Teide volcano*, J. Volcanol. Geotherm. Res. *160*, 285–299.

BAUBRON, J.C., RIGO, A., and TOUTAIN, J.P. (2002), *Soil gas profiles as a tool to characterise active tectonic areas: the Jaut Pass example (Pirenees, France)*, Earth Planet. Sci. Lett. *196*, 69–81.

CANAS, J.A., UGALDE, A., PUJADES, L.G., CARRACEDO, J.C., SOLER, V., and BLANCO, M.J. (1998), *Intrinsic and scattering seismic wave attenuation in the Canary Islands*, J. Geophys. Res. *103* (B7), 15,037–15,050.

CHIRKOV, A.M. (1975), *Radon as a possible criterion for predicting eruptions as observed at Karymsky volcano*, Bull. Volcanol. *39*, 126–131.

CORNELIUS, R.R. and VOIGHT, B. (1994), *Seismological aspects of the 1989–1900 eruption at Rebout volcano, Alaska: The Materials Failure Forecast Method with RSAM and SSAM seismic data*, J. Volcanol. Geotherm. Res. *62*, 469–498.

CORNELIUS, R.R. and VOIGHT, B. (1995), *RSAM and SSAM seismic analyses with the Materils Failure Forecast Method (FMM), June 1991 explosive eruption at Pinatubo volcano, Philippines*, U.S. Geological Survey Prof. Paper.

EFF-DARWICH, A., MARTÍN-LUIS, C., QUESADA, M., DE LA NUEZ, J., and COELLO, J. (2002), *Variations on the concentration of ^{222}Rn in the subsurface of the volcanic island of Tenerife, Canary Islands*, Geophys. Res. Lett. *29*(22): doi: 10.1029/2002GL015387. issue: 0094–8276.

ETIOPE, G. and MARTINELLI, G. (2002), *Migration of carrier and trace gases in the geosphere: an overview*, Phys. Earth Planet. Int. *129*, 185–204.

FLEROV, G.N., CHIRKOV, A.M., TRETYAKOVA, S.P., DZHOLOS, L.V., and MERKINA, K.I. (1986), *The use of radon as an indicator of volcanic processes*. Earth Phys. *22*, 213–216.

GALINDO, I. (2005), *Estructura Volcano-Tectónica y Emisión Difusa de gases de Tenerife (Islas Canarias).*, Ph.D. Thesis, University of Barcelona.

GIAMMANCO, S., SIMS, K.W.W., and NERI, M. (2007), *Measurements of ^{220}Rn and ^{222}Rn and CO_2 emissions in soil and fumarole gases on Mt. Etna volcano (Italy): Implications for gas transport and shallow ground fracture*, Geochem. Geophys. Geosyst. *8*, Q10001, doi:10.1029/2007GC001644.

GOTTSMANN, J., WOOLLER, L., MARTÍ, J., FERNÁNDEZ, J., CAMACHO, A.G., GONZÁLEZ, P.J., GARCÍA, A., and RYMER, H. (2006), *New evidence for the reawakening of Teide volcano*, Geophys. Res. Let. *33*, L20311, doi: 10.1029/2006GL027523.

GUERRA, M. and LOMBARDI, S. (2001), *Soil-gas meted for tracing neotectonic faults in clay basins: the Pisticci field (Southern Italy)*, Tectonophysics *339*, 511–522.

HARLEY, N.H., CHITTAPORN, P., MEDORA, R., MERRILL, R., and WANITSOOKSUMBUT, W. (2005), *Thoron versus radon: measurement and dosimetry*, International Congress Series *1276*, 72–75.

HEILIGMANN, M., STIX, J., WILLIAMS-JONES, G., SHERWOOD-LOLLAR, B., and GARZÓN, G. (1997), *Distal degassing of radon and carbon dioxide on Galeras volcano, Colombia*, J. Volcanol. Geotherm. Res. *77*, 267–283.

HERNÁNDEZ, P.A., PÉREZ, N.M., SALAZAR, J.M.L., NAKAI, S., NOTSU, K., and WAKITA, H. (1998), *Diffuse emission of carbon dioxide, methane, and helium-3 from Teide volcano, Tenerife, Canary Islands*, Geophys. Res. Lett. *25*, 17, 3311–3314.

HERNÁNDEZ, P.A., PÉREZ, N., SALAZAR, J.M.L., SATO, M., NOTSU, K., and WAKITA, H. (2000), *Soil gas CO_2, CH_4, and H_2 distribution in and around Las Cañadas caldera, Tenerife, Canary Islands, Spain*, J. Volcanol. Geotherm. Res. *103*, 425–438.

HERNÁNDEZ, P.A., PÉREZ, N.M., SALAZAR, J., REIMER, G.M., KENJI NOTSU, and WAKITA, H. (2004), *Radon and helium in soil gases at Cañadas Caldera, Tenerife, Canary Island, Spain*, J. Volcanol. Geotherm. Res. *2721*, 1–18.

HERNÁNDEZ, P.A., PÉREZ, N.M., PADRÓN, E., MELIÁN, G., and PEREDA, E. (2006a), *Diffuse CO_2 emission changes at the summit cone of Teide volcano and relation to seismic activity in and around Tenerife, Canary Islands*, Garavolcan International Meeting. Session 6: Tenerife's experience: scientific results and the recent seismicvolcanic crisis, Garachico, Tenerife, Spain.

HERNÁNDEZ, P.A., PÉREZ, N., PADRÓN, E., and MELIÁN, G., (2006b), *Continuous monitoring of dissolved gases by means of QMS and radon sensors for Tenerife's volcanic surveillance*, Garavolcan International Meeting. Session 6: Tenerife's experience: Scientific results and the recent seismicvolcanic crisis, Garachico, Tenerife, Spain.

HIROTAKA, U.I., MORIUCHI, H., TAKEMURA, Y., TSUCHIDA, H., FUJII, I., and NAKAMURA, M., (1988), *Anomalously high radon discharge from Atotsugawa Fault prior to the western Nagano Prefecture earthquake (M 6.8) of September 14, 1984*, Tectonophysics *152*, 147–152.

HOLUB, R.F., and BRADY, B.T., (1981), *The effect of stress on radon emanation from rock*, J. Geophys. Res. *86*(B3), 1776–1784.

HOPKE, P.K. (1987), *Radon and its decay products: An overview*. In (HOPKE, P.K., eds.), *Radon and its Decay Products: Occurrence, Properties, and Health e!ects*, Am. Chem. Soc., Washington, DC, pp. 1–10.

IGARASHI, G. and WAKITA, H. (1990), *Groundwater radon anomalies associated with earthquake*, Tectnophysics *180*, 237–254.

IGARASHI, G., SAEKI, S., TAKAHATA, N., SUMIKAWA, K., TASAKA, S., SASAKI, Y., TAKAHASHI, M. and SANO, Y. (1995), *Groundwater radon anomaly before the Kobe earthquake in Japan*, Science, *269*, 60–61.

IMMÈ, G., LA DELFA, S., LO NIGRO, S., MORELLI, D., and PATANÈ, G. (2006), *Soil radon concentrations and volcanic activity of Mt. Etna before and after the 2002 eruption*, Rad. Meas. *41*, 241–245.

KING, C.Y. (1978), *Radon emanation on San Andreas fault*, Nature *271*, 516–519.

KING, C.Y. (1986), *Gas geochemistry applied to earthquake prediction: An overview*, J. Geophys. Res. *91*, 12269–12281.

LABRECQUE, J.J. (2002), *Simple and rapid methods for on-site determination of radon and thoron in soil-gases for seismic studies*, J. Radioanalytical. Nuclear Chem. *254*, 3,439–444.

LÓPEZ, C., BLANCO, M. J., and CARREÑO E. (2006), *Analysis of IGN seismic series in Tenerife that triggered the 2004 seismovolcanic alert*, Garavolcan International Meeting. Session 6: Tenerife's experience:sicientif results and the recient seismovolcanic crisis, Garachico, Tenerife, Spain.

MARRERO, R., SALAZAR, P., LOPEZ, D., HERNÁNDEZ, P.A., and PÉREZ, N.M. (2005), *Hydrogeochemical monitoring for volcanic surveillance at Tenerife, Canary Islands*, Geophys. Res. Abstr. *7*, 09928.

MARRERO, R., MELIÁN, G., PADRÓN, E., BARRANCOS, J., CALVO, D.1, NOLASCO, D., PADILLA, G., LÓPEZ, D.L., HERNÁNDEZ, P.A., and PÉREZ, N. *Physical-chemical hydrological changes related to the recent volcanic unrest at Tenerife, Canary Islands, M.*, J. Volcanol. Geothem. Res., submitted to JVGR.

MARTÍ, J., MITJAVILA, J., and ARAÑA, V. (1994), *Stratigraphy, structure and geochronology of the Las Cañadas caldera (Tenerife, Canary Islands)*, Geol. Mag. *131*, 715–727.

MARTÍ, J. and GUDMUNDSSON, A. (2000), *The Las Cañadas caldera (Tenerife, Canary Island): An overlapping collapse caldera generated by magma-chamber migration*, J. Volcanol. Geothem. Res. *103*,161–173.

MEZCUA, J., BUFORN, E., UDIAS, A., and RUEDA, J. (1992), *Seismotectonics of the Canary Islands*, Tectonophysics *208*, 447–452.

NERI, M., BEHNCKE, B., BURTON, M., GALLI, G., GIAMMANCO, S., PECORA, E., PRIVITERA, E. and REITANO, D. (2006), *Continuous soil radon monitoring during the July 2006 Etna eruption*, Geophys. Res. Lett. *33*, L24316, doi: 10.1029/2006GL028394.

ORTÍZ, R., MORENO, H., GARCÍA, A., FUENTEALBA, G., ASTIZ, M., PEÑA, P., SÁNCHEZ, N., and TÁRRAGA, M. (2003), *Villarrica volcano (Chile): characteristics of the volcanic tremor and forecasting of small explosions by means of a material failure method*, J. Volcanol. Geotherm. Res. *128*, 247–259.

PÉREZ, N.M., STURCHIO, N.C, AREHART, G., HERNÁNDEZ, P.A., and WAKITA, H. (1996), *Short-term secular variations of carbon and radon isotopes and relation to seismic activity in the Canary Islands, Spain*, Bull. Lab. Erathquake Chem. *31–33*.

PÉREZ, N.M., HERNÁNDEZ, P.A., LIMA, N., MELIÁN, G., GALINDO, I., PADRÓN, E., MARRERO, R., SALAZAR, P., GÓMEZ, L., GONZÁLEZ, P., COELLO, C., and PÉREZ, V., (2004). *Reducing volcanic risk in the Canary Islands: Are we doing the homework?* Abstracts of the Internat. Symp. *Reducing Volcanic Risk in Islands*, June *2–6*, Tenerife, Canary Islands, Spain.

PÉREZ et al. (2005). *Premonitory geochemical and geophysical signatures of volcanic unrest at Tenerife, Canary Islands*, Geophys. Res. Abstracts, Vol. *7*, 09993.

PINAULT, J. and BAUBRON, J. (1996), *Signal processing of soil gas radon, atmospheric pressure, moisture and soil temperature data: A new approach for radon concentration modelling*, J. Geophys. Res. *101*, 3157–3171.

RICHON, P.1 SABROUX, J.-C., HALBWACHS, M., VANDEMEULEBROUCK, J., POUSSIELGUE, N., TABBAGH, J., and PUNONGBAYAN, R. (2003), *Radon anomaly in the soil of Taal volcano, the Philippines: A likely precursor of the M 7.1 Mindoro earthquake (1994)*, Geophys. Res. Lett. *30*(9), 1481, doi:10.1029/2003GL016902.

ROMERO, C. (1991), *Las manifestaciones volcánicas históricas del archipiélago canario (2 vols)*, Gobierno de Canarias, Sta. Cruz de Tenerife, Spain.

SMITH, A.Y., BARRETO, P.M.C., and POURNIS, S. (1976), *Radon methods in uranium exploration*, In *Proc. Symp. Exploration for Uranium Ore Deposits*, IAEA, Vienna, pp. 185–211.

TOUTAIN, J.-P., and BAUBRON, J.-C. (1999), *Gas geochemistry and seismotectonics: A review*, Tectonophysics *304*, 1–27.

VIRK, H.S. (1986), *Radon monitoring and earthquake prediction. In Proc. International Syposium Earthquake Prediction-Present Status*, University of Poona, Pune, India 157–162.

VIRK, H.S., WALIA, V., and KURMAR, N. (2001), *Helium/radon precursory anomalies of Chamoli earthquake, Garhwal Himalaya, India*, J. Geodynamics 31, 201–210.

VOIGHT, B. (1988), *A method for prediction of volcanic eruptions*, Nature *332*, 125–130.

WALIA, V., SU, T.C., FU, C.C., and YANG, T.F. (2005), *Spatial variations of radon and helium concentration in soil-gas across the Shan-Chiao fault, Nothern Taiwan*, Rad. Measurem. *40*, 513–516.

WILLIAMS, S.N., (1985), *Soil radon and elemental mercury distribution and relation to magmatic resurgence at Long Valley Caldera*, Science *229*, 551–553.

YAMAOKA, K. (1993), *State of stress and magma movement inferred from seismic activity during 1986–1987 eruption of Izu-Oshima volcano*, Workshop on Volcanic Disaster Prevention, 8–12 March 1992, Menlo Park, CA, 16–22.

YANG, T.F., WALIA, V., CHYI, L.L., FU, C.C., CHEN, C.-H., LIU, T.K., SONG, S.R., LEE, C.Y., and LEE, M. (2005), *Variations of soil radon and thoron concentrations in a fault zone and prospective earthquakes in SW Taiwan*, Rad. Measurements *40*, 496–502.

YOSHIKAWA, H., NAKANISHI, T., and NAKAHARA, H. (2006), *Determination of thoron and radon ratio by liquid scintillation spectrometry*, J. Radioanal. Nuclear Chem. *267*, 195–203, doi: 10.1007/s10967-006-0027-7.

ZMAZEK, B., ZIVCIC, M., TODOROVSKI, L., DZEROSKI, S., VAUPOTIC, J., and KOBAL, I. (2005), *Radon I soil gas: How to identify anomalies caused by earthquakes*, Appl. Radiat. Isot. *20*, 1106–1109.

To access this journal online:
www.birkhauser.ch/pageoph

Soil H_2 and CO_2 Surveys at Several Active Faults in Japan

TURHAN DOGAN,[1,2] TOSHIYA MORI,[1] FUMIAKI TSUNOMORI,[1] and KENJI NOTSU[1]

Abstract—Soil H_2 and CO_2 surveys were carried out along seven active faults and around the aftershock region of the 2000 Tottori-ken Seibu earthquake in Japan. Diffuse CO_2 effluxes were also measured along one fault and around the 2000 aftershock region. The results show highly variable H_2 concentration in space and time and it seems that the maximum H_2 concentration at each active fault correlates with fault activity as exemplified by the time of the latest big earthquakes. Even though observed H_2 concentrations in four faults were markedly lower than those collected previously in the latter half of the 1970s, it is evident that the higher H_2 concentrations in this study are due to the addition of the fault gases. Comparing the chemical composition of trapped gases (H_2: 5–20% and CO_2/H_2: 0.5–12) in fractured rocks of drill cores bored at the Nojima fault, a soil gas sample with the highest H_2 concentration showed large amounts of the trapped fault gas, diluted with atmospheric component. The profile experiment across a fracture zone at the Yamasaki fault showed higher H_2 concentrations and lower CO_2/H_2 ratios as was observed in soil gas from the fracture zone. A few days after the 2000 Tottori-kei Seibu earthquake, no CO_2 effluxes related to the occurrence of earthquakes were observed at the aftershock region. However, only above the epicenter zone, relatively high H_2 concentrations in soil gases were observed.

Key words: Active fault, soil H_2, Co_2 degassing, fault gas.

1. Introduction

Volatile species such as Rn, H_2, CO_2, and He are observed to seep through active faults during quiescent periods when only micro-earthquakes occur intermittently at depth. Experimentally, these seeping species can be detected by analyzing the chemical composition of soil gases or by measuring soil gas efflux along active faults. Soil Rn measurements have been conducted since the 1950s at active seismic areas. KING (1978) found a good correlation between Rn emanation and local seismicity at the San Andreas fault. High H_2 concentrations up to 3% were observed in soil gases along a strike of the Yamasaki fault (WAKITA *et al.*, 1980) and SUGISAKI *et al.* (1983) reported a relationship between soil H_2 contents and fault activity, based on comprehensive soil H_2 surveys at several active faults in Japan. IRWIN and BERNES (1980) suggested that discharge of CO_2 might indicate areas with high pore pressure at depth and can be used for fault mapping.

[1] Laboratory for Earthquake Chemistry, Graduate School of Science, University of Tokyo, Hongo, Bunkyo-ku, Tokyo 113-0033, Japan. E-mail: notsu@eqchem.s.u-tokyo.ac.jp
[2] TUBITAK-MAM, Earth and Marine Science Institute, 41470 Gebze-KOCAELI, Turkey.

In spite of above observations, the origin of volatile species released from active faults remains obscure and is presumed to be multiple. Two mechanisms are proposed for the origin of Rn emanating along active faults (IMAIZUMI *et al.*, 1992): (1) Release of Rn in deep rocks associated with formation of micro-cracks through seismic activity; (2) release of Rn in the fault gauge (clay) with selective enrichment of U and/or Ra at subsurface depth. Regarding the origin of H_2, chemical reactions of new rock surfaces exposed at the time of micro-crack formation with local water also have been proposed (KITA *et al.*, 1982). However, other possible mechanisms, such as ferrous reduction (KING and LUO, 1990) and serpentinization (SATO *et al.*, 1986), were proposed, and microbial formation should be examined. SUGISAKI *et al.* (1983) presumed that CO_2 in fault zones is a mixture of some of several sources (mantle, thermogenic, biogenic etc.), and LEWICKI and BLANTLY (2000) and LEWICKI *et al.* (2003) studied CO_2 efflux at the San Andreas fault, showing that the efflux anomalies are consistent with fault-related biogenic gas flow, not attributed to a deep gas source. While KENNEDY *et al.* (1997) found mantle helium with a higher ^{3}He/^{4}He ratio than atmospheric value along the San Andreas fault, and DOGAN *et al.* (2006) also found the helium release from the mantle along the Median Tectonic Line, a major active fault in Japan. To monitor fault activity or seismic activity using these volatile species, it is still necessary to comprehensively understand chemical processes occurring at active faults.

In Japan, soil H_2 and CO_2 surveys along active faults have not been conducted during the last 25 years, which has brought big inland earthquakes such as the 1995 Hyogo-ken Nanbu earthquake (M 7.3) and the 2000 Tottori-ken Seibu earthquake (M 7.3). These large earthquakes provided us with a good chance to investigate changes in soil gas nature immediately after the occurrence of the earthquakes. The purpose of this work is to present new H_2 and CO_2 data of soil gases along several active faults in Japan and to clarify the behavior of volatile species being released through active faults in relation to seismic activity.

2. Surveyed Areas and Methods

Figure 1 shows the location of the seven active faults and the aftershock region in western and central Japan surveyed in this study. We selected the Atera, Atotsugawa, Neodani and Yamasaki faults because of previously reported high H_2 concentrations in soil gases (WAKITA *et al.*, 1980; SUGISAKI *et al.*, 1983) and large earthquakes (>M 7) which occurred in historical times. Studies on geomorphology, geology, historical seismic activity and others of these active faults are compiled by the RESEARCH GROUP FOR ACTIVE FAULTS OF JAPAN (2001). At each active fault, observations were carried out at selected sites where clear surface displacements were morphologically observed and/or fractured rocks or fault gauges exposed as outcrops.

Along a part of the Atera fault (ca. 40-km long), seven sites, where surface displacements were observed as outcrops (TSUKUDA *et al.*, 1993), were surveyed. We
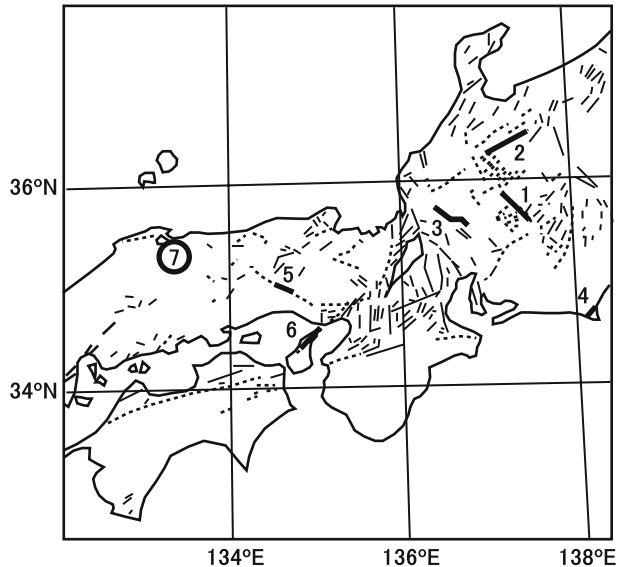
Figure 1
Locations of active faults surveyed in this study. 1. Atera fault, 2. Atotsugawa fault, 3. Neodani fault, 4. Serizawa and Hirosawa fault, 5. Yamasaki fault, 6. Nojima fault, 7. aftershock region of the 2000 Tottori-ken Seibu earthquake.

carried out a soil gas survey at four sites along the western part of the Atotsugawa fault (ca. 30-km long). We also surveyed five sites along a strike (ca. 10-km long) of the Neodani fault, where surface displacement was formed during the occurrence of the 1891 Nobi earthquake (M 8.0) (OKADA, 1987). Along the Yamasaki fault, soil gas surveys were carried out in February 2004 and March 2005 across a fracture zone (Fig. 2) close to the C site, where WAKITA *et al.* (1980) found values as high as 31,000 ppm H$_2$ in November 1979. For comparison, we carried out soil gas surveys at the Serizawa and Hirosawa faults located at the Cape Omaezaki of the Shizuoka prefecture (KATSURAJIMA *et al.*, 1987), as examples of active faults with low fault activity, i.e., very small slip rate. Averages of slip rates are respectively 0.04 and 0.06 m/10^3 year for the Serizawa and Hirosawa faults; accordingly, both are classified as C-class active faults (RESEARCH GROUP FOR ACTIVE FAULTS OF JAPAN, 2001). We collected at each fault two soil gas samples along the surface displacements and one from a background site, 2 km east of the Serizawa fault.

In order to investigate the effects on the soil gas composition after the occurrence of large earthquakes, we carried out a soil gas survey in December 2003 along the Nojima fault, which was displaced at the time of the Hyogo-ken Nanbu earthquake which occurred on 17 January, 1995 (M 7.3), almost nine years after the mainshock. We collected soil gas samples from twelve sites along the earthquake fault (Fig. 3), which
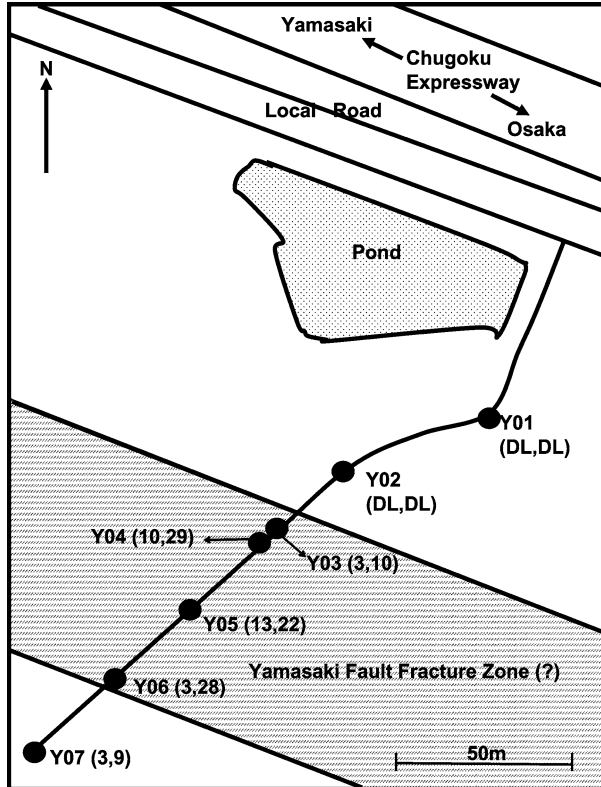
Figure 2

H$_2$ concentrations (ppm) in soil gas across the Yamasaki fault. Surveyed site is close to C-site of WAKITA *et al.* (1980). Two numbers in (,) after each sampling point are H$_2$ concentrations (ppm) in soil gases collected on Feb. 26 and 28, 2004. DL shows H$_2$ concentration below the detection limit of 1ppm.

ruptured with a maximum displacement of 2.5 m (AWATA and MIZUNO, 1998). Soil gas samples were repeatedly collected in 2004 and 2005 at a site (Noj05) where the maximum H$_2$ content was measured during the 2002 survey. In addition, we carried out a soil gas survey at 26 sites in the aftershock region of the Tottori-ken Seibu earthquake (M 7.3), which occurred on October 6, 2000 (OHMI *et al.*, 2002), one week after the mainshock. This earthquake was an inland-type; its magnitude was similar to that of the 1995 Hyogo-ken Nanbu earthquake, but no clear surface displacement caused by the earthquake fault was apparent. Instead, surface fault ruptures with a total length of about 6 km appeared above the epicenter (FUSEJIMA *et al.*, 2001).

At each survey site, soil gases were collected at 30-cm depth using a metallic probe (MU type gas collection tube; GL Sciences Inc., Japan) for chemical and carbon isotope analyses. This probe is a stainless tube of 50-cm long with a filter at the bottom and a septum at the top to prevent leakage of the inside gas with approximately 0.5 ml. After
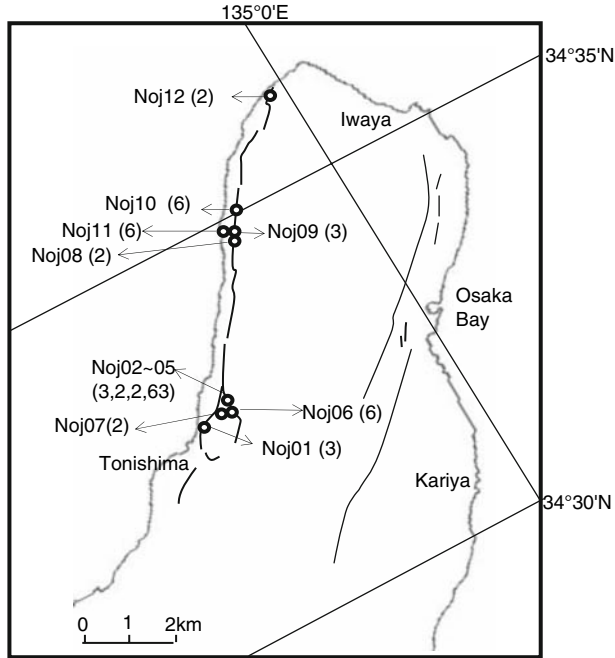
Figure 3

H$_2$ concentrations (ppm) in soil gas along the Nojima fault in December 2003. H$_2$ concentrations at Noj05 site are 510 ppm in March 2004 and 105 ppm in March 2005.

inserting this probe into soil, the original gas which resided inside was exchanged with soil gas by sucking the original gas using a syringe. Then approximately 10 ml of the soil gas was sucked with the syringe and was removed into a glass container with a rubber cock, which had been evacuated before use. At the Atera fault and aftershock region of the 2000 Tottori-ken Seibu earthquake, diffuse CO$_2$ efflux measurements were also performed using a portable CO$_2$ flux meter (WEST System Srl., Italy), which was designed based on the accumulation chamber method (CHIODINI *et al.*, 1998). Detection limit of this flux meter was 3 g CO$_2$ m^{-2}d^{-1} and the reproducibility was about $\pm$ 10% for the efflux range over 100 g CO$_2$ m^{-2}d^{-1}.

Concentrations of CO$_2$, He, H$_2$, O$_2$, N$_2$ and CH$_4$ in soil gases were determined using a micro-gas chromatograph (Micro-GC CP2002; Varian Inc.). A Pora PLOTQ column and He carrier gas were used for CO$_2$ and CH$_4$ determinations, whereas a molecular sieve column and Ar carrier gas were used for other species. Detection limits of H$_2$ and CH$_4$ determination were 1 ppm and 5 ppm, respectively. Carbon isotope measurements for CO$_2$ in soil gases were carried out using a MAT delta-S GC/C/MS system (Finigan MAT, GmbH). Correction for mass discrimination in analyses was done with the measurement of a standard gas (CO$_2$ > 99.95%, δ^{13}C = -30.92‰) intermittently injected into the mass spectrometer during sample analyses.

3. *Results and Discussion*

Table 1 lists H_2 and CO_2 concentrations of soil gas samples from seven active faults. Since all samples except three samples from the Yamasaki fault have CH_4 concentrations below the detection limit (5 ppm), the CH_4 data of these three samples are shown in the column "comment" of Table 1. The $\delta^{13}C$ (CO_2) data are also listed in the same column, if available. Major components of all gas samples are N_2 and O_2 with almost atmospheric composition. The O_2 depletion was observed in samples with large amounts of CO_2. Overall range of H_2 concentrations in soil gases was from <1 ppm to 510 ppm, which was significantly lower than the reported H_2 data (SUGISAKI *et al*., 1983). While CO_2 concentrations in soil gases range from 530 ppm to 2.5% with $\delta^{13}C(CO_2)$ values at the Atera and Neodani faults ranging from −25.3 to −19.6‰ and −22.7 to −20.7‰, respectively. These results suggest biogenic origin of CO_2 and they are similar to those measured at the San Andreas fault (LEWICKI *et al*., 2003).

3.1. *Spatial and Temporal Variation of Soil Gases*

It is well known that soil gas concentrations and fluxes are highly variable in space and time, even along a given fault trace. WAKITA *et al*. (1980) reported that H_2 concentrations at identical sampling points can change drastically over time. For example, H_2 concentrations at the A site of the Yamasaki fault were respectively 3060 and 3 ppm in November 1978 and November 1979. This variation is not attributable to seasonal variations, because this drastic decreasing occurred in a one-year interval. SUGISAKI *et al*. (1983) compiled the soil H_2 data, showing extremely large spatial variations in H_2 concentrations for each active fault. In the case of the Atera fault, soil H_2 concentrations varied from 1 ppm to 100,000 ppm from place to place. Our H_2 data in Table 1 also show significant spatial and temporal variations at each fault.

At the Yamasaki fault, soil gas samples were collected at seven sites aligned across the fracture zone in two different days during February 2004. Figure 2 shows a map of sampling locations with soil H_2 concentration values. Soil gases in the fracture zone showed considerably higher H_2 concentrations than surrounding areas also with temporal variations (almost two times) during only two-days interval. We again conducted measurements along a traverse following the same route in March 2005, confirming the observed trend of 2004. The maximum H_2 concentration (22 ppm) was measured at Y505 site, close to Y05 site in the 2004 survey.

In the case of the Nojima fault, the spatial variation in soil H_2 content is shown in Figure 3. Among 12 sites, the highest H_2 concentration (63 ppm) was measured at the Noj05 site, where a fresh fault plane was exposed on the southern shore of a small pond. Here, the gas sample was collected in the mudstone-conglomerate layer. Other gas samples were collected in the surface soil layer along an earthquake fault which was displaced at the time of the earthquake occurrence. Four samples collected in a narrow area (Noj02∼Noj05) showed different soil H_2 concentrations (see Table 1). Soil H_2

Table 1

Soil H$_2$ and CO$_2$ data of seven active faults in Japan

Active fault	Site number	Sampling date	H$_2$ ppm	CO$_2$ ppm	CO$_2$/H$_2$	Comment
Atera	Ate01	2003-12-05	26	1200	46	δ^{13}C = −19.6‰
	Ate02	2003-12-05	13	6200	480	δ^{13}C = −23.9‰
	Ate03	2003-12-05	9	1800	200	δ^{13}C = −21.5‰
	Ate04	2003-12-05	8	1800	230	δ^{13}C = −24.6‰
	Ate05	2003-12-06	32	3300	103	δ^{13}C = −25.2‰
	Ate06	2003-12-06	22	15000	680	δ^{13}C = −25.3‰
	Ate07	2003-12-06	11	4600	420	δ^{13}C = −24.6‰
Atotsugawa	Awa01	2004-04-30	<1	1000	—	
	Awa02	2004-04-30	1.2	1000	830	
	Awa03	2004-04-30	16	1000	63	
	Awa04	2004-04-30	19	2000	105	
Neodani	Neo01	2003-12-15	<1	8000	—	δ^{13}C = −22.7‰
	Neo02	2003-12-15	<1	6000	—	δ^{13}C = −20.7‰
	Neo03	2003-12-15	5	2000	400	δ^{13}C = −21.9‰
	Neo04	2003-12-15	3	11000	3700	δ^{13}C = −21.1‰
	Neo05	2003-12-15	3	2000	670	δ^{13}C = −22.2‰
Hirosawa	Omz01	2004-12-16	<1	10000	—	
	Omz02	2004-12-16	<1	8000	—	
Serizawa	Omz03	2004-12-16	<1	2000	—	
	Omz04	2004-12-16	<1	3000	—	
	Omz05	2004-12-16	<1	7000	—	2 km from the fault
Yamasaki	Y01-1	2004-02-26	<1	1100	—	far from the fracture
	Y01-2	2004-02-28	<1	1100	—	far from the fracture
	Y02-1	2004-02-26	<1	690	—	outside the fracture
	Y02-2	2004-02-28	2	1100	550	outside the fracture
	Y03-1	2004-02-26	3	710	240	
	Y03-2	2004-02-28	10	600	60	CH$_4$ = 27 ppm
	Y04-1	2004-02-26	10	660	66	
	Y04-2	2004-02-28	29	730	25	
	Y05-1	2004-02-26	13	800	62	CH$_4$ = 16 ppm
	Y05-2	2004-02-28	22	1900	86	
	Y06-1	2004-02-26	7	1200	171	
	Y06-2	2004-02-28	28	1100	39	
	Y07-1	2004-02-26	3	710	240	outside the fracture
	Y07-2	2004-02-28	9	700	78	outside the fracture
	Y501	2005-03-17	5	5000	1000	far from the fracture
	Y502	2005-03-17	2	1100	550	outside the fracture
	Y503	2005-03-17	2	800	400	
	Y504	2005-03-17	2	700	350	
	Y505	2005-03-17	22	1100	50	CH$_4$ = 18 ppm
	Y506	2005-03-17	5	1400	280	outside the fracture
Nojima	Noj01	2003-12-26	3	900	300	
	Noj02	2003-12-26	3	25000	8300	
	Noj03	2003-12-26	2	1600	800	
	Noj04	2003-12-26	2	1400	700	
	Noj05	2003-12-26	63	3000	48	
	Noj06	2003-12-26	6	2600	430	
	Noj07	2003-12-26	2	3100	1550	
	Noj08	2003-12-26	2	800	400	
	Noj09	2003-12-26	3	1300	430	
	Noj10	2003-12-26	6	2600	430	
	Noj11	2003-12-26	6	13000	2200	
	Noj12	2003-12-26	2	5400	2700	
	N04-1	2004-03-04	510	530	1.0	
	N04-2	2004-03-04	3	1250	420	
	N04-3	2004-03-04	35	1460	42	
	N05-1	2005-03-22	107	900	8	
	N05-2	2005-03-22	11	1900	170	
	N05-3	2005-03-22	3	3100	1030	

concentrations decrease drastically to 2 ppm (Noj03 and Noj04) and 3 ppm (Noj02), located approximately 1 m or less distant from the highest Noj05 site. We repeated the measurement of H_2 concentration in the soil at the Noj05 site to verify the temporal reproducibility of the observed high H_2 concentrations: The results were 510 ppm in March 2004 and 105 ppm in March 2005, indicating containment of a considerable amount of H_2 despite large temporal variation.

Figure 4 shows our survey sites in the aftershock region of the 2000 Tottori-ken Seibu earthquake. Among the 26 sampling sites, the site No. 15, just close to a surface fault rupture above the epicenter (FUSEJIMA *et al.*, 2001), was the only one showing a considerably high content of H_2 (40 ppm and 24 ppm), whereas all other sites were characterized by very low soil H_2 concentrations less than the detection limit of 1 ppm.

In summary, the spatial distributions of soil H_2 concentrations for the surveyed faults showed that higher H_2 concentrations are observed at fracture zones of active faults, compared with surrounding areas. Since the higher H_2 concentrations along active fault strikes were variable in time and in space, continuous monitoring of soil H_2 concentration will help us gain a better understanding of these phenomena.

3.2. *Correlation between Soil H_2 Concentration and Fault Activity*

Although soil H_2 shows a significant spatial and temporal variation in a given active fault, it is important to compare the soil H_2 content with other parameters of active faults, such as the average slip rate and age of the latest large earthquake (Table 2). Table 2 also shows soil H_2 data measured in late 1970 (WAKITA *et al.*, 1980; SUGISAKI *et al.*, 1983) for comparison. Studied active faults with very low average slip rate, represented by the Serizawa and Hirosawa faults, resulted in soil H_2 concentrations less than 1 ppm. However, it is difficult to find the correlation between the maximum H_2 concentration with the average slip rate. SUGISAKI *et al.* (1983) pointed out that soil H_2 concentrations from active faults with historical earthquakes were significantly higher than those from Quaternary faults not associated with historical earthquakes. Our new data support this observed relationship. The maximum H_2 concentration measured in this study was observed at the Nojima fault, which moved about 10 years ago, whereas for active faults without historical earthquakes H_2 contents were always below the detection limit. However, a clear relationship between the maximum H_2 concentration and the time from the latest large earthquake is not observed among several active faults with historically big earthquakes.

3.3. *Chemical Features of Subsurface Soil Gas along Active Faults*

Table 1 also shows that our observed H_2 concentrations in soil gas collected during 2003–2005 are markedly lower than those of previous data collected in the late 1970s (WAKITA *et al.*, 1980; SUGISAKI *et al.*, 1983). This substantial difference in H_2 concentrations might result from the different soil gas sampling methods. We adopted

Table 2

Soil H$_2$ concentrations of several active faults in Japan

Active fault	Average slip rate[1]	Latest big earthquake			Soil H$_2$ concentration (ppm)[2]	
		Year	Name	Magnitude	This work	Late 1970
Atera	1–7	1586	Tensho	7.8	8 ∼ 32 (7)	1 ∼ 100000 (73)[3]
Atotsugawa	2–4	1858	Hietsu	7.0–7.1	0 ∼ 19 (4)	1 ∼ 25000 (47)[3]
Neodani	>2	1891	Nobi	8.0	0 ∼ 5 (5)	100 ∼ 9000 (5)[3]
Yamasaki	0.03–0.3	868	Harima	>7.0	0 ∼ 29 (20)	0.5 ∼ 30600 (28)[4]
Nojima	1	1995	Hyogo-ken Nanbu	7.3	2 ∼ 510 (18)	—
(not identified)	—	2000	Tottori-ken Seibu	7.3	0 ∼ 40 (27)	—
Serizawa	0.04		(not identified)		<1	—
Hirosawa	0.06		(not identified)		<1	—

[1] RESEARCH GROUP for ACTIVE FAULTS of JAPAN (2001).
[2] Numbers in ( ) are numbers of samples.
[3] SUGISAKI *et al.* (1983).
[4] WAKITA *et al.* (1980).

a simpler and more convenient method than WAKITA *et al.* (1980) or SUGISAKI *et al.* (1983). We collected soil gases at 30-cm deep using a commercial metallic probe, while WAKITA *et al.* (1980) drilled 50–100-cm deep holes reaching the bedrock, then inserted polyvinyl chloride pipes with sealed tops into the holes. After about 12 h storage time, sample gases were extracted with a hypodermic syringe. A collecting method devised by SUGISAKI *et al.* (1983) was described by SUGISAKI *et al.* (1980) by means of sampling with a tube buried in a hole about 1-m deep within the fault zone. It may be possible that our soil gas samples are substantially diluted with atmospheric component, because basement rocks in the fracture zone associated with the displacement of active faults are usually covered with soils of considerable depth. The gas component possibly generated and stored in fracture zones might migrate into the overlapping soils, with the involvement of a large amount of atmospheric component.

The alternative explanation for our low H$_2$ concentration is due to the temporal change in seismic activity. Assuming that H$_2$ production is related to the rock fracture because of the micro-earthquake activity which intermittently occurred underneath the active faults (KITA *et al.*, 1982), soil H$_2$ concentrations might be affected by temporal changes in seismic activity. Around the Yamasaki and Atotsugawa faults, precise seismic observation networks have been operating since the 1970s. The annual number of earthquakes larger than M 1.6 in the 5th sector of NAKAO *et al.* (2004), which includes our sampling site, was low in 1978 and 1979, when WAKITA *et al.* (1980) collected gas samples, reaching a peak in 1993, which has not changed remarkably after 2002 (Japan Meteorological Agency, personal communication). Therefore, it seems difficult to attribute higher soil H$_2$ concentrations in 1978 and 1979 to intense micro-crack formation caused by active micro-seismicity. In the southwestern part of the Atotsugawa fault, the monthly frequency distribution of micro-earthquakes larger than M 2 has been constant

between 1977 and 1994, except during the period of swarm activity from December 1986 to January 1987 (WADA and ITO, 1995). After 1995, the monthly frequency of micro-earthquakes increased gradually to 2002 (WADA *et al.*, 2002). This trend also indicates that a drastic decrease in soil H_2 concentration is inexplicable in terms of micro-earthquake activity changes.

ARAI *et al.* (2001) measured the chemical composition of extracted gases from core samples drilled at the Nojima fault, showing that those from the fracture zone deeper than 1560 m contain 5–20% H_2 of the total $(CH_4 + CO_2 + H_2 + C_2H_6 + He)$ gas mixture, whereas those shallower than 1560 m contain a negligible amount of H_2. Since the CO_2 concentrations of the extracted gases from the fracture zone are 10–60% of the total gas mixture, the CO_2/H_2 ratios of trapped gas in the fracture zone of the Nojima fault are from 0.5 to 12, which are similar to those of soil gases with high H_2 concentrations (Noj05: 48, N04-1: 1.0, N05-1: 8). Figure 5 shows the relationship between H_2 concentrations and CO_2/H_2 ratios of soil gases from the Nojima and Yamasaki faults. In this figure, chemical data of extracted gases from core samples of the fracture zone of the Nojima fault (ARAI *et al.*, 2001) and of fault gases from the Yamasaki fault (WAKITA *et al.*, 1980) are also shown. The CO_2/H_2 ratios of H_2-rich gas
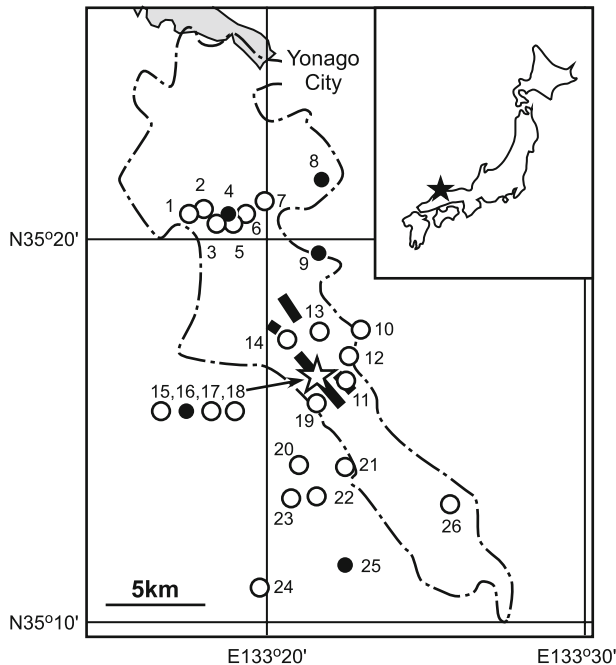
Figure 4

Spatial distribution of CO_2 efflux in the aftershock region of the 2000 Tottori-ken Seibu earthquake. ● 3–6 gCO_2 /m²/d, ○ < 3 gCO_2 /m²/d. A large open star shows the epicenter, the aftershock region is the interior area bordered by chain lines. Solid bars show surface fault ruptures.

samples along the Yamasaki fault strikes can be estimated to be less that 9, because WAKITA *et al.* (1980) reported that fault gases with H$_2$ of 0.1–3.0% contained CO$_2$ less than 0.9%. This low ratio is in the range of CO$_2$/H$_2$ ratios of trapped gas in fractured rocks from the Nojima fault.

Figure 5 indicates that the soil gases with high H$_2$ concentrations from the Nojima fault contain a considerable amount of trapped gas in fractured rocks and diluted atmospheric component. For other samples with a few ppm of H$_2$ and CO$_2$/H$_2$ ratio above 100, the trapped gas component in fractured rocks (CO$_2$/H$_2$ = 0.5–12) is more diluted with atmospheric component with CO$_2$ enrichment under the subsurface soil environment or it is negligible. Furthermore, Figure 5 illustrates that most of the Yamasaki soil gas samples in this study contain a fault gas component. Our traverse experiment across the fracture zone also demonstrates that the CO$_2$/H$_2$ ratio in soil gas from the fracture zone (<100) is systematically lower than that from beyond the fracture zone (>500), indicating involvement of fault gas components in the gas samples from the fracture zone.

3.4. *Changes in Soil Gases Associated with Earthquakes*

A recent monitoring study of CO$_2$ efflux in El Salvador showed a marked increase in soil CO$_2$ efflux related to a M 5.1 earthquake that occurred 12 km east of the observation station (SALAZAR *et al.*, 2002). According to this, it is important to examine characteristic changes in soil gas chemistry and efflux prior to and at the time of the occurrence of an earthquake. We had the chance to carry out a soil gas survey immediately after the 2000 Tottori-ken Seibu earthquake (M 7.3). This earthquake occurred where no active faults had been recognized previously (RESEARCH GROUP FOR ACTIVE FAULTS OF JAPAN, 2001), so that a fractured terrain, which is typically formed at repeated earthquakes over a prolonged period, might not be developed.

Among the soil gas samples collected from 26 sites shown in Figure.4, only one site (No. 15), located above the epicenter region of the earthquake where surface fault ruptures appeared, showed a marked high level of H$_2$ (40 ppm). The soil H$_2$ concentrations measured at all other sites extending from the aftershock distribution, which represents a lineament of a buried active fault, were below the detection limit (1 ppm). Under the condition of no previous fault activities, trapped H$_2$ can only be seeped through a fault rupture region, assuming that H$_2$ is concentrated in the trapped gas of the fracture zone, as observed at the Nojima fault (ARAI *et al.*, 2001).

The low soil degassing revealed by the soil H$_2$ survey is consistent with the diffuse CO$_2$ efflux data (Fig. 4). In general, soil CO$_2$ efflux values were lower than the detection limit of approximately 3 g m^{-2}d^{-1}, except for the higher effluxes at several sites with the maximum of 6 g m^{-2}d^{-1} measured at No. 4 and No. 9 sites. If we compare these values with the ones measured along the Atera fault strike, which range between below the detection limit of 3 g m^{-2}d^{-1} and 24 g m^{-2}d^{-1}, the efflux in the aftershock region is
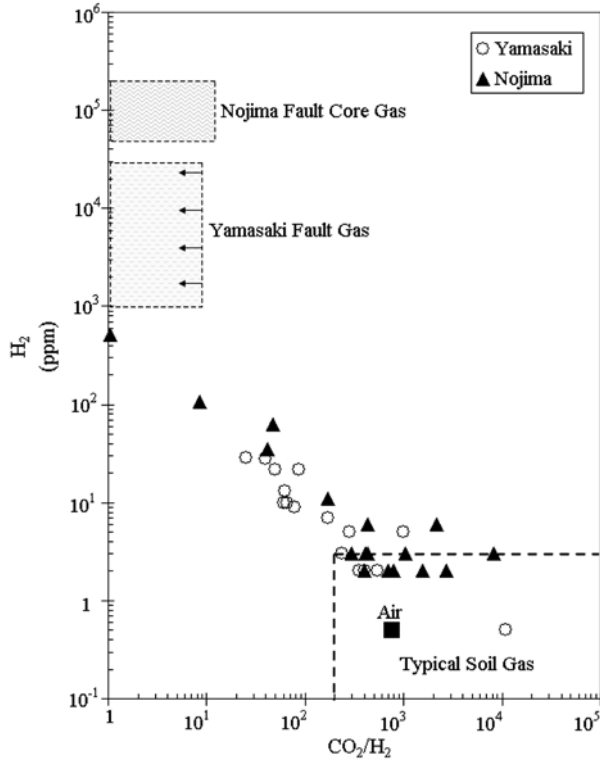
Figure 5

H_2 vs. CO_2/H_2 diagram of soil gas samples from the Yamasaki and Nojima faults. Data of extracted gases from core samples of fracture zone of the Nojima fault are from ARAI *et al.* (2001) and those of fault gases from the Yamasaki fault are from WAKITA *et al.* (1980).

very low, suggesting that degassing attributable to the movement of a presumed underground active fault was not observed.

Soil gas surveys at the Nojima fault displaced in 1995 and around the aftershock region of the 2000 Tottori-ken-Seibu earthquake suggest that release of H_2 is related to the occurrence of earthquakes. To better understand these phenomena and to catch a precursory signal of earthquakes, a continuous monitoring of soil gases could be a good way.

4. *Summary*

1. Soil H_2 and CO_2 surveys were carried out along seven active faults and around the aftershock region of the 2000 Tottori-ken Seibu earthquake in Japan. The

results show that soil H$_2$ concentrations are highly variable in space and time for each active fault. The maximum H$_2$ concentration at each active fault seems to correlate with fault activity as exemplified by the time to the latest big earthquakes.

2. Observed soil H$_2$ concentrations in four faults were markedly lower than those collected in the latter half of the 1970s. These differences in H$_2$ concentration may be related to different sampling depth or material in the active fault system. Even though we did not measure the same maximum values, we could observe that higher H$_2$ concentrations due to the addition of the fault gases which occur close to the fault strikes. Since we collected subsurface soil gas of 30-cm deep, this gas contains a mixture of trapped gas in the fractured rocks with high H$_2$ concentration and low CO$_2$/H$_2$ ratio, as exemplified by extracted gas from fractured rocks at the Nojima fault (ARAI *et al*., 2001), and atmospheric component with CO$_2$ enrichment. A sample with the highest H$_2$ concentration in our study obtained at the Nojima fault showed a similar low CO$_2$/H$_2$ ratio to that of trapped gas. The traverse experiment across the fracture zone at the Yamasaki fault showed higher H$_2$ concentration and lower CO$_2$/H$_2$ ratio in soil gas from the fracture zone.

3. A few days after the 2000 Tottori-kei Seibu earthquake, higher H$_2$ concentrations in soil gases were observed only above the epicenter, and no CO$_2$ efflux related to the earthquake occurrence was observed in the aftershock region. This might coincide with the fact that this earthquake occurred where no active faults had been recognized previously.

REFERENCES

ARAI, T., OKUSAWA, T. and TSUKAHARA, H. (2001), *Behavior of gases in the Nojima fault zone revealed from the chemical composition and carbon isotope ratio of gases extracted from DPRI 1800 m dill core*, The Island Arc *10*, 430–438.

AWATA, Y. and MIZUNO, K. (1998), *Explanatory text of the strip map of the surface fault ruptures associated with the 1995 Hyogo-ken Nanbu earthquake, central Japan - the Nojima, Ogura and Nadagawa earthquake fault, scale 1:10,000*, Tectonic map series (12), Geol. Surv. Japan, 74pp. (in Japanese with English abstract).

CHIODINI, G., CIONI, R., GUIDI, M., RACO, B. and MARINI, L. (1998), *Soil CO₂ flux measurements in volcanic and geothermal areas*, Appl. Geochem. *13*, 543–552.

DOGAN, T., SUMUNO, H., NAGAO, K. and NOTSU, K. (2006), *Release of mantle helium from forearc region of the Southwest Japan arc*, Chem. Geol. *233*, 235–248.

FUSEJIMA, Y., YOSHIOKA, T., MIZUNO, K., SHISHIKURA, M., IMURA, R., KOMATSUBARA, T. and SASAKI, T. (2001), *Surface ruptures associated with the 2000 Tottori-ken Seibu earthquake*, Ann. Rep. Active Fault Paleoearthq. Res. *1*, 1–26 (in Japanese with English abstract).

IMAIZUMI, M., KOMAE, T. and HAMADA, H. (1992), *Gamma-ray spectrometry for prospecting faults around Atera fault in Yamaguti village, Nagano prefecture*, J. Japan Soc. Engineer. Geol. *33*, 91–103 (in Japanese with English abstract).

IRWIN, W.P. and BARNES, I. (1980), *Tectonic relations of carbon dioxide discharges and earthquakes*, J. Geophys. Res. *85*, 3115–3121.

KATSURAJIMA, S., SANGAWA, A., HASHIMOTO, T., MIYAZAKI, J., WATANABE, K. and SAITO, E. (1987), *Active structures of Omaezaki region, Shizuoka prefecture*, Bull. Geol. Surv. Japan *38*, 319–330 (in Japanese with English abstract).

KENNEDY, B.M., KHARAKA, Y.K., EVANS, W.C., ELLWOOD, A., DEPAOLO, D.J., THORDSEN, J., AMBATS, G. and MARINER, R.H. (1997), *Mantle fluids in the San Andreas fault system, California*, Science *278*, 1278–1281.

KING, C.-Y. (1978), *Radon emanation on San Andreas fault*, Nature *271*, 516–519.

KING, C.-Y. and LUO, G. (1990), *Variations of electric resistance and H₂ and Rn emissions of concrete blocks under increasing uniaxial compression*, Pure Appl. Geophys. *134*, 45–56.

KITA, I., MATSUO, S. and WAKITA, H. (1982), *H₂ generation by reaction between H₂O and crushed rock: An experimental study on H₂ degassing from the active fault zone*, J. Geophys. Res. *87*, 10789–10795.

LEWICKI, J.L. and BLANTLEY, S.L. (2000), *CO₂ degassing along the San Andreas fault, Parkfield, California*, Geophys. Res. Lett. *27*, 5–8.

LEWICKI, J.L., EVANS, W.C., HILLEY, G.E., SOREY, M.L., ROGIE, J.D. and BRANTLEY, S.L. (2003), *Shallow soil CO₂ flow along the San Andreas and Calaveras faults, California*, J. Geophys. Res. *108*, 2187, doi:10.1029/2002JB002141.

NAKAO, S., SHIBUTANI, T. and KARAO, H. (2004), *Seismicity around the Yamasaki fault*, Ann. Disas. Prev. Res. Inst., Kyoto Univ. *47* B-1, 713–720 (in Japanese with English abstract).

OHMI, S., WATANABE, K., SHIBUTANI, T., HIRANO, N. and NAKAO, S. (2002), *The 2000 Western Tottori earthquake –Seismic activity revealed by the regional seismic networks*, Earth Planets Space *54*. 819–830.

OKADA, A. (1987), *Neodani Fault in Nobi earthquake faults system*, Active Fault Res. *4*, 71–90 (in Japanese).

RESEARCH GROUP FOR ACTIVE FAULTS OF JAPAN (2001), *Active faults in Japan* (revised edition), University of Tokyo Press, 437 pp. (in Japanese with English summary).

SALAZAR, J.M.L., PEREZ, N.M., HERNANDEZ, P.A., SORIANO, T., BARAHONA, F., OLMOS, R., CARTAGENA, R., LOPEZ, D.L., LIMA, R.N., MILIAN, G., GALINDO, I., PADRON, E., SUMINO, H. and NOTSU, K. (2002), *Precursory diffuse carbon dioxide degassing signature related to a 5.1 magnitude earthquake in El Salvador, central America*, Earth Planet. Sci. Lett. *205*, 80–89.

SATO, M., SUTTON, A.J. and MCGEE, K.A. (1986), *Monitoring of hydrogen along the San Andreas faults in central California in 1980–1984*, J. Geophys. Res. *91*, 12315–12326.

SUGISAKI, R., ANNO, H., ADACHI, M. and UI, H. (1980), *Geochemical features of gases and rocks along active faults*, Geochem. J. *14*, 101–112.

SUGISAKI, R., IDO, M., TAKEDA, H., ISOBE, Y., HAYASHI, Y., NAKAMURA, N., SATAKE, H. and MIZUTANI, Y. (1983), *Origin of hydrogen and carbon dioxide in fault gases and its relation to fault activity*, J. Geol. *91*, 239–258.

TSUKUDA, E., AWATA, Y., YAMAZAKI, H., SUGIYAMA, Y., SHIMOKAWA, K. and MIZUNO, K. (1993), *Explanatory text of the strip map of the Atera Fault system, scale 1:25,000*, Tectonic map series (7), Geol. Surv. Japan, 39 pp. (in Japanese with English abstract).

WADA, H. and ITO, K. (1995), *Seismic activity in the vicinity of the Atotsugawa fault, central Japan*, Ann. Disas. Prev. Res. Inst., Kyoto Univ., 38 B-1, 235–250 (in Japanese with English abstract).

WADA, H., ITO, K., OHMI, S. and HIRANO, N. (2002), *Recent ultra-micro-earthquake activity in the Hida Mountain range*, Tech. Res. Rep., Earthq. Res. Inst., Univ. Tokyo, *8*, 1–8 (in Japanese with English abstract).

WAKITA, H., NAKAMURA, Y., KITA, I., FUJII, N. and NOTSU, K. (1980), *Hydrogen release: New indicator of fault activity*, Science *210*, 188–190.

To access this journal online:
www.birkhauser.ch/pageoph

Diffuse Emission of Hydrogen from Poás Volcano, Costa Rica, America Central

Gladys V. Melián,[1] Inés Galindo,[1,2] Nemesio M. Pérez,[1] Pedro A. Hernández,[1] Mario Fernández,[3] Carlos Ramírez,[3] Raúl Mora,[4] and Guillermo E. Alvarado[4]

Abstract—We report the results of four soil H_2 surveys carried out in 2000–2003 at Poás volcano, Costa Rica, to investigate the soil H_2 distribution and evaluate the diffuse H_2 emission as a potential surveillance tool for Poás volcano. Soil gas H_2 contents showed a wide range of concentration from 0.2 to 7,059 ppmV during the four surveys. Maps of soil gas H_2 based on Sequential Gaussian Simulation showed low H_2 concentration values in the soil atmosphere (<0.7 ppmV) for most of the study area, whereas high soil gas H_2 values were observed inside the active crater of Poás. A significant increase in soil gas H_2 concentration was observed inside the active crater during 2001 and 2002 with respect to year 2000, followed by a decrease in 2003. The observed spatial and temporal variations of soil H_2 concentration have been well correlated with seismicity, microgravimetry and fumarolic chemistry changes which occurred during this study. These observations evidence changes in the shallow magmatic-hydrothermal system of Poás, and it might be related to a potential magmatic intrusion during the period 1998–2004. Therefore, monitoring diffuse H_2 emission of Poás has become an important geochemical tool for the monitoring of its volcanic activity.

Key words: Hydrogen, soil gas, Poás, Costa Rica.

1. Introduction

The study and monitoring of volcanic gases have provided important information about the process occurring at depth at volcanoes, and have become a useful tool to evaluate the volcanic activity (Matsuo, 1960; Noguchi and Kamiya, 1963; Matsuo *et al.*, 1975, 1982; Casadevall *et al.*, 1983; Gerlach and Graeber, 1985; Hirabayashi *et al.*, 1986; Symonds *et al.*, 1990; Sano *et al.*, 1991; Giggenbach, 1996; Chiodini *et al.*, 1998; Hernández *et al.*, 2001a; Carappezza *et al.*, 2004). Recently, new techniques have

---

[1] Environmental Research Division, Instituto Tecnológico y de Energías Renovables (ITER), 38611 GranadillaS/C de Tenerife, Spain. E-mail: gladys@iter.es

[2] Instituto Geológico y Minero de España. Oficina de Proyectos de Canarias, Alonso Alvarado, 43, 2°A. 35003 Las Palmas de Gran Canaria, Las Palmas, Spain.

[3] Centro de Investigaciones Geofísicas, University of Costa Rica (UCR), 1000 San José, Costa Rica.

[4] Escuela Centroamericana de Geología, University of Costa Rica (UCR), 1000 San José, Costa Rica.

enabled the measurement of volcanic gases from safe distances (MORI *et al.*, 1993; MORI and NOTSU, 1997; OPPENHEIMER *et al.*, 1998; ALLARD, 1999; GALLE *et al.*, 2002; BURTON, *et al.*, 2003; ALLARD *et al.*, 2005; MCGONIGLE *et al.*, 2005; MATSUSHIMA, 2005; SHINOHARA, 2005; WEIDMANN *et al.*, 2005). Significant amount of gases are emitted in to the atmosphere by active volcanoes through visible manifestations such as plumes, fumaroles and hot springs, but nonvisible emanations through the surface environment known as diffuse degassing are also a significant source of deep-seated gases released to the atmosphere by active volcanoes (ALLARD *et al.*, 1991; BAUBRON *et al.*, 1990). During the last 20 years significant contributions of soil degassing studies related to volcanic activity have been reported (WAKITA *et al.*, 1980; SATO and MCGEE, 1981; LOMBARDI and REIMER, 1990; CHIODINI *et al.*, 1996, 2001; PÉREZ *et al.*, 1996, 2006; D'ALESSANDRO and PARELLO, 1997; HERNÁNDEZ *et al.*, 2000, 2001a, b, 2003; SALAZAR *et al.*, 2001, 2002; ROGIE *et al.*, 2001; GERLACH *et al.*, 2001; AIUPPA *et al.*, 2004; CARAPEZZA *et al.*, 2004; FRONDINI *et al.*, 2004; MCGEE *et al.*, 2006). A few of these studies have been focused on hydrogen in the soil atmosphere (SATO and MCGEE, 1981; SATO, 1988; GIAMMANCO *et al.*, 1998; HERNÁNDEZ *et al.*, 2000; MELIÁN *et al.*, 2003).

Hydrogen is an important component of volcanic gases and its use as a tool to monitor the volcanic activity started with SATO and MCGEE (1981). Because of its chemical and physical characteristics, H_2 moves easily though the crust and constantly escapes to the atmosphere. The atmospheric H_2 concentration is relatively low (0.5 ppmV), and its light solubility in groundwater coupled with its low concentration in the air makes direct contamination of this gas from atmospheric sources negligible. These characteristics make H_2 an excellent tracer for processes operating deep in the crust. H_2 can be generated abundantly by several chemical reactions induced by water-rock interaction. High concentrations of H_2 often have been detected in soil gases and dissolved gases from fault zones and volcanic emissions (WHITE and WARING, 1963; WAKITA *et al.*, 1980; KAZAHAYA *et al.*, 1988; SATO, 1988; GIAMMANCO *et al.*, 1998; HERNÁNDEZ *et al.*, 2000). The interaction between the infiltrated water and rock at depth may also favor reduced condition and enhance formation of the H_2. Hydrogen can be generated in the earth's crust by different processes. The main source is probably the reaction of water with FeO in extrusive magmas. Other sources for H_2 are reaction of water with carbon of mantle origin, thermal decomposition of organic matter in reactions of water with freshly cleaved surfaces of rocks in areas of fault activity (SATO, 1988).

This article describes and discusses the results obtained during the four surveys of soil H_2 carried out at Poás volcano, Costa Rica, in the period 2000–2003. The objectives of this paper are to evaluate the spatial and temporal distribution of diffuse degassing of soil H_2 at Poás volcano during this period and to discuss the origin of this gas. This study demonstrates the importance of geochemical monitoring of volcanic gases in andesitic volcanoes and provides important information for the identification of possible geochemical precursors of volcanic unrest at Poás volcano.

2. Geological Setting of the Study Area

Poás volcano is one of the most active volcanoes in Costa Rica. It is located within the Cordillera Central, the southernmost volcanic front associated with the subduction of the Cocos plate beneath the Caribbean plate (Fig. 1) and is one of the 41 active volcanoes of the volcanic chain of America Central, which extends along 1100 km from Guatemala to Panama (SINKIN and SIEBERT, 1994). It is a broad well-vegetated basaltic-andesite strato volcano rising at an elevation of about 2708 m a.s.l., with a summit area containing three cones aligned at the N-S direction and the eroded remnants of two elongated calderas.

The topography at the summit manifests three different eruptive centers: (1) Von Frantzius, 2639 m a.s.l., a vegetated and eroded cone that lies to the north of the present active crater; (2) Botos 2708, m a.s.l., a younger cone formed to the south with a freshwater lake about 15-m deep in the center (RYMER et al., 2000), and (3) the present active crater located at a lower elevation between the former two (Fig. 2).

The active crater of Poás shows two main features: (1) A 300-m diameter pit crater partially filled with a hot (temperature range between 30 and 60°C) acidic crater lake
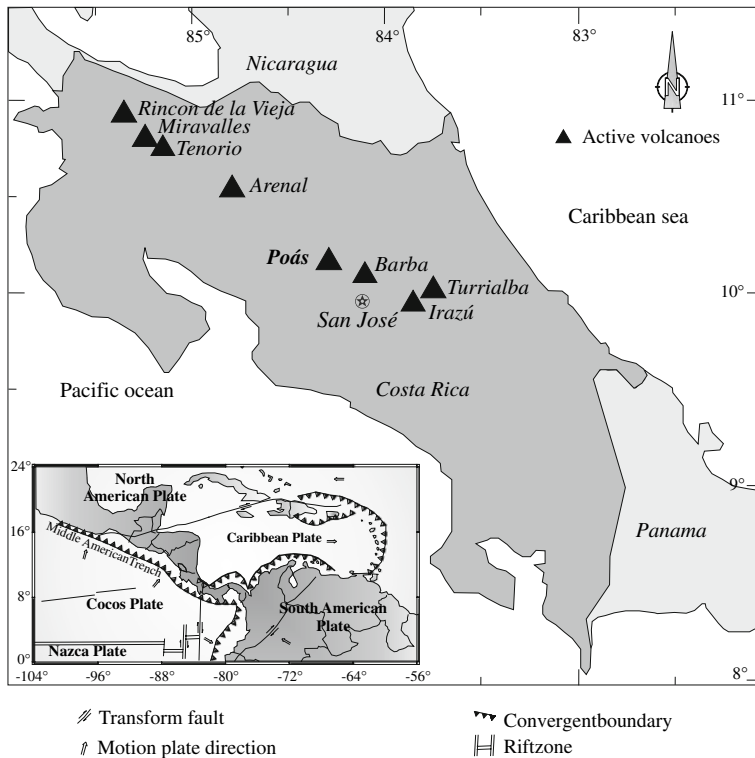
Figure 1
Tectonics of America Central and the Caribbean area and location of Poás volcano, Costa Rica.
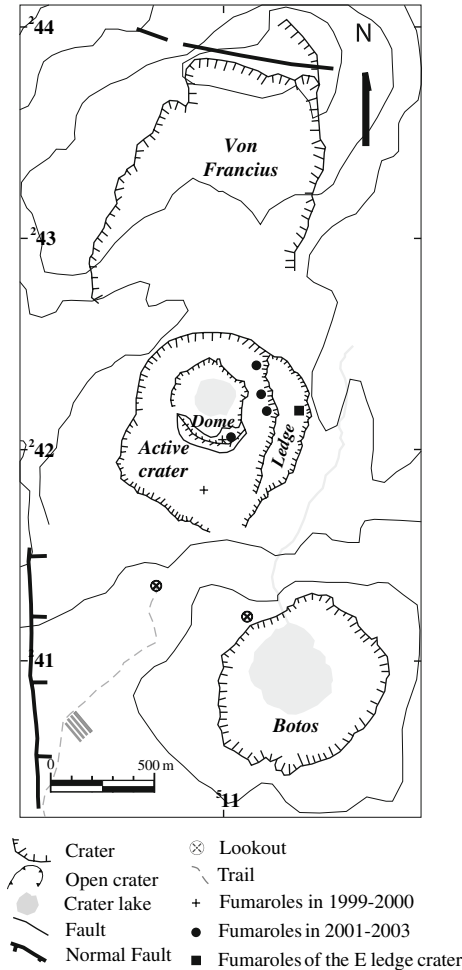
Figure 2
Map of summit region of Poás volcano with fumarolic locations.

(pH $\approx$ 0) whose volume, temperature and water chemistry vary sharply in response to rainfall and volcanic activity (BROWN *et al.*, 1989; ROWE *et al.*, 1992a, b); and (2) A 30-m high dome formed during the last phreatomagmatic eruption of Poás in 1953–1954 (CASERTANO *et al.*, 1985, 1987; ROWE *et al.*, 1992a). At present, the main fumarolic activity is located along the northeastern flank of this cone, which together with the gases emanated from the acid lake, is responsible for the volcanic plume. The active crater hosts an active hydrothermal system (CASERTANO *et al.*, 1987) supplied with heat and volatiles by a small magma body located at a relatively shallow depth (about 500 m) at Poás (RYMER and BROWN, 1989). Based on the lake temperature, seismicity and geochemical data, some authors suggested that pressure and temperature changes in the

volcanic-hydrothermal system of Poás at depth might explain the observed increases in heat and volatiles fluxes of the active crater (CASERTANO et al., 1987; ROWE et al., 1992a; VASELLI et al., 2003). Variables as rock permeability, thickness of the water table, gas-gas, rock-fluid and water-gas interactions could influence the composition of gases released from Poás volcano (CASERTANO et al., 1987; ROWE et al., 1992a, b, 1995; VASELLI et al., 2003).

3. Seismic activity

Seismicity is one of the most representative geophysical features of Poás volcano showing a good correlation with the level of volcanic activity (CASERTANO et al., 1987; FERNÁNDEZ, 1990; ROWE et al., 1992a). Seismicity at Poás is characterized by typical A-type events (high-frequency >3 Hz), B-type events (low-frequency <3 Hz) and tremors (MINAKAMI, 1969). Seismic data provided by a short-period seismic station (VPS-2) located close to the main crater of Poás, and belonging to the National Seismic Network (RSN. ICE-UCR), indicate that a steady background level of 50–100 A-Type events per day is the most common of Poás seismic activity. A-type events have been erratic in their frequency of occurrence during this study (2000–2003), as was also observed between 1980 and 1996 (RYMER et al., 2000), with notable peaks in September-November 1999, March-August and October-December, 2001 and February-May, 2003 (Fig. 3). These peaks might also be triggered by regional earthquakes which occurred during the same period (OVSICORI-UNA). Following ROWE et al. (1992a), the A events observed might represent externally triggered stress released within the volcanic edifice.

Long-term B-type seismic activity showed also an erratic distribution with peaks in September-November 1999, December 2000, March 2001 and March-May 2003. Increases in B-type events are well correlated with increases in A-type events and water temperature changes in the lake, suggesting the occurrence of stronger hydrothermal activity, pherhaps caused by an initial overpressure in the volcanic-hydrothermal system of Poás. The observed changes in the rate of B-type activity might also reflect changes in the volatile flux from the magma beneath Poás and water exolution through fractures (ARAÑA and ORTIZ, 1984; FERRUCCI, 1995; MARTÍNEZ et al., 2000).

4. Procedures and Methods

During years 2000–2003, four diffuse degassing surveys were carried out in and around the active crater of the Poás volcano, after taking into consideration the geology and structure of the study area as well as accessibility. The 2000 survey was carried out between April 14 and May 4, with 109 sampling sites covering an area of about 3.6 km^2. The surveys were carried out in 2001 (February 27 to March 10), 2002 (March 19 to April 06) and 2003 (April 4 to 21). The covered areas for these three surveys were the same as
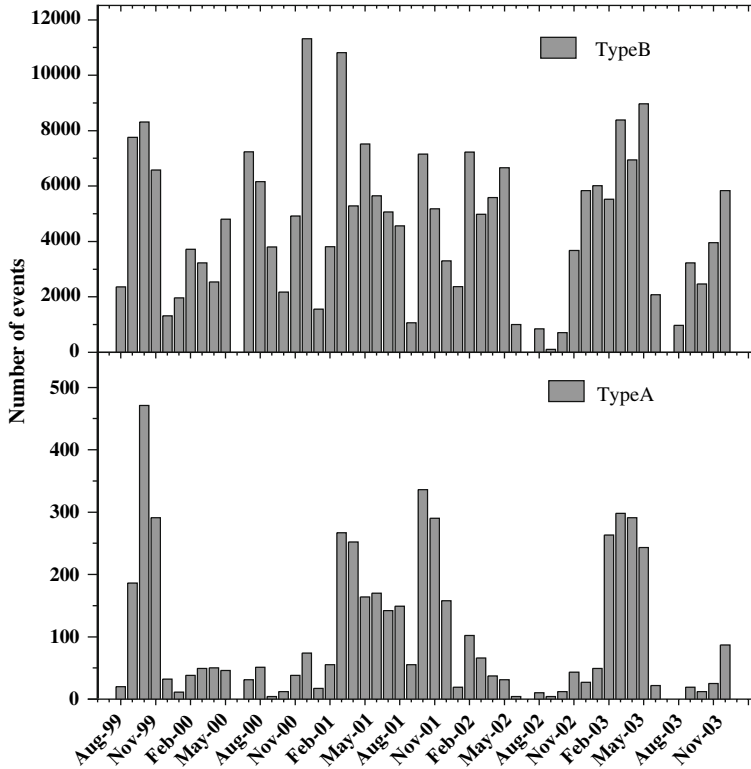
Figure 3
Monthly variation of number of seismic events at Poás volcano between August 1999 and December 2003.
Seismic data recorded at VPS-2 station which belonged to the National Seismic Network (RSN. ICE-UCR). (a)
A-Type seismicity and (b) B-Type seismicity.

the 2000 survey and the numbers of sampling sites were 182, 244 and 238 for the 2001, 2002 and 2003 surveys, respectively. The surveys were performed during the dry season and under similar meteorological conditions. These conditions ensured minimal soil gas variations from external changes and minimized disturbances from soil moisture changes during the measurements. Meteoric water may play an important role in gas chemistry since precipitations are variable at Poás, with dry and wet seasons not well defined (VASELLI *et al.*, 2003).

The sampling sites were selected in order to obtain a good spatial distribution. Soil gases were sampled at each sampling site together with ground temperature measurements at a depth of 30–50 cm using a metallic soil probe and 30 cc hypodermic syringes. The gas samples were introduced in 10 cc vacutainers (HINKLE and KILBURN, 1979) filled with deionised water. Later the water was displaced until the vacutainer was filled with the gas sample to avoid air contamination.

The composition of soil gas was determined in the laboratory by means of a gas double column micro-chromatograph VARIAN model CP2002P. Hydrogen was analyzed with a thermal conductivity detector (TDC) and a 20 m MolSieve 5 Å column using Ar as carrier gas. The temperatures of the column and injector were 60°C and 30°C, respectively, and the injection time was 20 msec. In this column, helium, oxygen and nitrogen were also determined. The detection limit for H_2 was estimated to be about 0.05 ppmV and the accuracy of the measurement about 2.5% on the basis of standard sample measurements. In another column (Poraplot-Q column of 10-m long, a TC detector, and helium as a carrier gas) we analyzed the soil CO_2 concentration. Soil temperature was also determined at each sampling site at a depth of 30–40 cm.

5. Results and Discussion

A summary of analytical results of the chemical composition for all soil gas samples is shown in Table 1. The soil H_2 concentration values from the survey carried out in 2000 ranged from 0.5 to 1.6 ppmV. To check whether the data came from a unimodal or a polymodal distribution, we applied the probability-plot technique (TENNANT and WHITE, 1959; SINCLAIR, 1974) to the entire soil H_2 data set of this survey. Soil H_2 concentration data showed a unimodal distribution, and the histogram of the log-normally distributed soil H_2 values (Fig. 4a) showed a skewness and kurtosis of 1.9 and 3.3, respectively. Only one distinct mode was found for the soil H_2 data (Fig. 4b), indicating the existence of one geochemical population, normal I (Table 2).

Soil H_2 values measured in the 2001, 2002 and 2003 surveys ranged from 0.4 to 1,910 ppmV, 0.9 to 7,060 ppmV and 0.2 to 270 ppmV, respectively (Table 2). Soil H_2 concentration data were also log-normally distributed, and the histograms of the log-normally distributed soil H_2 data showed a skewness and kurtosis of 1.5 and 2.3, 1.5 and 2.8, and 0.6 and 0.4 for the 2001, 2002 and 2003 surveys, respectively (Figs. 5a, 6a and 7a). At least three distinct modes were found for these three soil H_2 data sets: normal I, normal II and the mode comprised between both distributions (Figs. 5b, 6b and 7b).

Table 1

Statistics of soil gas data at Poás volcano, Costa Rica, for the 2000, 2001, 2002 and 2003 surveys

	2000			2001			2002			2003		
	Min.	Max.	Med.	Min.	Max.	Med.	Min.	Max.	Med.	Min.	Max.	Med.
He (ppmV)	4.2	6.2	5.6	4.4	6.0	5.4	4.8	6.1	5.8	3.5	7.6	6.3
H_2 (ppmV)	0.5	1.6	0.7	0.4	1910	20.5	1.0	7059	94.9	0.2	271	7.4
O_2 (%)	20.7	21.5	19.5	12.3	23.2	21.0	0.3	21.5	20.1	18.7	22.9	19.8
N_2 (%)	78.1	80.6	79.6	41.7	80.5	78.0	74.0	81.7	77.6	70.7	82.8	79.3
CO_2 (%)	0.03	58.5	0.92	0.03	53.9	1.9	0.03	80.9	2.2	0.03	4.28	0.22
T soil (°C)	7.2	92.7	17.9	8.3	92.0	18.1	10.0	94.3	18.1	10.4	93.3	19.4
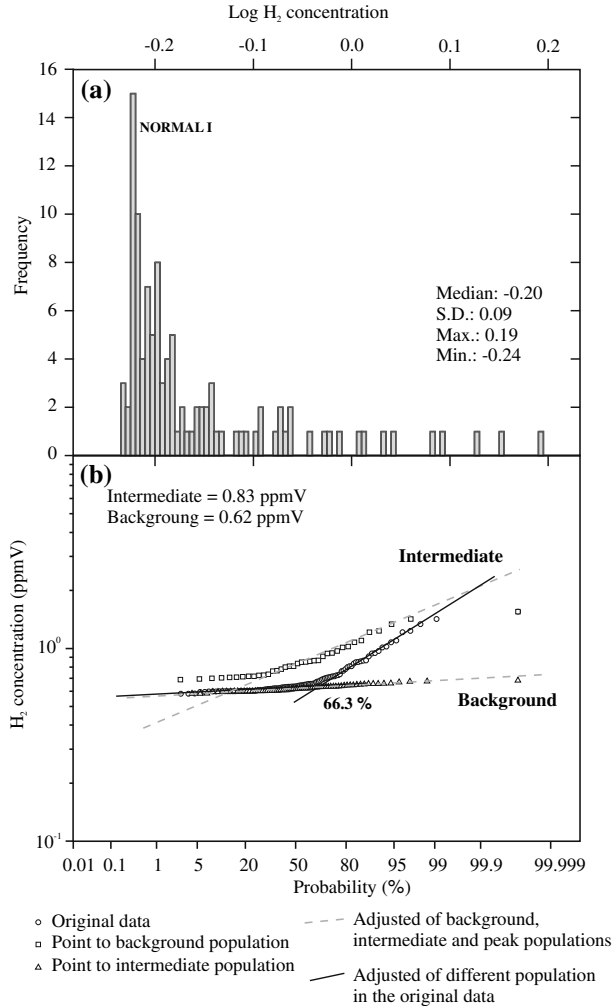
Figure 4

(a) Histogram of the log-transformed soil H_2 concentration values showing the existence of one mode within the sampling frequency distribution. (b) Probability plot of soil H_2 concentration values observed in 109 sampling sites at Poás volcano in 2000.

These three distinct populations are known as background, peak, and intermediate mixed-population, respectively (Table 2). The existence of more than one geochemical population of soil H_2 measured at the surface environment of Poás volcano suggests the occurrence of a deep perturbation of the volcanic-hydrothermal system.

Soil H_2 distribution maps for the four surveys were constructed based on the application of Stochastic Gaussian Simulation algorithms (SGS) provided by GSLIB program (DEUTSCH and JOURNEL, 1998). The steps of data treatment included: (1)

Table 2

Estimated parameters of partitioned populations for soil H_2 concentration values at Poás volcano, Costa Rica

	Population	No. of points	Proportion (%)	Average H_2 Concentration (ppmV)	Standard deviation 95% confidence interval (ppmV)
Poás volcano 2000	I	72	66.3	0.6	0.58–0.66
	II	37	33.7	0.8	0.51–1.4
	total	109	100		
Poás volcano 2001	I	36	20.2	0.6	0.31–1.2
	II	115	63.0	1.9	1.2–3.0
	III	31	16.8	12	0.34–405
	total	282	100		
Poás volcano 2002	I	85	35.2	4.1	2.6–6.4
	II	142	58.2	18	3.7–86
	III	17	6.6	394	47–3298
	total	244	100		
Poás volcano 2003	I	151	63.6	1.1	0.24–4.5
	II	81	19.1	7.1	1.5–34
	III	6	17.3	85	48–151
	total	238	100		

Declustering of the original data distribution, higher weights given to areas with less data density; (2) n-score normalization of the declustering data of soil H_2 concentration; (3) computation of the experimental variograms of n-score values; (4) definition of the variogram model and (5) simulations of the soil H_2 concentration using the SGS algorithm provided by GSLIB.

Experimental variograms and variogram models of soil H_2 concentration of 2000, 2001, 2002 and 2003 surveys are showed in Figure 8. The variogram models were adjusted with a spherical model for 2000, 2001 and 2003 surveys, whereas for the 2002 survey an exponential model was used. Parameters to define the variogram, nugget effect and range, are shown in Figure 8 (DEUTSCH and JOURNEL, 1998).

Soil H_2 distribution maps (Figs. 9 and 10) were constructed using the average of 50 simulations for each survey. H_2 distribution of the soil atmosphere showed a different pattern for each survey, with a clear increase in both the spatial extension of the anomalies and the magnitude of diffuse emission rates from 2000 to 2002 surveys. Most of the studied areas showed background values for soil H_2 concentration (0.6 ppmV, 2000; 0.6 ppmV, 2001; 4.1 ppmV, 2002, and 1.1 ppmV, 2003) in all the surveys. During the 2000 survey the highest soil H_2 concentrations were measured at the NE sector inside the active crater (Fig. 9) with values up to 1.2 ppmV. Other areas showing relatively high values of soil H_2 concentration were located at the N and SE part of the studied area, with values up to 1.0 ppmV. In 2001, an increase in the soil H_2 concentration was observed (Fig. 10a), with values reaching 400 ppmV, being mainly measured at the eastern wall of the active crater where an intensive fumarolic activity started in 2000 (MORA, 2001;
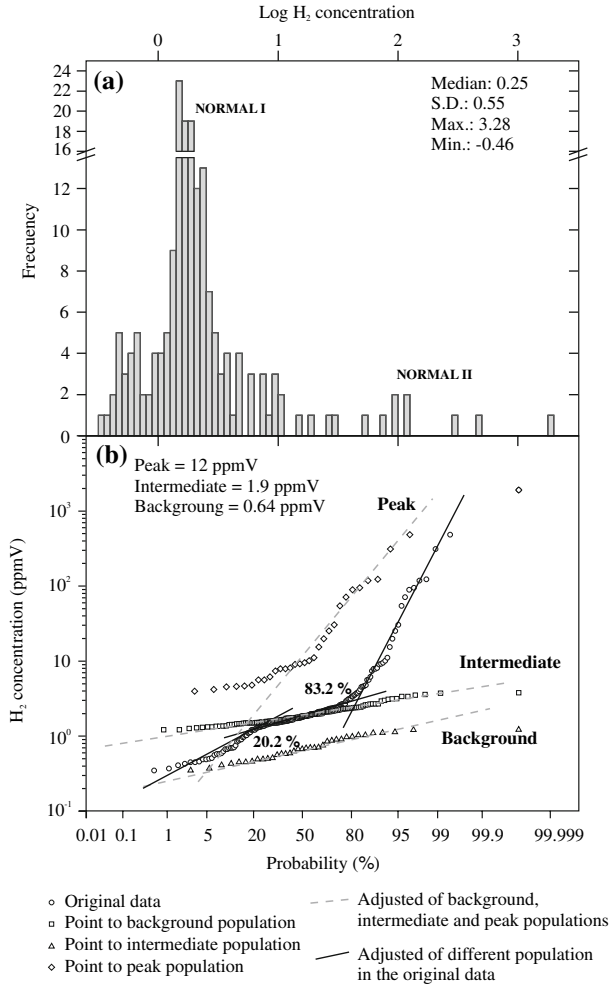
Figure 5

(a) Histogram of the log-transformed soil H_2 concentration values showing the existence of two modes within the sampling frequency distribution. (b) Probability plot of soil H_2 concentration values observed in 182 sampling sites at Poás volcano in 2001.

MORA *et al.*, 2003; FERNÁNDEZ *et al.*, 2003). Other areas registering high soil H_2 concentration (>120 ppmV) were S of the volcanic dome and inside the active crater. It is important to note the observed increase in the soil H_2 concentration (from 1.0 to 30 ppmV) from 2000 to 2001 at the volcanic dome.

During the 2002 survey, a general increase in the soil H_2 emissions was observed at the summit of Poás. The fumarolic activity remained strong at the eastern wall of the active crater with soil H_2 concentration values reaching 1,000 ppmV (Fig. 10b). The highest values (> 800 ppmV) were measured along the ledge located inside the eastern
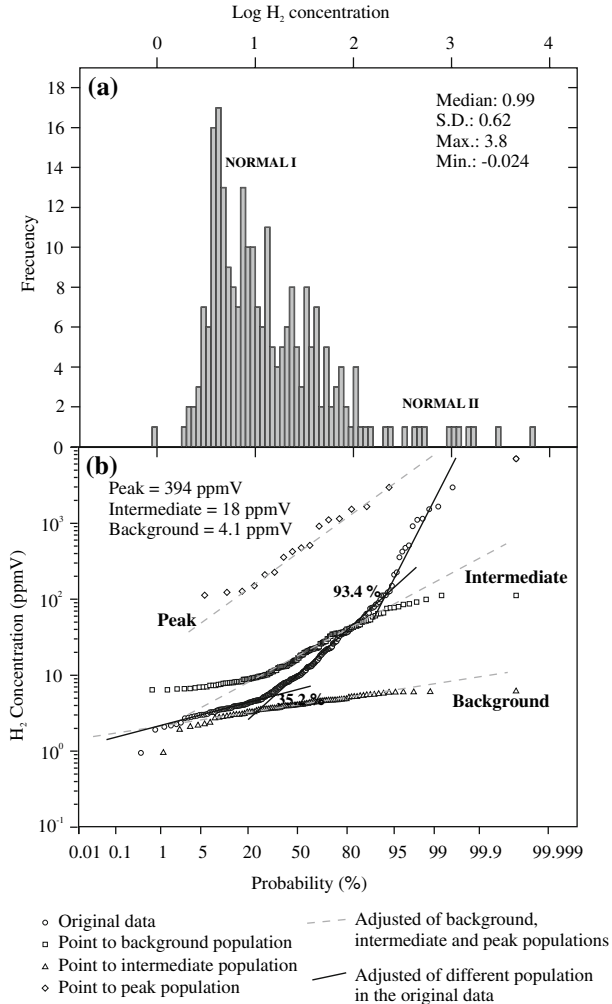
Figure 6
(a) Histogram of the log-transformed soil H_2 concentration values showing the existence of two modes within the sampling frequency distribution. (b) Probability plot of soil H_2 concentration values observed in 244 sampling sites at Poás volcano in 2002.

part of the active crater, where fumarolic activity started to increase at the end of 2000 (MORA et al., 2003). Other relatively high soil H_2 concentrations (>500 ppmV) were measured at the volcanic dome. These results showed a clear increase in the soil H_2 concentration at the summit of Poás volcano from 2000 to 2002. Other areas displaying relatively high values of soil H_2 concentration were located at the N part and NE of the studied area, with values up to 300 ppmV. Inspection of the soil H_2 concentration contour map for the 2003 survey shows a clear decrease in the diffuse emission of H_2 at Poás with
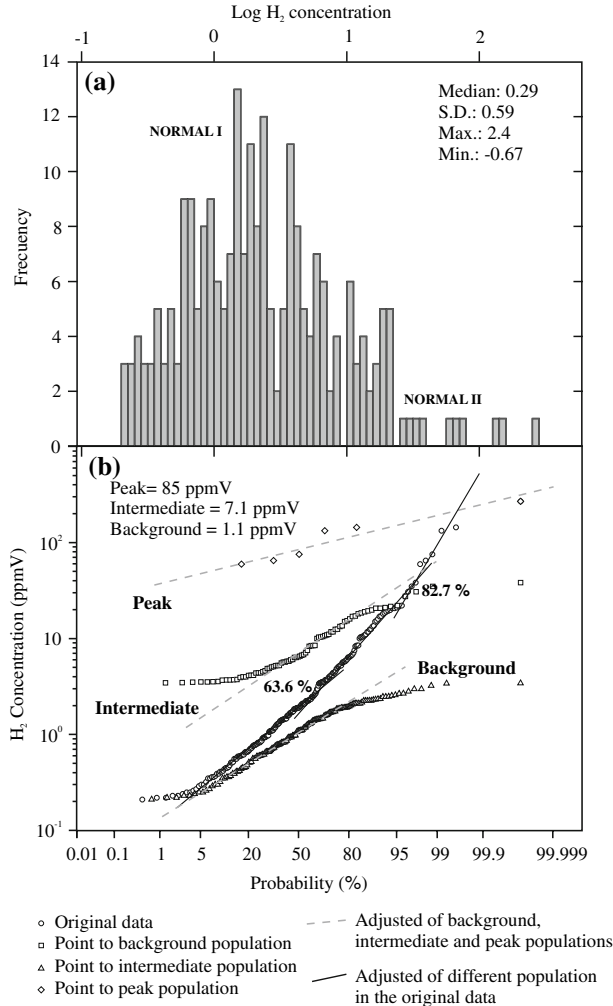
Figure 7

(a) Histogram of the log-transformed soil H_2 concentration values showing the existence of two modes within the sampling frequency distribution. (b) Probability Plot of soil H_2 Concentration values observed in 238 sampling sites at Poás volcano in 2003.

the existence of only one anomaly with soil H_2 concentration values up to 200 ppmV (Fig. 10c), at the NE sector inside the active crater with values up to 90 ppmV.

If we compare these results with the diffuse H_2 emission data reported for other volcanic areas such as Sabatini volcano, Italy (BERTRAMI *et al.*, 1990) and Teide volcano, Spain (HERNÁNDEZ *et al.*, 2000), soil H_2 emission values during the 2001 and 2002 surveys at Poás volcano are in general higher. BERTRAMI *et al.* (1990) measured soil H_2 concentrations between 5 and 52 ppmV with 10% of the total data over the detection
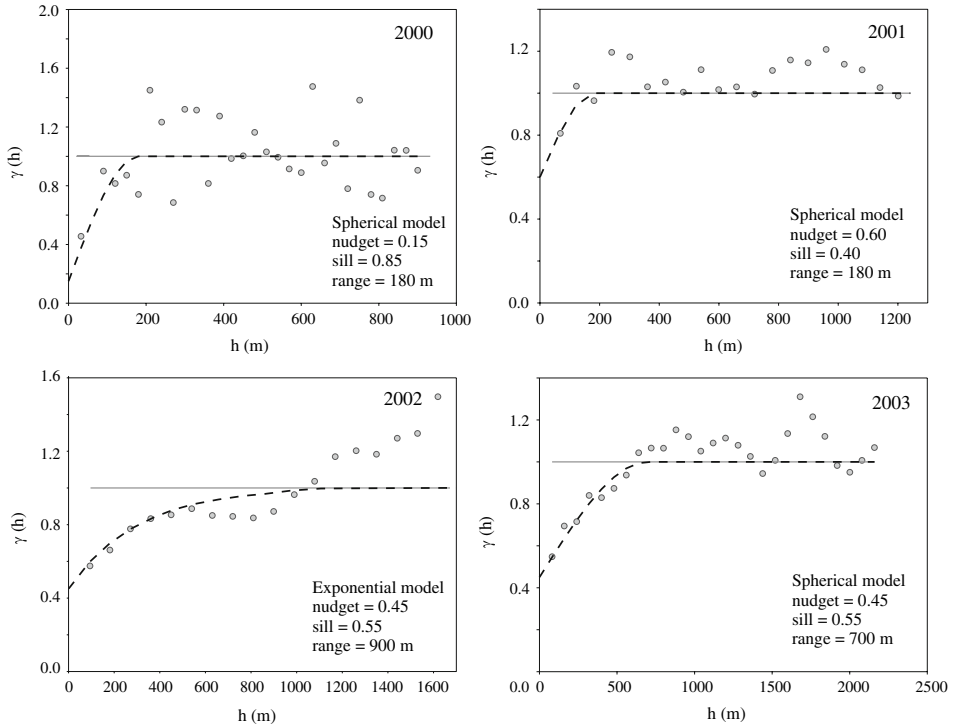
Figure 8.
Experimental variogram (grey points) and variogram model (dashed line) of soil H_2 concentration at Poás volcano.

limit, whereas HERNÁNDEZ et al. (2000) measured soil H_2 concentration values between the air content (0.5 ppmV) and 620 ppmV. The maximum soil H_2 values measured at Poás were 1,910, 7,059 and 271 ppmV in 2001, 2002 and 2003, respectively. These differences may be related to the level of volcanic activity of each volcanic system. Other geochemical and geophysical data at these two volcanic systems support these observations (DE RITA et al., 1983; ALBERT-BELTRÁN et al., 1990; PÉREZ et al., 1992; HERNÁNDEZ, 1997; KARNER et al., 2001).

Soil temperature measured at Poás showed a similar temporal variation to that observed for the diffuse emission of H_2, with an increase in 2002. Soil temperatures ranged from 7.2 to 92.7°C in 2000, 8.3 to 92.0°C in 2001, 10 to 94.3°C in 2002 and 10.4 to 101°C in 2003. Experimental variograms and variogram models of soil temperature data for 2000, 2001, 2002 and 2003 surveys are depicted in Figure 11. The variogram models for the 2000, 2001 and 2002 surveys were adjusted with a spherical model, whereas the variogram of the 2003 survey was adjusted with a hole effect model. Most of the studied area exhibited soil temperatures up to 20°C except inside the summit crater and especially next to the fumaroles, where higher temperatures were measured during all
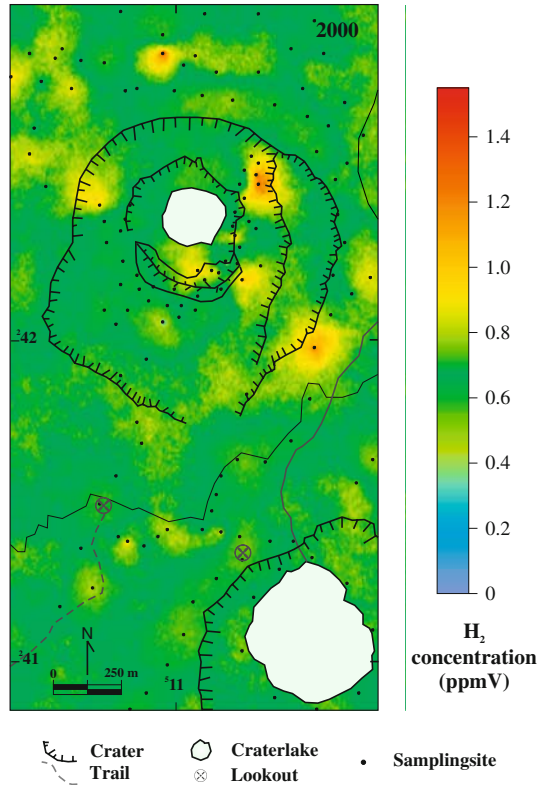
Figure 9

Contour map of the soil H_2 concentration values (ppmV) measured at Poás volcano, Costa Rica (April 2000). Dots indicate sampling sites.

these studies (Fig. 12). Thermal anomalies at Poás volcano occur mainly where the fumarolic activity is stronger. In 2002, an increase at the areas affected by thermal anomalies was observed together with the occurrence of the strongest fumarolic activity during all this study, affecting the east summit rim and the ledge located inside the active crater (VASELLI *et al.*, 2003). During 2003, a general decrease in ground temperature was observed at Poás with respect to the 2001 and 2002 surveys. Heat flow, steam and acidic gas emissions were clearly identified along those areas of high soil H_2 emission (MARTÍNEZ *et al.*, 2003; MELIÁN *et al.*, 2002, 2003).

Temporal and spatial distribution of soil H_2 evidenced a pattern similar to the observed for other gases such as CO_2 (MELIÁN *et al.*, 2001). The correlation coefficients between soil H_2 and CO_2 concentrations, and soil temperature are shown in Table 3. Soil H_2 data of the 2000 survey showed a poor correlation factor with the soil CO_2 concentration ($r^2 = 0.290$), whereas for 2001, 2002 and 2003 the correlation coefficients were 0.473, 0.732 and 0.741, respectively. During 2001 and 2002 an increase of the
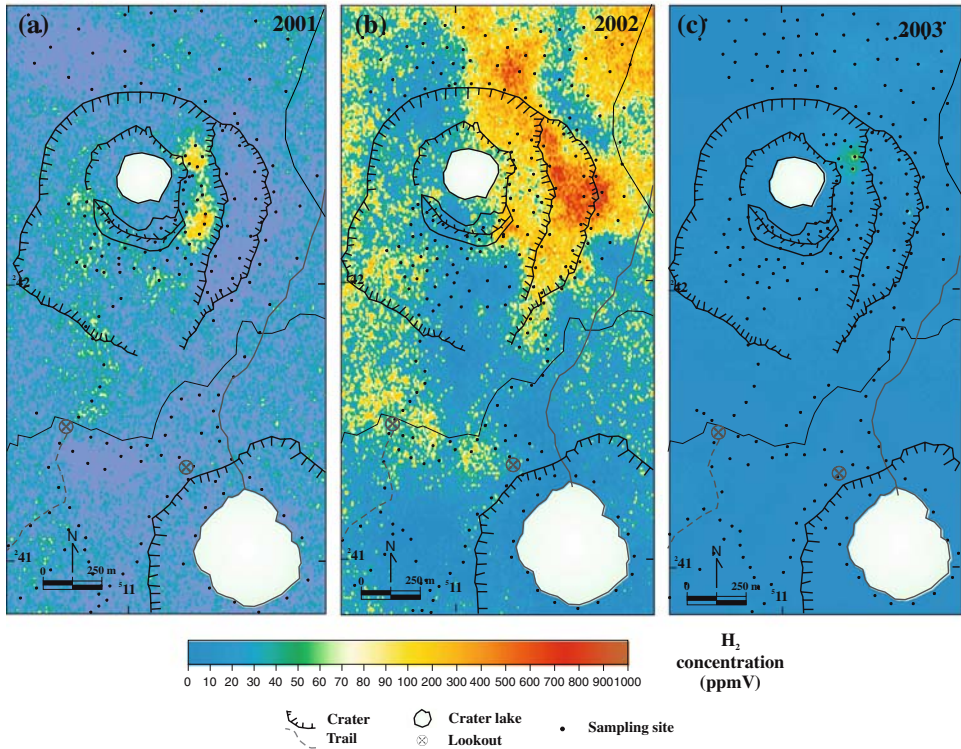
Figure 10

Contour map of the soil H_2 concentration values (ppmV) measured at Poás volcano, Costa Rica (a) March 2001, (b) March 2002 and (c) April 2003. Dots indicate sampling sites.

correlation coefficients between soil H_2 and soil temperature was observed, varying from 0.073 in 2000 to 0.477, 0.478 and 0.557 in 2001, 2002 and 2003, respectively. The spatial correlation between soil CO_2 and soil temperature manifests the same behavior, increasing from 0.056 in 2000 to 0.610, 0.610 and 0.244 in 2001, 2002 and 2003, respectively. These observations suggest that the increase in gas emission, steam and heat flow might be related to changes in the shallow magmatic-hydrothermal system of Poás.

RYMER *et al*. (2005) reported new microgravity data from the active crater of Poás during the period 2002–2004. They found during this study a significant increase in the microgravimetry in the western and southern areas of the active crater, whereas a sharp decrease was observed east and northeast of the same area. The observed decrease in microgravimetry was explained in terms of drainage of cooling degassed magma beneath the eastern part of the lake and the possible magma intrusion below the southwestern part of the lake during the period 1998–2004. VASELLI *et al*. (2003) studied the gas composition of the fumarolic gases at Poás during 1998–2001, finding a considerable temporal variability in its chemical composition. During this period, dissolved gases in
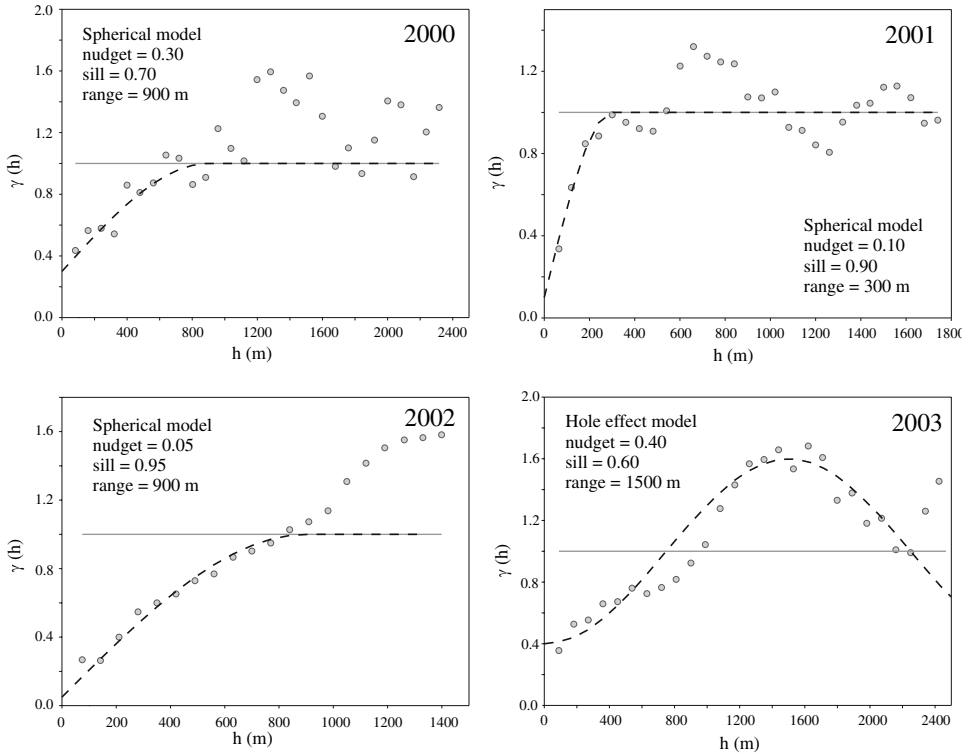
Figure 11

Experimental variograms (grey point) and variograms model (dashed line) of soil T.

the acidic waters of crater lake and fumaroles gases showed high H_2 contents of up to 1.2%vol, made possible magma intrusion below the southwestern part of the lake during the period 1998–2004 become related to variations of both temperature and redox conditions of the magmatic-hydrothermal system. The occurrence of fumarolic activity and the observed soil H_2 anomalies at the northern part of the active crater during the period 2000–2004, are surface evidence of the changes which occurred in the magmatic-hydrothermal system of Poás. Magma drainage beneath this sector of the active crater together with the observed mass loss might have enhanced the circulation and entrance of water favoring the hydrothermal alteration and changing the redox conditions in the shallow environment of the system. They assumed that these variations were a consequence of the permeability changes due to hydrofracturing in the system.

During September-November 1999, high A-type seismicity was observed at Poás volcano, maybe related to stress release from the volcanic edifice. During this period, an increase in the B-type seismicity was also observed. This increase was interpreted in terms of magma intrusion enhancing hydrofracturing, which favored the drainage of water into the system, increasing the reducing conditions and producing intense fumarolic
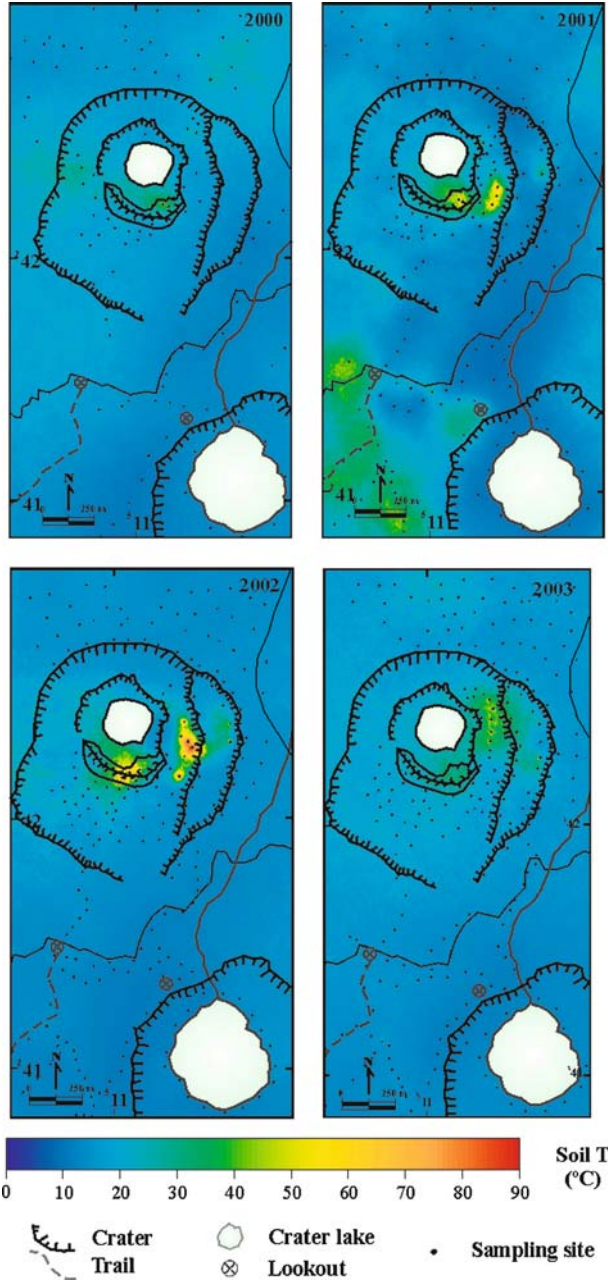
Figure 12
Contour map of the soil temperature measured at 20-cm depth at Poás volcano, Costa Rica (2000, 2001, 2002 and 2003). Dots indicate sampling sites.

Table 3

Correlation coefficients between soil H_2 and CO_2 concentration and soil temperature at Poás, Costa Rica

	2000		2001		2002		2003	
	H_2 (ppmV)	CO_2 (ppmV)	H_2 (ppmV)	CO_2 (ppmV)	H_2 (ppmV)	CO_2 (ppmV)	H_2 (ppmV)	CO_2 (ppmV)
CO_2 (ppmV)	0.290	1.0	0.473	1.0	0.732	1.0	0.741	1.0
T(°C)	0.073	0.056	0.477	0.610	0.478	0.610	0.557	0.244

activity at the south part of the active crater (VASELLI *et al.*, 2003; RYMER *et al.*, 2005). Between January 2000 and February 2001, no significant A-type seismicity was observed at Poás volcano. More reducing conditions in the magmatic-hydrothermal system of Poás were assessed from the chemical composition of fumarolic gases (VASELLI *et al.*, 2003), starting to appear from strong fumarolic activity along the eastern rim of the active crater. The persistent fumarolic activity was explained in terms of water excess in the system. The soil H_2 concentrations measured at the surface environment of the summit at Poás during 2000 showed low concentration values close to the air (average value of 0.7 ppmV), suggesting that gases escaped preferentially through breaks and conduits opened due to stress changes. Between March 2001 and November 2002, A-type seismicity increased strongly again, coupled with a peak on the B-type seismicity, indicating a new stage of the volcanic activity level and may be related to pressure changes on the volcanic fluids below SW of the crater's lake . At this time, a significant increase in the soil H_2 concentration was observed, being measured during the March 2002 soil gas survey as the highest concentration values during this study (7,059 ppmV) with an average value of 95 ppmV. Even when in February-May 2003 a new increase of the A-type seismicity was observed, soil H_2 decreased to an average value of 7.4 ppmV. These observations suggest that the shallow hydrothermal system of Poás volcano degassed, keeping the heat and mass transport required to maintain persistent fumarolic activity. The seismic events may have resulted from the hydrofracturing of carapace of the magma body with a consequent increase in the volatiles flux in the system. Because of its high diffusivity, most of the H_2 might have escaped in the atmosphere in 2002 due to the observed change in the volcanic-hydrothermal system.

In addition, spatial distribution of peak values of soil H_2 concentration at the eastern sector of the summit crater followed a N-S trending parallel to a local faulting system. Generally soils at the areas of high soil H_2 concentration are characterized by high temperatures (T > 60°C) whereas the areas with low soil H_2 concentration are characterized by lower temperatures (20°C T). Assuming a common origin for the H_2 discharged from the fumaroles and the areas having relatively high H_2 diffuse degassing, water-rock interaction and redox conditions of the magmatic-hydrothermal system seem to be the main mechanisms controlling the observed soil H_2 anomalies at the crater of Poás volcano. This positive correlation between soil H_2 concentration and temperatures in soils is supported by both spatial distribution of soil H_2 concentration and soil

temperature maps, suggesting that part of the energy coming from the shallow heat source beneath the Poás volcano (ROWE *et al.*, 1995) is used to heat the water. Drainage of water into the system together with vapor excess from the hydrothermal system seem to be responsible for the reducing conditions. The observed increase of the soil temperatures at the surface environment in 2002 seems to be an expression of an increase of heat flux related to a possible magma intrusion below the Southwestern part of the lake during the period 1998–2004 (RYMER *et al.*, 2005), which might have enhanced water-rock interaction and favored the production of H_2. The presence of fumarolic fields linked to the fracturing system suggests that permeable structures act as preferential pathways to the surface for deep gases.

The observed temporal variations in the diffuse H_2 emission together with other gases and volatiles (MELIÁN *et al.*, 2001; NOLASCO *et al.*, 2003) and soil temperature suggest that H_2 at the surface environment of Poás volcano is not coming only from the thermal reactions between the meteoric water infiltrated through fissures and the rocks beneath Poás but also from the additional contribution of deep-seated gases to the diffuse degassing. Changes in the physical and chemical conditions at depth in a volcanic-hydrothermal system can produce an increase in the gas and volatile emission to the surface (HERNÁNDEZ *et al.*, 2001a).

6. Conclusions

Diffuse H_2 degassing data from four soil gas surveys carried out at Poás volcano during the period 2000–2003 proved useful in evaluating the physical-chemical changes observed in the shallow magmatic-hydrothermal system of Poás and related to the possible magma intrusion beneath the SW and crater lake during the same period. The magma body at depth and the superficial aquifer control and regulate the volcanic activity of Poás volcano. The magmatic intrusion which occurred in this period is associated with the transport of mass and heat from depth. Boiling of the hydrothermal aquifer might have favored water-rock interaction processes, which seem to be the main factor controlling the observed spatial and temporal changes in the soil H_2 at Poás. Meteoric water infiltrated into the system and vapor excess related to an increase of heat flux due to a possible magma intrusion below the Southwestern part of the lake may have changed the redox conditions favoring H_2 production. The observed changes also occurred when fumarolic activity was stronger at the active crater.

The good spatial correlation between soil H_2 concentration and soil temperature during the period of study indicates the existence of areas of high heat flow which may have a higher permeability and therefore better connection with the system at depth. The observed temporal variations in the intensity of diffuse H_2 degassing makes diffuse degassing studies at Poás a useful tool to distinguish between steady-state degassing due to magma convection and gas pulses due to magma intrusion and/or changes in the pressure of the fluids in the magmatic-hydrothermal system.

Acknowledgements

REFERENCES

AIUPPA, A., CALECA, A., FEDERICO, C., GURRIERI, S., and VALENZA, M. (2004), Diffuse degassing of carbon dioxide at Somma-Vesuvius volcanic complex (Southern Italy) and its relation with regional tectonics, J. Volcanol. Geotherm. Res. 133, 55–79.

ALBER-BELTRÁN, J., ARAÑA, V., DIEZ, J., and VALETIN, A. (1990), *Physical-chemical conditions of the Teide volcanic system (Tenerife, Canary Islands)*, J. Volcanol. Geotherm. Res. *43*, 321–332.

ALLARD, P., BURTON, M., and MURÈ, P. (2005), Spectroscopic evidence for a lava fountain driven by previously accumulated magmatic gas, Nature 433, 407–409.

ALLARD, P., CARBONELLE, J., DAJLEVIC, D., BRONCE, J., MOREL, P., ROBE, M., MAURENADS, J., FAIVRE-PIERRET, R., MARTIN, D., SABROUX, J., and ZETTWOOG, P. (1991), *Eruptive and diffuse emissions of CO$_2$ from Mount Etna*, Nature *351*, 387–391.

ARAÑA, V., and ORTIZ, R., Vulcanología XV. Consejo Superior Invest. Cient. (ed. Rueda) (Madrid 1984) 150pp.

BAUBRON, J., ALLARD, P., and TOUTAIN, J. (1990), *Diffuse volcanic emissions of carbon dioxide from Vulcano Island, Italy*, Nature 344, 51–53.

BERTRAMI, R., BUONASORTE, G., CECCARELLI, A., LOMBARDI, S., PIERI, S., and SCANDIFFIO, G. (1990), *Soil gas in geothermal prospecting: Two case histories (Sabatini volcanoes and Alban Hills, Latium*, Central Italy, J. Geophys. Res. *95*, 21475–21481.

BROWN, G., DOWDEN, J., KAPADIA, P., STEVENSON, D., BARQUERO, J., and MORALES, L. (1989), *Energy budget analysis for Poás Crater Lake: Implications for predicting volcanic activity*, Nature *339*, 370–373.

BURTON, M., ALLARD, P., MURÈ, F., and OPPENHEIMER, C., (2003), *FTIR remote sensing of fractional magma degassing at Mt. Etna, Sicily*. In *Volcanic Degassing*, Geolog. Soc. Spec. Public. *213*, 281–293.

CARAPEZZA, M.L., INGUAGGIATO, S., BRUSCA, L., and LONGO, M. (2004), *Geochemical precursors of the activity of an open-conduit volcano: The Stromboli 2002–2003 eruptive events*, Geophys. Res. Lett. *31*, L07620, doi:10.1029/2004GL019614.

CASADEVALL, T., ROSE, W., GERLACH, T., GREENLAND, L., EWERT, J., WUNDERMAN, R., and SYMONDS, R. (1983), *Gas emissions and the eruptions of Mount St. Helens through 1982*, Science *221*, 1383–1385.

CASERTANO, L., BORGIA, A., CIGOLINI, C., MORALES, L., GOMEZ, M., and FERNÁNDEZ, J. (1987), *A integrated dynamic model for the volcanic activity at Poás Volcano, Costa Rica*, Bull. Volcanol. *49*, 588–598.

CASERTANO, L., BORGIA, A., CIGOLINI, C., MORALES, L., MONTERO, W., GÓMEZ, M., and FERNÁNDEZ, J. (1985), *Investigaciones geofísicas y características geoquímicas de las aguas hidrotermales: Volcán Poás, Costa Rica*, Geofis. Int. *24* (2), 315–332.

CHIODINI, G., FRONDINI, F., CARDELLINI, C., GRANIERI, D., MARINI, M., and VENTURA, G. (2001), *CO$_2$ degassing and energy release at Solfatara volcano, Campi Flegrei, Italia*, J. Geophys. Res. *106* (B8), 16.213–16,221.

CHIODINI, G., CIONI, R., GUIDI, M., RACO, B., and MARINI, M. (1998), *Soil Flux measurements in volcanic and geothermal areas*, Appl. Geochem. *13* (5), 543–552.

CHIODINI, G., FRONDINI, F., and RACO, B. (1996), Diffuse emission of CO$_2$ from the Fossa crater, Vulcano Island (Italy), Bull. Vulcanol. *48*, 41–50.

D'ALESSANDRO, W., and PARELLO, F. (1997), Soil gas prospection of He, ^{222}Rn and CO$_2$: Vulcano Porto area, Aeolian Islands, Italy, Appl. Geochem. 12, 213–224.

DE RITA, D., FUNICIELLO, R., ROSSI, U., and SPOSATO, A. (1983), *Structure and evolution of the Sacrofano-Baccano Caldera, Sabatini Volcanic Complex, Rome*, J. Volcanol. Geotherm. Res. *17*, 219–236.

DEUTSCH, C. and JOURNEL, A., *GSLIB: Geostatistical Software Library and Users Guide*, (2nd Ed., Oxford University Press) (New York 1998) 369 pp.

FERNÁNDEZ, E., DUARTE, E., SÁENZ, W., MALAVASI, E., BARBOZA, V., MARTÍNEZ, M., and VALDÉZ, J. (2003), *Volcanic gas condensates from Poás volcano 1999–2000. Eighth Field Workshop on Volcanic Gases*, IAVCEI and CCVG, 30pp.

FERNÁNDEZ, M. (1990), La actividad del Volcán Poás (Costa Rica): *Análisis sísmico durante el periodo 1980– 1989. Tesis de Licenciatura. Escuela Centroamericana de Geología*, Univ. Costa Rica, 185.

FERRUCCI, F. In: (McGuire, W.J. Kilburn, C Murray, J.B. eds.) *Seismic Monitoring at Active Volcanoes* (UCL, London 1995), 60, 92.

FRONDINI, F., CHIODINI, G., CALIRO, S., CARDELLINI, C., GRANIERI, D., and VENTURA, G. (2004), *Diffuse CO_2 degassing at Vesuvio, Italia*, Bull. Volcanol. *66*, 642–651. doi:10.1007/s00445–004-0346.

GALLE, B., OPPENHEIMER, C., GEYER, A., McGONIGLE, A., EDMONDS, M., and HORROCKS, L. (2002), *A miniaturised ultraviolet spectrometer for remote sensing of SO_2 fluxes: A new tool for volcano surveillance*, J. Volcanol. Geotherm. Res. *119*, 241–254.

GERLACH, T. DOUKAS, M., McGEE, K., and KESSLER, R. (2001), Soil efflux and total emission rates of magmatic CO_2 at the Horseshoe tree kill, Mammoth Mountain, California, 1995–1999, Chem. Geology *177*, 101–116.

GERLACH, T., and GRAEBER, E. (1985), *Volatile budget of Kilauea Volcano*, Nature *313*, 273–277.

GIAMMANCO, S., INGUAGGIATO, S., and VALENZA, M. (1998), *Soil and fumarole gases of Mount Etna: geochemistry and relations with volcanic activity*, J. Volcanol. Geoth. Res. *81*, 297–310.

GIGGENBACH, W., *Chemical composition of volcanic gases*. In *Monitoring and Mitigation of Volcanic Hazards* (ed. Scarpa and R. Tilling) (Springer-Verlag, Berlin-Heidelberg 1996) pp. 221–256.

HERNÁNDEZ, P., NOTSU, K., TSURUMI, M., MORI, T., OHNO, M., SHIMOIKE, Y., SALAZAR, J., and PÉREZ, N. (2003), *Carbon dioxide emissions from soils at Hakkoda, North Japan*, J. Geophys. Res. *108*, doi:10.1029/ 2002JB001847.

HERNÁNDEZ, P., NOTSU, K., SALAZAR, J., MORI, T., NATALE, G., OKADA, H., VIRGILI, G., SHIMOIKE, Y., SATO, M., and PÉREZ, N. (2001a), *Carbon dioxide degassing by advective flow from Usu Volcano, Japan*, Science *292*, 83–86.

HERNÁNDEZ, P., SALAZAR, J., SHIMOIKE, Y., MORI, T., NOTSU, K., and PÉREZ, N. (2001b), *Diffuse emission of CO_2 from Miyakejima Volcano, Japan*, Chem. Geol. *177*, 175–185.

HERNÁNDEZ, P., PÉREZ, N., SALAZAR, J., SATO, M., NOTSU, K., and WAKITA, H. (2000), *Soil gas CO_2, CH_4 and H_2 distribution in and around Las Cañadas Caldera, Tenerife, Canary Islands, Spain*, J. Volcanol. Geotherm. Res. *103*, 425–438.

HERNÁNDEZ, P. (1997), Estudio geoquímico de gases y volátiles en la Caldera de Las Cañadas del Teide, Tenerife, Islas Canarias España, Univ. Autónoma de Madrid, Tesis Doctoral, 409 pp.

HINKLE, M., and KILBURN, J. (1979), *The use of vacutainer tube for collection of soil sample for helium analysis*, U. S. Geol. Surv. Open File Rep. 79, 1441.

HIRABAYASHI, J., OSSAKA, J., and OZAWA, T. (1986), *Geochemical study on volcanic gases at Sakurajima Volcano, Japan*, J. Geophys. Res. *91*, 12167–12176.

KARNER, D., MARRA, F., and RENNE, P. (2001), The history of the Monti Sabatini and Alban Hills volcanoes: Groundwork for assessing volcanic-tectonic hazards for Rome, J. Volcanol. Geotherm. Res. 107 (1–3), 185–219.

KAZAHAYA, K., TAKAHASHI, M., OHSUMI, T., SOYA, T., ANDO, N., HIRABAYASHI, J., KUSAKABE, M., and HAMADA, R. (1988), *Chemical monitoring of volcanic gas from crater of Mt. Nihara, Izu-Oshima*, Bull. Volcanol. Soc. Jpn. Ser. *2* (33), 13–19 (in Japanese, with English abstract).

LOMBARDI, S., and REIMER, G. (1990), *Radon and helium in soil gases in the Phlegraean Fields, Central Italy*, Geophys. Res. Lett. *17* (6), 849–852.

MARTÍNEZ, M., FERNÁNDEZ, E., VALDÉS, J., BARBOZA, V., VAN DER LAAT, R., DUARTE, E., MALAVASSI, E., SANDOVAL, L., BARQUERO, J., and MARINO, T. (2000), *Chemical evolution and volcanic activity of the active crater lake of Poás volcano, Costa Rica, 1993–1997*, J. Volcanol. Geotherm. Res. 97, 127–141.

MARTÍNEZ, M., VAN BERGEN, M., FERNÁNDEZ, E., MALAVASSI, E., MARINO, T., BARQUERO, J., VALDÉS, J., BARBOZA, V., DUARTE, E., VAN DER LAAT, R., SÁENZ, R., SAÉNZ, W., and CHAVARÍA, F. (2003), *Volcanic gas condensates from Poás volcano 1999–2000*, Eighth Field Workshop on Volcanic Gases. IAVCEI and CCVG, 45pp.

MATSUO, S., OSSAKA, J., HIRABAYASHI, J., OZAWA, T., and KIMISHIMA, K. (1982), *Chemical nature of volcanic gases of Usu volcano in Japan*, Bull. Volcanol. *5*, 261–264.

MATSUO, S., SUZUKI, T., KUSAKABE, M., WADA, H., and SUZUKI, M. (1975), *Isotopic and chemical composition of volcanic gases from Satsuma-Iwojima, Japan*, Geochem. J. *8*, 165–173.

Matsuo, S. (1960), *On the origin of volcanic gases*, J. Earth Science 8, 222–245.

Matsushima, N. (2005), H₂O emission rate by the volcanic plume during the 2000–2002 Miyakejima volcanic activity, Geophys. Res. Lett., *32*, L14307, doi:10.1029/2005GL023217.

McGee, K., Sutton, A., Elias, T., Doukas, M., and Gerlach, T. (2006), *Puhimau Thermal Area: A Window into the Upper East Rift Zone of Kilahuea Volcano, Hawaii?* Pure Appl. Geophys. *163*, 837–851.

McGonigle, A., Inguaggiato, S., Aiuppa, A., Hayes, A., and Oppenheimer, C. (2005), Accurate measurement of volcanic SO₂ flux: Determination of plume transport speed and integrated SO₂ concentration with a single device, Geochem. Geophys. Geosyst. 6, Q02003, doi:10.1029/2004GC000845.

Melián, G., Galindo, I., Pérez, N., Hernández, P., Salazar, J., Fernández, M., Ramírez, C., Mora, R., and Alvarado, G. (2003), *Emisión Difusa de Hidrógeno en el Volcán Poás, Costa Rica, América Central*. en: Soto, G.J. and Alvarado, G.E. (eds): *La Vulconología y su entorno geoambiental. Número especial*, *Revista Geológica de América Central 30*, 167–177.

Melián, G., Galindo, I., Salazar, J., Pérez, N., Hernández, P., Fernández, M., Ramírez, C., Mora, R., and Alvarado, G. (2002), *Hydrogen emission from Poás volcano, Costa Rica, Central America: A premonitory geochemical signature of volcanic unrest?* EOS, Transac. Am. Geophy. Union 83, F1489.

Melián, G., Galindo, I., Salazar, J., Hernández, P., Pérez, N., Ramírez, C., Fernández, M., and Notsu, K. (2001), *Spatial and secular variations of diffuse CO₂ degassing from Poás Volcano, Costa Rica, Central America*, EOS, Transac. American. Geophys. Union 82, F1332.

Minakami, T. (1969), *Earthquake originating from volcanoes at XVIII*, Covn. ASS. Geof. Ital., Napoli 1–4 October.

Mora, R., Ramírez, C., and Fernández, M. (2003), *La actividad de los volcanes de la Cordillera Central, 1998–2002, Costa Rica*. In (Soto, G.J. and Alvarado, G.E. eds), *La Vulconología y su entorno geoambiental. Número especial*, Revista Geológica de América Central 30, 189–197.

Mora, R. (2001), Informe semestral de la actividad volcánica en la Cordillera Volcánica Central Enero-Junio 2001. Informe Interno, Sección de Sismología, Volcanología y Exploración Geofísica, Escuela Centroamérica de Geología, Univ. Costa Rica. 35 pp.

Mori, T., and Notsu, K. (1997), Remote CO, COS, CO₂, SO₂, HCl detection and temperature estimation of volcanic gas, Geophys. Res. Lett. *24*, 2047–2050.

Mori, T., Notsu, K., Tohjima, Y., and Wakita, H. (1993), *Remote detection of HCl and SO₂ in volcanic gas from Unzen Volcano, Japan*, Geophys. Res. Lett. 20, 1355–1358.

Noguchi, K., and Kamiya, H., (1963), Prediction of volcanic eruption by measuring the chemical composition and amount of gases, Bull. Volcanol. 26, 367–378.

Nolasco, D., Melián, G., Galindo, I., Salazar, J., Pérez, N., Hernández, P., Fernández, M., Ramírez, C., Mora, R., and Alvarado, G. (2003), *Diffuse mercury degassing at Poás Volcano, Costa Rica, Central America, AGU Fall Meeting 2003, San Francisco, USA. EOS*, Transac. Am. Geophys. Union 84, 46, F11513.

Oppenheimer, C, Francis, P., and Maciejewski, A. (1998), *Spectroscopic observation of HCl degassing from Soufriere Hills volcano, Montserrat*, Geophys. Res. Lett. 25, 3689–3692.

Pérez, N., Hernández, P., Padrón, E., Cartagena, R., Olmos, R., Barahona, F., Melián, G., Salazar, P., and López, D. (2006), *Anomalous Diffuse CO₂ Emission prior to the January 2002 Short-term Unrest at San Miguel Volcano, El Salvador, Central America*, Pure Appl. Geophys. 163 (4), 883–896.

Pérez, N., Wakita, H., Lolok, D., Patia, H., Talai, B., and Mckee, C. (1996), *Anomalous soil gas CO₂ concentrations and relation to seismic activity at Rabaul Caldera, Papua New Guinea*, Geogaceta 20, 1000–1003.

Pérez, N., Williams, S., Sano, Y., Carracedo, J., Coello, J., and Wakita, H. (1992), *Helium-3 emision from The Canarian Volcanoes, Spain*, III *Congreso Geológico de España y VII Congreso Latinoamericano de Geología*, Salamanca, actas tomo *1*, 468–472.

Rogie, J., Kerrick, D., Sorey, M., Chiodini, G., and Galloway, D. (2001), *Dynamics of carbon dioxide emission at Mammoth Mountain, California*, Earth Planet. Sci. Lett. *188*, 535–541.

Rowe, G., Brantley, S., Fernández, J., and Borgia, A. (1995), *The chemical and hydrologic structure of Poás volcano, Costa Rica*, J. Volcanol. Geotherm. Res. *64*, 233–267.

Rowe, G., Brantley, S., Fernández, M., Fernández, J., Barquero, J., and Borgia, A. (1992a), *Fluid-volcano interacting in an active stratovolcano: the Crater Lake system of Poás volcano, Costa Rica*, J. Volcanol. Geotherm. Res. *49*, 23–51.

Rowe, G., Ohsawa, S., Takano, B., Brantley, S., Fernández, J., and Barquero, J. (1992b), *Using Crater Lake chemistry to predict volcanic activity at Poás volcano, Costa Rica*, Bull. Volcanol. *54*, 494–503.

RYMER, H., LOCKE, C., BRENES, J., and WILLIAMS-JONES, G. (2005), *Magma plumbing processes for persistent activity at Poás volcano*, Geophys. Res. Lett. *32*, L08307, doi: 10.1029/2004GL22284.

RYMER, H., CASSIDY, J., LOCKE, C., BARBOZA, M., BARQUERO, J., BRENES, J., and VAN DER LAAT, R. (2000), *Geophysical studies of the recent 15-year eruptive cycle at Poás volcano, Costa Rica*, J. Volcanol. Geotherm. Res. *97*, 425–442.

RYMER, H., and BROWN, G. (1989), *Gravity changes as a precursor to volcanic eruption at Poás volcano, Costa Rica*, Nature *342*, 902–905.

SALAZAR, J., PÉREZ, N., HERNÁNDEZ, P., SORIANO, T., BARAHONA, F., OLMOS, R., CARTAGENA, R., LÓPEZ, D., LIMA, N., MELIÁN, G., PADRÓN, E., GALINDO, I., and NOTSU, K. (2002), *Precursory diffuse carbon dioxide degassing related to a 5.1 magnitude earthquake in El Salvador, Central America*, Earth Planet. Sci. Lett. *205*, (1–2), 81–89.

SALAZAR, J., HERNÁNDEZ, P., PÉREZ, N., MELIÁN, G., ÁLVAREZ, J., SEGURA, F., and NOTSU, K. (2001). *Diffuse emission of carbon dioxide from Cerro Negro Volcano*, Nicaragua. Geophys, Res. Lett. *28*, 4275–4278.

SANO, Y., NOTSU, K., ISHIBASHI, J., IGARASHI, G., and WAKITA, H. (1991), *Secular variations in helium isotope ratios in an active volcano: Eruption and plug hypothesis*, Earth Planet. Sci. Lett. *107*, 95–100.

SATO, M. (1988), Continuous monitoring of hydrogen in volcanic areas: petrological rationale and early experiments, Rendiconti Della Società Italiana Di Mineralogia Petrologia *43*, 1.265–1.281.

SATO, M. and MCGEE, F. (1981), Continuous monitoring of hydrogen on the south flank of Mount St. Helens, In (Lipman, P. W., Mullineaux, D. R. eds.), The 1980 eruption of Mount St. Helens, Washington. U.S. Geol. Surv. Prof. Pap., *1250*, 209–219.

SHINOHARA, H. (2005), A new technique to estimate volcanic gas composition: plume measurements with a portable multi-sensor system, J. Volcanol. Geotherm. Res. 143, 319–333.

SINCLAIR, A. (1974), Selection of thresholds in geochemical data using probability graphs, J. Geochem. Explor. *3*, 129–149.

SINKIN, T. and SIEBERT, L., *Volcanoes of the world*, 2nd Ed., Geosci. Press. Tucson, Arizona (1994), 349pp.

SYMONDS, R., ROSE, W., GERLACH, T., BRIGGS, P., and HARMON, R., (1990), Evaluation of gases, condensates, and SO_2 emissions from Augustine volcano, Alaska: the degassing of a Cl-rich volcanic system, Bull. Volcanol. *52*, 355–374.

TENNANT, C. and WHITE, M. (1959), *Study of the distribution of some geochemical data*, Econ. Geol. *54*, 1281–1290.

VASELLI, O., TASSI, F., MINISSALE, G., MONTEGROSSI, G., DUARTE, E., FERNANDEZ, E., and BERGAMASCHI, F. (2003), *Fumarole migration and fluid geochemistry at Poás Volcano (Costa Rica) from 1998 and 2001*, (Eds. Oppenheimer, C., Pyle D., and Barclay J.), Volcanic Degassing. Geological Society, London, Special Publication, *213*, 247–262. 0305–8719/03.

WAKITA, H., NAKAMURA, Y., KITA, I., FUJI, N., and NOTSU, K. (1980), *Hydrogen Release: New Indicator of Fault Activity*, Science *210*, 188–190.

WEIDMANN, D., WYSOCKI, G., OPPENHEIMER, C., and TITTEL, F. (2005), Development of a compact quantum cascade laser spectrometer for field measurement of CO_2 isotopes, Applied Physcs B. 80, 255–260.

WHITE, D., and WARING, G. (1963), *Volcanic Emanations*, *In Chapter 6 K*, Data of Geochemistry (6th Ed.) U.S. Geological Survey Prof. Pap. 440-K, K1-K27.

To access this journal online:
www.birkhauser.ch/pageoph

Pure and Applied Geophysics

Anomalous Emissions of SO_2 During the Recent Eruption of Santa Ana Volcano, El Salvador, Central America

Rodolfo Olmos,[1] José Barrancos,[2] Claudia Rivera,[3] Francisco Barahona,[1]
Dina L. López,[4] Benancio Henriquez,[1] Agustín Hernández,[1] Efrain Benitez,[1]
Pedro A. Hernández,[2] Nemesio M. Pérez,[2] and Bo Galle[3]

Abstract—Santa Ana volcano in western El Salvador, Central America, had a phreatic eruption at 8:05 am (local time) on October 1, 2005, 101 years after its last eruption. However, during the last one hundred years this volcano has presented periods of quiet degassing with fumarolic activity and an acidic lake within its crater. This paper presents results of frequent measurements of SO_2 degassing using the MiniDOAS (Differential Optical Absorption Spectroscopy) system and a comparison with the volcanic seismicity prior to the eruption, during, and after the eruption. Vehicle measurements of SO_2 flux were taken every hour during the first nine days of the eruption and daily after that. The period of time reported here is from August to December, 2005. Three periods of degassing are distinguished: pre-eruptive, eruptive, and post-eruptive periods. The intense activity at Santa Ana volcano started in July 2005. During the pre-eruptive period up to 4306 and 5154 ton/day of SO_2 flux were recorded on October 24 and September 9, 2005, respectively. These values were of the same order of magnitude as the recorded values just after the October 1st eruption (2925 ton/day at 10:01 am). Hourly measurements of SO_2 flux taken during the first nine days after the main eruptive event indicate that explosions are preceded by an increase in SO_2 flux and that this parameter reaches a peak after the explosion took place. This behavior suggests that increasing accumulation of exsolved magmatic gases occurs within the magmatic chamber before the explosions, increasing the pressure until the point of explosion. A correlation between SO_2 fluxes and RSAM (Real Time Seismic Amplitude Measurements) is observed during the complete sampling period. Periodic fluctuations in the SO_2 and RSAM values during the entire study period are observed. One possible mechanism explaining these fluctuations it that convective circulation within the magmatic chamber can bring fresh magma periodically to shallow levels, allowing increasing degasification and then decreasing degasification as the batch of magma lowers its gas content, becomes denser, and sinks to give space to a new magma pulse. These results illustrate that the measurements of SO_2 flux can provide important warning signals for incoming explosive activity in active volcanoes.

Key words: Sulfur dioxide flux, RSAM, magma degassing, volcanic eruption, Santa Ana volcano.

[1] Consejo de Investigaciones Cientìficas, Universidad de El Salvador, El Salvador, Centro America. E-mail: rolmos99@yahoo.com

[2] Enviromental Research Division, ITER, 38611 Granadilla, Tenerife, Canary Island, Spain.

[3] Department of Radio and Space Science, Chalmers University of Technology, 41296 Gothenburg, Sweden.

[4] Department of Geological Sciences, Ohio University, Athens, Ohio 45701, USA.
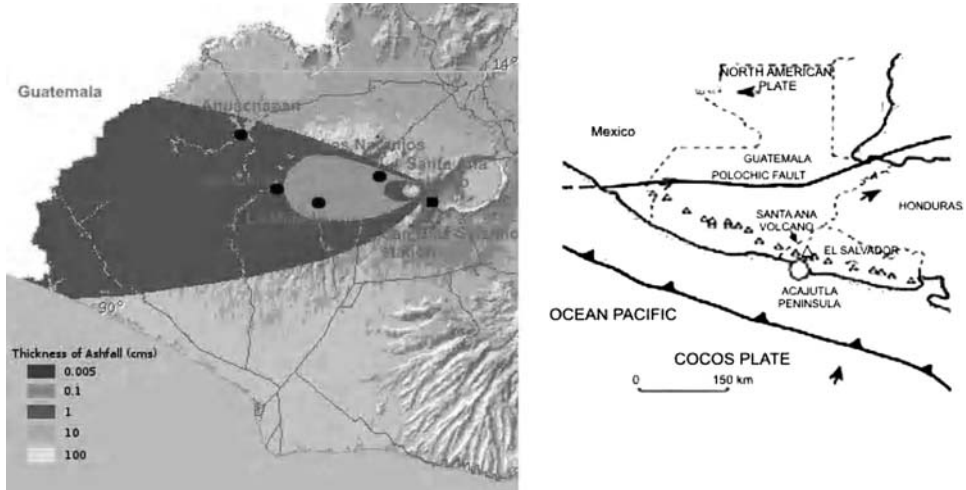
Figure 1
Map of pyroclastic products of the October 1, 2005 at Santa Ana volcano, El Salvador. Central America.
Servicio Nacional de Estudios Territoriales de El Salvador SNET, October (2005).

1. Introduction

In October 1, 2005, Santa Ana volcano in western El Salvador, Central America (Fig. 1) finally erupted after several years of quiet degassing and seismic activity. Prior to the October 1st phreatic eruption, from 2001 to 2005, several discrete measurements of the SO_2 fluxes emitted with the plume by Santa Ana volcano were measured occasionally (see Table 1) using a COSPEC (correlation spectrometer) (RODRIGUEZ *et al.*, 2004). More recently, frequent measurements of SO_2 fluxes using the Mini-DOAS system (GALLE *et al.*, 2002) were taken before the eruption until December 2005. These measurements started two months before the October 1st eruption. At the same time, the Servicio Nacional de Estudios Territoriales of El Salvador (SNET) had been monitoring the seismic activity of this volcano using three seismic stations at the volcano. These measurements have allowed us to compare the emissions of SO_2 with the seismic and explosive activity of Santa Ana volcano. This paper presents the results of these investigations and their significance for the monitoring of the Santa Ana volcano and other similar volcanoes.

Santa Ana volcano, with a summit of 2365 m, is located in western El Salvador at 13°51′ N and 89°38′ W, to the west of Coatepeque caldera (Fig. 1). It forms part of the volcanic system known as the Coatepeque-Izalco-Santa Ana volcanic complex, one of the most active volcanic systems in the Central American volcanic arc. The volcanism in Central America is related to the subduction of the Coco's plate below the Caribbean plate (MOLNAR and SYKES 1969). Santa Ana volcano was the source of the debris avalanche that formed the Acajutla peninsula in the Pleistocene or early Holocene

Table 1

SO$_2$ Flux from Santa Ana Volcano, 2001–2005. Units in tons/day. VS: vertical scans.

Date	No. Of Meas.	Min	Max	Average	S.D	Technique	Reference	Periods	
1/8/01	13	30	260	393	60	Stationary (VS)	COSPEC/ Rodriguez,2004	PRE-ERUPIVE PERIOD	
1/9/01	42	100	950	280	140	Vehicular	COSPEC/ Rodriguez,2004		
1/9/01	3	190	420	270	130	Vehicular	COSPEC/ Rodriguez,2004		
5/9/01	n.r.d.a.	-	-	170	-	Stationary (VS)	COSPEC/ Rodriguez,2004		
1/24/02	8	10	220	80	80	Stationary (V S)	COSPEC/ Rodriguez,2004		
1/25/02	4	10	40	30	10	Stationary (VS)	COSPEC/ Rodriguez,2004		
1/26/02	14	20	180	50	40	Stationary (VS)	COSPEC/ Rodriguez,2004		
8/24/04				586			COSPEC/INSIVUMEH		
8/25/04				400			COSPEC/INSIVUMEH		
8/26/04				176			COSPEC/INSIVUMEH		
8/27/04				526			COSPEC/INSIVUMEH		
4/13/05				523			COSPEC/INSIVUMEH		
4/14/05				520	39		COSPEC/INSIVUMEH		
4/15/05				581			COSPEC/INSIVUMEH		
8/20/05	5	880	1928	1434	466	Vehicular			Stage A Incandescente increases
8/24/05	2	4265	4306	4285	29	Vehicular			
8/29/05	4	2642	3737	3040	509	Vehicular			
8/31/05	4	301	482	370	85	Vehicular			
9/2/05	7	2317	3768	3129	600	Vehicular			Stage B Higher incandescence
9/3/05	4	1405	3593	2315	1052	Vehicular		PRE-ERUPIVE PERIOD	
9/10/05	2	1747	2653	2200	640	Vehicular			
9/11/05	12	1348	2541	1881	401	Vehicular			
9/12/05	2	2033	2409	2221	266	Vehicular			
9/13/05	2	3329	5154	4241	917	Vehicular			
9/14/05	4	3324	5099	3882	820	Vehicular			
9/15/05	10	1917	4326	3320	777	Vehicular			
9/16/05	6	757	4326	1603	1130	Vehicular	MiniDOAS, this paper		
9/17/05	9	1135	2191	1731	354	Vehicular			
9/18/05	7	1001	1713	1432	281	Vehicular			
9/20/05	4	1233	3848	1653	793	Vehicular			
9/21/05	1			1866		Vehicular			
9/22/05	4	844	1838	1184	446	Vehicular			
9/24/05	6	1312	3329	2401	839	Vehicular			
9/25/05	8	793	2634	1601	650	Vehicular			
9/26/05	3	2879	3633	3315	391	Vehicular			
9/27/05	3	713	828	770	57	Vehicular			
9/28/05	2	1742	2384	2063	454	Vehicular			
9/29/05	3	1363	1798	1564	219	Vehicular			
9/30/05	3	1382	1747	1623	291	Vehicular			
10/1/05	2	212	2925	1568	1919	Vehicular			Eruption
10/2/05	18	240	986	547	229	Vehicular			Stage C Small Explosion
10/4/05	6	152	1104	438	344	Vehicular			
10/6/05	2	507	521	514	10	Vehicular			
10/7/05	12	380	1158	755	243	Vehicular			
10/8/05	5	69	1685	743	726	Vehicular			

Table 1

(Contd.)

10/9/05	11	207	2074	727	632	Vehicular			from crater
10/10/05	3	276	320	291	25	Vehicular			and an
10/11/05	5	86	562	399	184	Vehicular			additional
10/12/05	10	26	492	245	137	Vehicular			input of
10/16/05	8	199	527	342	104	Vehicular			magmatic
10/17/05	9	311	674	470	124	Vehicular			gases
10/18/05	4	570	726	652	81	Vehicular			
10/19/05	5	363	847	627	204	Vehicular			
10/23/05	2	1140	1495	1318	250	Vehicular			
10/24/05	2	873	1201	1037	232	Vehicular			
10/25/05	3	752	994	858	124	Vehicular	POST- ERUPTIVE PERIOD		
10/26/05	7	294	475	386	63	Vehicular			
10/27/05	6	415	1140	710	269	Vehicular			
10/28/05	4	181	337	257	66	Vehicular			
10/29/05	4	311	415	372	48	Vehicular			
10/31/05	6	95	207	154	38	Vehicular			
11/1/05	6	276	389	314	40	Vehicular			Stage D
11/2/05	6	847	1210	1024	151	Vehicular			Fluctuant-state
11/3/05	5	82	138	110	22	Vehicular			degassing
11/4/05	10	311	648	483	110	Vehicular			interval
11/5/05	7	708	1452	1159	279	Vehicular			
11/7/05	3	544	562	553	9	Vehicular			
11/8/05	4	380	821	639	230	Vehicular			
11/12/05	9	423	527	490	58	Vehicular			
11/26/05	7	294	475	386	63	Vehicular			
11/27/05	6	415	1140	710	269	Vehicular			
11/28/05	4	181	337	257	66	Vehicular			
12/2/05	4	233	605	438	161	Vehicular			
12/4/05	4	769	933	829	72	Vehicular			
12/5/05	6	372	1123	753	275	Vehicular			

(a) COSPEC/Rodriguez, (2004); (b) COSPEC/INSIVUMEH.

(SIEBERT *et al.*, 2004; PULLINGER, 1998). The later activity of Santa Ana volcano produced volcanic deposits that have filled the depression formed by this volcanic collapse. The new volcano presents several crescent-shaped concentric craters and several flank vents along a fault system that extends around 20 km in the NNW direction bisecting the volcano (PULLINGER, 1998). Moderate eruptions from the summit and flank vents have characterized Santa Ana's activity since the 16th century. One of those vents is the San Marcelino cinder cone that erupted in 1722, producing lava flows that traveled 13 km to the east (PULLINGER, 1998).

The last recorded eruption of Santa Ana volcano, prior to the October 1, 2005 eruption, occurred in 1904. A crateric acid lake and a fumarolic field on the crater wall were formed after this eruption (PULLINGER, 1998; BERNARD *et al.*, 2004). The latter crater has a diameter of about 0.5 km. During the past century, Santa Ana volcano emitted important gas emissions consisting of a mixture of magmatic gases and steam from the magmatic-hydrothermal system. During the most recent period of degassing, 2001–2005, the acid rain associated with the volcanic plume has produced extensive damage to the surrounding vegetation, particularly in the south and southwest flanks of the volcano.

HERNÁNDEZ *et al.* (this volume) reported a significant increase in the extent and intensity of the fumarolic field inside the crater rim and of the surface temperature of the crater's lake a few days before the October 1, 2005 eruption. SO_2 flux measurements were taken using COSPEC during this period of time, showing average values around 140 tons/day (BERNARD *et al.*, 2004; RODRIGUEZ *et al.*, 2004).

The surface covered by the pyroclastic products ejected during the October 1, 2005 eruption are shown in Figure 1 (SNET, 2005). The eruption produced ashfall on the west side of the volcano. Ash layers about 3–5 cm were observed in Los Naranjos village. In addition, the eruption produced lahars and launched ballistic material (up to 2 m in diameter) at distances up to 3 km from the crater. About 80% of the vegetation in an area defined by a radial distance of 3 km from the crater was damaged during this eruption. The villages more affected by ash fall were Los Naranjos, La Majada and Apaneca, as well as Ahuachapán city.

Increased emissions of volcanic gases usually precede eruptive activity (MALINCONICO, 1979; YOUNG *et al.*, 1998; TARAN *et al.*, 2002). Research and monitoring of these emissions can provide warning signals for possible eruptions such as has happened in other global volcanoes, for example the March-April, 1982 eruption of Mount St. Helens (SWANSON *et al.*, 1985). Previous work on diffuse CO_2 at Santa Ana volcanic complex was carried out by SALAZAR *et al.*, 2001, finding that most of the CO_2 degassing at Santa Ana is limited to the central area of the volcano. An important challenge in volcanic research and monitoring has been the sampling of volcanic gases within the crater, which is dangerous during active periods. Therefore, optical remote sensing methods such as Ultraviolet and Infrared Spectroscopy are suitable to measure volcanic gas emissions. The UV sensor COSPEC has been used for remote monitoring of volcanic plumes since the early eighties (STOIBER *et al.*, 1983). COSPEC was a major change from direct gas sampling to remote sensing. Sampling of gases within craters and determination of their composition are more accurate than remote methods. However, better safety and increased sampling frequency are the benefits of remote sensing, greatly improving the ability to evaluate degassing trends. More recently, Differential Optical Absorption Spectroscopy (DOAS) has allowed highly sensitive and specific detection of many gases using artificial sources or scattered sunlight (GALLE *et al.*, 2002). The MiniDOAS is compact, lightweight, portable, and relative simple equipment, which was successfully introduced for remote sensing of SO_2 fluxes in volcanoes in 2002 (GALLE *et al.*, 2002). In this paper, we present measurements of SO_2 emissions performed using a miniDOAS system before, during, and after the last phreatic eruptive period of the Santa Ana volcano.

2. Methodology

The miniDOAS system is based on a spectrometer (Ocean Optics S2000) coupled to a telescope through a quartz optical fiber (diameter 800 μm). The unit is powered via the USB-port of a laptop computer, which also supports data transfer. The spectrometer is

calibrated using a mercury lamp. The software used for controlling the spectrometer was developed at Chalmer University of Technology and it is called MobileDoas. In our work, the spectra were re-evaluated using DOASIS (DOAS Intellingent System). DOASIS is a software that filters the interference of other chemical species with the SO_2 spectrum, generating a cleaner spectrogram and a better determination of the SO_2 fluxes. In a typical measurement the mini-DOAS was carried on a car and spectra were recorded while the car moved under the volcanic plume. The plane formed by the moving car with the MiniDOAS and the trajectory of the car is approximately perpendicular to the direction of movement of the plume. The distance from the transect to the crater is between 5 and 15 km. The car position was tracked using a handheld GPS receiver. The parameter obtained at every measurement point along the transect is concentration of SO_2 times meter (ppm.m or mass.length^{-2}) or SO_2 column density. The direction of plume transport was found using the GPS position of the maximum SO_2 column density and the crater position. Integrated path values were obtained by adding the products of the SO_2 column density and perpendicular displacement for each segment along the path (mass.length^{-1}). SO_2 flux values were obtained multiplying the integrated path values times the mean value of the wind speed during the time of the measurements (mass.time^{-1}). Values of wind speed were estimated using the FNL model of the National Oceanic and Atmospheric Administration (NOAA) at 700 and 850 HPa (Hectopascals). Typical transects for this study are shown in Figure 2.

During the time period of this investigation, SO_2 flux measurements were taken at variable time intervals. From August 24 to December 5, 2005, almost daily measurements were taken. The number of transects measured every day varied from 1 to 18. When several transects were measured in one day, the average daily flux is reported. Variations in SO_2 flux at different times of the day were investigated on October 2, 7, and 9. The results for the different SO_2 flux measurements taken by other authors before 2005 and the values obtained in this work are shown in Table 1.

3. Results and Discussion

3.1. Pre-eruptive Period (June–September 2005)

The relatively low values of SO_2 flux measurements taken using COSPEC during 2001 and 2002 (140 tons/day; Bernard *et al.*, 2004; Rodriguez *et al.*, 2004) are in good agreement with the low RSAM (Real Time Seismic Amplitude Measurements) values measured during April–June 2005 (< 20 RSAM units), as shown in Figure 3. This value of around 20 RSAM units will be considered in this paper as the base line for volcanic seismicity. The RSAM system was developed by the USGS to study seismic activity during volcanic crises (Ewert *et al.*, 1993). During volcanic crisis, it is often difficult to distinguish individual seismic events. Instead of focusing on individual events, the average amplitude over 10-minutes intervals is computed and stored (RSAM). If the
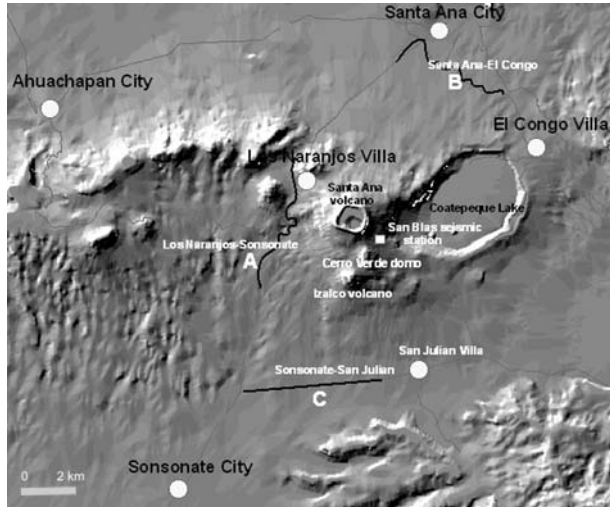
Figure 2
Typical transect A: Los Naranjos-Sonsonate B:Santa Ana-El Congo, October (2005).

amplitude or rate of the volcanic tremor increases, RSAM also increases. The importance of seismicity as a precursor to eruptive activity has been demonstrated (CHOUET, 1996). This increase in seismicity can be related to magma or gas movement.

At Santa Ana volcano, two stages can be identified during the pre-eruptive period as shown in Table 1 and Figure 3. Stage A comprises the period between 05/13/2005 and 09/02/2005, as it can be observed in the increase in RSAM and SO$_2$ happening around that date in May. During stage A, from 05/13/2005 to 08/20/2005, we observed an anomalous increase in SO$_2$ flux of 893 tons/day (from 541 ± 34 tons/day to 1434 ± 466 tons/day), as shown in Table 1. In comparison, from 08/20/2005 to 08/24/2005 the flux increased ∼2850 tons/day (from 1434 ± 466 to 4285 ± 29 tons/day, respectively). This emission of SO$_2$ is up to 30 times greater than the 140 tons/day found during the previous period. Increases in SO$_2$ emissions at Santa Ana volcano have been reported during non-erupting periods. In February, 2001, COSPEC measurements showed a noticeable increase of SO$_2$ by a factor higher than 8 (WUNDERMAN and ED VENZKE, 2001). However, that increase is considerable lower than the factor of 30 observed at Santa Ana during the period prior to the eruption of 2005. This increase of SO$_2$ flux suggested the rise of magma to a level that promoted gas emission and/or gas transmission through the hydrothermal system. The increase of volcano-tectonic (VT) seismicity is in good agreement with this interpretation (Fig. 3). The RSAM values, measured at the San Blas Station increased to values of 54 RSAM units on 08/20/2005. This value represents an increase of more than 30 RSAM units with respect to the base line seismicity. Two seismic events occurred on 08/24/2005 on the south flank of the Santa Ana volcano. These events were located between Cerro Verde and San Blas
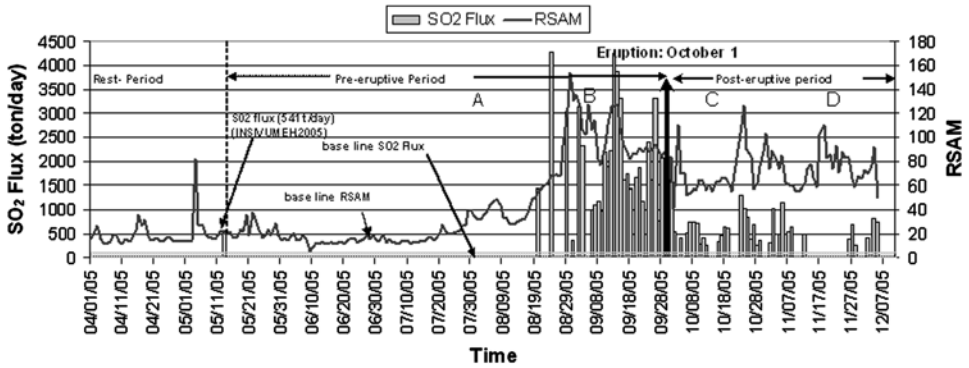
Figure 3

SO$_2$ flux variations in the pre-eruptive, eruptive and post-eruptive periods and the RSAM signal of Seismic Station San Blas at Santa Ana Volcano during 2005. SO$_2$ flux was measured with a MiniDOAS system.

Seismic Station (see Fig. 2). On 08/30/2005 a maximun RSAM of 154 units was observed. This increase in seismicity occurred at the time that high incandescence appeared in the volcano crater. Starting on 09/02/2005 a decrease of the SO$_2$ emissions was observed. These changes can be interpreted as a partial sealing of the conduit by a solidified plug of magma, which will cause later overpressurization of the system as suggested by CASADEVALL *et al.* (1981).

Stage B comprises events taking place from 09/03/2005 to 09/30/2005 which follows a cyclic behavior similar to stage A but with a much higher incandescence in the volcano main crater (visual observations). During the first part of stage B, SO$_2$ flux increased, reaching a daily maximum of 4241 ± 917 tons/day on 09/13/2005 followed by a decrease to 1184 ± 446 tons/day on 09/22/2005. Subsequently SO$_2$ flux increased again reaching a daily average of 3315 ± 391 tons/day on 09/26/2005. The two peak values of the SO$_2$ flux on 09/13/2005 and 09/26/2005 correlated with increases in VT-seismic events during the subsequent days, reaching 14 and 23 events, respectively (Demetrio Escobar, SNET, personal communication). According to DAAG *et al.* (1996), an increase in SO$_2$ flux to a peak value suggests the rise of magma to a level that promotes gas exsolution, water displacement, and gas transmission through the hydrothermal system.

The observations during stage B can be summarized as follows. The SO$_2$ flux appears to have been variable prior to the 10/01/2005 eruption. This behavior may indicate periodic fracturing of the rocks that had been sealing and pressurizing the magma in the conduit. This fracturing of the sealing cap is due to increased pressure and allows gases to be exsolved more easily from the magma head, but in a cyclic way following the fracturing events. The changes observed in the rates of SO$_2$ flux reflect changes in the magmatic degassing. These changes are also reflected in the heating rate of the crater as reflected in variations in incandescence. Two days prior to the October 1st eruption

changes in the predominant seismic frequency (from 8 to 5 Hz) were observed (Demetrio Escobar, SNET, personal communication). The observed changes in gas release could be the main cause of the changes in seismic frequency. Modeling studies of degassing in magmatic chambers by BENOIT and MCNUTT (1997) and NEUBERG et al. (2000) show that gas concentration affects the seismic velocity and the observed spectra in the low frequency region. Changes in seismic frequency are produced by cycles of pressure within the magma conduit due to different types of resonance sources at different depths. As a gas pulse moves upward within the magmatic conduit towards the magma head intercepts fractures. The magma conduit acts as a resonance source that changes resonance frequency due to the fractures and produces the changes in spectral frequencies measured in the seismograms. The degassing and bubbling of magma also changes due to changes in acoustic vibration. Changes in gas concentrations can produce changes in dominant seismic frequency and shift in spectral frequencies during hybrid and long-period seismic events (NEUBERG et al., 1998; BAPTIE et al., 2002; NEUBERG and O'GORMAN, 2002).

3.2. Phreatic Eruption (1st October 2005)

The phreatic eruption occurred at 08:05 a.m. on 10/01/2005 as shown with the arrow in Figure 3. Two transects were performed during this day around 10:00 am and 04:00 pm producing SO_2 flux values of 2925 ± 29 tons/day and 212 ± 21 tons/day, respectively. These values are a factor of 3 and 47 lower than the 10,000 tons measured in the erupted cloud by the Ozone Monitoring Instrument (OMI) on board NASA's Aura satellite during the phreatic eruption of Santa Ana Volcano (NASA EARTH OBSERVATORY, 2005). Ground-based and satellite-based measurements can give different values due to the uncertainties in the measurements and the different methodologies (fluxes in the ground-based measurements and SO_2 mass content in the OMI measurement). However, these values show order of magnitude differences. On the other hand, the RSAM values reached values up to 1368 RSAM units at the time of the eruption, extremely higher than all previous values. However, similar to the SO_2 fluxes, the RSAM values decreased dramatically after the eruption. At 07:00 pm (11 hours after the eruption), the RSAM went down to 20 RSAM units.

Observations by the OMI instrument (NASA EARTH OBSERVATORY, 2005) show that the cloud of gas displaced to the southwest. This is in agreement with the mapped ash fall as shown in Figure 1 that presents a thickness of up to 10 m close to the crater and the plume spreading towards the southwest with 2 mm thickness at Ahuchapán City.

3.3. Post-eruptive Period (October 2 – December 5, 2005)

Stage C corresponds to small explosions in the crater from October 2 to October 31, 2005. Measurements of SO_2 flux from active volcanoes are not done very frequently due to instrumental limitations, changes in wind conditions, expensive equipment and time

consumption (Andres and Rose, 1995). However, on the days following the eruption, transects of SO_2 were measured approximately every hour with the purpose of observing variations of this parameter and its relationship with subsequent events in the Santa Ana volcano. The results for the SO_2 flux measured at the Santa Ana volcano plume are presented in Figures 4, 5, and 6 for the dates October 2, 7, and 9. In these graphs, the occurrence of explosions as detected by San Blas seismic station is also shown. Seismic tremor, and lahars are indicated with arrows. It should be noted that Hurricane Stan was hitting El Salvador during early October, increasing the risk for lahars and other related phenomenon. On October 2nd, an increase from 262 ± 21 to 866 ± 104 tons/day of SO_2 flux preceded an explosion. Later that day, a landslide to the east and southeast of the crater generated a lahar that traveled 5 km away from the crater towards Coatepeque Lake. In addition, the Stan storm and the small explosions produced during this day considerable damage to the west and northwest flanks. On October 7 (Fig. 5) peaks of SO_2 flux were observed at 9:14 am,12:30 and 15:32 pm. In addition, a marked increase of the VT-seismic events at 11:40 am, 14:00 and 20:17 pm due to small explosions was observed. On October 9 (Fig. 6), the SO_2 flux started to increase clearly before an explosion occurred around 11 a. m. and reached peak values around 12 m. In all these explosive events, SO_2 flux started to increase before the explosions and reached a peak after the explosions took place. Note that on the explosion of October 2, the peak value was probably not detected because measurements were not taken during the few hours after the event. The observational results imply that increased degassing occurs before the explosions. A low permeability degassed magma cap on top of the magma head can generate an accumulation of gases and over-pressurization on the magma head. As the pressure rises, the magma cap starts to break and allows the release of small fluxes of gases before the explosions. However, before the explosions the rate of accumulation of gases is greater than the fluxes released to the atmosphere and the pressure continues to increase. This high pressure is transferred throughout the magmatic conduit and the magmatic chamber until it is high enough to produce the observed explosions and subsequent high release of gases. These conditions can be considered similar to those
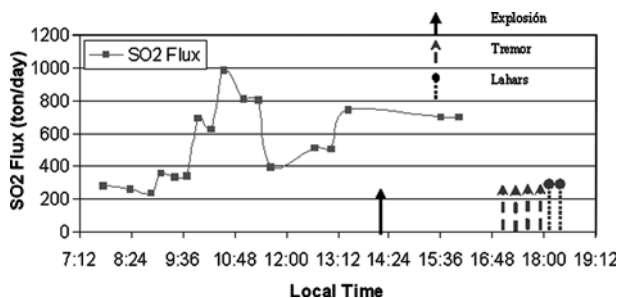
Figure 4
Hourly SO_2 flux at Santa Ana volcano plume during October 2, 2005.
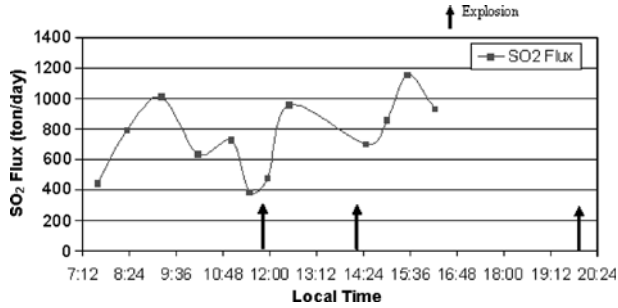
Figure 5
Hourly SO$_2$ flux at Santa Ana volcano plume during October 7, 2005.

happening on Soufriere Hills volcano, Montserrat, where long period seismic events have been recorded and occurred at the same time with visual observations of ash and gas venting at the surface, and immediately preceding rockfalls (LUCKETT et al., 2002).

Increased SO$_2$ emissions often precede and/or occur simultaneously to increases in eruptive activity (MALINCONICO, 1979; YOUNG et al., 1998). In Figure 3, an additional input of magmatic gases into the feeding system is suggested during October 24–26, due to an increase of SO$_2$ flux. At that time, a new crisis of the volcano was suspected with values of 103 y 127 RSAM units registered at the San Blas seismic station. These high RSAM values occurred on October 23 and 24, 2005. At the same time, SO$_2$ flux increased reaching values of 1318 ± 250 and 1037 ± 232 tons/day, respectively. These fluctuations in SO$_2$ flux can be interpreted as decreases in pressure in the magma head that allows the ascent of intermittent, less dense bubble-bearing magma through the magma conduit and produces changes in the RSAM signal. On the other hand, LP-events and hybrid earthquakes are generated from the excitation and resonance of a fluid magma body surrounded by an elastic medium (FERRAZZINI and AKI, 1987).
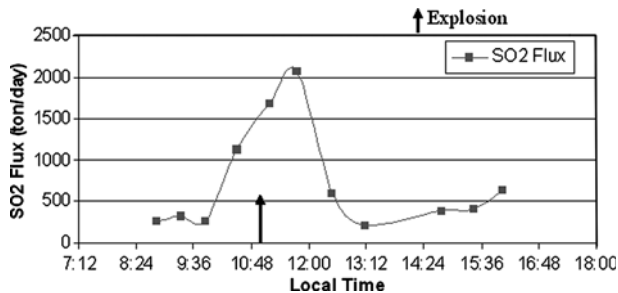
Figure 6
Hourly SO$_2$ flux at Santa Ana volcano plume during October 9, 2005.

3.4. *Stage D Fluctuant-state Degassing Interval (November–December, 2005)*

During the months of November and December, 2005, measurements of SO_2 flux were done more irregularly (Fig. 3). The changes of SO_2 flux observed during this time correlate with small variations in the seismicity of the volcanic system. Visual observations were done on November 4, at a distance of 2 km from the crater, at the west side. These observations allowed us to identify a small plume ascending approximately three hundred meters above the crater (Fig. 7a). In another inspection of the summit crater on November 11, a change in color in the crater lake was observed (Fig. 7b), from green before the eruption to turquoise after the eruption. This change in color could correspond to the deposition of new sulfate minerals that were not present before the eruption. The fumarolic area that existed at the walls of the crater was found sealed, and an intensive bubbling was occurring at the crater lake. This bubbling indicates direct interaction of the lake with the magmatic-hydrothermal system. More recently (March, 2006), a reduction in the size of the crater lake was observed (Fig. 7c) if it is compared with its original area before the eruption. Heat and gas transfer is changing the chemical composition and temperature of the lake (Figs. 7b and 7c). For the entire stage D, a maximum value of SO_2 flux of 1024 ± 151 ton/day was measured in November 2, 2004, and a minimum value of 110 ± 22 ton/day in November 3, 2004, with an average of 599 ± 218 tons/day.

At Santa Ana volcano, frequencies of 2 and 4 Hz (Demetrio Escobar, SNET, personal communication) in the spectrograms were recorded during stage D. These dominant frequencies correlated with the decreasing and fluctuating flux of SO_2. JOHNSON and LEES (2000) explains that signals between 1 and 5 Hz can be classified as degassing "chugging" events. At Pinatubo volcano, similar bands with frequencies between 3.5 and 4.5 Hz were present on June 12, 1991, and continued until June 16, 1991. These bands were explained as magma movement and release of associated volatiles into a new system of cracks before the eruption of June 15, 1991 (POWER *et al.*, 1996). The displacement of frequency patterns correlated well with the RSAM signal.
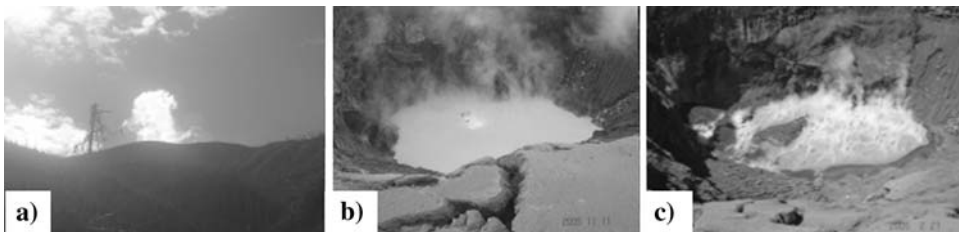
Figure 7
a) Small plume at Santa Ana volcano on November 4, 2005. b) Sulphurous lake at the Santa Ana volcano crater as observed on November 12, 2005. c) Sulphurous lake at the Santa Ana volcano crater as observed on February 26, 2006.

These changes in the frequency pattern (long-period earthquakes and tremor) have been observed in other global volcanoes, for example: Arenal in Costa Rica (HAGERTY *et al.*, 2000), Karymsky in Russia (JOHNSON and LEES, 2000), Montserrat in West Indies (NEUBERG *et al.*, 2000), Erebus in Antartica (ROWE *et al.*, 2000), and Lascar in Chile (HELLWEG, 2000).

The gas pulses identified in the frequent SO$_2$ measurements taken during stage D are probably explained by changes in the partially sealed conduit of the crater as well as possible changes in the density of the magma (JAUPART and VERGNIOLLE, 1989). The pressure within the magma head decreases due to the released gases. The gas composition of the remaining gases changes because different magmatic gases have different partition coefficients (GIGGENBACH, 1980). These changes in composition also generate changes in magma density. The decreasing trends of SO$_2$ flux have also revealed the influence of the hydrothermal system covering the degassing magma. Open or partially open conduits in the interior of the crater make possible the leak and rapid ascent of gases through the hydrothermal system that surrounds the magmatic environment (DOUKAS and GERLACH, 1995). However, the magma that does not have the right pressure for the gases to ascend and leave the crater, remains trapped in the magma conduit until more gases accumulate or new batches of magma reach shallower levels. The fluctuations of SO$_2$ flux also can reflect a convective magma circulation and transfer of gases within the magmatic chamber, such as is observed in the large period events registered in the seismograms. New batches of magma arriving at shallow levels by convective circulation from deeper levels within the chamber should provide higher release of gases. In addition, convection of magma within the magma conduit has been proposed as a mechanism to transport volatiles to shallow levels (KAZAHAYA *et al.*, 2004; WITTER *et al.*, 2004). The geometry of the magma conduit controls the exsolution of gases. KAZAHAYA *et al.* (2004) have modeled the ascent of magma within a pipe showing that gas exsolution is affected by the radius of the magmatic conduit. As heat and gases are transferred to the surrounding rocks and to the atmosphere, changes in the radius of the magmatic conduit can occur due to channel erosion or rock collapses. These processes can also produce changes in the emitted SO$_2$. Variations in density due to the degasification process have been proposed to drive magmatic convection within magmatic conduits. As magma degas, the denser magma in the magma head sinks and allows the lighter magma, richer in gases, to ascend producing an increase in gas release at the magma head (STEVENSON and BLAKE, 1998). This mechanism explains the degasification process in non-erupting volcanoes that release gases continuously at their craters (KAZAHAYA *et al.*, 1994; ALLARD, 1997; STEVENSON and BLAKE, 1998). As the magma batch degasses decreasing the volatile concentration, the exsolved fluxes should decrease. As convection is a periodic phenomenon, the fluxes should also behave periodically. Another possible explanation for the decrease in SO$_2$ flux is the decreasing degasification of the magma as the concentration of dissolved gases decreases with time (ANDRES *et al.*, 1993; GARDNER and WHITE, 2002).

3.5. *Correlation between RSAM and SO₂ Flux*

The SO_2 flux and RSAM data versus time plotted in Figure 3 suggest that both variables are correlated in time. Higher values of both variables occur almost at the same days. However, the construction of a cross-correlogram between both variables can allow the identification of any time lag between these two variables (DAVIS, 2002). Figure 8 shows the cross-correlogram between SO_2 and RSAM. In this Figure, a clear lag of zero days can be observed between the two variables because the cross-correlogram has a peak at zero days with a correlation coefficient equal to 0.58. The test of significance of the correlation coefficient (DAVIS, 2002) for the correlation coefficient of 0.58 and 61 data points gives a *t statistics* equal to 5.41, which is significant at a confidence level higher than 99.99%. The lag phase between the two variables is probably lower than 1 day, as suggested by Figures 4–6, and the occurrence of explosions and seismic events. These figures suggest that the phase lag is probably only minutes or hours. Time intervals between measurements smaller than 1 day are needed to find the right phase lag between the variables.

4. *Conclusions*

At Santa Ana volcano, seismic measurements (RSAM) and fluxes of SO_2 have proved to be a good tool to detect changes in volcanic activity during the recent eruptive period. Both parameters showed an increase, with some variability, several months before the eruption. SO_2 flux reached thousands of tons/day a few days before the eruption and RSAM showed similar trends. This behavior indicates that the measurement of these two parameters in active volcanoes such as Santa Ana is essential to forecast future eruptions as has happened in other worldwide volcanoes (e.g., Pinatubo and Montserrat volcanoes).
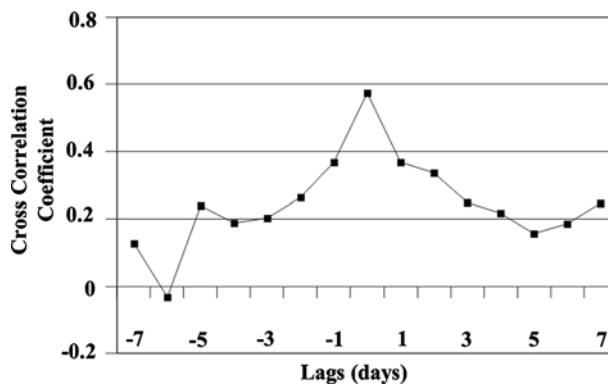
Figure 8

Cross-correlogram of RSAM and SO_2 flux at Santa Ana volcano from August to December, 2005. A maximum in the cross-correlogram at zero lag indicates that the lag phase between the two variables is smaller than one day.

Within a few days of the eruption, variations in emissions of SO$_2$ were closely related to seismic and explosive activity at Santa Ana volcano. Increases in SO$_2$ emissions were observed prior to explosive events and the flux increased to peak values after the explosion. This initial increase seems to occur within an hour of the explosion. This situation probably also happens when major eruptions occur but we have not detected it because SO$_2$ fluxes are not measured very frequently in volcanoes. These changes are probably even more dramatic at the time of large eruptions as found for Santa Ana volcano by the OMI instrument on board NASA's Aura satellite. Consequently, methods to monitor SO$_2$ more frequently are needed. COSPEC and MiniDOAS measurements made from an Air planes or from vehicles take too long and can be made only during the day. New sensors that can be operated remotely and that measure the fluxes at night and day are needed, as well as the improvement of the resolution of the remote sensors used by satellites.

According to the behavior of the SO$_2$ flux from Santa Ana volcano and the RSAM, SO$_2$ degassing of magma at Santa Ana volcano after the anomalous changes that started in May of 2005 have been caused mainly by a high accumulation of volatiles at shallow levels (magma head) in the magmatic conduit. The periodic fluctuations in SO$_2$ degassing and seismicity at Santa Ana volcano are probably the result of a combination of processes such as the convective circulation of magma within the magmatic chamber that transports fresh magma rich in gases to shallower levels and releases high fluxes as it arrives. Later the gas fluxes decrease until the magma becomes denser and sinks again to give path to another magma batch. another possible mechanism is the plugging and unplugging of the conduits as magma cools and solidifies, then the increase in pressure inside the chamber can again break the seal, and gases again are released abundantly. Finally, during the periods of low to moderate release of magmatic gases, external factors such as tidal and atmospheric effects can also generate cyclic behavior in the seismicity and probably in the gas released (López *et al.*, 2006; Neuberg, 2000a, b; Rydelek *et al.*, 1988).

Acknowledgments

References

Allard, P. (1997), *Endogenous magma degassing and storage at Mount Etna*, Geophys. Res. Lett. *24*, 2219–2222.

Andres, R.J. and Rose, W.I., *Remote sensing spectroscopy of* volcanic *plumes and clouds*. In *Monitoring Active Volcanoes*, (McGuire, B., Kilburn, C.R.J., and Murray, J., eds.), (UCL Press 1995).

ANDRES, R.J., ROSE, W.I., STOIBER, R.E., WILLIAMS, S.N., MATIAS, O., and MORALES, R. (1993), *A summary of sulfur dioxide emission rate measurements from Guatemalan volcanoes*, Bull. Volcanol. *55*, 379–388.

BAPTIE, B., LUCKETT, R., and NEUBERG, J. (2002), *Observations of low-frequency earthquakes and* volcanic *tremor at Soufriere Hills Volcano, Montserrat*. In *The Eruption of Soufriere Hills Volcano, Montserrat, from 1995 to 1999*, (Druitt, T.H. and Kokelaar, B.P., eds.), Geological Society, London, Memoirs *21*, 611–620.

BENOIT, J. and MCNUTT S. (1997), *New constraints on sources processes of* volcanic *tremor at Arenal Volcano, Costa Rica, using broadband seismic data*, Geophys. Res. Lett. *24*, 449–452.

BERNARD, A., ESCOBAR, C.D., MAZOT, A., and GUTTIERREZ, R.E. (2004), *The acid crater lake of Santa Ana volcano, El Salvador*. In (Rose, W.I., Bommer, J.J., López, D,L., Carr, M.J., and Major, J.J., eds.) *Natural Hazards in El Salvador: Boulder, Colorado*, Geological Sociey of America Special Paper 375.p. 5–23.

CASADEVALL, T.J., JOHNSTON, D.A., HARRIS, D.A., ROSE, W.I., Jr., MALINCONICO, L.L., Jr., STOIBER, R.E., BORNHORST, T.J., WILLIAMS, S.N., WOODRUFF, L., and THOMPSON, J.M. (1981), SO_2 *emission rates at Mount St. Helens from March 29 through December, 1980*. In (Lipman, P.W., and Mullineaux, D.R., eds.), *The 1980 eruptions of Mount St. Helens*, U.S. Geological Survey Professional Paper 1250, pp. 193–200.

CHOUET, B. (1996), *Long-period volcano seismicity: Its source and use in eruption forecasting*, Nature *380*, 309–316.

DAAG, A.S., TUBIANOSA, B.S., NEWHALL, C.G., TUNGOL, N.M., JAVIER, D., DOLAN, M.T., REYES, P.J.D., ARBOLEDA, R.A., MARTINEZ, M.M.L., and REGALADO, M.T.M. (1996), *Monitoring sulfur dioxide emission at Mount Pinatubo*. In *Fire and Mud: Eruptions and Lahars of Mount Pinatubo*, (Newhall, C.G. and Punongbayan, R.S., eds.), Phillipines, Philippine Institute of Volcanology and Seismology, Quezon City, and University of Washington Press, Seattle, pp. 409–414.

DAVIS, J.C., *Statistics and Data Analysis in Geology*, 3rd edition (Wiley, New York 2002).

DOUKAS, M.P. and GERLACH, T.M. (1995), *Sulfur dioxide scrubbing during the 1992 eruptions of Crater Peak, Mount Spurr Volcano, Alaska*. In *The 1992 Eruptions of Crater Peak Vent, Mount Spurr Volcano, Alaska*, (Keith, T.E.C., ed.), U.S. Geolog Survey Bull. *2139*, 47–57.

EWERT, J.W., MURRAY, T.L., LOCKHART, A.B., and MILLER, C.D. (1993), *Preventing Volcanic Catastrophe: The U.S. International Volcano Disaster Assistance Program*, Earthquakes and Volcanoes 24, 6.

FERRAZZINI, V. and AKI, K. (1987), *Slow waves trapped in a fluid-filled infinite crack: Implication for* volcanic *tremor*, J. Geophys. Res. *92*, 9215–9223.

GALLE B., OPPENHEIMER, C., GEYER, A., MCGONIGLE, A.J.S ., EDMONS, M., and HORROCS L.A. (2002), *A miniaturized UV spectrometer for remote sensing of SO_2 fluxes: A new tool for volcano surveillance*, J. Volcanol. Geotherm. Res. *119*, 241–254.

GARDNER, C.A. and WHITE, R.A. (2002), *Seismicity, gas emission and deformation from 18 July to 25 September 1995 during the initial phreatic phase of the eruption of Soufriere Hills Volcano, Montserrat*. In *The Eruption of Soufriere Hills Volcano, Montserrat, from 1995 to 1999* (Druitt, T.H. and Kokelaar, B.P., eds.), Geological Society, London, Memoirs. *21*,567–581.

GIGGENBACH, W. F., *Chemical composition of volcanic gases*, In (Scarpa, Tilling, eds.) *Monitoring and Mitigation of Volcano Hazard* (Springer, 1996) pp. 221–256.

HAGERTY, M., SCHWARTZ, S., GARCES, M., and PROTTI, M. (2000), *Analysis of seismic and accoustic observations at Arenal Volcano*, Costa Rica, 1995–1997, J. Volcanol. Geotherm. Res. *101*, 27–65.

HELLWEG, M. (2000), *Physical models for the source of Lascar's harmonic tremor*, J. Volcanol. Geotherm. Res. *101*, 183–198.

HERNÁNDEZ, P. A., PÉREZ, N. M., VAREKAMP, J. C., HENRIQUEZ, B., HERNÁNDEZ, A., BARRANCOS, J. PADRÓN, E. CALVO, D., and MELIÁN, G. (2007), *Crater Lake temperature changes of the 2005 eruption of Santa Ana volcano, El Salvador, Central America*, Pure Appl. Geophy. (this volume).

JAUPART, C. and VERGNIOLLE, S. (1989), *The generation and collapse of a foam layer at the roof of basaltic magma chamber*, J. Fluid Mech. *203*, 247–380.

JOHNSON, J. and LEES, J. (2000), *Plugs and chugs-seismic and acoustic observations of degassing explosions at Karymsky, Russia and Sangay, Ecuador*, J. Volcanol. Geotherm. Res. *101*, 67–82.

KAZAHAYA, K., SHINOHARA, H., and SAITO, G. (1994), *Excessive degassing of Izu-Oshima Volcano: Magma convection in a conduit*, Bull. Volcanol. *56*, 207–216.

KAZAHAYA, K, SHINOHARA, H., UTO, K., ODAI, M., NAKAHORI, Y., MORI, H., IINO, H., MIYASHITA, M., and HIRABAYASHI, J. (2004), *Gigantic SO_2 emission from Miyakejima volcano, Japan, caused by caldera collapse*, Geology *32*, 425–428.

López, D.L., Bundschuh, J., Soto, G.J., Fernández, J.F., and Alvarado, G.E. (2006), *Chemical evolution of thermal springs at Arenal Volcano, Costa Rica: Effect of volcanic activity, precipitation, seismic activity, and Heat tides*, J. Volcanol. Geotherm. Res. *157*, 166–181.

Luckett, R., Baptie, B., and Neuberg, J. (2002), *The relationship between degassing and rockfall signals at Soufriere Hills Volcano, Montserrat*. In *The Eruption of Soufriere Hills Volcano, Montserrat, from 1995 to 1999* (Druitt, T.H. and Kokelaar, B.P., eds.), Geological Society, London, Memoirs *21*, 595–601.

Malinconico, L.L., Jr. (1979), *Fluctuations in SO$_2$ emission during recent eruptions of Etna*. Nature *278*, 43–45.

Molnar, P. and Sykes, L. (1969), *Tectonics of the Caribbean and Middle America regions from focal mechanisms and seismicity*, Geol. Soc. Am. Bull. *80*, 16–1684.

Nasa's Earth Observatory web page. (October, 2005), (http://earthobservatory.nasa.gov/NaturalHazards/ natural_hazards_v2.php3?img_id=13191).

Neuberg, J. and O'Gorman, C. (2002), *A model of the seismic wavefield in gas-charged magma: application to Soufriere Hills Volcano, Montserrat*. In *The Eruption of Soufriere Hills Volcano, Montserrat, from 1995 to 1999* (Druitt, T.H. and Kokelaar, B.P. eds.), Geological Society, London, Memoirs *21*, 603–609.

Neuberg, J. (2000a), *External modulation of volcanic activity*, Geophys. J. Internat. *142*, 232–240.

Neuberg, J. (2000b), *Characteristics and causes of shallow seismicity in andesite volcanoes*, Philos. Trans. R. Soc. Lond. *358*, 1533–1546.

Neuberg, J., Luckett, R., Baptie, B., and Olsen, K. (2000), *Models of tremor and low-frequency earthquake swarms on Montserrat*, J. Volcanol. Geotherm. Res. *101*, 83–104.

Power, J. A., Murray, T. L., Marso, J. N., and Laguerta, E. P. (1996), *Preliminary observations of seismicity at Mount Pinatubo by use of the seismic spectral amplitude measurement (SSAM) system, May 13–June 18, 1991*. In (Newhall, C. G. and Punongbayan, R. S., eds.), *Fire and Mud: Eruptions and Lahars of Mount Pinatubo, Philippines*, Philippine Institute of Volcanology and Seismology, Quezon City, and University of Washington Press, Seattle, pp. 269–283.

Pullinger, C. (1998), *Evolution of the Santa Ana volcanic complex, El Salvador*. Submitted in Partial fulfillment of the requirements for the degree of Master of Science in Geology, Michigan Technological University.

Rodriguez, L., Watson, M., Rose, W., Brannan, Y., Bluth, G., Chigna, G., Matias, O., Escobar, D., Carn, S., and Fischer, T. (2004), *SO$_2$ emission to the atmosphere from active volcanoes in Guatemala and El Salvador, 1999–2002*, J. Volcanol. Res. *138*, 325–344.

Rowe, C., Aster, R., Kyle, P., Dibble, R., and Schlue, J. (2000), *Seismic and accoustic observations at Mount Erebus volcano, Ross Island, Antartica, 1994–1998*, J. Volcanol. Geotherm. Res. *101*, 105–128.

Rydelek, P.A., Davis, P.M., and Koyanagi, R.Y. (1988), *Tidal triggering of earthquake swarms at Kilauea volcano, Hawaii*, J. Geophys. Res. *93*, 4401–4411.

Salazar J.M.L., Hernández P.A., Pérez N.M., Olmos R., Barahona F., Cartagena R., Soriano T., Lopez K., and Notsu K., (2004), *Spatial and temporal variations of diffuse CO$_2$ degassing at Santa Ana-Izalco-Coatepeque volcanic complex, El Salvador, Central America*. Bulletin Geological Society of America Special Paper, *375*, 135–146.

Siebert, L., Kimberly, P., and Pullinger, C.R. (2004), *The voluminous Acajutla debris avalanche from Santa Ana volcano, western El Salvador, and comparison with other Central American edifice-failure events*. In (Rose, W.I., Bommer, J.J., López, D.L., Carr, M.J., and Major, J.J., eds.), *Natural hazards in El Salvador: Boulder, Colorado*, Geological Society of America Special Paper *375*, pp. 5–23.

Snet (2005), (http://www.snet.gob.sv/Geologia/Vulcanologia/erupcion12005vsa.htm).

Stevenson, D.S. and Blake, S. (1998), *Modeling the dynamics of volcanic degassing*, Bull. Volcanol. *60*, 307–317.

Stoiber, R.E., Malinconico, L.L. Jr., and Williams, S.N. (1983), *Use of the correlation spectrometer at volcanoes*. In *Forecasting Volcanic Events* (Tazieff, H. and Sabroux, J.C., eds.), (Amsterdam-New York 1983), pp. 425–444.

Swanson, D.A., Casadevall, T.J., Dzurisin, D., Holcomb, R.T., Newhall, C.G., Malone, S.D., and Weaver, C.S. (1985), *Forecast and predictions of eruptive activity at Mount St. Helens, USA: 1975–1984*, J. Geodynamics *3*, 397–423.

Taran, Y.A., Gavilanes, J.C., and Cortes, A. (2002), *Chemical and isotope composition of fumarolic gases and the SO$_2$ flux from volcan de Colima, Mexico, between 1994 and 1998 eruptions*, J. Volcanol. Geoth. Res. *117*, 105–119.

YOUNG, S.R., FRANCIS, P.W., BARCLAY, J., CASADEVALL, T.J., GARDNER, C.A., DAROUX, B., DAVIES, M.A., DELMELLE, P., NORTON, G.E., MACIEJEWSKI, A.J.H., OPPENHEIMER, C.M.M., STIX, J., and WATSON, I.M. (1998), *Monitoring SO_2 emission at the Soufriere Hills Volcano: Implications for changes in eruptive conditions*, Geophys. Res. Lett. *25*, 3681–3684.

WITTER, J.B., KRESS, V.C, DELMELLE, P., and STIX, J. (2004), *Volatile degassing, petrology, and magma dynamics of the Villarrica Lava Lake, Southern Chile*, J. Volcanol. Geotherm. Res. *134*, 303–337.

WUNDERMAN, R. and VENZKE, E. eds (2001), *Santa Ana (El Salvador) 2000–2001, Observations of glowing fumaroles and release of magmatic gas*, Bull. Global Volcanism Network, BGVN 26, 04.

To access this journal online:
www.birkhauser.ch/pageoph

▐ Pure and Applied Geophysics

Crater Lake Temperature Changes of the 2005 Eruption of Santa Ana Volcano, El Salvador, Central America

P. A. Hernández,[1] N. M. Pérez,[1] J. C. Varekamp,[2] B. Henriquez,[3] A. Hernández,[3] J. Barrancos,[1] E. Padrón,[1] D. Calvo,[1] and G. Melián[1]

Abstract—A sudden eruption at Santa Ana occurred on 1 October 2005, producing an ash-and-gas plume to a height in excess of 10 km above the volcano. Several days before, thermal infrared images of the crater provided precursory signals of the eruption. A significant increase in the extent and intensity of the fumarolic field inside the crater rim and of the surface temperature of the crater's lake was observed. Changes in energy input was also estimated to explain the increase in lake temperature based on energy/mass balance calculations.

Key words: Santa Ana, crater lake, volcanic eruption, thermal precursors.

1. Introduction

Santa Ana volcano is located 40 km west of San Salvador, in Central America. This massive stratovolcano rises 2,381 m above mean sea level (Fig. 1) and forms a part of the Central American volcanic chain, which results from the convergence of the Cocos and the Caribbean plates. It is located at the intersection of a NW-SE system of regional faults (Williams and Meyer-Abich, 1955) and the southern boundary of the so-called 'Central American Graben', an extensional structure parallel to the Pacific coastline of El Salvador (Rotolo and Castorina, 1998). The NW-SE system of faults is considered a major structural feature of El Salvador's geology (Wiesemann, 1975), found over the entire country, and expressed in the Santa Ana region by fissures and alignments of volcanic edifices and eruptive centers. This volcanic complex consists of the Coatepeque collapse caldera, a 6.5×10.5 km elliptical depression about 0.22 Ma (Pullinger, 1998), the Santa Ana and Izalco volcanoes, as well as numerous cinder cones and explosion craters (Fig. 1).

[1] Environmental Research Division, Instituto Tecnológico y de Energías Renovables (ITER), 38611 Granadilla de Abona, S/C de Tenerife, Spain. E-mail: phdez@iter.es
[2] Earth and Environmental Sciences, Wesleyan University, 265 Church Street, Middletown, CT 06459-0139, USA.
[3] Instituto de Ciencias de la Tierra, Universidad de El Salvador, El Salvador, Central America.
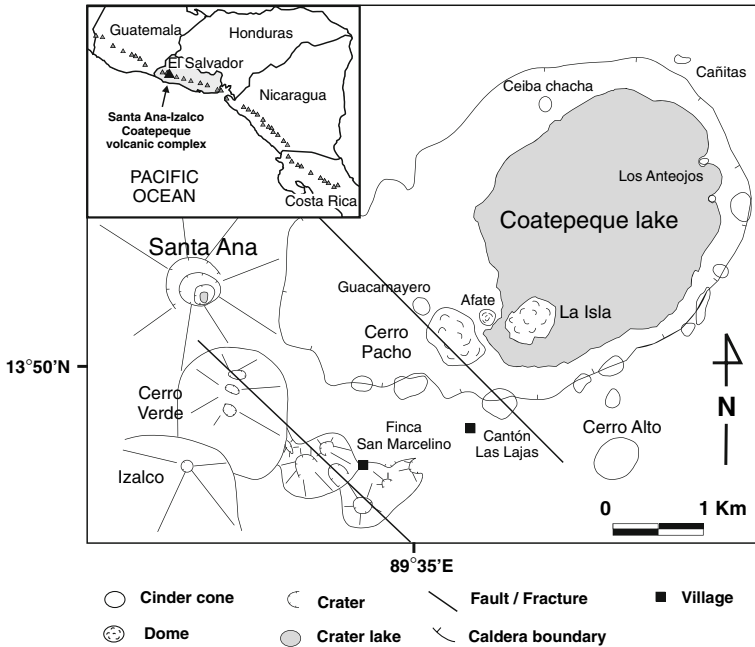
Figure 1

Simple morphological and structural map of Santa Ana volcano complex and its surroundings, El Salvador, Central America. In the map of Central America, closed triangles represent active volcanic systems of the Central American Volcanic Belt.

The activity during the last few thousand years has been characterized by phreatic or phreatomagmatic eruptions at the central summit vent (PULLINGER, 1998), suggesting the existence of a large and permanent hydrothermal system beneath the Santa Ana volcano. With 12 historic eruptions, it is one of the most active volcanoes in El Salvador. Its summit contains an acid lake with an average surface temperature of 18–20°C within a 0.5-km diameter explosion crater that was formed during the most recent eruption in 1904. Hot springs, gas bubbling and intense fumarolic emissions are observed along the shoreline of this crater lake. A volcanic gas plume, usually driven by the NE trades, may be seen rising to 500 m from the summit crater of the Santa Ana volcano.

The presence of a lake in the crater represents an interesting opportunity for long-term monitoring since it acts as a calorimeter and chemical condenser, integrating most of the heat flux and volatiles released by the shallow magma (BERNARD *et al.*, 2004). The physico-chemical characteristics of a volcanic lake depend largely on the magnitude of the volcanic/hydrothermal heat and mass influx and the capacity of the lake to dissipate the heat. BERNARD *et al.* (2004) observed changes in the depth and volume of the crater's lake between 2000 and 2002 from 27 m to 20 m and from 4.5×10^5 m^3 to 3.10^5 m^3, respectively. Changes of the temperature and chemical and physical parameters of the

volcanic gases and volcanic lakes have been observed before volcanic eruptions and became useful tools to monitor the activity of the volcanoes (GIGGENBACH, 1974, 1983; TAKANO, 1987; ROWE *et al.*, 1992; BADRUDIN, 1994; PASTERNACK AND VAREKAMP, 1997; VANDERMEULEBROUCK *et al.*, 2000; HERNÁNDEZ *et al.*, 2001; VAREKAMP *et al.*, 2001, DEHN *et al.*, 2002).

In the beginning of July 2005, the seismic network of the Servicio Nacional de Estudios Territoriales (SNET) of El Salvador at Santa Ana volcano detected an anomalous seismic activity (09/2005, BGVN 30:09). After the detection of these possible volcanic precursors, a monitoring of the SO_2 emission in the volcanic plume of Santa Ana by means of remote sensors (COSPEC and miniDOAS) started. University of El Salvador (UES) scientists carried out most of the measurements under a collaborative scientific project UES-ITER (Institute of Technology and Renewable Energy) financed by the Spanish Aid Agency (AECI), finding a significant increase of the SO_2 emission rate at the beginning of September 2005 (OLMOS *et al.*, 2007). Subsequently, a more intensive survey was carried out at Santa Ana volcano several days before the volcanic eruption on October 1, 2005. A thermal survey of the summit crater fumaroles and the volcanic lake together with intensive monitoring of the volcanic plume before and after the volcanic eruption provided information on precursory signals of the pending volcanic eruption.

This paper reports the thermal precursors detected before the 2005 eruption of Santa Ana and estimates the energy/mass balance associated with the volcanic heat transfer during the volcanic unrest.

2. *Chronology of the Volcanic Eruption*

Based on the monthly Smithsonian reports of the volcanic activity of Santa Ana (04/2001, BGVN 26:04; 09/2005, BGVN 30:09) since June 2005, strong degassing occurred at the summit area with an ash emission on 16 June. A slight increase in the seismicity together with a significant increase in the gas emission rate were observed from 27 July until at least 30 August. SNET scientists recorded on a daily basis surface temperature at the center of the lake, documenting an increase of the from 20°C to 25°C during the period April–June 2005. No more data are available since then due to accessibility problems. Observations made by SNET scientists on 29 August revealed incandescent rocks in the fumarolic fields inside the summit crater, effects attributed to hot gases heating the rocks. At that time, a significant increase in SO_2 emission was recorded (OLMOS *et al.*, 2007), together with a gas-and-steam plume rising 500–1,000 m above the volcano's crater. After these volcanic unrest signals, seismicity and gas emissions continued above normal levels. During the first two weeks of September, the SO_2 flux was over 1,000 metric tons per day and from 5 September, satellite imagery detected a thermal anomaly. On 16 September SO_2 flux reached a maximum of 3,320 metric tons per day (14–20 September/2005, BGVN; OLMOS *et al.*, 2007). Microseis-

micity remained at relatively high levels and incandescence was visible inside some cracks. During 21–26 September, seismicity and gas emissions showed the highest values (1000–4000 tn SO_2; BARRANCOS, 2005; OLMOS *et al.*, 2007), indicating the possibility of the occurrence of a volcanic eruption.

On 1 October 2005, a volcanic eruption occurred at Santa Ana, producing a plume of 14 km of altitude and several lahar deposits as far as 2 km SE of the volcano (28 September – 4 October/2005, BGVN). Following the eruption of 1 October, small explosions, degassing, and low-to-moderate seismicity occurred at Santa Ana during 5–11 October. Surprisingly, during an aerial inspection of the volcano by the scientific staff of SNET on 11 October, no important changes were observed at the crater. On 11 October, SO_2 measurements were around 600–700 metric tons per day.

The volcanic activity of Santa Ana remained high until February 2006, with relatively high SO_2 emission rates (500–1000 *t/d*) (Barrancos, personal communication), seismicity above background levels, and strong evaporation of the summit crater lake.

3. Procedures and Methods

With the aim to detect thermal precursors of the volcanic eruption of Santa Ana volcano, a handheld thermal camera FLIR (Forward Looking Infrared Radiometer) model P65 was used to collect thermal images from the crater's lake and fumarolic area at the summit of the volcano. FLIR data were collected on a daily basis between September 19 and 26, 2005, and between February 20 and 26, 2006. This type of handheld thermal camera has been used at other volcanoes such as Etna and Stromboli volcanoes (DEHN *et al*. 2002, CALVARI and PINKERTON, 2004; CALVARI *et al*. 2005) and other volcanic areas (CALVO *et al*., 2006, PADRÓN *et al*., 2006). The FLIR consists of an uncooled microbolometer detector with a thermal sensitivity of 0.05°C (50/60 Hz 50 mk at 30°C) which allows us to clearly see the smallest temperature differences. A total of 76,000 pixels provide real-time, crisp, high-resolution 16-bit thermal images. The built-in visual camera provides digital images linked with corresponding thermal images. The field of view/min focus distance is 19 × 14°/0.3 m with a spatial resolution (IFOV) of 1.1 mrad. Internal calibration together with an atmospheric correction based on user input for reflected ambient temperature, distance, relative humidity, atmospheric transmission, and external optics allow the FLIR to calculate realistic digital source temperatures. Ambient temperature and relative humidity were measured every ten minutes at the start of the thermal measurements with specific sensors, whereas an emissivity correction factor was taken at 0.95 for hot rocks at the fumarolic areas and at 0.96 for the lake water surface. Accuracy of the instrument (% of reading) was ± 2 °C or ± 2%.

Depending on the lens installed in the camera, different ranges of temperature are available: −40°C to +120°C, 0°C to +250°C, +150°C to +500°C, and up to +1500°C, which we did not have at the time of the September 2005 survey. During the collection of
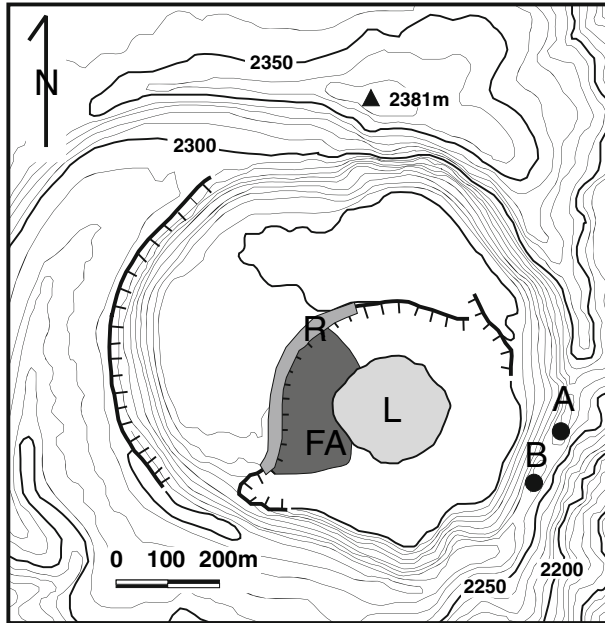
Figure 2

Summit area of Santa Ana volcano showing the sites (A and B) from where the thermal IR images were recorded
in both surveys, September 2005 and February 2006. Abbreviations are as follows: FA, Fumarolic Area; L,
Lake; R, NE Rim of inner crater.

images, it is very important to select the correct range as well as the long line-of-sight.
Since the distances from the measuring points to the crater's lake were about 400 m
(Fig. 2), we used the low-temperature range ($-40°$C to $+120°$C) for the detection of
small temperature gradients. Solar reflection was avoided since most of the measurements
were carried out after sunset. To check if reflection on the lake surface due to the thermal
energy radiated from the high temperature fumarolic field was affecting the observed
thermal anomalies, several pictures were taken from the west side of the rim. The results
were similar to the images taken from A and B sites (Fig. 2). The middle temperature
range ($+150°$C to $+500°$C), which can measure extrapolated temperatures up to $+850°$C,
was used for observing the incandescent fumarolic areas. To minimize the effect of gas
and aerosols absorption, most of the measurements were carried out from the opposite
side of the crater where the volcanic plume occurred. We assumed following CALVARI
et al. (2005), the associated errors to the thermal images collected during this field work
to be between 6–20%, depending mainly on the wind direction during the measurements.
Once measurements in the field were completed, images were optimized with the
software TherrmaCAM at the field lab.

    SO_2 flux measurements were taken by means of two different remote sensors, mini-
DOAS and COSPEC. Mini-DOAS was used in all the measurements whereas COSPEC

was used only during several days to compare the fluxes obtained with both instruments (BARRANCOS, 2005).

Mini-DOAS is based on an Ocean Optics USB2000 spectrometer, taking the light caught by the telescope and guided through an optical fiber to the spectrometer. The detector, which can operate at ambient temperature, is a CCD-array of 2048 elements (13 μm (width) × 200 μm (height)) treated for enhanced sensitivity below 360 nm resolution, a 50 μm slit and spectal resolution of ∼0.6 nm over the wavelength range of 245–380 nm. The COSPEC is a correlation spectrometer designed for vertical or slant column measurements of SO_2 concentration using zenith sky-scattered sunlight. The calibration always was performed *in situ* by placing cells containing known amounts (ppm•m) of gas in the path of the radiance dispersed by the instrument ('high and low'). The detection limit of the COSPEC is lower than 5 ppm with short time constants (1 s), and higher than 10% during adverse meteorological conditions which affect the intensity of light.

Measurements by COSPEC and mini-DOAS were carried out as mobile measurements by placing the instruments on a car and traversing beneath and roughly perpendicularly to the volcanic plume of Santa Ana (BARRANCOS, 2005). Total integrated concentration cross-sections of SO_2 were obtained and later multiplied by the estimated plume velocities to yield the total source emission rates (ton/day).

4. Summit Crater's Lake and Fumarole Temperatures

Measurements of temperature were focused at the summit crater lake and the active fumarolic areas by means of a thermal camera FLIR. During the September 2005 survey, a significant increase in the extent and intensity of the fumaroles and the surface temperature of the lake was observed. For several years, the fumarolic area located at the west side of the lake has been present, with temperatures of 532°C measured in January 2000, 875°C in June 2002 due to a sudden increase in the fumarolic activity (BERNARD *et al.*, 2004) and decreasing in December 2003 to 264°C and January 2004 to 360°C (SNET, Monthly Report). Due to technical and accessibility problems, no more temperature measurements in the high temperature fumarolic area have been carried out since February 2004.

Surface temperature of volcanic lakes is a good indicator of volcanic activity. During periods of low volcanic activity, temperatures of the water at the crater's lake of Santa Ana volcano range near ambient atmospheric values (17–21°C). Heating episodes increase the temperature of the lake water and reflect changes in the flow rate or in the enthalpy of hot fluids entering the lake (BERNARD *et al.*, 2004). The only way to obtain temperature data of the fumarolic area and crater's lake at the time of both surveys was the use of a handheld thermal camera. For this reason thermal IR images were taken at the lake's surface during September 2005 and February 2006 surveys. During both thermal
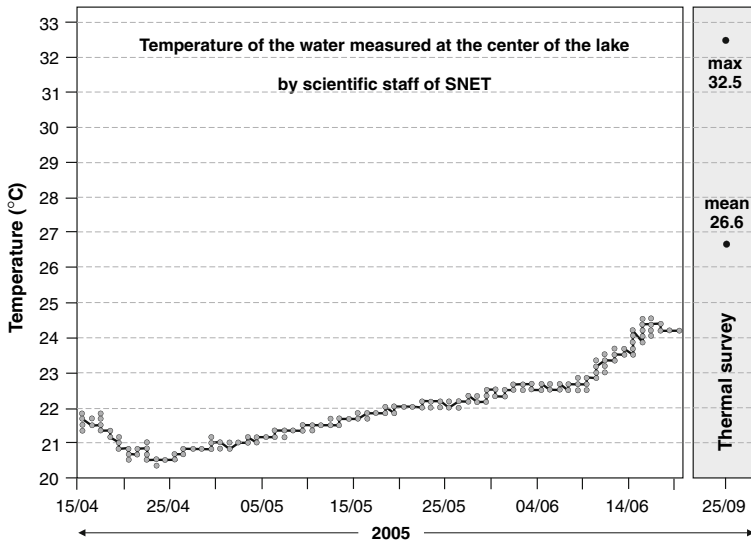
Figure 3

Time series of temperature measured at the center of Santa Ana volcano crater's lake by scientific staff of SNET (El Salvador) during the period April to July 2005. Also shown are the maximum and average temperatures measured at the center of the crater's lake with the thermal camera FLIR in September 25, 2005.

surveys, measurements were carried out under stable weather conditions, avoiding cloudy days and rain.

During the measurements carried out in September 2005, we used an average value of 65% for atmospheric humidity, 22°C for atmospheric temperature and 0.88 for atmospheric transmission. The viewing distance for the measurements was 400 m, resulting in a pixel size of 50 cm; such a small pixel size can reduce apparent peak temperatures. One of the most important observations was the significant increase of the temperature at the center of the lake surface's, compared to the temperatures measured at the same area by the SNET scientific staff until July 2005 (Fig. 3). This increase was higher in those areas closer to the fumarolic field, where bubbling was also observed, indicating changes in the flow of hot gases entering the lake. These observations, together with the increase in the seismicity and the relatively high SO_2 flux emission rates measured during this survey, indicated precursory signals of renewal magmatic activity at Santa Ana and suggested the possibility of an incoming high volcanic activity in the immediate future. From the observed temperature gradient at the lake's surface in 20 September 2005, we distinguished four areas characterized by different colors (different temperatures) which we called areas 1, 2 3, and 4 (Fig. 4). Table 1 shows the average and maximum surface temperatures of the four colored areas selected at the lake during the September 2005 thermal survey. The maximum apparent temperature measured at the surface of the lake at that time was 58°C and close to the fumarolic field with an average temperature of 29°C for the lake surface.
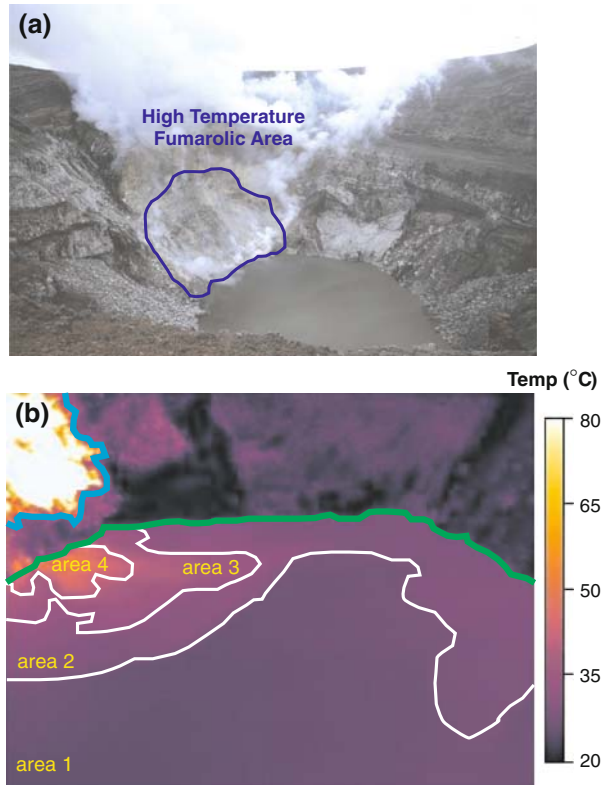
Figure 4

(a) View of Santa Ana's summit crater and hosted crater's lake taken September 20, 2005, from the southeast rim. Dark blue line indicates the area affected by intensive fumarolic activity. (b) Thermal image of the lake's surface taken from the southeastern rim of Santa Ana volcano on 20 September 2005. White lines indicate separately the four different thermal areas selected in this study. Green line denotes the crater's lake shore line. The yellow bright spot at the high left end of the image is the high temperature fumarolic area.

Thermal images of the fumarolic field were taken on 20, 21 and 25 of September 2005, the last one five days before the volcanic eruption (Figs. 5a, 5b and 5c). These three images have been corrected with the atmospheric and internal parameters of the FLIR for comparison. The IR images show the concentric and incandescent fractures which

Table 1

Surface lake's apparent temperatures measured at Santa Ana crater lake on September 20, 2005

Area	Average Temperature (°C)	Maximum Temperature °C
1	27	33
2	29	37
3	36	47
4	46	58
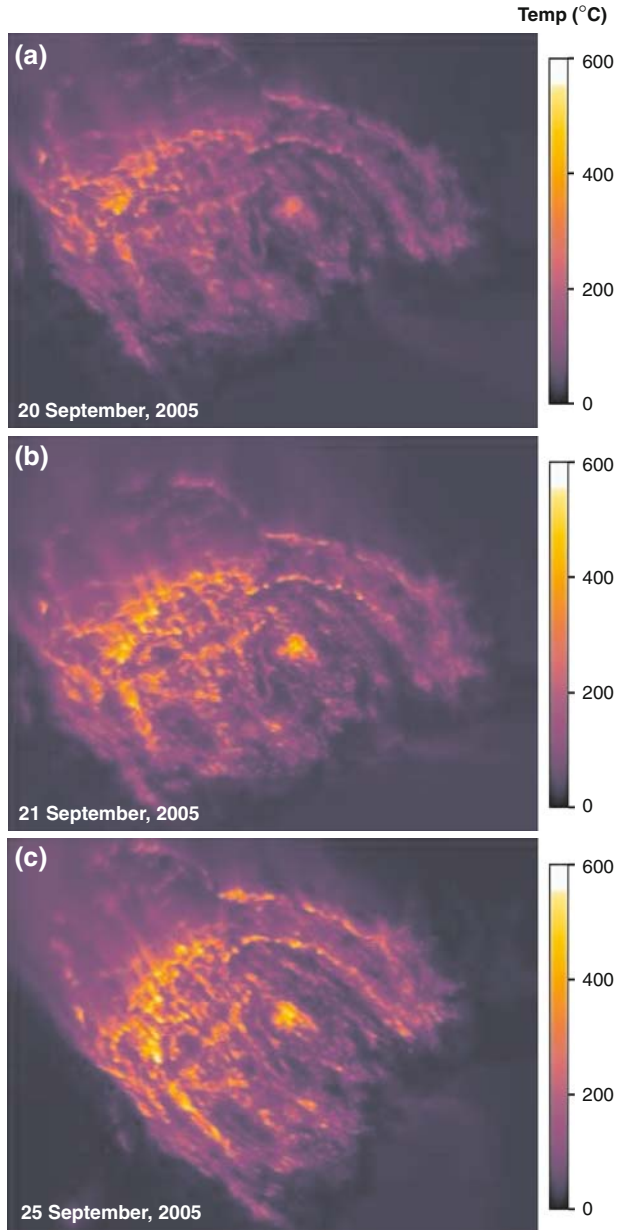
Figure 5
Thermal images taken on the high temperature fumarolic area (FA) on (a) 20 September 2005, (b) 21 September 2005 and (c) 25 September 2005, just few days before the volcanic eruption of Santa Ana volcano.

resulted from inflation of the fumarolic field due to the high pressure of endogenous hot gases. An increased intensity of the hotter areas is observed, indicating the increase of the hydrothermal activity beneath Santa Ana volcano a few days before the volcanic eruption.

In February 2006, four months after the volcanic eruption, a new thermal survey was performed at Santa Ana summit crater. At this time the crater's lake showed a continuous lowering of the water lake level. Thermal IR images were recorded at the same sites as those in September 2005. A significant decrease in the apparent temperature of the remaining fumaroles at the summit crater was observed. As was mentioned above, the area affected by hot degassing and incandescence was "cut" and disappeared with the volcanic explosions during the eruption, leaving just a vertical escarpment. During this second thermal survey, the remaining vertical escarpment showed no significant high temperature (Fig. 6a). At the time of the volcanic eruption, the incandescent area disappeared due to the volcanic explosions that occurred inside the summit crater. This fact, together with the decreasing hydrothermal activity, explains the observed relatively low fumarolic temperatures. However, a different behavior was observed at the surface lake temperature. At the time of the February 2006 thermal survey, a significant increase in the water lake surface temperatures was observed, this time quite homogeneous over the lake (Fig. 6b). The maximum recorded apparent temperature was about 67°C, close to a small island that formed on the east
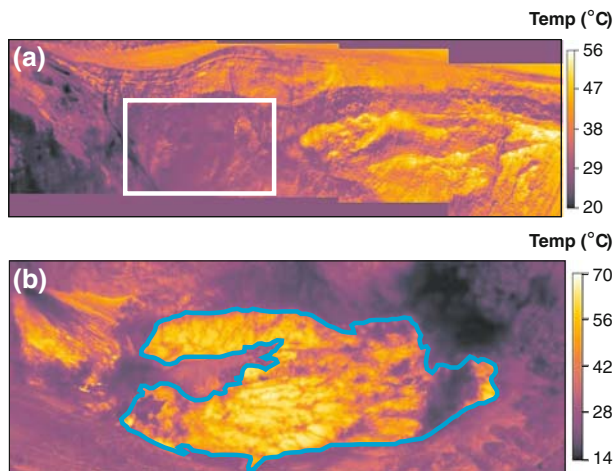
Figure 6

(a) Thermal image of the remaining vertical escarpment left after the volcanic eruption taken during the February thermal survey (R in Fig. 2). White square indicates the location of the Fumarolic area before the volcanic eruption. No significant thermal anomalies are observed. (b) Thermal image of the lake's surface taken from the southeastern rim of Santa Ana volcano on 24 February 2006, blue line shows the crater's lake shore line.

side of the lake due to the strong evaporation. The fast evaporation process occurring at the crater lake of Santa Ana after the volcanic eruption was possibly due to the residual heat in hot rocks remaining beneath the volcano.

Lack of evidence regarding the presence of "fresh rocks" suggests that the anomaly that led to the explosion was fed by a shallow, strongly degassing magma body. The closeness to the surface was responsible for the high measured temperatures, and possibly water that drained into heated cracks served as the trigger of the eruption. Seismic data provided by SNET shows that banded as well as polychromatic tremor, and also LP and VT events were indicating the ascent of magmatic gases, however no evidence of extruding magma has been provided. In 2002, 875 °C was measured in the fumarolic field without an eruption, consequently we can assume a vertical oscillation of a magmatic body beneath the volcano. Thermal imagery is then essential for detecting future changes in the dynamics of Santa Ana volcano.

5. Energy and Mass Balance Calculation

The observed increase of temperature at the surface of the lake of the Santa Ana volcano during the volcanic unrest of 2005 indicated the existence of changes in the heat input into the lake system of the volcano. To evaluate the magnitude of volcanic energy input during the volcanic crisis, we used a box model developed by PASTERNACK and VAREKAMP (P&V, 1997). Since the physico-chemical characteristics of a volcanic lake depend largely on the magnitude of the volcanic/hydrothermal heat and mass influx and the capacity of the lake to dissipate the heat, the P&V model uses outgoing energy and mass fluxes as a function of lake temperature, basin geometry and atmospheric parameters. Water mass balance with inputs of meteoric water and geothermal vapor or liquid and outputs of water lost by evaporation, seepage, or stream outflow determine whether a lake will maintain its volume or not (BRANTLEY et al., 1993). For a steady-state, energy balance is expressed as:

$$E_{\text{cond}}^{\text{volc}} + E_{\text{rad}}^{\text{sun}} + E_{\text{volc}} + E_{\text{rad}}^{\text{atm}} = E_{\text{rad}}^{\text{lake}} + E_{\text{evap}} + E_{\text{cond}}^{\text{lake}} + E_{\text{meteoric}} \tag{1}$$

This equation shows that the energy inputs expressed as the sum of conductive heat input from a shallow magma body ($E_{\text{cond}}^{\text{volc}}$), the short-wavelength solar flux ($E_{\text{rad}}^{\text{sun}}$), the enthalpy of the volcanic/hydrothermal flux (E_{volc}) and the long-wavelength radiative input from the atmosphere ($E_{\text{rad}}^{\text{atm}}$) must equal the lake surface long-wavelength radiation ($E_{\text{rad}}^{\text{lake}}$), heat loss due to surface evaporation (E_{evap}), lake surface conduction ($E_{\text{cond}}^{\text{lake}}$) and heating of meteoric influxes up to the lake's temperature (E_{meteoric}). To yield a conceptual and generic model Pasternack and Varekamp made several simplifications and assumptions (see P&V, 1997).

The model currently runs in Mathematica 5.2 and solves simultaneously all the energy and mass-balance statements. Atmospheric parameters such as average annual

air temperature, cloudiness and precipitation rate were entered, based on local observations or derived from the geographical location (latitude) and altitude. The temperature of the volcanic gas input is expressed as a function of the gas mass flux, using a step function (a small flux of gas cools rapidly whereas a big gas flux maintains magmatic temperatures). Following P&V (1997), we used a 'standard arc gas' with the composition of 2% SO_2, 5% CO_2 and 93% of H_2O. Gas inputs were expressed in MW as well as in equivalent SO_2 fluxes (*t/d*) for comparison with COSPEC data (BARRANCOS, J., 2005; OLMOS *et al.*, 2007). Ultimately, since the main energy input comes from the conversion of steam to liquid water (enthalpy of condensation), gas temperature and gas composition are not critical parameters (P&V., 1997). The current version of the P&V model uses the evaporation expressions after SILL (1983) conformed to STEVENSON (1992), nonetheless an important difference is the phrasing of the long wavelength heat input from the atmosphere. The P&V model uses an empirical expression that relates measured long wavelength heat fluxes to the surface temperature (following LINACRE, 1992), whereas most other models simply use Boltzman's Law with the surface temperature (STEVENSON, 1992, BERNARD *et al.*, 2004). The latter approach creates larger atmospheric heat inputs into a lake (up to 30%), with resulting smaller volcanic heat inputs needed to obtain a given temperature.

Running the model with various air surface temperatures at different elevations from El Salvador, we calculated the surface temperature from the latitude and the elevation of Santa Ana volcano (using a lapse rate of 6°C per km), getting a satisfactory relation between elevation and air temperature. With this fitting we used a mean September 2005 temperature for the town of Santa Ana of 26.1°C (http://www.tutiempo.net/en/Climate/Santa_Ana_El_Palmar/09-2005/786550.htm) which gave an air temperature in the crater
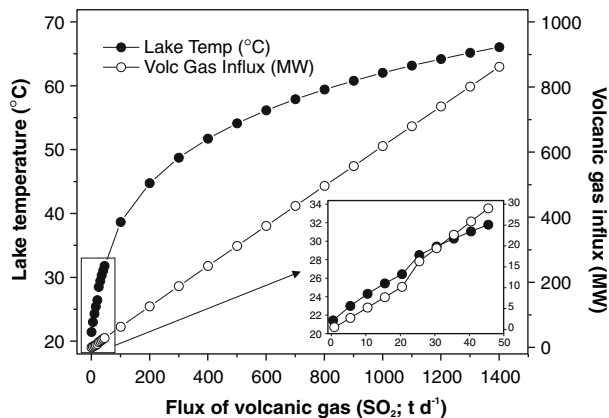
Figure 7

Energy model results for a volcanic gas input and the resulting lake water temperature, with parameters specific for Santa Ana volcano. The flux of volcanic gas is expressed in MW as well as in equivalent SO_2 fluxes (*t/d*). Also shown in more detail are the results for lake water temperature range 20–34°C.
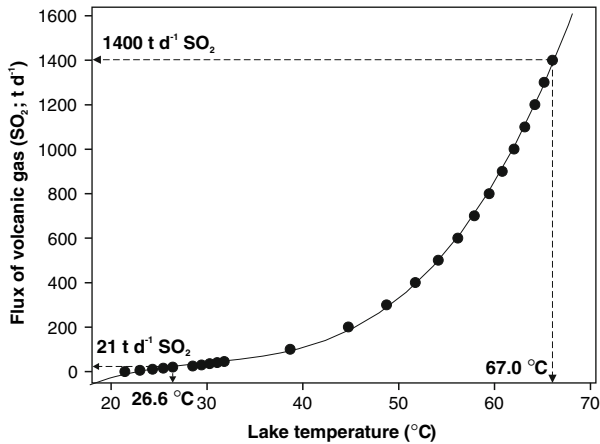
Figure 8
Relationship between the calculated flux of volcanic gas (SO₂, *t/d*) and surface lake's temperature for September 2005.

of 16.6°C, very close to locally measured temperatures *in situ*. We used a gas temperature of 875°C, as measured in 2002 in the crater. The results of the model calculations are shown in Figure 7.

Assuming an average temperature of 26.6°C for the entire lake's surface during our field work in September 2005, we estimated the flux of volcanic gas necessary to maintain the observed lake temperature. Our calculations yielded a total of 21 *t/d* of SO_2 (Fig. 8) or 10 MW for Santa Ana volcanic lake (20 m depth and 200 m of diameter), a value in the range of similar volcanic lakes (PASTERNACK and VAREKAMP, 1997). BERNARD *et al*. (2004) reported an energy flux of 16 MW when the lake surface was at its peak temperature (30°C) in July-August 2000, which would give with the P&V model an energy flux of 24 MW (using a crater air temperature of 15.7°C for June 2000), a slightly larger value for model specific reasons that were discussed above. These values reflected changes in the dynamics of the volcanic gas entering the lake and a clear sign of volcanic unrest. Most of reported values of SO_2 flux measured with COSPEC and miniDOAS during our thermal measurements (OLMOS *et al*., 2007) were in the range of 500–1500 *t/d*, which are considerably higher than the calculated values for the lake. In situ observations at the crater area during our measurements showed that most of the volcanic gas (volcanic plume) escaped through the fumarolic field and not from the lake's surface. Only part of this gas was heating the water of the lake to the observed temperature. Those areas of the lake showing higher temperatures (max. of 54°C) were located close to the fumarolic field, indicating that only these areas of the lake (areas 3 and 4 in Fig. 4) were affected by the hot gases entering the lake.

During the volcanic eruption which occurred on October 1, part of the lake was "ejected" due to the phreatic explosion. Since the meteorological conditions did not

allow scientists to make visual inspections of the summit crater, later on (November 2005) again a volcanic lake with slight changes in the color (light green), shape, level of water and with a strong bubbling at its center (SNET, Informe mensual N°7) was observed. Our observations made in February 2006 indicated a higher lake temperature (67°C) and a fast evaporation rate indicating that the lake was not going to keep its mass for a longer period of time. The loss of mass was so fast that during the 10-days field work the level of the lake decreased about 1 meter. The volcanic input required to create a lake temperature of 67 $^{\circ}$C is 1400 t SO$_2$/day or 860 MW energy input (Fig. 8).

6. *Conclusions*

Two thermal surveys conducted before and after the occurrence of a volcanic eruption of Santa Ana volcano on 1 October 2005 enabled detection of crater's lake temperature changes related to the eruption. The strong degassing observed before the eruption seems to be responsible for the recorded thermal anomalies at the crater's lake surface. The observed changes in the apparent temperatures in the fumarolic field and lake, together with the magnitude of volcanic energy input, reflected changes in the dynamics of the volcanic gas entering the lake and were a clear sign of a volcanic unrest. The use of a thermal imaging system at Santa Ana volcano provides a clear potential for detecting changes in the dynamics of active volcanic systems.

Acknowledgements

REFERENCES

BADRUDIN, M. (1994), *Kelut volcano monitoring, Hazards, mitigation and changes in water chemistry prior to the 1990 eruption*, Geochem. J. *28*, 233–241.

BARRANCOS, J. (2005), *Determinación de emisiones de dióxido de azufre (SO2) procedentes de fuentes naturales y antrópicas mediante el uso de sensores ópticos remotos, COSPEC & miniDOAS*. Master degree, University of La Laguna, 132pp.

BERNARD, A., ESCOBAR, D., MAZOT, A., and GUTIERREZ, R. (2004), *The acid volcanic lake of Santa Ana volcano, El Salvador*. In: *Natural Hazards in El Salvador*. Geological Society of America, Special Paper *375*, 121–133.

BRANTLEY, S.L., ÁGÚSTSDÓTTIR, A.M., and ROWE, G.L. (1993), *Crater Lakes Reveal volcanic heat and volatile fluxes*. GSA Today *3* (7), 175–178.

CALVARI, S. and PINKERTON, H. (2004), *Birth, growth and morphologic evolution of the 'Laghetto' cinder cone during the 2001 Etna eruption*, J. Volcanol. Geotherm. Res. *123*, 225–239.

CALVARI, S, SPAMPINATO, L., LODATO, L., HARRIS, A., PATRICK, M., DEHN, J., BURTON, M., and ANDRONICO, D., (2005), *Chronology and complex volcanic processes during the 2002–2003 flank eruption at Stromboli volcano (Italy) reconstructed from direct observations and surveys with a handheld thermal camera*, J. Geophys. Res. Solid Earth, Section B *110* (2).

CALVO, D., HERNÁNDEZ, P.A., PÉREZ, N., AURÍA, G., MELIÁN, G., PADRÓN, E., NOLASCO, D. and BARRANCOS, J, (2006), *Thermal monitoring using a portable IR camera in Central America volcanoes*, GARAVOLCAN Internat. Symp., Session 2, May 2006.

DEHN, J., DEAN, K.G., ENGLE, K., and IZBEKOV, P. (2002), *Thermal precursors in satellite imagery of the 1999 eruption of Shishaldin*, Bull. Volcanol. *64*, 525–534.

GIGGENBACH, W.F. (1974), *The chemistry of Crater Lake, Mt. Ruapehu (New Zealand) during and after the 1971 active period*, New Zealand J. Sci. *17*, 33–45.

GIGGENBACH, W.F. (1983), *Chemical surveillance of active volcanoes in New Zealand*, In: *Forecasting Volcanic Events* (Tazieff, H. and Sabroux, J.C., eds.) (Elsevier, Amsterdam, 1983), pp. 311–322.

HERNÁNDEZ, P.A., NOTSU, K., SALAZAR, J.M., MORI, T., NATALE, G., OKADA, H., VIRGILI, G., SHIMOIKE, Y., SATO, M., and PÉREZ, N.M. (2001), *Carbon dioxide degassing by advective flow from Usu volcano, Japan*, Science *292*, 83–86.

LINACRE, E., *Climate Data and Resources. A Reference and Guide*. (Routledge, London 1992).

OLMOS, R., BARRANCOS, J., RIVERA, C., BARAHONA, F., LÓPEZ, D., HENRIQUEZ, B., HERNÁNDEZ, A., BENITEZ, E., HERNÁNDEZ, P.A., PÉREZ, N.M., GALLE, B., and RUDAMAS, C. (2007), *Anomalous emissions of SO_2 during the recent eruption of Santa Ana Volcano, El Salvador, Central America*. Pure Appl. Geophys. (this volume).

PADRÓN, E., PÉREZ, N., HERNÁNDEZ, P.A., MELIÁN, G., BARRANCOS, J., NOLASCO, D., CALVO, D. and AURÍA, G, (2006), *Thermal monitoring program for the volcanic surveillance in the Canay Islands*, GARAVOLCAN Internat. Symp. Session 2, May 2006.

PASTERNACK, G.B. and VAREKAMP, J.C. (19970, *Volcanic lake systematics. I. Physical constraints*, Bull. Volc. *58*, 528–538.

PULLINGER, C. (1998), Evolution *of the Santa Ana volcanic complex, El Salvador* [M.S. Thesis], Houghton, Michigan Technologycal University, 151 pp.

ROTOLO, S.G. and. CASTORINA, F. (1998), *Transition from mildly-tholeiitic to calc-alkaline suite: The case of Chichontepec volcanic center, El Salvador, Central America*, J. Volcanol. Geotherm. Res. (Elsevier, Amsterdam) 86, 117–136.

ROWE, G., OHSAWA, S., TAKANO, B., BRANTLEY, S., FERNÁNDEZ, J.F., and BARQUERO, J. (1992), *Using crater lake chemistry to predict volcanic activity at Poás volcano, Costa Rica*, Bull. Volcanol. *54*, 494–503.

SILL, W.R. (1983), Self-*potential modeling from primary flows*, Geophysics 48, 76–86.

SMITHSONIAN INSTITUTION (2001), Bulletin of the Global Volcanism Network, April, 2001.

SMITHSONIAN INSTITUTION (2005), Bulletin of the Global Volcanism Network. 14–20, September 2005.

SMITHSONIAN INSTITUTION (2005), Bulletin of the Global Volcanism Network. 30: 09, September 2005.

SMITHSONIAN INSTITUTION (2005), Bulletin of the Global Volcanism Network. 28:09–4:10, October 2005.

STEVENSON, D.S. (1992), *Heat transfer in active volcanoes: Models of crater lake systems* [Ph.D. thesis], Cambridge, UK, Department of Earth Sciences, The Open University, 234 pp.

TAKANO, B. (1987), *Correlation of volcanic activity with sulfur oxyanion speciation in a crater lake*, Science, *235*, 1445.

VANDEMEULEBROUCK, J., SABROUX, J.-C., HALBWACHS, M., SURONO, POUSSIELGUE, N., GRANGEON, J., and TABBAGH, J. (2000), *Hydroacoustic noise precursors of the 1990 eruption of Kelut volcano, Indonesia*, J. Volcan. Geotherm. Res. *97*, 443–456.

VAREKAMP, J.C., OUIMETTE, A., HERMAN, S., BERMUDEZ, A., and DELPINO, D. (2001), *Hydrothermal element fluxes during the 2000 eruptions of Copahue, Argentina, A 'Beehive' Volcano in Turmoil*, Geology *29*, 1059–1062.

WIESEMANN, G. (1975), *Remarks on the geologic structure of the Republic of El Salvador*. Mitt. Geol.-Palaeontol. Inst. Univ. Hamburg *44*, 557–574.

WILLIAMS, H. and MEYER-ABICH, H. (1955), *Volcanism in the southern part of El Salvador.* Univ. Calif. Publ. Geol. Sci. *32*, 1–64, 7 Fig., 8 Pl., Berkeley-Los Angeles.

To access this journal online:
www.birkhauser.ch/pageoph

Temporal Variability of Major and Trace Element Concentrations in the Groundwaters of Mt. Etna (Italy): Effects of Transient Input of Magmatic Fluids Highlighted by Means of Cluster Analysis

SALVATORE GIAMMANCO,[1] MASSIMO OTTAVIANI,[2] and ENRICO VESCHETTI[2]

Abstract—Data for major, minor and trace elements in groundwaters from Mt. Etna volcano collected in 1994, 1995 and 1997 were analyzed using Cluster Analysis (CA). Two groups of sampling sites were identified (named clusters A and B), mainly on the basis of their different salinity and content of dissolved CO_2. The highest levels of both of these parameters were observed in the sites of cluster A, located in the lower southwestern and central eastern flanks of the volcano. For both of the statistical groups CA was repeated, taking into account the mean values of each parameter in time, and the results allowed us to recognize four distinct groups of parameters for each group of sites on the basis of their temporal patterns. Four different types of temporal patterns were recognized: concave, convex, increasing, decreasing. The observed changes were basically interpreted as a result of the different response of dissolved chemical elements to changes in the aqueous environment and/or in their solubility/mobility in water due to different rates of input of magmatic gases to Etna's aquifers. The main changes occurred in 1995, when Etna's volcanic activity resumed after a two-year period of rest. The temporal changes of the majority of the studied parameters (water temperature, water conductivity, Eh, pH, Al, Mg, B, Ca, Cl^-, Hg, Mn, Mo, Na, Ni, Se, Si, Sr, Cr Zn and pCO_2) were not cluster-dependent, therefore they were not apparently affected by differences in water salinity between the two groups of sampling sites. A limited number of parameters (Ti, K, Li, HCO_3^-, As, Fe, SO_4^{2-}, Cu and V), however, manifested different behaviors, depending on the cluster of sites to which they belonged, thus suggesting their apparent dependency on water salinity.

Key words: Trace elements, groundwater, Mount Etna, cluster analysis, volcanic activity.

1. Introduction

The chemical characteristics of groundwaters in the absence of human perturbations, are the result of several geochemical processes that are closely linked to the local natural environment. Underground water acquires salts from leaching of the host rock, a phenomenon strictly dependent upon the chemical composition of host rocks, the residence time of water—that in turn is a consequence of water flow velocity and length of the flow path—and the presence of reactive gas species, such as carbon dioxide (CO_2),

[1] Istituto Nazionale di Geofisica e Vulcanologia – Sezione di Catania, Piazza Roma 2, Catania 95123, Italy. E-mail: giammanco@ct.ingv.it
[2] Istituto Superiore di Sanità, Viale Regina Elena 299, Roma 00161, Italy.

that dissolve into water and enhance water aggressiveness towards the rock. In an active volcanic environment such as Mt. Etna, the latter is a highly efficient process (ANZÀ *et al.*, 1989; GIAMMANCO *et al.*, 1998; AIUPPA *et al.*, 2000). Actually, magma-derived gases, in particular CO_2, are abundantly released through the flanks of Etna besides their massive emission through the volcanic plume (ALLARD *et al.*, 1991; GIAMMANCO *et al.*, 1995; D'ALESSANDRO *et al.*, 1997), and strongly interact with the aquifers. DONGARRÀ *et al.* (1993) and BONFANTI *et al.* (1996) found that the concentration of the major species in solution, and particularly the calculated values of partial pressure of CO_2 with which waters equilibrated, can be subject to marked variations in time. Such variations were found to be caused both by seasonal effects and, more significantly, by increases in the volcanic activity of Etna.

Previous works on minor and trace elements in Etna's groundwaters (GIAMMANCO *et al.*, 1996, 1998; AIUPPA *et al.*, 2000) showed that their concentrations mostly derive from the geochemical processes mentioned above. However, many of those dissolved elements can also be directly supplied by magma-derived fluids and/or by hydrothermal fluids. Lastly, the pH and redox conditions of water can greatly affect the mobility of several trace elements in solution. These conditions in turn depend on the amount of reactive gas interacting with groundwater, and are expected to change markedly with time chiefly as a function of the intensity of volcanic activity.

2. *Geological and Hydrogeological Settings*

The large volcanic edifice of Mt. Etna (3,340 m of altitude and about 1200 km^2 of total surface) has matured during the last 500,000 years on the eastern coast of Sicily (Southern Italy) with the alternate superimposition of lava flows and pyroclastic deposits (ROMANO, 1982; CHESTER *et al.*, 1985). During the last 5,000 years Etna has been persistently active and has erupted volcanic products essentially made of lavas, with a composition that ranges from alkali-basalt to hawaiite (CHESTER *et al.*, 1985). Etna's volcanic products lie over a thick (>15 km) sedimentary substratum which is mostly composed of clays (Messinian age) to the east and south, and of clay, marl and quartz-arenite units, aging from Triassic to upper Pliocene, to the west and north (LENTINI, 1982). These units belong to the so-called Appenninian-Mahgrebian Chain that runs along northern Sicily from east to west, linking the Appennines to the Atlas Mountains of North Africa, and is structurally a part of the Indo-European plate (LENTINI, 1982). The units are reduced into several south-verging thrust sheets which progressively thrusted over each other during the collision with the African plate, from Eocene to the Quaternary (LENTINI, 1982).

The permeability of Etna's volcanics is generally high (2.5×10^{-7} to 2.9×10^{-6} cm^2, according to AURELI, 1973 and FERRARA, 1975), while that of the sediments of Etna's basement is on the contrary much lower (average value of 1×10^{-10} cm^2, according to SCHILIRÒ, 1988). Such a large permeability contrast, together with the remarkable amount

of water and snow precipitation that characterizes the area, implies that Mt. Etna volcano is also an important reservoir of groundwater (about 7×10^8 m^3 of water available per year, according to OGNIBEN, 1966).

The circulation of groundwater inside Mt. Etna is strongly influenced by the morphology of the sedimentary basement of the volcano. In fact, most of the waters that fall on the ground surface as rain and/or snow percolate through the permeable volcanic rocks. After reaching the impermeable basement, such waters move along radial directions towards the outer boundaries of the volcanic edifice. However, since Etna's basement reaches its maximum height (about 1200 m a.s.l.) slightly NW of the summit of the volcano and has a general slope towards SE, groundwaters tend to move and accumulate in the southern and eastern flanks of the volcanic edifice, where the number of springs and water-wells is actually highest (OGNIBEN, 1966). On the basis of the groundwater circulation, three main hydrogeological basins can be distinguished on Etna (OGNIBEN, 1966; FERRARA, 1990): The first roughly corresponds to the northern sector of the volcano, the second includes a great part of the western and southern flanks and the third, which is the largest one, includes most of the eastern part of it (Fig. 1). Regardless of the hydrogeological basin considered, the seasonal variation of water discharge from all of the springs of Mt. Etna normally shows two maxima, from November to January and from May to June (AURELI, 1973). The first period of high water discharge follows the period of highest rainfall in the area, whereas the second period of high discharge is related to spring melting of the abundant snow cover of Mt. Etna, with a consequent transitory increase in the recharge of water into the local aquifers (OGNIBEN, 1966).

3. Sampling and Analytical Methods

Twelve sampling sites at Mt. Etna were chosen for the collection of groundwater samples to be analyzed for their contents of major, minor and trace elements. Samplings were carried out in August 1994, November 1995 and September 1997 from 4 springs, 6 water wells and 2 drainage galleries, quite uniformly distributed over the surface of the volcano (Fig. 1). These sampling sites are part of a larger group that was first surveyed in 1994, and the results of that study can be found in GIAMMANCO *et al.* (1998). Hence, in the present work the sampling sites will be indicated with the same names used by GIAMMANCO *et al.* (1998). Before sampling from wells, tap water was allowed to run for several minutes. Samples for laboratory analyses were collected into 500 ml polythene flasks with screw caps. Prior to the sample collection, the flasks were rinsed at least four times with groundwater directly at the tap or at the spring and then three more times with filtered water, using a 0.45 μm membrane filter (GELMAN Sciences, Ann Arbor, Michigan, U.S.A.). After collection, each sample was filtered using the 0.45 μm Gelman filter, acidified with Ultrapur nitric acid to pH < 2 (0.2% v/v) and then stored at approximately 4°C. Water temperature, pH, Eh and electrical conductivity values were measured in the field with portable electronic instruments. Values of pH, Eh and
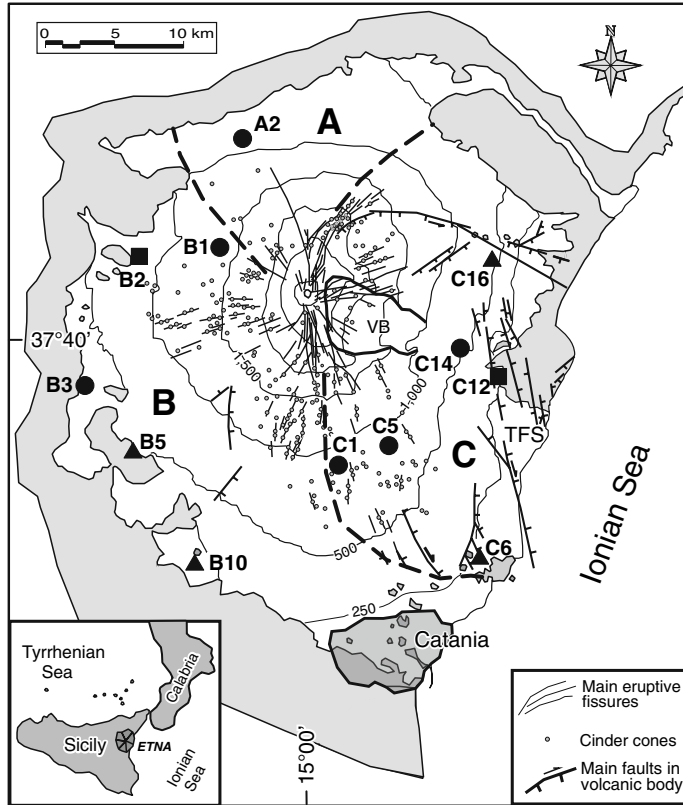
Figure 1

Simplified volcano-tectonic map of Mt. Etna (modified from ACOCELLA and NERI, 2003) showing the location of the groundwater sampling points and the main hydrogeological basins (separated by thick dashed lines: A = Northern basin; B = Western basin; C = Eastern basin) according to FERRARA (1990). Filled circles indicate wells, filled triangles indicate springs and filled squares indicate the entrance of drainage galleries. The white area encloses Etna's volcanic rocks. TFS = Timpe Fault System. VB = Valle del Bove morphological depression. Altitudes in meters.

conductivity are referred to the sampling temperature. The content of bicarbonate ion was also determined in the field by titration with standard hydrochloric acid 0.1 N using a bromocresol green-methyl red mixture as a colorimetric indicator. Values of $p(CO_2)$ were calculated from pH and HCO_3^- values.

Collected samples were quantitatively analyzed at the Istituto Superiore di Sanità, Rome, for the determination of major species (Ca, K, Mg, Na, Si, Cl^- and SO_4^{2-}) and minor and trace elements (Li, B, Al, Ti, V, Cr, Mn, Fe, Co, Ni, Cu, Zn, As, Se, Sr, Mo, Cd, Hg and Pb), after stabilization of samples with nitric acid. The concentration of sulphate ion was determined through the turbidimetric method. Chloride anion was measured by potentiometric titration with a standardized silver nitrate solution. The concentrations of Ca, K, Mg, Na, Li, Sr, as well as Fe and Mn for a few samples

particularly enriched in the two elements, were analyzed by means of inductively coupled plasma emission spectroscopy using a Perkin-Elmer PLASMA 400 spectrometer. Cold-vapor and hydride generation methods were applied to the determination of Hg and of the couple As - Se. These measurements were performed by a Perkin - Elmer 5000 atomic absorption spectrometer fit with Perkin - Elmer MHS − 20 Mercury/Hydrade System and electrically heated cylindrical quartz cells. The concentrations of B, Al, Ti, V, Cr, Mn, Fe, Co, Ni, Cu, Zn, Mo, Cd and Pb were determined by an Ati - Unicam SOLAAR 939QZ atomic absorption spectrometer using a SOLAAR GF90 Zeeman electrothermal atomizer and a SOLAAR FS90 PLUS furnace autosampler.

The accuracy of the analytical procedures was verified using both certified reference materials (CRM 398 and CRM 399, Community Bureau of Reference, BCR, Brussels, Belgium) and synthetic aqueous solutions, following the procedure indicated by GIAMMANCO et al. (1998). The precision of the values obtained by atomic absorption spectroscopy was determined as the percentage relative to the standard deviation of three consecutive measurements of the reference and synthetic solutions. Both accuracy and precision concerning the other parameters were those indicated in literature (APHA, AWWA and WEF, 1992; BAUER et al., 1985). Detection limits (LOD) were set as three times the standard deviation of the blank.

4. Results and Discussion

4.1. Geochemical Characterization of Sampled Waters

The analytical results of the three surveys carried out on Mt. Etna are reported in Tables 1 and 2. The results for the major chemical species (Table 1) show that ten out of twelve samples displayed a bicarbonate alkaline-earth composition, typical of most groundwaters of Mt. Etna (ANZÀ et al., 1989; GIAMMANCO et al., 1996, 1998; AIUPPA et al., 2000, 2004). Major elements in solutions are generally more abundant where the highest values of HCO_3^- concentrations are observed, which is an indication of the important role of the interaction between groundwater and CO_2 in enhancing basalt weathering. According to the model first proposed by ANZÀ et al. (1989), Etna's groundwaters are of meteoric origin, based on their Deuterium/Hydrogen and [18]Oxigen/[16]Oxigen isotopic ratios. When rain waters enter the aquifer, they become enriched in CO_2 which, according to the $\delta^{13}C$ values already available in literature, is mostly of magmatic origin (ANZÀ et al., 1993; ALLARD et al., 1997; AIUPPA et al., 2004). This process is ubiquitous on Mt. Etna, although it is enhanced in the most fractured and seismically active zones of the volcano (i.e., the SW and the E flanks), and it seems to mask any evolution of water chemistry from recharge to discharge areas (AIUPPA et al., 2004, and literature therein cited).

Sample C6 shows a chloride-sulphate alkaline-earth composition, being enriched in Cl^- and particularly in SO_4^{2-} ions. Sample B1 falls instead into the chloride-sulphate

Table 1

Analytical results for physico-chemical parameters and major species in the three surveys of Etna's ground water

Sample[a]	Date	T (°C)	Cond. (μS/cm)	Eh (mV)	pH	Na (mg/L)	Mg (mg/L)	K (mg/L)	Ca (mg/L)	HCO$_3^-$ (mg/L)	SO$_4^=$ (mg/L)	Cl$^-$ (mg/L)
A2	1994	12.5	377	244	7.01	24	16	7	36	194	26	19
A2	1995	10.4	672	117	6.44	58	69	9	32	308	103	39
A2	1997	13.2	480	162	7.02	37	26	6	55	281	55	26
B1	1994	9.1	1220	−265	6.84	288	46	22	17	308	20	347
B1	1995	9.0	1920	−336	6.74	365	19	14	54	342	13	513
B1	1997	9.7	1468	87	8.03	165	52	11	17	354	31	338
B2	1994	13.0	1123	253	6.91	148	58	46	24	417	164	97
B2	1995	10.2	1206	106	6.75	167	29	21	85	442	269	103
B2	1997	13.2	1127	162	7.63	119	78	19	15	439	222	94
B3	1994	14.4	1129	292	7.03	142	66	30	31	539	161	93
B3	1995	12.2	1161	135	6.64	145	36	23	84	549	148	197
B3	1997	18.4	1198	440	7.77	119	89	22	37	610	145	101
B5	1994	17.3	1816	270	6.89	252	119	40	33	887	221	126
B5	1995	16.7	1825	93	6.73	227	38	24	119	891	153	130
B5	1997	17.4	137	358	8.14	152	122	23	33	915	156	148
B10	1994	19.2	1874	67	6.75	192	131	26	110	1439	148	85
B10	1995	19.2	1921	−21	6.55	198	143	23	156	1440	24	127
B10	1997	19.8	1778	112	6.09	133	113	17	128	1379	34	63
C1	1994	19.3	1269	402	6.76	105	79	25	48	652	121	112
C1	1995	19.1	1302	163	6.85	120	58	30	101	668	92	98
C1	1997	18.1	1155	221	6.36	77	46	12	42	634	85	106
C5	1994	14.5	375	310	7.03	46	16	12	11	176	43	24
C5	1995	14.3	338	129	6.89	43	9	8	15	151	26	19
C5	1997	14.7	363	354	7.57	57	21	8	12	195	35	28
C6	1994	17.7	842	184	7.04	63	26	30	51	111	127	89
C6	1995	17.3	850	118	6.35	67	60	30	28	122	101	93
C6	1997	17.6	855	229	7.24	78	35	30	62	134	152	104
C12	1994	20.2	1710	216	6.91	214	74	50	29	870	260	110
C12	1995	19.8	1779	127	6.24	247	86	51	101	886	219	118
C12	1997	19.7	1586	150	6.36	103	86	28	35	805	233	127
C14	1994	21.8	1795	253	6.71	276	78	68	21	920	251	83
C14	1995	20.3	1923	128	6.18	229	68	49	86	940	263	140
C14	1997	19.2	1715	191	6.28	154	98	48	73	830	275	152
C16	1994	13.8	204	174	6.89	23	6	4	6	67	14	19
C16	1995	11.8	226	51	6.53	26	16	3	5	81	19	17
C16	1997	13.1	314	380	7.31	42	13	3	25	159	39	22
LOD		–	–	–	–	1	1	1	1	1	1	1

[a] LOD = Limit of detection. Letters in samples names refer to the hydrogeological basins (see Fig. 1).

alkaline category, being particularly enriched both in alkali ions (Na$^+$ and K$^+$) and in Cl$^-$ ions. The peculiar compositions of these two samples have been explained by GIAMMANCO *et al.* (1998) as a result of the interaction between groundwaters and evaporitic deposits rich in gypsum and chlorides, respectively at shallow (oxidizing) and deep (reducing)

Table 2

Analytical results for minor and trace elements in the three surveys of Etna's ground water[a]

Sample[b]	Date	Li (mg/L)	B (mg/L)	Al	Si (mg/L)	Ti	V	Cr	Mn	Fe	Co	Ni	Cu	Zn	As	Se	Sr (mg/L)	Mo	Cd	Hg	Pb
A2	1994	<LOD	0.1	13	13	<LOD	39	0.2	3	4	<LOD	<LOD	0.3	2	0.8	<LOD	0.13	4.1	<LOD	<LOD	<LOD
A2	1995	0.07	0.5	<LOD	20	1	23	0.1	2	<LOD	<LOD	1.5	0.9	<LOD	0.5	1	0.23	4.7	<LOD	1	<LOD
A2	1997	0.05	0.2	8	1	<LOD	25	1.9	2	1	<LOD	0.8	1.5	73	1.1	0.5	0.09	4.2	<LOD	<LOD	<LOD
B1	1994	0.20	0.9	1	19	4	37	<LOD	4	4	0.6	0.6	<LOD	4	1.6	0.5	0.74	8.1	<LOD	<LOD	<LOD
B1	1995	0.28	1.8	11	23	2	11	<LOD	80	1	<LOD	1.1	0.7	2	0.7	3.0	0.81	6.2	<LOD	39	<LOD
B1	1997	0.20	0.9	9	13	<LOD	32	0.3	<LOD	122	<LOD	0.4	<LOD	<LOD	1.3	2.8	0.14	3.6	<LOD	0.13	<LOD
B2	1994	0.20	0.9	2	18	<LOD	220	<LOD	1	1	<LOD	<LOD	0.9	2	7.8	0.8	0.24	32.0	<LOD	<LOD	<LOD
B2	1995	0.21	0.8	1	21	2	284	0.1	1	6	<LOD	1.2	1.5	17	8.8	2.0	0.23	51.5	<LOD	10	<LOD
B2	1997	0.20	0.8	12	1	<LOD	160	0.7	<LOD	1	<LOD	0.8	0.8	36	8.0	1.6	0.10	23.9	<LOD	0.06	<LOD
B3	1994	0.20	0.7	<LOD	19	<LOD	200	0.1	1	1	<LOD	1.1	0.4	<LOD	4.2	<LOD	0.27	37.6	<LOD	<LOD	<LOD
B3	1995	0.16	0.7	<LOD	26	3	246	0.2	1	4	<LOD	0.6	1.9	<LOD	8.8	1	0.26	66.6	<LOD	13	<LOD
B3	1997	0.20	1.2	3	25	6	134	1.3	2	2	<LOD	0.5	3.3	47	6.3	<LOD	0.14	34.7	0.06	0.05	<LOD
B5	1994	0.50	1.2	<LOD	19	<LOD	72	0.9	1	2	<LOD	0.7	0.9	<LOD	1.3	<LOD	0.34	20.0	0.09	<LOD	<LOD
B5	1995	0.48	1.0	1	32	4	60	1.3	1	7	<LOD	1.9	1.3	<LOD	2.1	<LOD	0.34	42.8	0.16	18	<LOD
B5	1997	0.50	0.7	2	1	2	43	1.1	2	2	<LOD	0.5	<LOD	51	1.7	1.3	0.21	19.2	0.06	0.09	<LOD
B10	1994	0.90	1.9	31	55	6	16	0.1	410*	8900*	1.9	6.7	1.3	25	1.3	1.2	0.57	11.7	0.09	<LOD	1.3
B10	1995	1.22	1.2	14	63	10	2	0.6	310*	8700*	3.2	14.9	2.6	27	0.5	0.5	0.55	12.4	0.16	228	1.4
B10	1997	1.10	1.1	2	1	1	1	7.9	5	3000*	3.7	10.1	15.9	<LOD	1.1	0.6	0.53	8.8	0.19	0.05	0.5
C1	1994	0.10	0.9	1	35	<LOD	62	<LOD	4	4	0.4	<LOD	1.4	<LOD	1.5	1.6	0.28	78.3	<LOD	1	<LOD
C1	1995	0.11	0.6	<LOD	35	4	56	0.1	3	3	<LOD	2.3	6.3	<LOD	1.3	4.0	0.30	121.1	<LOD	16	<LOD
C1	1997	0.10	0.2	9	15	<LOD	63	0.9	5	<LOD	<LOD	0.7	2.2	121	1.7	2.5	0.07	54.6	0.05	0.05	<LOD
C5	1994	0.10	0.2	7	23	<LOD	51	<LOD	2	2	0.5	<LOD	<LOD	5	5.9	<LOD	0.12	10.2	<LOD	<LOD	<LOD
C5	1995	0.02	0.2	6	35	1	47	0.1	5	20	<LOD	3.6	7.2	67	3.7	<LOD	0.06	6.6	<LOD	17	6.2
C5	1997	0.05	0.3	6	3	<LOD	33	0.8	2	2	<LOD	0.7	2.5	66	6.7	<LOD	0.03	8.3	<LOD	0.10	<LOD
C6	1994	<LOD	0.4	267	21	<LOD	28	0.2	1	8	<LOD	3.1	1.2	12	0.8	1.7	0.42	3.1	<LOD	2	<LOD
C6	1995	0.07	0.5	9	20	3	20	1.1	1	13	<LOD	1.3	4.9	2	1.2	<LOD	0.41	8.1	0.08	22	<LOD
C6	1997	0.05	<LOD	14	8	4	13	3.0	7	6	0.9	0.3	0.4	125	<LOD	1.3	0.38	3.8	0.10	0.10	<LOD
C12	1994	0.50	0.8	1	32	3	84	<LOD	2	1	<LOD	1.0	0.4	<LOD	0.9	0.7	0.43	23.0	<LOD	<LOD	<LOD
C12	1995	0.54	0.8	1	27	3	94	0.3	3	<LOD	<LOD	1.7	2.6	<LOD	1.9	5.0	0.45	128.7	<LOD	39	<LOD
C12	1997	0.10	0.6	8	1	1	73	3.0	1	11	<LOD	1.5	0.7	10	1.6	4.6	0.45	39.8	<LOD	0.14	<LOD
C14	1994	0.50	1.3	<LOD	25	<LOD	145	0.1	1	<LOD	<LOD	<LOD	0.1	<LOD	0.8	2.6	0.35	33.1	<LOD	4	<LOD
C14	1995	0.41	2.1	<LOD	24	4	16	0.1	1	<LOD	<LOD	0.7	4.4	33	3.7	<LOD	0.47	160.8	<LOD	<LOD	<LOD
C14	1997	0.50	<LOD	9	9	1	81	1.3	9	17	<LOD	5.1	<LOD	206	<LOD	<LOD	0.24	5.8	<LOD	0.14	<LOD
C16	1994	<LOD	<LOD	45	15	<LOD	8	0.2	1	8	<LOD	<LOD	0.4	49	0.7	<LOD	0.20	2.8	<LOD	<LOD	<LOD
C16	1995	0.03	<LOD	10	21	1	15	0.6	2	11	0.7	3.2	2.3	30	<LOD	1.0	0.19	2.2	<LOD	50	<LOD
C16	1997	0.05	<LOD	13	5	<LOD	9	1.5	2	8	<LOD	1.6	5.6	97	<LOD	<LOD	0.19	2.3	0.11	0.10	<LOD
LOD		0.01	0.1	1	1	1	1	0.1	1	1	0.3	0.3	0.1	1	0.5	0.5	0.05	0.3	0.05	0.05**	0.5

[a] Values in µg/L, except where indicated.

[b] LOD = Limit of detection. Letters in samples names refer to the hydrogeological basins (see Fig. 1).

*Values obtained with flame atomic absorption spectrometry.

**Detection limit for the analytical results of 1997 survey.

conditions. The presence of such sedimentary deposits underneath Etna's volcanic products is inferred also from geological data (LENTINI, 1982).

Water temperatures in the collected samples were in general low (9.0 to 21.8°C) throughout the three surveys, indicating a relatively shallow and fast circulation of water within the volcanic edifice.

4.2. Statistical Treatment of Data

The chemical and physico-chemical determinations of the groundwater samples collected on Mt. Etna generated a series of data structured in a multidimensional matrix (32 variables × 12 sites × 3 sampling surveys). In order to obtain the largest amount of information from the acquired data, it was necessary to perform a multivariate statistical analysis. In particular, we identified the Cluster Analysis (CA) as the most appropriate one to carry out in this study. Actually, the low number of sampling sites (cases) compared to the number of parameters determined (variables), did not allow us to perform a Principal Component Analysis, which was used in a previous work on the geochemical characterization of Etna's groundwaters (GIAMMANCO *et al.*, 1998).

Differently from other statistical procedures, some of the algorithms used in the CA are applied when it is not possible to formulate *a priori* hypotheses on the taxonomy of the data. Those algorithms recognize the most significant classification, starting from the information included in the matrix of the examined values. The grouping of the data into clusters is based on their degree of similarity. Every object is correlated with the others so as to identify the couple of objects with the highest similarity (i.e., with the shortest distance in the multidimensional space) to be merged into a cluster. Among the criteria developed to merge single clusters into progressively larger ones, that of Ward is thought to be the most efficient, because it minimizes the increment in heterogeneity that occurs when two clusters unite. The initial or final heterogeneity of each group is calculated *a posteriori* by summing the squares of the distances between the centroid and the objects. A drawback of this method is its tendency to form clusters of small dimensions.

In this work the CA was used to find eventual relations not only among the parameters determined, but also among the sampling sites, as already performed in non-volcanic areas (GÜLER and THYNE, 2004). Grouping the sites was necessary in order to elaborate separately data sets with a stronger affinity among them. Actually, the data in Table 1 clearly indicate large differences in the geochemical characteristics of the groundwaters sampled from one site to the other within the same survey, thus suggesting different types and/or intensity of geochemical processes affecting them.

Figure 2 depicts the dendrograms resulting from the application of the CA to the matrices of data obtained in each of the three surveys, after assigning a zero value to a parameter in each case that it was below detection limit. They display the clusters of sampling sites in each survey, in decreasing order of similarity. Sites belonging to the same cluster imply a high degree of similarity among the chemical and physico-chemical characteristics of the relevant waters. The initial distances d among the objects (sampling

sites) were calculated starting from the linear correlation coefficient r using the following equation:

$$d = 1 - r. \tag{1}$$

In the computation we did not include Cd, Co and Pb, because they were found only a very few times in a very limited number of sites, and their valid values were too few to be computed for a significant analysis.

The three dendrograms show a good similarity in their results: All of them present a high correlation among sites B5, B10, C12 and C14, which form a small cluster (named A) that is poorly correlated with the rest of the other sites (grouped into cluster B). We therefore calculated the average values of the parameters belonging to each of the two clusters found with the CA for each survey, and the resulting values are plotted with time in the diagrams of Figure 3. The figure shows that practically all of the considered parameters changed in their average values throughout the three surveys, but not all in the same way. Several patterns of change can be actually recognized (basically: increasing, decreasing, concave and convex), which suggest a possible grouping of parameters according to their behavior.

As a first approach to investigate the similarities among parameters, a correlation matrix was calculated for the parameters of each cluster. In the two correlation matrices, the average values of each parameter in time were correlated with those of all the other parameters according to their pattern of changes from 1994 through 1997, and the resulting values of the correlation coefficients are shown in Tables 3 and 4. In order to visualize the correlations between parameters obtained from the correlation matrices, CA was again used. Figure 4 shows the dendrograms resulting from the application of the CA to the matrices of data obtained from both of the clusters of sampling sites considering the average values of each parameter in time. The dendrogram for cluster A (Fig. 4a) highlights four families of parameters with high similarity. Family I includes Temperature, Al, SO_4^{2-}, V, K, Eh, Mg and pH; these parameters manifest either a concave pattern, that is they decrease from 1994 to 1995 and then slightly increase or remain low in 1997, or a decreasing pattern (only for element K). Family II includes Conductivity, Si, HCO_3^-, Ti, Sr, Na, B and Mn; these parameters show a slight convex pattern, with a marked decrease in 1997. Family III includes Ca, As, Mo, Hg, Li, Fe, Cl^-, Ni, Se and pCO_2; these parameters show a clear convex pattern, apart from pCO_2 which shows a slight increasing pattern. Lastly, family IV includes Cr, Zn and Cu, which show an increasing pattern. Actually the pattern of pCO_2 shows a greater similarity with the pattern of parameters in family IV, and the relevant values of the correlation coefficient between this parameter and those of family IV would support this indication (Table 3), thus leading either to the reallocation of this parameter into family IV or to its affinity to both family III and family IV. Besides, some of the parameters in family II, namely Conductivity, Si, HCO_3^-, Ti and Sr, display patterns that are similar to those of the parameters in family III. Also in this case the correlation matrix for cluster A parameters indicates high values of the correlation coefficients among the above indicated
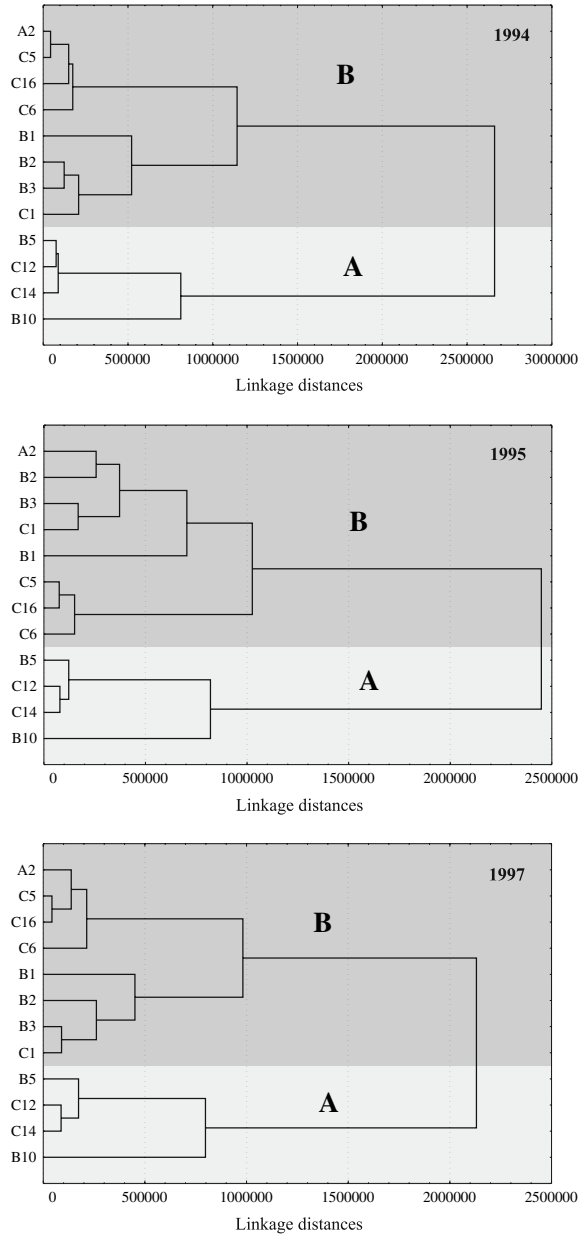
Figure 2
Dendrograms resulting from the application of the CA to the matrices of data obtained in each of the three surveys of Mt. Etna's groundwaters. Distances among groups were evaluated using the Ward's method. Distances among objects were calculated using Euclidean distances. Computation performed using STATISTICA for Windows software. The graphs show the clusters of sampling sites in each survey (two clusters recognized, indicated with A and B), in decreasing order of similarity. Linkage distances in arbitrary units.

(a)
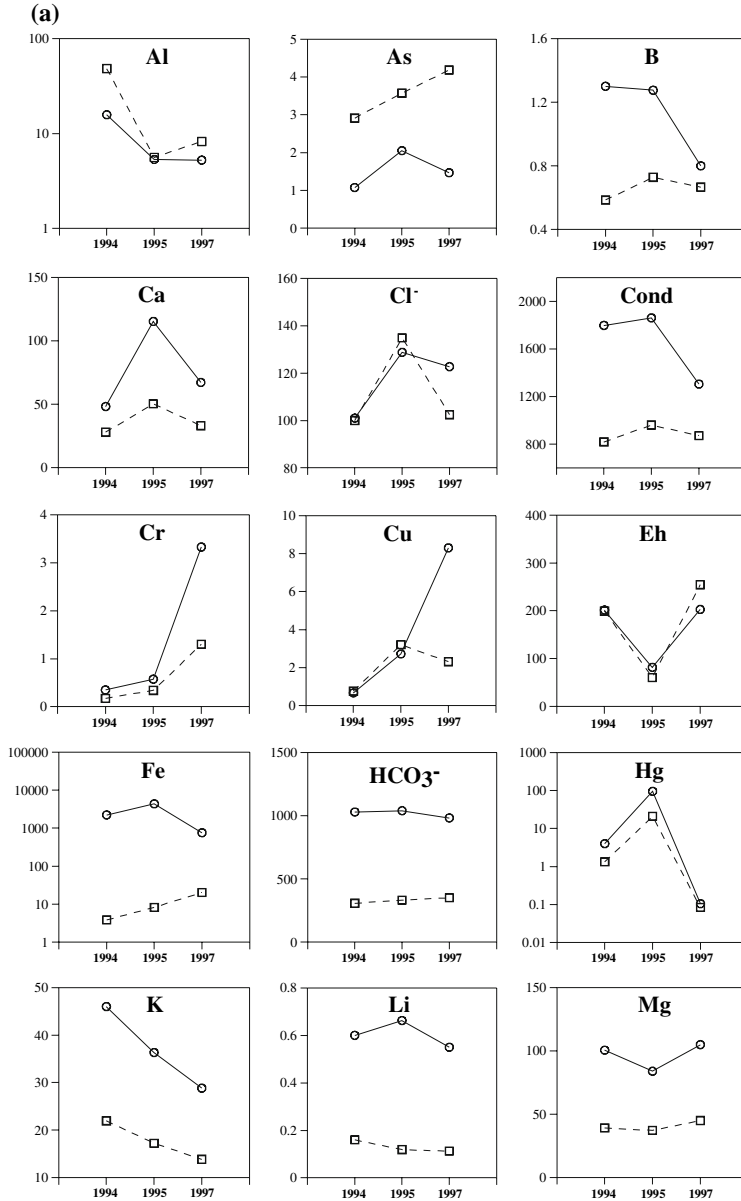
Figure 3

Temporal evolution of the parameters measured in the three surveys of Mt. Etna's groundwaters, divided by the two clusters of sampling sites found with the CA. Pairs of symbols for each sampling year (open circles connected with solid lines for cluster A sites, open squares connected with dashed lines for cluster B sites) represent the average values of the indicated parameter calculated for the sites relevant to that cluster (sites B5, B10, C12, C14 for cluster A, all the other sites for cluster B). Temperature is in °C; Conductivity is in μS/cm; pH is in pH units; Eh is in mV; calculated $p(CO_2)$ is in atm; Ca, K, Mg, Na, Si, Cl^-, SO_4^{2-}, HCO_3^-, Li, B, Si and Sr are in mg/L; all other elements are in μg/L.

(b)

Figure 3
(Contd.)

Table 3

Correlation matrix for the parameters of cluster A sites. Average values of each parameter in time are correlated with those of all the other parameters. Correlation factors with a significant correlation (r > 0,80) are highlighted in grey

	T	Cond	Eh	pH	Na	Mg	K	Ca	HCO_3^-	SO_4^{2-}	Cl^-	pCO_2	Li	B	Al	Si	Ti	V	Cr	Mn	Fe	Ni	Cu	Zn	As	Se	Sr	Mo	Hg
T	-	0.38	0.52	0.72	0.53	0.35	0.88	-0.74	0.32	0.99	-0.98	-0.98	-0.10	0.51	1.00	0.37	0.31	0.99	-0.53	0.67	-0.14	-0.98	-0.68	-0.53	-0.82	-0.93	0.28	-0.49	-0.50
Cond		-	-0.59	-0.38	0.98	-0.73	0.76	0.34	1.00	0.25	-0.21	-0.55	0.89	0.99	0.41	1.00	1.00	0.25	-0.99	0.94	0.87	-0.18	-0.93	-0.98	0.22	0.00	0.99	0.62	0.62
Eh			-	0.97	-0.44	0.06	0.31	-0.96	-0.64	0.63	-0.66	-0.35	-0.90	-0.47	0.49	-0.60	-0.65	0.63	0.45	-0.28	-0.92	-0.69	0.27	0.45	-0.91	-0.80	-0.67	-1.00	0.62
pH				-	-0.20	0.90	0.31	-1.00	-0.43	0.80	-0.83	-0.57	-0.76	-0.23	0.69	-0.38	-0.44	0.80	0.21	-0.03	-0.79	-0.85	0.02	-0.98	-0.99	-0.93	-0.47	-0.96	-0.96
Na					-	-0.60	-0.12	-0.89	-0.78	0.42	-0.38	-0.69	0.79	1.00	0.57	0.98	0.97	0.42	-1.00	0.99	0.76	-0.35	-0.98	-1.00	0.04	-0.18	0.96	0.47	0.47
Mg						-		-0.34	0.72	0.82	-0.79	-0.96	0.38	0.85	0.90	0.76	0.72	0.81	-0.86	0.94	0.34	-0.54	-0.94	-0.86	-0.46	-0.65	0.69	-0.03	-0.04
K							-		0.40	0.19	0.85	0.60	0.74	0.20	-0.71	0.35	0.41	-0.82	-0.18	0.00	0.77	-0.11	0.02	-0.18	0.99	0.94	0.44	0.95	0.66
Ca								-	-0.34	0.99	-1.00	0.17																	
HCO_3^-									-	0.99	-0.17	-0.96																	
SO_4^{2-}										-	-1.00	-0.49																	
Cl^-											-	-0.95	0.27	-0.35	-0.98	-0.21	-0.14	-1.00	0.37	0.57	-0.27	1.00	0.55	-0.42	0.91	0.98	-0.11	0.63	0.64
pCO_2												-	-0.10	-0.67	-0.99	-0.55	-0.48	-0.95											
Li													-	0.81	-0.06	0.89	0.92	-0.23	-0.79	0.30	0.30	-0.66	-0.66	-0.79	0.64	0.46	0.93	0.92	0.91
B														-	0.54	0.99	0.98	0.39	-1.00	0.98	0.78	-0.32	-0.98	-1.00	0.07	-0.15	0.97	0.50	0.49
Al															-	0.41	0.35	0.98	-0.56	0.70	-0.10	-0.97	-0.71	-0.57	-0.80	-0.91	0.32	-0.45	-0.46
Si																-	0.92	-0.55	0.68	-0.80	-0.05	0.92	0.81	0.68	0.70	0.84	-0.46	0.32	0.32
Ti																	-	0.18	-0.98	0.67	0.90	-0.10	-0.90	-0.97	0.29	0.07	1.00	0.68	0.67
V																		-	-0.98	0.94	0.87	-0.17	-0.93	-0.98	-0.89	-0.97	0.15	-0.60	-0.61
Cr																			-	-0.98	0.87	-0.17	-0.93	-0.98	0.22	0.00	0.90	0.63	0.62
Mn																				-	0.87	-0.50	-1.00	-0.98	-0.13	-0.35	0.90	0.32	0.31
Fe																					-	0.64	-0.63	-0.77	0.68	0.50	0.91	0.93	0.93
Ni																						-	0.34	0.34	0.92	0.68	-0.07	0.66	0.67
Cu																							-	0.52	0.15	0.36	-0.89	-0.30	-0.29
Zn																								-	-0.04	0.18	-0.96	-0.48	-0.47
As																									-	0.98	0.31	0.90	0.90
Se																										-	0.10	0.78	0.79
Sr																											-	0.70	0.69
Mo																												-	0.78
Hg																													-

Figure 4

Dendrograms resulting from the application of the CA to the matrices of data obtained correlating the temporal patterns of the average values of each analyzed parameter in a) cluster A and b) cluster B of sampling sites. Distances among groups were evaluated using the Ward's method. Distances among objects were calculated using (1-r) distances. Computation performed using STATISTICA for Windows software. Both of the graphs highlight four families of parameters with high similarity (indicated with roman numbers).

parameters of family II and many parameters of family III, particularly Li and Fe. Thus, in the case of cluster A the basic temporal patterns recognized can be reduced to three: concave, convex and increasing.
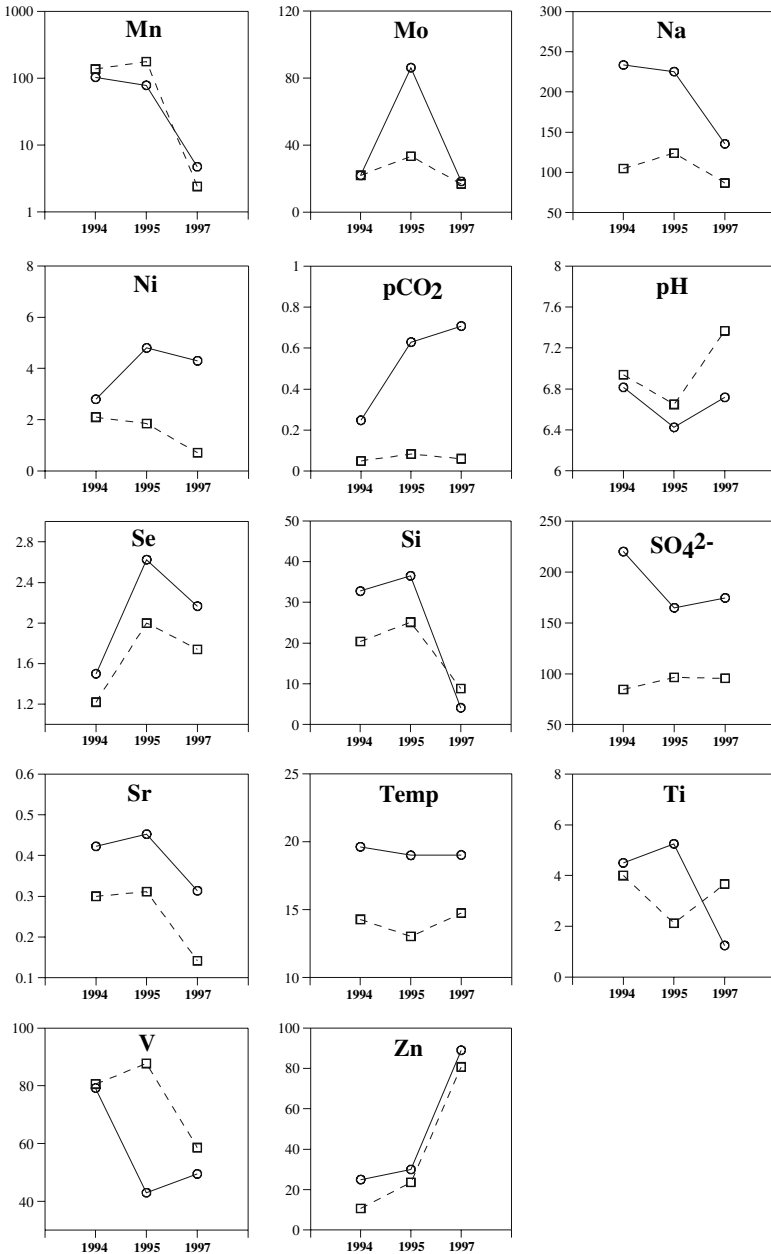
Table 4

Correlation matrix for the parameters of cluster B sites. Average values of each parameter in time are correlated with those of all the other parameters. Correlation factors with a significant correlation (r > 0.80) are highlighted in grey

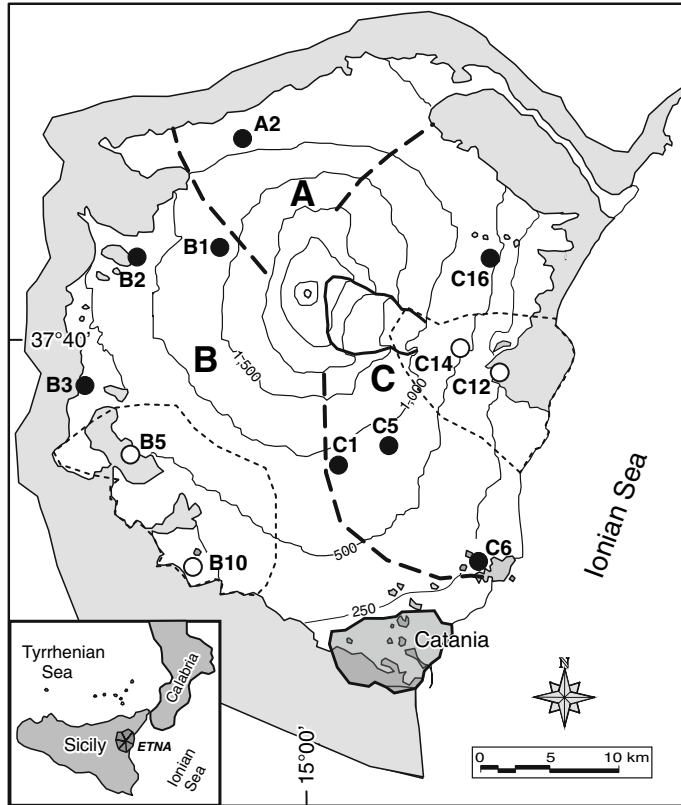|	T	Cond	Eh	pH	Na	Mg	K	Ca	HCO_3^-	SO_4^{2-}	Cl^-	pCO_2	Li	B	Al	Si	Ti	V	Cr	Mn	Fe	Ni	Cu	Zn	As	Se	Sr	Mo	Hg
T	-	-0.80	0.93	0.94	-0.97	0.86	-0.17	-0.88	0.17	-0.31	-0.95	-0.83	0.14	-0.65	0.31	-0.88	0.91	-0.85	0.61	-0.85	0.50	-0.58	-0.59	0.58	0.24	-0.56	-0.75	-1.00	-0.98
Cond		-	-0.79	-0.53	0.63	-0.39	-0.45	0.99	0.45	0.82	0.95	1.00	-0.70	0.97	-0.82	0.42	-0.98	0.38	-0.01	0.36	0.11	-0.02	0.96	0.03	0.39	0.94	0.21	0.78	0.91
Eh			-	0.87	-0.97	0.87	-0.18	-0.88	0.19	-0.30	-0.94	-0.82	0.12	-0.64	0.30	-0.89	0.90	-0.86	0.62	-0.86	0.52	-0.59	-0.58	0.59	0.26	-0.55	-0.76	-1.00	-0.97
pH				-	-0.99	0.99	-0.51	-0.66	0.52	0.05	-0.77	-0.58	-0.23	-0.33	-0.05	-0.99	0.70	-0.98	0.85	-0.98	0.78	-0.83	-0.26	0.83	0.57	-0.22	-0.94	-0.95	-0.97
Na					-	-0.96	0.40	0.74	-0.41	0.07	0.84	0.67	0.11	0.45	-0.07	0.97	-0.78	0.95	-0.78	0.95	-0.70	0.76	0.38	-0.76	-0.47	0.34	0.89	0.98	-0.84
Mg						-	-0.65	-0.52	0.65	0.21	-0.65	-0.43	-0.39	-0.17	-0.22	-1.00	0.57	-1.00	0.93	-1.00	0.87	-0.91	-0.10	0.91	0.70	-0.06	-0.98	-0.88	0.90
K							-	-0.31	-1.00	-0.88	-0.16	-0.41	0.95	-0.64	0.89	0.62	0.26	0.66	-0.89	0.67	-0.94	0.90	-0.70	-0.90	-1.00	-0.72	0.78	0.21	-0.73
Ca								-	0.31	0.72	0.99	0.99	-0.58	0.93	-0.72	0.56	-1.00	0.51	-0.16	0.50	-0.04	0.13	0.90	-0.13	0.24	0.88	0.35	0.86	-0.04
HCO_3^-									-	0.88	0.15	0.40	-0.95	0.64	-0.88	-0.62	-0.25	-0.66	0.89	-0.67	0.94	-0.90	0.69	0.90	0.90	0.72	-0.78	-0.22	0.96
SO_4^{2-}										-	0.60	0.79	-0.98	0.93	-1.00	-0.17	-0.68	-0.22	0.57	-0.24	0.66	-0.59	0.95	0.59	0.85	0.96	-0.39	0.04	0.04
Cl^-											-	0.97	-0.45	0.86	-0.60	0.68	-0.99	0.64	-0.32	0.63	-0.20	0.29	0.82	-0.28	0.08	0.80	0.50	0.27	0.51
pCO_2												-	-0.66	0.96	-0.79	0.47	-0.99	0.42	-0.06	0.41	0.06	0.03	0.94	-0.03	0.34	0.92	0.26	0.93	0.99
Li													-	-0.84	0.98	0.35	0.54	0.40	-0.71	0.41	-0.79	0.73	-0.88	-0.73	-0.93	-0.90	0.55	0.81	0.93
B														-	-0.92	0.21	-0.91	0.16	0.21	0.15	0.33	-0.24	1.00	0.25	0.58	0.99	-0.02	-0.09	-0.34
Al															-	0.18	0.54	0.23	-0.91	0.24	-0.67	0.60	-0.95	-0.60	-0.85	-0.96	0.40	0.62	0.79
Si																-	-0.60	1.00	0.22	1.00	0.10	0.90	0.14	-0.90	-0.67	0.10	0.97	-0.27	-0.50
Ti																	-	-0.56	-0.93	-0.55	-0.88	-0.19	-0.87	0.18	-0.19	-0.85	-0.40	0.90	0.76
V																		-	-0.92	0.99	0.99	0.92	0.09	-0.92	-0.71	0.05	0.98	-0.89	-0.98
Cr																			-	-0.93	-0.94	-1.00	0.28	1.00	0.92	0.32	-0.98	0.88	0.73
Mn																				-	0.99	-0.89	0.07	-0.92	-0.72	0.03	0.99	-0.64	-0.43
Fe																					-	0.90	0.40	1.00	0.96	0.44	-0.95	0.87	0.72
Ni																						-	-0.32	-1.00	-0.93	-0.35	0.97	-0.54	-0.31
Cu																							-	0.32	0.64	1.00	-0.09	0.61	0.40
Zn																								-	0.93	0.36	-0.97	0.55	0.75
As																									-	0.67	-0.82	-0.61	-0.39
Se																										-	-0.13	-0.28	-0.03
Sr																											-	0.52	0.72
Mo																												-	0.59
Hg																													-

Figure 5

Spatial distribution of sampling sites at Mt. Etna, according to their respective cluster, following the results shown in Figure 2. Open circles = Cluster A sites; filled circles = Cluster B sites. Light dashed lines enclose cluster A sites. Thick dashed lines indicate the main hydrogeological basins (A = Northern basin; B = Western basin; C = Eastern basin) according to Ferrara (1990). Altitudes in meters.

The dendrogram for cluster B (Fig. 4b) also highlights four families of parameters with high similarities among them. Family I includes Temperature, Eh, pH, Ti and Mg; these parameters show a concave pattern. Family II includes HCO_3^-, As, Cr, Zn and Fe, which show an increasing pattern. Family III includes Conductivity, pCO_2, Ca, Cl^-, Hg, SO_4^{2-}, B, Cu, Se, Na, Mo, Si, V, Mn, Ni and Sr, which show a convex pattern. Family IV includes only K, Li and Al, which show a concave (Al) or decreasing (K and Li) pattern. As for cluster A, also in the case of cluster B some similarities can be found among parameters belonging to different families. In particular, Al shows a similar pattern to that of the parameters of family I; the highest correlation being with Ti (Table 4).

Table 5

Percentages of Etna's ground water samples, divided by the two clusters of sites (cluster A = 4 sites; cluster B = 8 sites), that in each survey showed saturation or oversaturation (SI > 0) in the phases listed. The horizontal dash indicates under saturation. Calculations carried out with PHREEQC software (PARKHURST, 1995)

Phases	Cluster A			Cluster B		
	1994	1995	1997	1994	1995	1997
Clay Minerals						
Annite	25	25	–	13	25	13
Ca-Nontronite	25	50	75	50	50	88
Halloysite	25	75	25	50	38	50
K-Nontronite	25	50	75	50	50	88
Kaolinite	25	75	75	63	63	100
Leonhardite	25	75	50	63	63	100
Mg-Nontronite	25	50	75	50	50	88
Montmorillonite	25	50	50	50	63	88
Muscovite	25	75	75	63	63	100
Na-Nontronite	25	50	75	50	50	88
Pyrophyllite	25	75	75	63	63	100
Talc	–	–	–	–	–	13
Tremolite	–	–	–	–	–	13
Carbonates						
Aragonite	25	–	–	–	–	–
Calcite	25	50	25	–	–	25
Dolomite	25	25	25	–	–	38
Magnesite	–	–	25	–	–	38
Siderite	25	25	–	–	–	–
Oxy-Hydroxides						
Cr_2O_3	–	25	100	–	25	88
$Cr(OH)_3$	–	–	25	–	–	38
Cuprite	–	–	–	–	25	–
Diaspore	25	75	100	13	63	100
Gibbsite (c)	25	25	50	13	13	38
Goethite	25	25	100	13	75	88
Hematite	25	50	100	13	75	88
Lepidocrocite	25	25	100	13	75	88
Maghemite	25	–	25	13	25	75
Magnetite	25	50	100	13	75	88

4.3. Geochemical Evaluation of the Temporal Variations of Data

Cluster A is characterized by waters with higher contents of dissolved salts than those of cluster B. This is highlighted mainly by the values of conductivity, although more generally by the contents of the major ions in solution. The concentrations of minor and trace elements are also generally higher in this cluster, and the higher values of pCO_2 combined with the lower values of pH indicate that the sites belonging to this cluster represent aquifers that are most subject to gas-water-rock interaction. The sites entailed by cluster A (B5, B10, C12 and C14, Fig. 5) are actually located in the areas of Mt. Etna

where degassing of magmatic volatiles into the aquifers is the highest (ANZÀ *et al.*, 1989; AIUPPA *et al.*, 2000, 2004; ALLARD *et al.*, 1997; BRUSCA *et al.*, 2001; GIAMMANCO *et al.*, 1995, 1998). These areas are located distant from the main craters of the volcano, but this is not surprising because leakage of magmatic gases from the flanks of Mt. Etna is strongly connected with the presence of deep tectonic faults (Timpe Fault System), largely belonging to the regional structural framework of eastern Sicily, that cut the crust down to the main magma reservoirs of Mt. Etna and act as high-permeability pathways for the escape of magmatic gases to the surface (e.g., AIUPPA *et al.*, 2004).

As regards the temporal changes observed in the parameters of cluster A from 1994 to 1997, it can be noted that the elements that showed a convex pattern, that is an increase in 1995 (groups II and III), are actually those whose mobility in solution is normally high and/or are particularly abundant in the basaltic rocks that constitute Etna's aquifers, because they are found as primary or secondary components in mineralogical phases like olivines, pyroxenes and Ca-plagioclases (e.g., CHESTER *et al.*, 1985). Therefore, alkalis and alkaline earth elements such as Na, Ca, Sr, as well as Si, Ni and Mo, show an expected increase of their concentration in solution when water-rock interaction is enhanced due to a higher input of CO_2 and other acid volcanic gases into the aquifer. This is suggested mostly by the higher values of conductivity, parameter normally related to the total content of solids in solution, measured in 1995. Other elements in these groups, particularly in group III, are volatiles (Cl^-, Hg, As, Se) associated to pCO_2, which suggests their input to groundwaters together with magmatic gases (mainly CO_2, but also HCl and other reduced gas species). Conversely, the parameters in group I mainly indicate significant changes in the redox and acid conditions of groundwaters belonging to cluster A. Particularly in 1995, waters became more acid and more reduced because of the higher input of CO_2 and possibly other magmatic gases in the sampled groundwaters. This in turn caused a marked decrease in V contents, because this element tends to form insoluble compounds (such as V_2O_4 and V_2O_3) with low pH and Eh values (GIAMMANCO *et al.*, 1998). Similarly, the low sulphate contents in 1995 may result from more reducing conditions of groundwater during that survey, which prevented the oxidation of volcanic H_2S. The low Al contents observed in 1995, as well as in 1997, can be explained by its uptake in secondary clay minerals precipitated from solution. Table 5 shows the percentage of saturation or oversaturation in a number of phases theoretically in equilibrium with the sampled groundwaters. The data of Table 5 indicate that the percentage of samples saturated with clay minerals generally increased after 1994, both in cluster A and in cluster B. Formation of secondary clay minerals, as well as carbonates, may also justify the low contents of Mg measured in the 1995 survey. Notwithstanding its high mobility in Etnean waters (AIUPPA *et al.*, 2000), Mg may be efficiently removed by secondary clay minerals like, for example, Mg-Nontronite or Mg-Smectite, as indicated by the data of Table 5.

Oxide and hydroxide anion-forming elements such as Se, Mo, As, along with Hg, should normally decrease with low pH and Eh values, opposite to what was observed. Their apparently strange behavior is reasonably to be ascribed to their direct input to

solution from volcanic fluids (GIAMMANCO *et al*., 1998), particularly in the case of volatile elements like Hg and Se. In the case of Hg, its relative high concentration found in Etna's groundwaters during the 1995 survey may be explained by a direct input of large amounts of mobile $Hg^0_{(aq)}$, transported as vapor and/or sulfide (HgS) (SYMONDS *et al*., 1992; NICHOLSON, 1993; BARNES and SEWARD, 1997), after exsolution from magma.

Elements in group IV (Cr, Zn, Cu and, possibly, pCO_2) show a constant increase from 1994 to 1997. This behavior can be ascribed either to a elemental affinity with the magmatic gas phase (as in the case of Cr, according to GIAMMANCO *et al*., 1998), or to increased selective mobilization of the elements under hydrothermal conditions (as in the case of Cu, according to ROSE *et al*., 1991; NICHOLSON, 1993; GIAMMANCO *et al*., 1998) that may have progressively developed in the aquifers feeding the sampled waters during the period of our observations, or to elemental mobilization under acid/reduced conditions, as in the case of Zn (GIAMMANCO *et al*., 1998), or to a combination of the above. Chromium and zinc should normally behave like iron, and this would explain why their contents in the 1995 survey were higher than those in the 1994 survey. However, their much higher values measured in 1997, particularly if compared to those of Fe, can be explained in different ways: Cr, like V, is actually more mobile in oxidized conditions (in the form of chromates, $HCrO_4^-$ or CrO_4^{2-}), hence its greatest concentration in water was found when Eh values were markedly higher, as in the case of the 1997 survey. The further increase in Zn contents in 1997, although the pH and Eh values for the sampled waters indicate a return to oxydized and less acid conditions, may instead suggest that the enhanced leaching of Etna's volcanic rocks continued even after 1995, although at a slower rate, and brought to solution less mobile species such as this element (AIUPPA *et al*., 2000). The decrease of HCO_3^- in 1997, which apparently seems to indicate a less intense water-rock interaction, may be in part explained by the above-mentioned increased saturation of groundwater in carbonates (Table 5).

In the low salinity waters belonging to cluster B some parameters show temporal changes that differ from those observed in cluster A waters. For example, Ti shows a concave pattern instead of convex; in this case the behavior of Ti is similar to that of Al and therefore it could be related to co-precipitation of Ti in titanium-containing clay minerals. Precipitation of secondary clay minerals, as discussed above in the case of group I of cluster A, could be the consequence of their saturation in water after increased leaching of the host rocks that was observed particularly in 1995. HCO_3^-, As and Fe show an increasing pattern, instead of convex, in association with Cr and Zn; in this case it is reasonable that their behaviour reflects an ever-increasing degree of water-rock interaction, which continued in 1997 even though the values of pCO_2 slightly decreased. SO_4^{2-}, Cu and V show a convex pattern instead of concave or increasing, as for Cu. In this case it seems that these parameters are not related with the redox conditions of water, but rather they seem more closely related with water-rock interaction driven by dissolved CO_2. In particular, the contemporaneous increase of both SO_4^{2-} and pCO_2 in 1995 may indicate a greater input of both H_2S and CO_2 in the groundwaters represented by the samples of cluster B. Lastly, Li and K display a decreasing pattern instead of convex and

concave, respectively. The concentrations of both of these elements in groundwater should be strongly affected by water-rock interaction, however their decrease, particularly in 1997, may be explained with their removal by secondary formation of amorphous silica and fine-grained, poorly crystalline K-rich clays (GOGUEL, 1983). This hypothesis is also strengthened by the thermodynamic data of Table 5, which indicate, as above-mentioned, a general increase in the percentage of samples that showed saturation or oversaturation in clay minerals, and hence also K-rich clays, from 1994 to 1997.

4.4. Correlation with Mt. Etna's Volcanic Activity

From the above discussion we can deduce that during the period 1994–1997 the changes in the chemical and physico-chemical characteristics of Mt. Etna's groundwaters are related, either directly or indirectly, to an increased input of magmatic fluids to the local aquifers due to a higher level of volcanic activity. The influence of recharge (due to infiltration of rain and snow) on the temporal variability of the studied waters seems to play a negligible role. This arises mostly from consideration that the only sampling that was carried out during a period of high discharge, i.e., in November 1995, when dilution of groundwaters should be close to its maximum (BONFANTI *et al.*, 1996), showed instead an increase in many parameters and particularly in those most closely linked to magmatic gas input.

Support for the hypothesis of chemical changes induced by the increased input of magmatic gas comes from many observations, mainly from the temporal evolution of SO_2 flux from the summit vents and of the partial pressure of dissolved CO_2 in groundwater during the studied period. Mt. Etna is actually one of the largest contributors of magmatic CO_2 and SO_2 to the atmosphere, even during non-eruptive periods (e.g., ALLARD *et al.*, 1991; ALLARD, 1997). Crater emissions from the four summit vents of the volcano provide mostly the totality of the emitted SO_2 and the large majority of CO_2 (ALLARD *et al.*, 1991; D'ALESSANDRO *et al.*, 1997). During the studied period both parameters showed a strong increase from 1994 to 1995 and then remained sensibly high in 1997, although with values slightly lower than in 1995. In fact, average pCO_2 values measured in the three hydrogeochemical surveys object of this study (based on the data of Tables 1 and 2) were 0.124 atm in 1994, 0.279 atm in 1995 and 0.277 atm in 1997. Accordingly, average crater SO_2 flux values were about 3440 t/day in August 1994, about 6180 t/day in November 1995 and about 5580 in August 1997 (data from BRUNO *et al.*, 1999, 2001). Such behavior is explained by the evolution of concurrent volcanic activity at Mt. Etna: after the huge 1991–1993 eruption a period of almost complete calm occurred at Etna from March 1993 to late July 1995, when mildly explosive magma ejection was again observed at the summit craters of the volcano (ARMIENTI *et al.*, 1996). The explosive activity continued with increasing intensity throughout the second half of 1995 and the beginning of 1996. During this period several episodes of violent lava fountaining took place in one of the four summit vents of Etna (namely, the North-East Crater). From February to August 1996 volcanic activity became more continuous, but
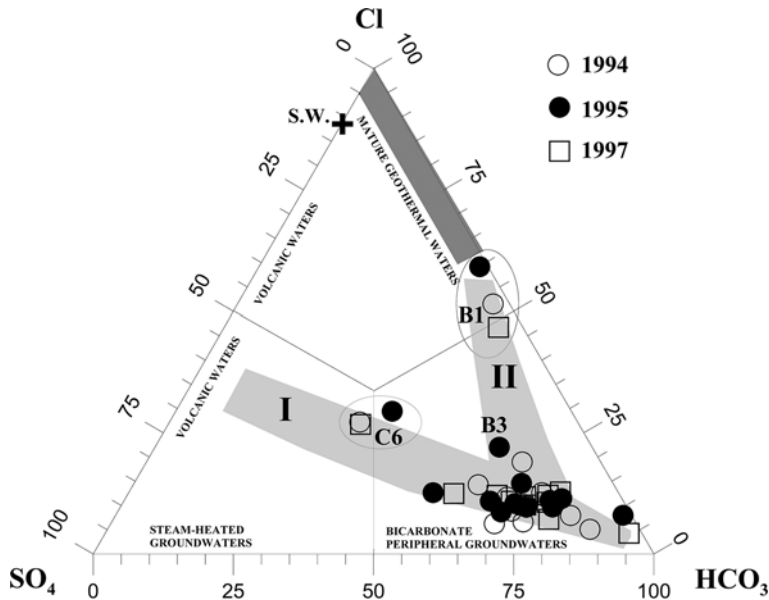
Figure 6

Cl–SO$_4$–HCO$_3$ triangular plot for the samples collected at Mt. Etna during 1994, 1995 and 1997 surveys (modified from Giggenbach, 1991). Ionic contents are in mg/kg. In the plot the compositional fields of the main types of water recognized by Giggenbach (1991) in volcanic and geothermal areas are also shown, along with the mixing trends (grey areas) that are likely to affect the sampled waters. The cross symbol with S.W. represents the composition of sea water. Most samples fall on a mixing trend between Bicarbonate Peripheral Groundwaters and Volcanic Waters (trend I). Other samples (e.g., all of those from site B1 and the 1995 sample from site B3) fall on a mixing trend between Bicarbonate Peripheral Groundwaters and Mature Geothermal Waters (trend II). The 1995 sample from site C6 seems to show as well a moderate influence from the geothermal component.

less vigorous, and was also characterized by modest lava outflows from the North-East Crater (Armienti et al., 1996). Since the second half of 1996 and throughout 1997 Etna's eruptive activity showed a lower intensity: Mild magma explosions occurred inside its summit vents, and the emission of small intra-crateric lava flows was frequent (La Volpe et al., 1999). Therefore, the overall level of volcanic activity at Etna was very low in 1994, high in 1995, particularly in late 1995 when our sampling was carried out, and then moderately high throughout 1997; an indication that since mid-1995 magma was almost continuously present within the shallowest portions of Etna's feeder system.

The increased gas-water interaction following the increased volcanic activity since 1995 is also responsible for the enhanced hydrothermal conditions in some of Etna's aquifers, as indicated by the triangular plot of Figure 6. The plot shows that all samples except those from sampling site B1 seem to derive from mixing between carbonate peripheral groundwaters and volcanic waters (trend A in Fig. 6). Samples from site B1 fall close to the composition of mature geothermal waters, with a sample from the 1995

survey being the closest to them. This would provide an alternative explanation for the peculiar composition of site B1 samples to that given by GIAMMANCO *et al.* (1998). Waters from site B1 would, therefore, derive from mixing between geothermal water and cold bicarbonate water (trend B in Fig. 6). Other samples show a possible transient interaction with geothermal waters, mostly in 1995 (e.g., the 1995 samples from sites C6 and B3).

5. Conclusions

In active volcanic areas, such as Mt. Etna, interaction among groundwater, the rocks hosting the aquifers and magmatic fluids is obviously strong, even during periods of relative volcanic quietness (GIAMMANCO *et al.*, 1998; AIUPPA *et al.*, 2000). Gas-water-rock interaction is particularly strong where deep faults cut the volcanic edifice down to the magma reservoirs and allow for an easier escape of magmatic volatiles to the surface. Examples of this can be found in the south western and eastern flanks of Mt. Etna. In these areas, groundwaters display a significantly higher salinity as a result of higher contents of most of the elements leached from host rocks and higher values of dissolved CO_2, so as to form a statistically distinct group of waters (cluster A obtained from CA).

Gas-water-rock interaction is generally enhanced when magma moves closer to the surface and releases a greater amount of high-enthalpy fluids (mostly water) and other incondensable gases, among which CO_2 is the most abundant. As a consequence, the aquatic environment of Mt. Etna is subject to sudden and marked changes in its chemical and physical conditions, particularly in the areas of highest flank emission of magmatic gases: leaching of soluble elements from volcanic rocks is enhanced, and volatile elements carried with volcanic gas increase their concentration in water. As the gas-water-rock interaction proceeds, secondary clay minerals and other insoluble minerals like carbonates and oxides form and precipitate, apparently at fast rates, thus causing a decrease in the concentration of the elements complexed by those mineral species. Lastly, increased interaction between hot magmatic fluids and groundwater could induce or intensify hydrothermalism at least in some parts of Etna's aquifers. Elements like Cr, Zn and Cu could be possible tracers of such conditions. Recent studies (CHIODINI *et al.*, 1996) demonstrated that some hiper-saline waters discharged by mud volcanoes located in the lower southwestern flank of Etna, near the town of Paternò, are fed by a hydrothermal system whose temperature was estimated at 100–150 °C. It must be noted that sites B5 and B10, both belonging to the high-salinity waters of cluster A, are located very close to this area. Other "stable" geothermal systems may exist in the Mt. Etna area, however they should be deeper than the aquifers of Etna and would not normally interact with them (BRUSCA *et al.*, 2001). However, temporary exchanges of fluids between "cold" and "hot" waters during periods of increased volcanic activity (e.g., because of increased flux of magmatic gases that carry deeper hot fluids to shallower levels of the crust) could also be invoked as an alternative explanation to the suggested hydrothermal conditions in Mt. Etna's shallow aquifers.

In conclusion, the results of this work demonstrate that the use of statistical tools such as Cluster Analysis in the elaboration of chemical data of groundwaters at Mt. Etna can provide useful information, both for modelling the gas-water-rock interaction in aquifers particularly subject to fast changes of the physical and chemical characteristics of their aqueous environment and for the strategies of geochemical surveillance of volcanic activity.

Acknowledgements

References

ACOCELLA, V. and NERI, M. (2003), *What makes flank eruptions? The 2001 Etna eruption and its possible triggering mechanisms*, Bull. Volcanol. *65*, 517–529, doi.: 10.1007/s00445-003-0280-3.

AIUPPA, A., ALLARD, P., D'ALESSANDRO, W., MICHEL, A., PARELLO, F., TREUIL, M., and VALENZA, M. (2000), *Mobility and fluxes of major, minor and trace metals during basalt weathering and groundwater transport at Mt. Etna volcano (Sicily)*, Geochim. Cosmochim. Acta *64*, 1827–1841.

AIUPPA, A., ALLARD, P., D'ALESSANDRO, W., GIAMMANCO, S., PARELLO, F., and VALENZA, M., *Magmatic gas leakage at Mount Etna (Sicily, Italy): relationships with the volcano-tectonic structures, the hydrological pattern and the eruptive activity*, In *Mt. Etna: Volcano Laboratory* (eds. Bonaccorso, A., Calvari, S., Coltelli, M., Del Negro, C., and Falsaperla, S.) (Am. Geophys. Union, Washington, D.C. 2004) pp. 129–145, doi.: 10.1029/143GM09.

ALLARD, P., CARBONELLE, J., DAJLEVIC, D., LE BRONEC, J., MOREL, P., ROBE, M.C., MAURENAS, J.M., FAIVRE-PIERRET, R., MARTIN, D., SABROUX, J.C., and ZETTWOOG, P. (1991), *Eruptive and diffuse emissions of CO$_2$ from Mount Etna*, Nature *351*, 387–391.

ALLARD, A., JEAN-BAPTISTE, P., D'ALESSANDRO, W., PARELLO, F., PARISI, B., and FLEHOC, C. (1997), *Mantle-derived helium and carbon in groundwaters and gases of Mount Etna, Italy, Earth Planet*, Sci. Let. *148*, 501–516.

ALLARD, P. (1997), *Endogenous magma degassing and storage at Mount Etna*, Geophys. Res. Lett. *24*, 2219–2222.

ANZÀ, S., DONGARRÀ, G., GIAMMANCO, S., GOTTINI, V., HAUSER, S., and VALENZA, M. (1989), *Geochimica dei fluidi dell'Etna: Le acque sotterranee, Miner*, Petrogr. Acta *32*, 231–251.

ANZÀ, S., BADALAMENTI, B., GIAMMANCO, S., GURRIERI, S., NUCCIO, P.M., and VALENZA, M. (1993), *Preliminary study on emanation of* CO$_2$ *from soils in some areas of Mount Etna (Sicily)*, Acta Vulcanol. *3*, 189–193.

APHA, AWWA, and WEF, *Standard methods for the examination of water and wastewater*, 18th Edition, (Am. Public Health Assoc., Washington, DC 1992).

ARMIENTI, P., D'ORAZIO, M., INNOCENTI, F., TONARINI, S., and VILLARI, L. (1996), *October 1995-February 1996 Mt. Etna explosive activity: Trace element and isotopic constraints on the feeding system*, Acta Vulcanol. *8* (1), 1–6.

AURELI, A. (1973), *Idrogeologia del fianco occidentale etneo*. Proc. 2nd Intl Congress on Underground Waters, Palermo, Italy, pp. 425–487.

BARNES, H.L., SEWARD, T.M., *Geothermal systems and mercury deposits, In Geochemistry of Hydrothermal Ore Deposits* (ed. Barnes, H.L.) (Wiley and Sons, New York 1997), pp. 699–736.

BAUER, H.H., CHRISTIAN, J.E., and O'REILLY, J.E., *Instrument Analysis* (Allin and Bacon, Inc. 1985).

BONFANTI, P., D'ALESSANDRO, W., DONGARRA, G., PARELLO, F., and VALENZA, M. (1996), *Mt. Etna eruption 1991–93: Geochemical anomalies in groundwaters*, Acta Vulcanol. 8(1), 107–109.

BRUNO, N., CALTABIANO, T., and ROMANO, R. (1999), *SO$_2$ emissions at Mt. Etna with particular reference to the period 1993–1995*, Bull Volcanol. 60, 405–411.

BRUNO, N., CALTABIANO, T., GIAMMANCO, S., and ROMANO, R. (2001), *Degassing of SO$_2$ and CO$_2$ at Mount Etna (Sicily) as indicator of pre-eruptive ascent and shallow emplacement of magma*, J. Volcanol. Geotherm. Res. 110, 137–153.

BRUSCA, L., AIUPPA, A., D'ALESSANDRO, W., PARELLO, F., ALLARD, P., and MICHEL, A. (2001), *Geochemical mapping of magmatic gas-water-rock interactions in the aquifer of Mount Etna volcano*, J. Volcanol. Geotherm. Res. 108, 199–218.

CHESTER, D.K., DUNCAN, A.M., GUEST, J.E., and KILBURN, C.R.J., *Mount Etna: The Anatomy of a Volcano* (Chapman and Hall, London 1985).

CHIODINI, G., D'ALESSANDRO, W., and PARELLO, F. (1996), *Geochemistry of the gases and of the waters discharged by the mud volcanoes of Paternò, Mt. Etna (Italy)*, Bull. Volcanol. 58, 51–58.

D'ALESSANDRO, W., GIAMMANCO, S, PARELLO, F., and VALENZA, M. (1997), *CO$_2$ output and δ^{13}C(CO$_2$) from Mount Etna as indicators of degassing of shallow asthenosphere*, Bull. Volcanol. 58, 455–458.

DONGARRÀ, G., GOTTINI, V., VALENZA, M., and BONFANTI, P. (1993), *Progress in hydrogeochemistry surveying*, Acta Vulcanol. 3, 318–321.

FERRARA, V. (1975), *Idrogeologia del versante orientale dell'Etna*. Proc. 3rd Intl Congress on Underground Waters, Palermo, Italy, pp. 91–144.

FERRARA, V. (1990), *Carta della vulnerabilità all'inquinamento dell'acquifero vulcanico dell'Etna* (C.N.R. Valutazione della Vulnerabilità degli Acquiferi), S.E.L.C.A., Firenze.

GIAMMANCO, S., GURRIERI, S., and VALENZA, M. (1995), *Soil CO$_2$ degassing on Mt. Etna (Sicily) during the period 1989–1993: Discrimination between climatic and volcanic influences*, Bull. Volcanol. 57, 52–60.

GIAMMANCO, S., VALENZA, M., PIGNATO, S., and GIAMMANCO, G. (1996), *Mg, Fe, Mn and V concentrations in the ground waters of Mount Etna (Sicily)*, Water Res. 2, 378–386.

GIAMMANCO, S., OTTAVIANI, M., VALENZA, M., VESCHETTI, E., PRINCIPIO, E., GIAMMANCO, G., and PIGNATO, S. (1998), *Major and trace elements geochemistry in the ground waters of a volcanic area: Mount Etna (Sicily)*, Water Res. 32, 19–30.

GIGGENBACH, W.F., *Chemical techniques in geothermal exploration*. In *Applications of Geochemistry in Geothermal Reservoir Development* (ed. D'Amore, F.) (UNITAR/UNDP Centre on small Energy Resources, Rome 1991) pp. 119–144.

GOGUEL, R.L. (1983), *The rare alkalis in hydrothermal alteration at Wairakei and Broadlands geothermal fields*, Geochim. Cosmochim. Acta 47, 429–437.

GÜLER, C. and THYNE, G.D. (2004), *Hydrologic and geologic factors controlling surface and groundwater chemistry in Indian Wells-Owens Valley area, southeastern California, USA*, J. Hydrol. 285, 1–4, 177–198.

LAPUKHOV, A.S., SIMONOV, V.A., MELNIKOVA, R.D., and PAVLOVA, L.K. (2001), *The influence of volatile components on the distribution of noble metals in rocks from the Mid-Atlantic Ridge*, Proc. 10th Intl Symposium on Water-Rock Interaction, Villasimius, Italy, pp. 973–975.

LA VOLPE, L., MANETTI, P., TRIGILA, R., and VILLARI, L. (1999), *Volcanology and chemistry of the earth's interior. Italian research activity (1995–1998) report to IAVCEI*, Boll. Geof. Teorica Appl. 40, 163–298.

LENTINI, F. (1982), *The geology of the Mt. Etna basement*, Mem. Soc. Geol. It. 23, 7–25.

NICHOLSON, K., *Geothermal Fluids* (Springer-Verlag, Berlin 1993).

OGNIBEN, L. (1966), *Lineamenti idrogeologici dell'Etna*, Riv. Min. Sic. 100–102, 1–24.

PARKHURST, D.L. (1995), *PHREEQC-a computer program for speciation, reaction path, advective transport, and inverse geochemical calculations*, USGS Water-Resources Investigations Report, 95–4227.

ROMANO, R. (1982), *Succession of the volcanic activity in the Etnean area*, Mem. Soc. Geol. It. 23, 27–48.

ROSE, A.W., HAWKES, H.E., and WEBB, J.S., *Geochemistry in Mineral Exploration* (Academic Press, London 1991).

SCHILIRÒ, F. (1988), *Proposta metodologica per una zonazione geologico-tecnica del centro abitato di Maletto*, Geologia Tecnica *3*/88, 32–53.

SYMONDS, R.B., REED, M.H., and ROSE, W.I. (1992), *Origin, speciation, and fluxes of trace-element gases at Augustine volcano, Alaska: Insights into magma degassing and fumarolic processes*, Geochim. Cosmochim. Acta *56*, 633–657.

To access this journal online:
www.birkhauser.ch/pageoph

Continuous, Direct Gas-Geochemical Monitoring in Hydrothermal Vents: Installation and Long-Term Operation on Nisyros Island (Greece)

Manfred Teschner,[1] Eckhard Faber,[1] Jürgen Poggenburg,[1]
Georgios E. Vougioukalakis,[2] and Georgios Hatziyannis[2]

Abstract—In this paper the installation and long-term operation of a system for continuous monitoring of fumarolic gases is described. Several physicochemical and gas-geochemical parameters such as the concentration of CO_2, H_2S and CO in the fumarolic emissions, as well as the temperatures of the hydrothermal steam and soil in close vicinity of the fumarole and steam pressure are measured in short-time intervals (typically 15 seconds). Data are logged on-site and in parallel transferred to a remote station by digital telemetry. Specially developed software enables the real-time observation of the local conditions in the crater and full bidirectional control of the monitoring system. Fluctuations in the monitored parameters are also reported. From the data presented it can be concluded that environmental conditions (direction and strength of wind, precipitation) will interact with some of the parameters monitored. These influences can only be revealed by continuously operated monitoring systems.

Key words: Aegean arc, Nisyros, Greece, fumaroles, hydrothermal vents, gas-geochemistry, continuous real-time monitoring, volcanic risk.

1. Introduction

Geochemical and geophysical phenomena observed on volcanoes and their fumaroles are initiated, influenced and controlled by a variety of complex processes. Mostly they are related to the transport of fluids in the magmatic and/or in the hydrothermal systems. These processes generate a broad variety of chemical and physical signals on different time scales which may be used as input for monitoring and possibly quantifying changes in the volcano's activity and for modelling the dynamic processes involved (Martinelli, 1997).

Whereas geophysical methods have been widely introduced as surveillance tools, gas-geochemical monitoring is still used only infrequently and lacks some general acceptance by the scientific community. Collection of fumarole gases is—depending on

---

[1] Bundesanstalt für Geowissenschaften und Rohstoffe (BGR), Stilleweg 2, 30655 Hannover, Germany. E-mail: manfred.teschner@bgr.de
[2] Institute for Geology and Mineral Exploration (IGME), 70, Messogion Street, Athens 11527, Greece. E-mail: gvoug@igme.gr

the state of volcanic activity, for logistics and other practical reasons – mostly performed discontinuously with time intervals of days, weeks or even months between consecutive sample collections (e.g., PECORAINO and GIAMMANCO, 2005). By this way any short-term variation in gas-geochemical parameters must be missed. These sampling frequencies are surely too low to allow for an efficient comparison between gas data and geophysical information. Therefore a strong need exists for continuously operated gas-geochemical monitoring systems.

Gas monitoring at volcanoes may have different motives: (i) it may be a contribution to risk mitigation by identifying potentially hazardous developments in quiescent or active volcanoes (e.g., ARAMAKI 1991; ANDAL *et al.*, 2005), or (ii) it may be applied to obtain a more complete understanding of the part gases may play in the magmatic and overlaying hydrothermal systems (e.g., ROSE *et al.*, 1986; ALLARD *et al.*, 1991; SYMONDS *et al.*, 1994; GIGGENBACH, 1996; YANG *et al.*, 1999, 2005; PECORAINO and GIAMMANCO, 2005; LEE *et al.*, 2005). A number of studies have pointed out that the composition of volcanic gas along with some reactive gas ratios changed dramatically before eruption (e.g., NOGUCHI and KAMIYA, 1963; CASADEVALL *et al.*, 1983; WALKER, 1974; OSKARSSON, 1984). The monitoring approach involves methodologies to quantify the rate and the amount of gases erupted and to characterize their composition. Besides that the general question arises as to how to distinguish a magmatic gas signature from that of a related hydrothermal system.

In recent papers by FRANCIS *et al.* (2000), DE NATALE *et al.* (2001), OPPENHEIMER and MCGONIGLE (2004), and DE ROSA *et al.* (2007) currently available direct sampling and remote sensing techniques for fumarolic gases have been reviewed and observations or interpretations made at some key volcanoes have been summarized. With the mostly applied remote techniques, gas concentrations within plumes are determined; a direct monitoring of individual fumaroles or hydrothermal vents by remote techniques is still difficult.

Few instrumental systems for continuous gas monitoring have been discussed in the literature. Investigation of gases from a well located at the foot of the active cone on Vulcano Island, Italy, has been presented by TOUTAIN *et al.* (1992) with data for CO_2, He and ^{222}Rn. Japanese scientists report on a monitoring system for volcanic gases extracted from an observation well in the vicinity of Izu-Oshima volcano (SHIMOIKE and NOTSU, 2000). They also review other papers describing the application of gas-monitoring equipment. Recently an automatically operated monitoring system based on a quadrupole mass spectrometer for the surveillance of seismic and geochemical variations on mud volcanoes in southwest Taiwan was described by YANG *et al.* (2006).

Due to the presence of hot water vapour and the variable content of corrosive components like CO_2, SO_2, H_2S, HF or HCl in the volcanic fluids, analytical equipment may be damaged in a short time. Only limited technical information is available in the literature and from manufacturers on suitable monitoring equipment which can be directly installed to active fumaroles. ZIMMER and ERZINGER (1998, 2003) and ZIMMER *et al.* (2000) applied a gas chromatographic system which has been operated continuously

at the summit of Merapi volcano (Indonesia). Another technical system which pumped fumarolic gases through an inert pipe to a remote station—equipped with a gas chromatograph, a mass spectrometer and several other physical instruments—operated at Galeras volcano (Colombia), was described by FABER *et al.* (1998).

In situ monitoring of CO_2, H_2S, Rn and other gases and physical parameters like fumarolic pressure requires lightweight and corrosion-resistant instruments with low power consumption. Here we present experience in long-term operation of a monitoring system which has been briefly described by FABER *et al.* (2000) and—after installation and operation for a longer period at Galeras volcano, Colombia, until its recent eruption in June 2004—in more detail by FABER *et al.* (2003), HELLWEG *et al.* (2004) and TESCHNER *et al.* (2004). Further instrumental development has been performed by our group on Nisyros Island, Greece, where a monitoring system has been installed at a hydrothermal vent and which is now in continuous operation for several years (TESCHNER *et al.*, 2005).

2. The Aegean Region

The volcanic island of Nisyros (27°15′E, 36°35′N) is located at the eastern end of the quaternary calc-alkaline Aegean active volcanic island arc, close to the coast of Turkey, where the Mediterranean oceanic lithosphere is subducting beneath the Aegean continental lithosphere (LE PICHON and ANGELIER, 1979). The Aegean arc also includes localities like (from E to W) Kos, Yali, Santorini, Milos, Aegina, Poros, Methana, and Crommyonia, and other minor eruptive centres. Further details may be found in a recently published book by FYTIKAS and VOUGIOUKALAKIS (2005).

2.1. Geological Framework

The island of Nisyros is built on a basement of Mesozoic limestones and Neogene sediments (GEOTERMICA ITALIANA, 1983; BARBERI *et al.*, 1988). Three main stages were distinguished in the evolution of the Nisyros volcanic island (DI PAOLA, 1974; KELLER, 1982; VOUGIOUKALAKIS, 1984; FRANCALANCI *et al.*, 1995): (i) an early submarine stage, (ii) a composite volcano stage, culminating in the formation of a central caldera, and (iii) a post-caldera stage, characterized by emplacement of several dacitic-rhyodacitic domes of unknown age in the western and northern sectors of the caldera. Today the island represents the emerged portion of an andesitic volcano built in the last 150,000 years, and truncated by a summit caldera of 3.8 km in diameter. Geochronology of Nisyros is poorly known: a K–Ar age of 200 ka was obtained for a pre-caldera dacite (DI PAOLA, 1974) and ages of 38 and 66 ka were obtained on dacite and rhyolite lavas from the flank of the stratovolcano, respectively (KELLER *et al.*, 1989). The formation of the caldera occurred in multiple stages and the first one, related to the eruption of the Lower Pumice deposit, was dated at 35 ka by tephrostratigraphic markers (HARDIMAN, 1999). Post-caldera activity

occurred as the intrusion of dacitic lava domes, raising the caldera rim to a maximum height of 698 m along a NE-trending tectonic.

The eastern and southern part of the caldera is called Lakki plain. It lies about 110–120 m above sea level and shows many signs of recent hydrothermal activity, indicated by the presence of craters as well as by deposits. Historical records describe the most recent hydrothermal explosions in 1871–1873 and 1887 (GORCEIX, 1873 a–d, 1874; MARTELLI, 1917; GEORGALAS, 1962; MARINI *et al.*, 1993). Hydrothermal explosive activity, focused in the eastern half of the caldera floor, produced numerous hydrothermal craters, at least 10 of them are well preserved. The island is today a site of intensive hydrothermal activity which feeds many fumaroles in the caldera floor area and hot springs along the coast line. The risk of a hydrothermal explosion is considered to be moderate to high (SEYMOUR and VLASSOPOULOS, 1989; MARINI *et al.*, 1993; FYTIKAS and VOUGIOUKALAKIS, 1995; VOUGIOUKALAKIS and FYTIKAS, 2005; CALIRO *et al.*, 2005).

Further details of the geological, volcanological and structural framework of the island have recently been supplemented by data collected during deep geothermal drilling projects which were carried out by the Hellenic Public Power Corporation in 1982–1983 (MARINELLI *et al.*, 1983, KOUTROUPIS, 1983, VROUZI, 1985). Research performed by the Lausanne University group on mapping, geochemistry of rocks and minerals and on geochronology on Nisyros Island has been recently documented in detail (HUNZIKER and MARINI, 2005).

2.2. *Past and Recent Seismicity of Nisyros*

Although the last magmatic activity on Nisyros is comparatively old, hydrothermal eruptions are recent. However, high seismic unrest and discharges of thermal water and fumarolic gases indicate the continuous activity of the volcano.

At the end of 1995, an intense seismic activity began on the island and lasted for about three years (VOUGIOUKALAKIS *et al.*, 1998; SACHPAZI *et al.*, 2002). Thousands of local, shallow, low magnitude seismic events have been manifested, located mainly in the area between Nisyros and Yali islands, with characteristics that do not permit the discrimination between tectonically and volcanically triggered events. In the same period ground deformation was manifested by the opening of two fractures on North Nisyros and Yali, along active faults previously mapped on land and underwater and by a vertical ground uplift of about 140 mm revealed by SAR interferometry (SACHPAZI *et al.*, 2002). Similar periods of intense seismic activity have been common to the past: It is known that violent seismic shocks accompanied the eruptions of 1871–1873 (GORCEIX, 1873a–d, 1874). Local swarms were also felt on Nisyros from time to time such as those of April 1887 which preceded by 5 months the last hydrothermal eruption of 1887 (GALANOPOULOS, 1953). Other swarms felt in Nisyros at the beginning of the century, in 1953 (BORNOVAS, 1953) and in 1970 (STIROS and VOUGIOUKALAKIS, 1996) were not associated with any change in the state of the volcano (VOUGIOUKALAKIS *et al.*, 1998).

After the strong seismic crisis in 1996–1997, PAPADOPOULOS *et al.* (1998) compared the recent seismic signatures with earlier seismic activity in the Dodecanese region and

came to the conclusion that the micro-earthquake properties seem to be characteristic in general for the region rather than for a precursor of forthcoming volcanic eruptions.

Between November 2001 and December 2002 a considerably long fissure (>400 m long) trending N-S, has been manifested on the central caldera flat floor (VOUGIOUKALAKIS, 2003; GALANOPOULOS and KOLETTIS, 2005). Fracturing developed in two distinct short–time periods, with no vertical or lateral movement. This fissure was probably created by the collapse of the caldera floor soft sediment cover in a maximum visible depth of 15–20 m. No changes have been detected in the activity state of the volcano before, during and after that period. All the observed, registered or measured parameters have been unchanged in respect to the post 1995–1998 seismic crisis state of the volcano.

The abnormally high precipitation rate during this period, combined with the denudation of the vegetation on the caldera walls and probable very shallow low magnitude local seismic events, could trigger the collapse of the upper sediment cover in the deepest pre-existing open spaces. The numerous 1995–1998 shallow intra-caldera earthquakes probably enhanced the existing discontinuities and open framework in the lower caldera filling deposits, facilitating the large-scale quasi linear collapse.

But these cracks gave rise to concern by local inhabitants and authorities. According to an article in a newspaper (Kathimerini News, Athens, 10.01.2003) and information in the Weekly Activity Report of the Smithsonian's Global Volcanism Program (8.-14.01.2003):

> … the crater of Nisyros was declared off limits to visitors, due to increasing temperatures and growing surface cracks. Evangelos Layios, the director of Athens University's geophysics laboratory, stated, "earthquakes in 1995–96 triggered changes in the general condition of the volcano. For example, the hydrothermal system has increased in heat [temperature] from 210 to 315 degrees Celsius, there is continuous microseismic activity as well as changes on the surface of the ground." The ban on visitors was prompted by a crack on the volcano that almost tripled in length over the past year to 139 m. …

In summer 2003 the ban for visiting the caldera and Stefanos crater, visited every summer by more than 60,000 day visitors, was cancelled.

Since April 2002 the National Earthquake Planning Organisation monitors continuously the geomagnetic field of the area at three sites, two on Nisyros and one on Yali Island (FOUNDULIS, D., personal communication). It is planned for the near future to establish and operate a volcano observatory structure, integrating the existing monitoring systems with a seismic and a ground deformation network.

2.3. Geochemistry of the Fumaroles

Two deep geothermal wells (Nis-1 and Nis-2) have been drilled at the Lakki plain in the central part of the caldera floor (Fig. 1; GEOTERMICA ITALIANA, 1983, 1984). They revealed the existence of two distinct hydrothermal aquifers. The hydrothermal mineral paragenesis of the shallow aquifer (250–700 m depth) indicates formation temperatures
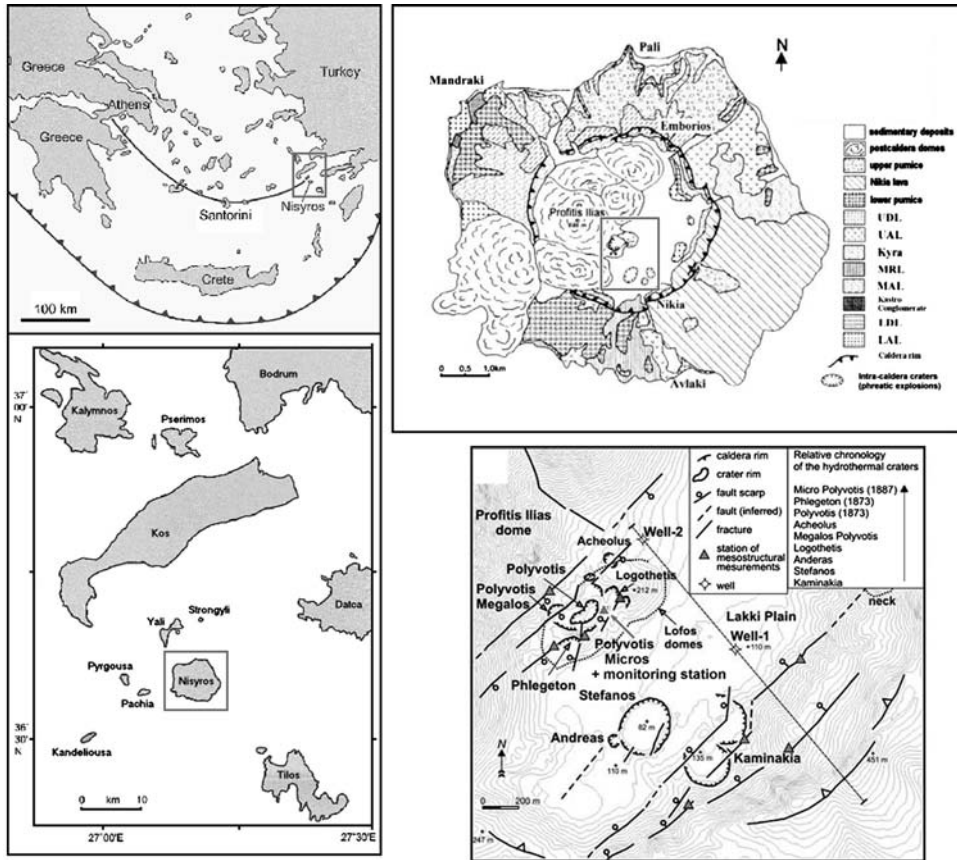
Figure 1
Location of Nisyros (Greece) and location of the gas geochemical monitoring station in the center of the caldera
(sketch maps after Vougioukalakis, 1993, slightly modified).

of 120–180°C. Temperatures of 330–340 and 300–320°C were measured at the bottom of Nis-1 (1,800 m depth) and Nis-2 (1,550 m depth) wells, respectively (Chiodini *et al.*, 1993a; Geotermica Italiana, 1983). However, the quartz equilibrium temperature (Fournier and Potter, 1982) of the Nis-2 reservoir liquid is only 290°C (Chiodini *et al.*, 1993a), which might correspond to the temperature of the productive zones of Nis-2 well, at a depth of 1,400 m.

Considerable gas anomalies were also detected in soil gas surveys of the area during 1995–1998. The Radon content registered in the fumaroles and soil gases of the caldera floor was very high during the whole seismic crisis (166.5 Bq/L [equivalent to 4,500 pCi/L] in soil gases). After this period it progressively declined to finally less than 11.1 Bq/L (300 pCi/L) in a 2000 soil gas survey (Vougioukalakis and Fytikas, 2005). Increased fumarolic activity was also observed from June to September, 1997. Intense

Table 1

Composition of gas samples taken from Polyvotis Mikros hydrothermal vent; original analytical data taken from BROMBACH et al. (2003) (sample number B-1 to B-6) and from FIEBIG et al. (2004) (sample number F-7)

Sample	Month	Year	Temp.	H_2O	CO_2	H_2S	H_2	N_2	CH_4	CO	He	Ar	O_2
				— original analytical data, composition given in µmol/mol —									
B-1	Nov.	1997	n.d.	988000	10000	1740	154	74.8	26.9	0.060	0.183	0.818	n.d.
B-2	Sept.	1998	99.0	989000	9230	1720	167	18.8	26.8	0.034	0.358	0.195	0.061
B-3	Sept.	1999	99.8	986000	12030	1570	223	18.4	24.9	0.121	0.535	0.120	0
B-4	May	2000	n.d.	988000	9600	2160	158	48.2	10.2	0.079	0.265	0.688	0
B-5	Sept.	2000	100	989000	8340	2210	153	30.1	10.3	0.115	0.259	0.571	0
B-6	Feb.	2001	99.9	990030	7867	1819	250	15.7	18.2	0.069	0.462	0.124	0
F-7	Sept.	2001	100.5	991000	6440	2420	136	8.6	7.2	0.072	0.190	0.100	0
				— recalculated to water-free gas, composition given in % —									
B-1	Nov.	1997	n.d.	–	83.35	14.50	1.28	0.62	0.22	0.0005	0.0015	0.0068	n.d.
B-2	Sept.	1998	99.0	–	82.68	15.41	1.50	0.17	0.24	0.0003	0.0032	0.0017	0.0005
B-3	Sept.	1999	99.8	–	86.75	11.32	1.61	0.13	0.18	0.0009	0.0039	0.0009	0
B-4	May	2000	n.d.	–	80.15	18.03	1.32	0.40	0.09	0.0007	0.0032	0.0057	0
B-5	Sept.	2000	100	–	77.62	20.57	1.42	0.28	0.10	0.0011	0.0024	0.0053	0
B-6	Feb.	2001	99.9	–	78.90	18.24	2.51	0.16	0.18	0.0007	0.0046	0.0012	0
F-7	Sept.	2001	100.5	–	71.46	26.85	1.51	0.10	0.08	0.0008	0.0021	0.0011	0

fumarolic activity appeared specifically in the southern flanks of the Polyvotis Megalos hydrothermal crater. The intensification of the fumarolic activity and the discharge of melted sulphur and hot mud on Stefanos crater floor took place one day after the recording of the two strongest earthquakes since the beginning of the recent unrest phase (M_L 5.3 and 5.2, August 28, 1997).

In historical times, several hydrothermal eruptions occurred in the southern part of the Lakki plain producing craters and partially destroying the small Lofos dome (Fig. 1). A large fumarolic field is now present in this area, which is affected by fracturing along the main NW- and NE-trending active fault systems (PAPADOPOULOS *et al.*, 1998). The fumaroles of the Lofos dome area, including those of the craters Polyvotis Megalos, Polyvotis Mikros, and Phlegethon, distribute along a NE fault located on the west of the fumarolic field, whereas the eastern NE–SW faults feed the fumaroles of the Kaminakia crater. The Stefanos crater fumaroles and Nis-1 well lie along another NE–SW fault.

Water vapour is the major constituent of all the hydrothermal vent gases, followed in concentration by CO_2, H_2S, H_2, N_2, CH_4, Ar, He, and CO. The fumarolic gases have hydrothermal rather than magmatic characteristics as indicated by their relatively high CH_4 and low CO content, and by the absence of highly acid gases, such as SO_2, HCl, and HF (GIGGENBACH, 1980, 1987; CHIODINI *et al.*, 1992, 1993b). The outlet temperature of all the fumaroles is close to 100°C.

Gas composition for the southern vent in Polyvotis Mikros (where our monitoring station is located) from recent sample collections is given by BROMBACH *et al.* (2003), FIEBIG *et al.* (2004) and MARINI and FIEBIG (2005); it can be summarized as given in Table 1 (original concentrations in the whole fumarolic gas steam escaping from the vent

expressed in µmol/mol, and recalculated gas concentrations after removal [condensation] of water vapour given in %).

Especially the concentration of H_2S in the (partially) de-watered gas is very high. Commercially available electrochemical sensors can only measure accurately considerably smaller concentrations and therefore gas streams have to be diluted to fit these measuring ranges.

CHIODINI *et al.* (2002) noted increasing H_2S/CO_2 and decreasing CH_4/CO_2 ratios for samples taken from several of the active fumaroles over the period 1990–2001 and interpreted these chemical changes as an increasing contribution of sulphur-rich, oxidizing magmatic fluids into the hydrothermal system below Nisyros Island. Considering the historical information about hydrothermal eruptions, the recent changes in the fumarolic gas composition and the physical phenomena affecting Nisyros may be interpreted as long-term precursors of a new period of volcanic unrest possibly culminating in a magmatic eruptive phase.

3. Monitoring System

We decided to connect a continuous gas extraction device directly into a hydrothermal vent. Hot vapour and gases escaping the fumaroles seem to be linked in a short way to regions influenced by the magmatic body of a volcano and/or to its overlaying hydrothermal systems. In the fumarole gases we believe to sense changes in temperature and gas composition at depth more rapidly than by analysing diffusive emanating soil gases.

The gas-geochemical monitoring station has been located close to one of the active fumaroles of the youngest hydrothermal intra-caldera crater (Polyvotis Mikros, opened up in 1887). The basic installation of the equipment was started during April 2003 and was supplemented by additional gas sensors and improved devices for gas extraction and flow control in 2003–2005. The operation of the monitoring system is performed in the frame of a BGR-IGME research project, in straight collaboration with the municipality of Nisyros in Mandraki.

The components of the gas monitoring system are shown schematically in Figure 2. The system is composed of the following main components:

— physical sensors to measure temperatures of vent gases and of surrounding soil;
— physical sensors to measure fumarolic (differential) and atmospheric pressure;
— a system to condensate water vapour and remove most of the water from the gas to be analysed;
— a system to transport and to dilute the vent gas so that standard electrochemical sensors may be used. For dilution ambient air from outside the crater is pumped by Thomas pumps (type Rietschle Thomas 3003 or 3013) and filtered over activated charcoal. The composition of this "fresh" air is checked occasionally, it shows very small concentrations of the analysed gas components with no variability over time;
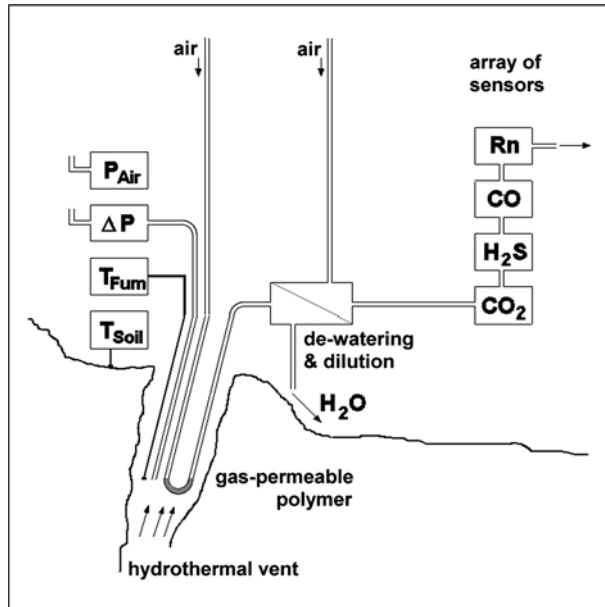— flow sensors in all gas streams;

Figure 2
Block diagram of the monitoring system.

— gas-geochemical sensors for the measurement of CO_2, H_2S, CO and ^{220}Rn / ^{222}Rn (Rn sensor temporarily disconnected due to technical reasons). Electrical signals from all gas-geochemical sensors have to be considered as proxies for a temporal variation of concentration (exact quantification of the gas components is not yet completed);

— an electronic system including A/D- and D/A-converters and a data logger, interconnected by a digital bus (RS-485);

— power supply using solar panels and back-up batteries;

— digital telemetry to a remote station in Emborios (a small village to the north on the caldera rim). From here connection to BGR or IGME office by standard telephone line or via GSM is used;

— software to control all components of the monitoring system and to store measured data (software developed by BGR – gas geochemistry group).

CO_2 concentration is monitored using an NDIR sensor (model AGM10, Sensors Europe, Ratingen, Germany). The gas enters a cabinet (volume about 6 cm^3) and diffuses through a membrane into the infrared cell (volume about 1 cm^3). The relative accuracy of the data is about $\pm$ 2% (specification given by the manufacturer). Gas leaving the CO_2 sensor enters flow-through cells of devices with electrochemical sensors for the measurement of H_2S and CO (model Polytron II, Draeger, Lübeck, Germany). Subsequently a radon sensor (model RTM 1688, SARAD GmbH, Dresden, Germany) is passed and then the gas escapes into the atmosphere. The radon sensor was operated

during a short period only and had to be disconnected due to signal timing problems between control software and instrument firmware.

The temperature inside the fumarole (determined at 50-cm depth) and at about 5 cm below the soil surface is measured using standard thermocouples (Pt-100). The soil temperature was determined at a location about 1.5 m away from the main opening of the hydrothermal vent, to the east, behind a huge stone. No direct connection of this location to hydrothermal vent openings was evident at the time of installation, however observations over the years showed the occasional dislocation of hydrothermal vent openings. At the same place a box with the electronic equipment was stored under a shelter.

A solid state sensor (type Motorola MPX 5100) measures the pressure in a pipe (8-mm wide) inserted ca. 50 cm into the fumarole and compares it to the atmospheric pressure. It is unlikely that the thermocouple, pressure sensor tube and gas extraction device disturb the flow of the gases emanating from the hydrothermal vent (which has an outlet diameter of about 15 cm), as inserting the devices into the fumarole did neither change the noise of the escaping gases nor were changes in the vapour plume apparent. All gas tubing is made from Teflon. It was noticed that standard polyethylene tubing could not withstand the high concentration of H_2S in the steam for a prolonged period.

The whole monitoring system is remotely controlled. Control commands to the system and data from the system are transmitted via digital telemetry to a computer in a station on the rim of the caldera at Emborios. Data are accessible worldwide via telephone line or GSM from this computer at Emborios. Under standard operation conditions data are measured and transmitted every 15 seconds. The telemetric system and the software developed include bi-directional communication, allowing all components (pumps, sensors) to be switched on/off (e.g., to save power in case of low battery voltage or component malfunction) or to be varied in their settings. A screen shot of the software used is shown in Figure 3.

The most demanding problem was to find a direct coupling of the analytical equipment to the hot steam. Because open tubes cannot be used due to the high temperature water vapour, various polymer tubing has been tested to find an acceptable solution for an efficient removal of most of the water vapour or condensate and a reproducible transfer of the gas components under investigation (POGGENBURG and FABER, 2004; LABED *et al.*, 1992, 1997; GUT *et al.*, 1998; SCHMID *et al.*, 2001).

4. Results and Discussion

Fluctuations recorded in time series of data may occur for various reasons. Firstly variations due to technical components have to be detected and corrected, which may be done by replacement with parts of different brands. This may be a long-lasting and tedious task. But it is a prerequisite to finally detect signals which are caused by geologic, volcanic, meteorological or other "natural" events.
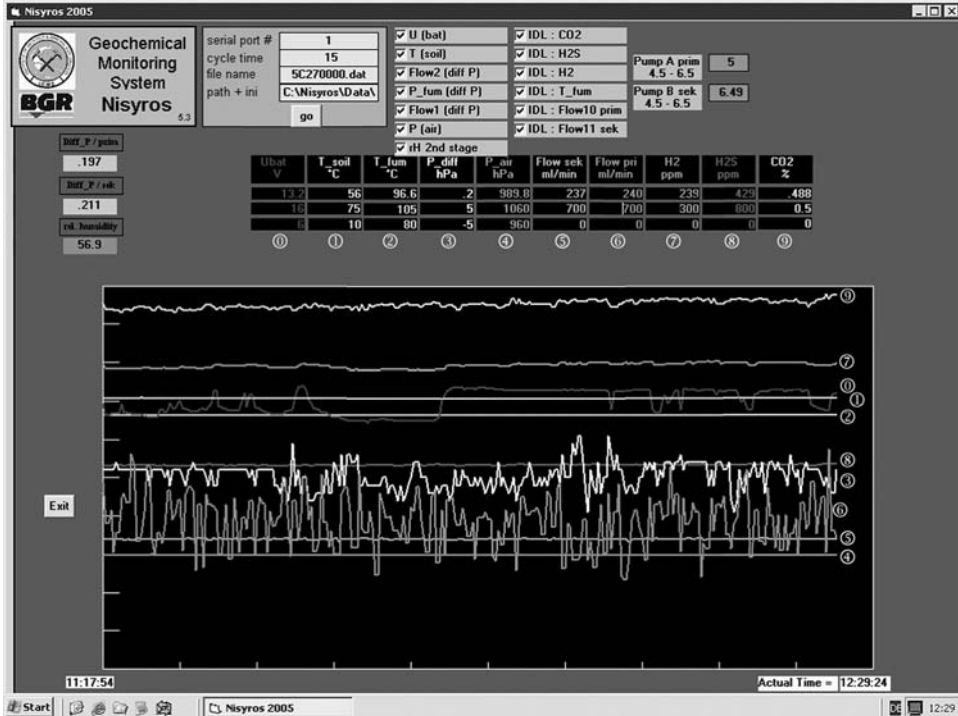
Figure 3

Control window of the software used with the monitoring station. Concentration data of gas components and flow rates shown are not calibrated and may only be taken as proxies.

Figure 4 shows a data set recorded over a three-week period in April/May, 2004. The pressure of the steam emanating from the fumarole at the vent opening is very low and does not exceed a few hectopascal. It fluctuates randomly without a clear correlation neither to atmospheric pressure, fumarole temperature nor to power supply conditions (as seen by the data for the battery voltage). The differential pressure data record contains some negative values which can be explained by steam condensation in the tubing connecting the sensor and the vent exit. After formation of a water drop in the tubing, the drop flows gravimetrically driven down and creates a slight vacuum until it leaves the tubing.

The temperature of the fumarolic gas stays rather constant at about 97.6–98°C. It shows a pronounced scattering to considerably lower values during short-time intervals, usually with durations of several hours. Afterwards it returns to the previous temperature range. These periods of lower fumarole temperature often coincide with adverse weather conditions (e.g., a clouded sky, which can be deduced from the profile of the battery recharge voltage). From these findings we conclude that bad weather conditions (including strong wind and rain) may influence the temperature of the steam escaping
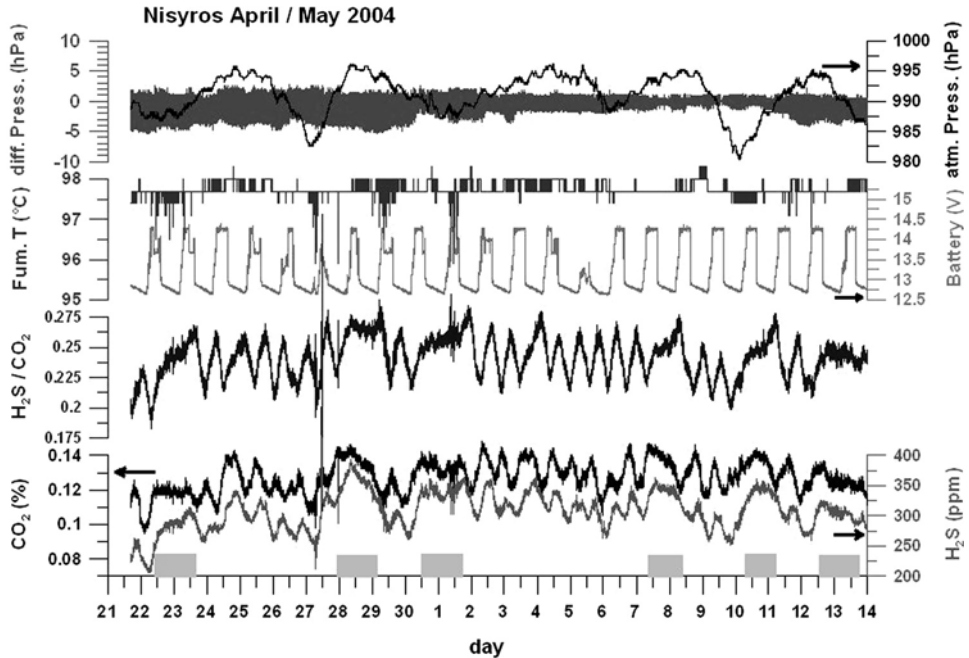
Figure 4
Typical data set, recorded in April/May 2004. Grey marks indicate periods of missing diurnal fluctuations.

from the vent. Here an influence on the temperature of the steam itself, coming from the hydrothermal system, has to be assumed because a superficial effect can be excluded due to insertion of the thermocouple about 50 cm deep into the opening of the vent. It has also to be noted from the data recorded during e.g., May 04, 2004, a clouded sky and lower fumarole temperatures are not necessarily interrelated in any case. These effects may be further evaluated with a weather record from a nearby meteorological station unavailable at the time of measurement.

The time series for CO_2 and H_2S concentration fluctuate in a very similar way. They show a prominent diurnal oscillation. A frequency of about 13 hours may be estimated in both data sets. Again there are time spans where the daily fluctuations are not well pronounced (e.g., April 23 or May 1, 2004). These temporal sections sometimes coincide with those where we find scattering in fumarole temperature (e.g., April 29, 2004), however this is not valid in any case. One may speculate that weather conditions will influence the fumarolic system close to the surface and that wind coming from a suitable direction entering through small cracks will dilute the gas stream originating from the hydrothermal system by ambient air.

The monitoring system is measuring a gas stream from which most of the water vapour has been removed and which is diluted by ambient air (taken from a place outside the crater). On-site calibration for gas concentration proved to be difficult and has not yet
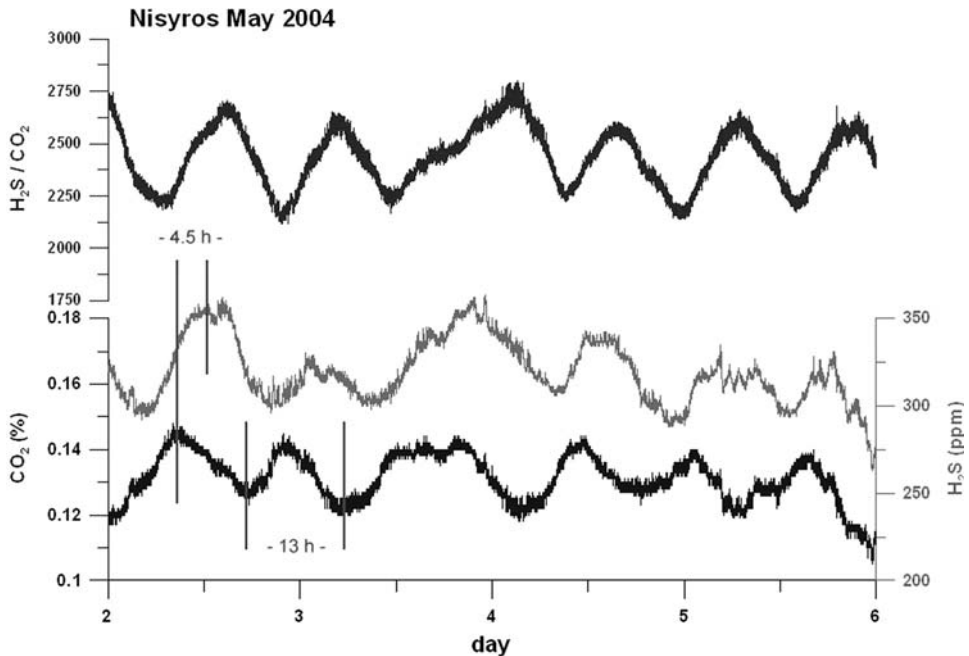
Figure 5
Detailed graph for the fluctuations of CO_2 and H_2S concentration including a plot of the H_2S/CO_2 ratio.

been completed. We estimate a dilution factor of 5–7 in comparison to the original steam. The concentration readings from the sensors of the monitoring system are in acceptable agreement with analytical gas geochemical data for Polyvotis Mikros fumaroles given by BROMBACH *et al.* (2003). In their sample B-6, taken during February 2001, a CO_2 concentration of 7867 ppm and a H_2S concentration of 1819 ppm have been determined in the total fumarolic gas mixture. The same applies for the data published by FIEBIG *et al.* (2004) for a sampling in September 2001, see Table 1 above.

A detailed comparison of the temporal variations of the CO_2 concentration and the H_2S concentration reveals that the graphs are very similar, although surprisingly there is a phase shift between both gases. This shift is of about 4.5 hours, and H_2S concentration is behind the CO_2 concentration (Fig. 5). This feature has been observed throughout the whole period the monitoring system is in operation with both sensors (i.e., from March 2004 onwards). To our best knowledge, similar observations have not been described in the literature and no explanation for this effect is evident. Technical reasons have to be ruled out because both sensors are connected in series by a short piece of tubing. Taking the typical flow rate in the monitoring system into account, a delay of a few seconds between the response onsets for both sensors will be calculated and rules out any chromatographic effect. Additionally, exchange of sensors, digitizers and loggers had no influence on the data set recorded.
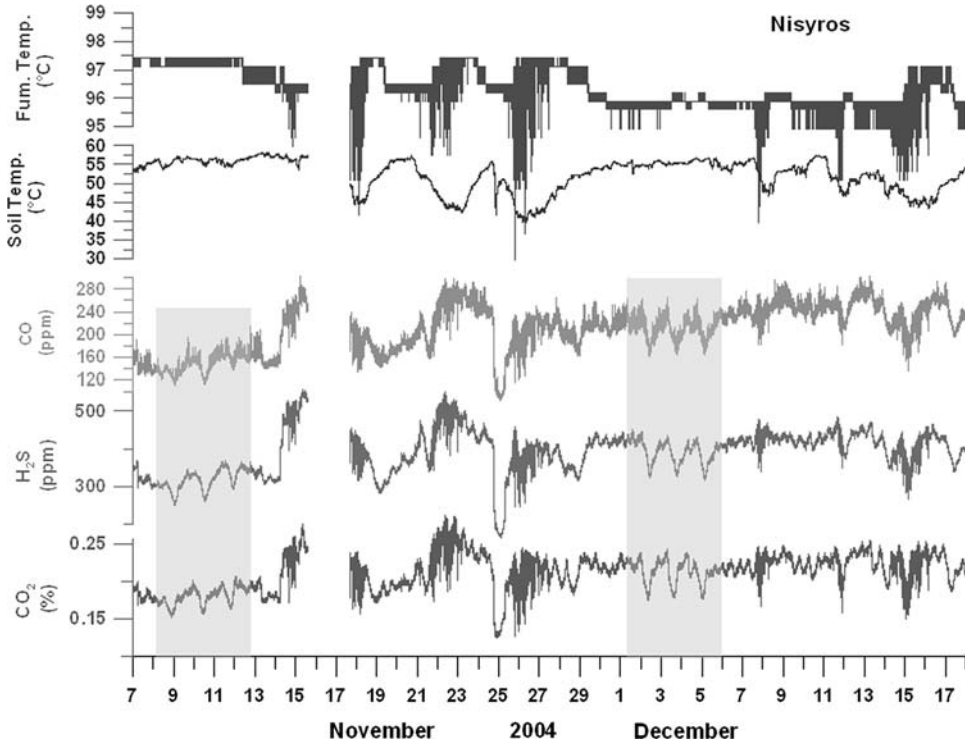
Figure 6
Graph of selected data for the observation period November to December, 2004. Grey marks indicate unusual fluctuations with in a period of about 33 hours.

The daily short-period fluctuations, which cover a relative concentration change of at least ± 10%, may misguide the interpretation of a series of discontinuous sample collections. Such a sampling may be executed when fluctuation shows high or low values or between both extremes. Consequently construction of gas concentration trends or concentration ratio trends over time may be influenced by the time of sampling and results may be misleading.

Another set of (selected) data is displayed in Figure 6 for the period November 2004 to December 2004. Comparing temperature data for steam and soil with gas data one notices the scattering of signals in all traces shown and described above. Besides that, another striking behaviour can be seen for the gas data during the periods around November 12, 2004 or December 2, 2004 (highlighted in grey). We see three consecutive drops in gas concentration, with minima which are separated by about 33 hours. This does not correlate with any change in gas flow data or with ambient weather conditions. An explanation for this observation is not obvious.
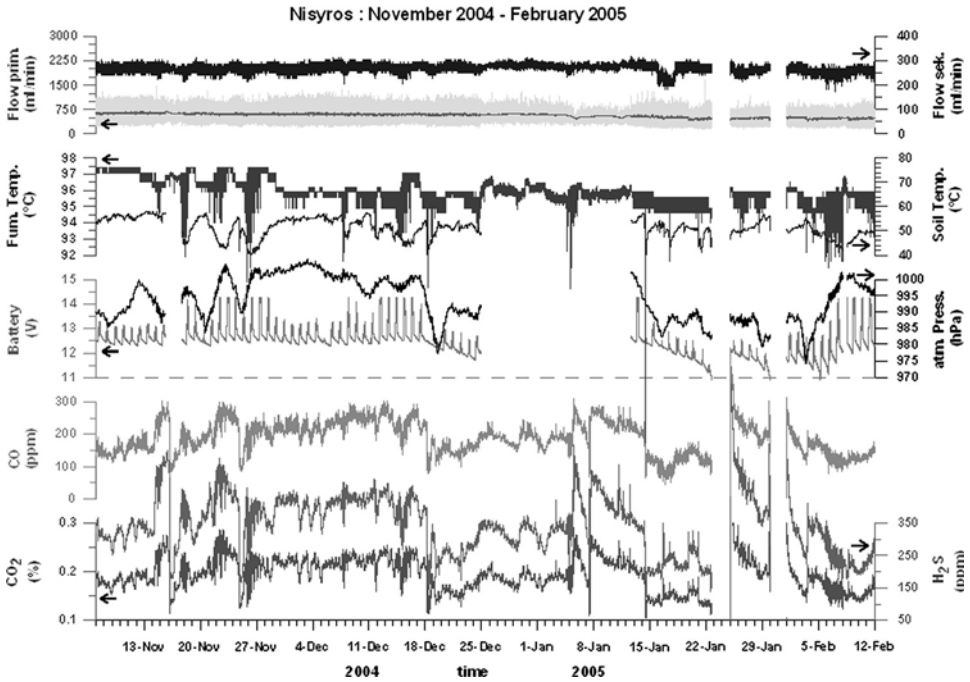
Figure 7
Graph of selected data for the observation period November 2004 to February 2005. Between December 20, 2004, and January 13, 2005, data were lost due to power failure.

In Figure 7 an extended set of (selected) data is displayed for the period November 2004 to February 2005. During this period the weather was rather bad at Nisyros with clouded sky, rain and thunderstorms. The recharging of the batteries by solar panels (2 * 50 W) was not sufficient to ensure a permanent operation of the monitoring station. Especially around January 25, 2005, and February 1, 2005, the system switched off due to low battery voltage, but resumed operation automatically about one day later. After restart the gas concentrations show immediately high values, decreasing to normal concentration over several hours. This is a typical behaviour of the monitoring system after a total power failure and restart. Probably some moisture condensed during switch-off on the inner walls of the tubing or the frits/membranes of the sensors and trapped some portion of the gas components (CO_2, H_2S) which had to be flushed out first after restart.

The data gap between December 22, 2004 and January 12, 2005 is due to a general power failure in the telecom station in Emborios. This small village at the caldera rim is mostly inhabited over the winter season and longer periods of power failures occurr frequently. Therefore, data transfer from the crater station to our offices was not possible; however data were additionally stored in an additional data logger directly in the box of
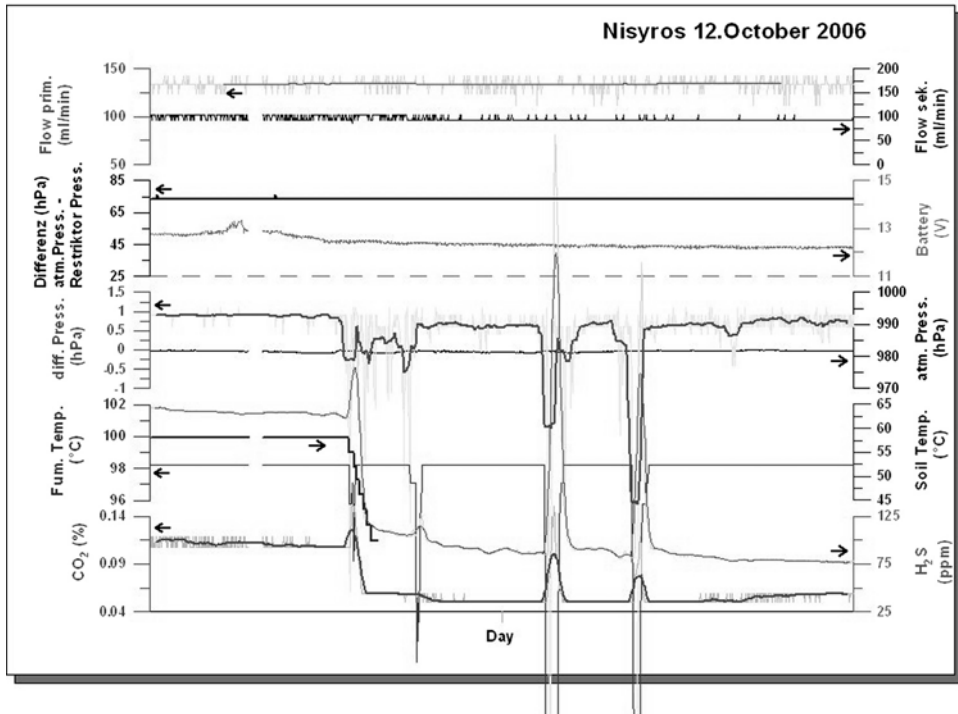
Figure 8
Data set for October 12, 2006, during thunderstorm with heavy rainfall events.

the monitoring system in the crater. After retrieval of this data set (which could be done under remote control) gas data were included into the long-term data set, only some physical data (soil temperature, differential pressure, battery voltage) were lost.

From Figure 7 it is obvious that there is a steady decrease in fumarole temperature from about 97.3°C in November 2004 to 94.8°C in February 2005. This is a result of the cool weather during winter time; over summer time (not shown here) steam temperature increases again to values close to 99°C. Nonetheless it cannot be excluded that also a geogenic/volcanological influence could be responsible for the observed temperature decrease.

During various visits on-site in 2003–2006, it was noticed that from time to time new vent openings occurred or that the shape of the vent exit changed its size over a period of several months. The sensor for soil temperature was at first installed for the surveillance of heat-sensitive electronic components. Unexpectedly, large fluctuations in soil temperature were noticed, very pronounced e.g., between November 17, 2004, and November 28, 2004 (Fig. 6). The soil temperature, which is typically between 50–60°C, decreased by about 15°C to less than 40°C and reverted to its previous value within several days.

This behaviour can be followed in detail in a data set for October 12, 2006 (Fig. 8). Beginning shortly after 07:00 UTC (10:00 local time) a thunderstorm with several heavy

rainfall events crossed Nisyros, coming from north-northeastern direction. It was observed that fast-flowing streams flushed the southern slope of the Polyvotis Micros crater and entered into several hydrothermal vent openings. As a result temperatures of emanating steam and soil dropped sharply (partly off-scale). The differential pressure signal turned to negative values, probably due to water droplet formation inside the connection tube to the sensor, as described above. But also signals from gas sensors were influenced: during the flushing of steam vents at first the concentration increases for several minutes and then drops to considerably lower values. This effect is most pronounced for the first event around 07:00 UTC which occurred after a long period with dry weather. Again we must notice a small phase shift between the data sets for CO_2 and H_2S, on the order of about 10–15 minutes. The reason for this small phase shift is still not known.

From these observations we must conclude that meteoric water (rain) will definitely enter the hydrothermal vent system at Polyvotis Micros site and will cause a cooling down of the gas stream and perhaps a washing out of gas components. This effect should be kept in mind when comparing discontinuously collected samples.

In Figure 6 variations in concentration for CO_2 and H_2S are similar to those shown in Figure 4. In addition to the former system, a sensor for CO was included in November 2004. But the readings of this sensor are several orders of magnitude higher than those concentrations determined by gas chromatographic analysis after classical sample collection (BROMBACH et al., 2003; FIEBIG et al., 2004). The manufacturer of the electrochemical CO sensor system admits a cross contamination by H_2S, however they claim to have an efficient and selective filter system to overcome this influence. This may be valid for an H_2S concentration in the ppm range, but in the fumarolic gas of Polyvotis Mikros we find H_2S concentrations on the order of 20% (Table 1), which exceeds clearly the efficiency of the selective filter system. Besides that the data sets of H_2S and CO have a correlation factor of close to unity (e.g., for November 2004 it is 0.981). This demonstrates that for the measurement of small concentrations of CO in the presence of high concentrations of H_2S no electrochemical sensor may be used reliably and either a suited type of sensor should be installed or H_2S has to be removed effectively prior to CO measurements.

Various drastic decreases of gas concentration were noted in Figure 7, e.g., on November 16, 2004 or on January 14, 2005. Here the concentration drops sharply within a few minutes. Simultaneously we also realize a sharp decrease in fumarole and soil temperature. From the weather archive of Rhodos airport (about 100 km ESE of Nisyros) heavy rainfall was recorded these days, e.g. on November 16, 2004, 23 mm was reported. Unfortunately no exact timing of the rainfall was available. Nonethless the sharp drop in gas concentration and simultaneously in temperatures may be explained by heavy rainfall entering the fumarolic system.

Periods of increased seismic unrest are noticed in the Dodecanese area and adjacent Turkey during the monitoring period. A crosscheck of recorded earthquakes with the time span of unusual data recordings for gas concentration and temperature as mentioned
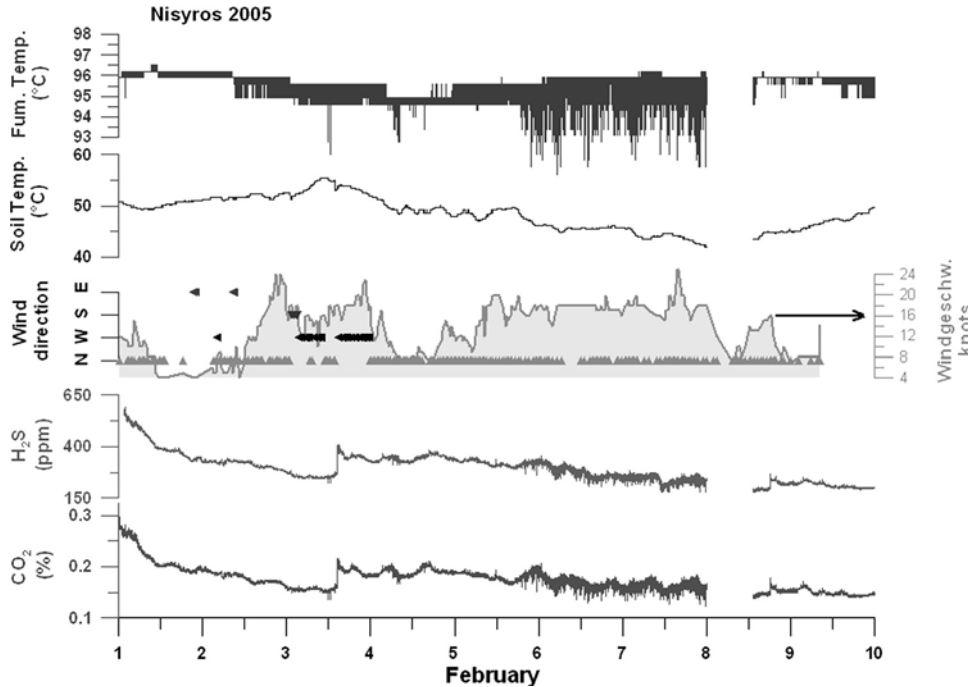
Figure 9

Graph of fumarole temperature, adjacent soil temperature and gas concentrations in fumarole steam in combination with wind speed and direction data from Kos airport weather archive. Wind from northern directions (▲, lowest trace, scale on left-hand side) is prevailing; wind from western directions is indicated by (◄), from southern directions by (▼), from eastern directions by (◄, uppermost trace). General power failures in Emborios telecom station on February 8, 2005.

above did not, however, correlate with these events. Also estimating the local effect of more distant earthquakes with high magnitude ($M_L \gg 3$), e.g., using the formulas given by FLEISCHER (1981), did not correlate with changes monitored. Unfortunately no seismic monitoring equipment is presently installed on Nisyros Island itself.

In Figure 9 gas and temperature data are shown in combination with weather data from Kos airport (about 15 km to the north of Nisyros Island). The weather data show that wind from the north is prevailing in this area of the Dodecanese. Wind speeds of 16 or 18 knots (roughly higher than 30 km/h) for prolonged periods coming from the north has a pronounced effect on the temperature of fumarole steams (and surrounding soil, too; cf. Fig. 9 for February 6 and 7, 2005). The main openings of the fumarole field are located at the southern wall of the Polyvotis Mikros crater and are therefore sensitive to wind blowing from the north.

Gas concentrations also are influenced by this combination of wind direction and wind speed in a way described above. Additionally we find some sudden increases in gas concentration, e.g. on February 3, 2005, around 13:00 UTC or on February 8, 2005,

around 18:00 UTC. These increases are not correlated with distinct weather situations as was deduced previously for the reported decreases in gas concentration. At present the reason for this behavior remains unknown.

5. Summary

The successful installation of a continuously operated monitoring station at a Polyvotis Mikros hydrothermal crater fumarole is described. The system developed comprises sensors for the most prominent gases CO_2 and H_2S as well as sensors for ambient parameters. During short periods additionally sensors for CO and for Rn have been included in the station although technical difficulties prevented a reliable and unattended operation. Due to numerous power-failure situations in the control center in Emborios telecom station, data logging on-site proved to be a necessary feature of the unattendedly operated station.

Interpretation of recorded data sets showed a strong influence on the long-term variation of parameters by meteorological data which were collected from archives of nearby airports. Unfortunately, only part of the necessary meteorological information (wind direction, wind speed) was available. The next supplementation planned for the monitoring system will be a local meteorological station on Nisyros. Some of the fluctuations in temperature and gas concentration graphs are easily related to meteoro-logical parameters, whereas other effects like short-term increases in gas concentration were not easily explained. Frequency analyses are needed to elucidate the origin of regular variations of gas concentrations. Regional seismic events or strong remote earthquakes do not reveal a clear correlation to the changes observed. Interpretation could probably be improved by correlation of the local seismic signal with gas data. Unfortunately appropriate equipment is not yet available.

With the exception of a general decrease in fumarole temperature over the winter season and short-term influences on temperatures and gas concentrations related to heavy rainfall, no significant deviation from the mean values of parameters monitored has been noticed. Thus proxies for a new period of increase in volcanic unrest are presently not deducible from the data set recorded.

Acknowledgements

REFERENCES

ALLARD, P., CARBONELLE, J., DAJLEVIC, D., LEBRONCE, J., MOREL, P., ROBE, M.C., MAURENADS, J.M., FAIVRE-PIERRET, R., MARTIN, D., SABROUX, J.C., and ZETTWOOG, P. (1991), *Eruptive and diffusive emissions of CO$_2$ from Mount Etna*, Nature *351*, 387–391.

ANDAL, E.S., YUMUL, Jr., G.P., LISTANCO, E.L., TAMAYO, Jr., R.A., DIMALANTA, C.B., and ISHII, T. (2005), *Characterization of the Pleistocene volcanic chain of the Bicol Arc, Philippines: Implications for geohazard assessment*, Terr. Atmos. Oceanic Sci. *16*, 865–883.

ARAMAKI, S. (1991), *Hazardous volcanic eruptions in Japan*, Episode *14*, 264–268.

BARBERI, F., NAVARRO, J.M., ROSI, M., SANTACROCE, R., and SBRANA, A. (1988), *Explosive interaction of magma with groundwater: Insights from xenoliths and geothermal drillings*, Rend. Soc. Ital. Mineral. Petrogr., Memorial Volume Marcello Carapezza *43*, 901–926.

BORNOVAS, J. (1953), *On the earthquakes of Nisyros in January 1953*, Unpublished report, Institute of Geology and Mineral Exploration, Athens (in Greek).

BROMBACH, T., CALIRO, St., CHIODINI, G., FIEBIG, J., HUNZIKER, J.C., and RACO, B. (2003), *Geochemical evidence for mixing of magmatic fluids with seawater, Nisyros hydrothermal system, Greece*, Bull. Volcanol. *65*, 505–516.

CALIRO, St., CHIODINI, G., GALLUZZO, D., GRANIERI, D., LaRocca, M., SACCOROTTI, G., and VENTURA, G. (2005), *Recent activity of Nisyros volcano (Greece) inferred from structural, geochemical and seismological data*, Bull. Volcanol. *67*, 358–369.

CASADEVALL, T.J., Rose, W., Gerlach, T., Greenland, L.P., Ewert, J., Wunderman, R., and Symonds, R. (1983), *Gas emissions and the eruptions of Mount St. Helens through 1982*, Science *221*, 1383–1385.

CHIODINI, G., CIONI, R., GUIDI, M., MARINI, L., RACO, B., and TADDEUCCI, G. (1992), *Gas geobarometry in boiling hydrothermal systems: A possible tool to evaluate the hazard of hydrothermal explosions*, Acta Vulcanologica, Marinelli vol. *2*, 99–107.

CHIODINI, G., CIONI, R., LEONIS, C., MARINI, L., and RACO, B. (1993a), *Fluid geochemistry of Nisyros Island, Dodecanese, Greece*, J. Volcanol. Geotherm. Res. *56*, 95–112.

CHIODINI, G., CIONI, R., and MARINI, L. (1993b), *Reactions governing the chemistry of crater fumaroles from Vulcano Island, Italy, and implications for volcanic surveillance*, Appl. Geochem. 8, 357–371.

CHIODINI, G., BROMBACH, T., CALIRO, St., CARDELLINI, C., MARINI, L., and DIETRICH, V. (2002), *Geochemical indicators of possible ongoing volcanic unrest at Nisyros Island (Greece)*, Geophys. Res. Lett. *29(16)*, 1759–1762, doi:10.1029/2001GL014355.

DE NATALE, P., GIANFRANI, L., and DE NATALE, G. (2001), *Optical methods for monitoring of volcanoes: techniques and new perspectives*, J. Volcanol. Geotherm. Res. *109*, 235–245.

DE ROSA, M., GAGLIARDI, G., ROCCO, A., SOMMA, R., DE NATALE, P., and DE NATALE, G. (2007), *Continuous in situ measurements of volcanic gases with a diode-laser-based spectrometer: CO$_2$ and H$_2$O concentration and soil degassing at Vulcano (Aeolian Islands: Italy)*, Geochem. Transact. *8*, 5; doi: 10.1186/1467-4866-8-5.

DI PAOLA, G.M. (1974), *Volcanology and petrology of Nisyros Island (Dodecanese, Greece)*, Bull. Volcanol. *38*, 944–987.

FABER, E., INGUAGGIATO, S., GARZÓN-VALENCIA, G., and SEIDL, D. (1998), *Continuous gas measurements at volcanic fumaroles*, Mitteilungen Deutsche Geophysikalische Gesellschaft e.V., DGG Special Volume III/1998, ISSN-Nr. 0947–1944: pp. 83–87.

FABER, E., POGGENBURG, J., GARZÓN, G., MORIÁN, C., and INGUAGGIATO, S. (2000), *Gas monitoring at volcanoes*, Mitteilungen Deutsche Geophysikalische Gesellschaft e.V., DGG Special Volume IV/2000, ISSN-Nr. 0947–1944: pp. 77–80.

FABER, E., MORÁN, C., POGGENBURG, J., GARZÁN, G., and TESCHNER, M. (2003), *Continuous gas monitoring at Galeras volcano, Colombia: first evidence*, J. Volcanol. Geotherm. Res. *125(1–2)*, 13–23.

FIEBIG, J., CHIODINI, G., CALIRO, St., RIZZO, A., SPANGENBERG, J., and HUNZIKER, J.C. (2004), *Chemical and isotopic equilibrium between CO$_2$ and CH$_4$ in fumarolic gas discharges: generation of CH$_4$ in arc magmatic-hydrothermal systems*, Geochim. Cosmochim. Acta *68*, 2321–2334.

FLEISCHER, R.L. (1981), *Dislocation model for radon response to distant earthquakes*, Geophys. Res. Lett. *8(5)*, 477–480.

FOURNIER, R.O. and POTTER II, R.W. (1982), *A revised and expanded silica (quartz) geothermometer*, Geotherm. Resour. Council Bull., 3–9.

Francalanci, L., Varecamp, J.C., Vougioukalakis, G., Defant, M.J., Innocenti, F., and Manetti, P. (1995), *Intricate processes occurring in the convecting, fractionating and assimilating magma chamber of Nisyros volcano, Aegean arc, Greece*, Bull. Volcanol. *56*, 601–620.

Francis, P., Horrocks, L., and Oppenheimer, C. (2000), *Monitoring gases from andesitic volcanoes*, Phil. Trans. Royal Soc. London A *358*, 1567–1584.

Fytikas, M. and Vougioukalakis, G., *Volcanic hazard in the Aegean Islands*. In (Horlick-Jones, T., Amendola, A., and Casale, R., Eds.), *Natural Risk and Civil Protection* (Spon, Brussels, (1995)), pp. 117–130.

Fytikas, M. and Vougioukalakis, G. (Eds.), *The South Aegean Active Volcanic Arc, Present Knowledge and Future Perspectives*; Developments in Volcanology, (Elsevier, Amsterdam (2005)), vol. *7*.

Galanopoulos, A. (1953), *Katalog der Erdbeben in Griechenland für die Zeit von 1879 bis 1892,* Ann. Geol. Pays Hellen. *5*, 144–229.

Galanopoulos, D. and Kolettis, G. (2005), *Investigating the formation of a superficial fracture on Nisyros Island, Greece with the DC resistivity method*. In (Fytikas, M. and Vougioukalakis, G.E., Eds.), *The South Aegean Active Volcanic Arc, Present Knowledge and Future Perspectives*; Developments in Volcanology (Elsevier, Amsterdam 2005), vol *7*, pp. 227–240.

Georgalas, G.C. (1962), *Catalogue of the Active Volcanoes of the World Including Solfatara Fields: Part XII, Greece,* Intern. Association of Volcanologists, Roma, 40 pp.

Geotermica Italiana (1983), *Nisyros-1 geothermal well*, PPC-EEC report, 106 pp.

Geotermica Italiana (1984), *Nisyros-2 geothermal well*, PPC report, 44 pp. (unpublished).

Giggenbach, W.F. (1980), *Geothermal gas equilibria*, Geochim. Cosmochim. Acta *44*, 2021–2032.

Giggenbach, W.F. (1987), *Redox processes governing the chemistry of fumarolic gas discharges from White Island, New Zealand*, Appl. Geochem. *2*, 143–161.

Giggenbach, W. F., *Chemical composition of volcanic gases*. In (Scarpa., R. and Tillinh, R.I., Eds.) *Monitoring and Mitigation of Volcanic Hazards* (Springer, Berlin, (1996)), pp. 221–256.

Gorceix, M.H. (1873a), *Sur l'état du volcan de Nisiros au mois de mars 1873*, C.R. Séances Acad. Sci., Paris, *LXXVII*, 597–601.

Gorceix, M.H. (1873b), *Sur la récente éruption de Nisyros*, C.R. Séances Acad. Sci. Paris, LXXVII, 1039.

Gorceix, M.H. (1873c), *Sur l'éruption boueuse de Nisiros*, C.R. Séances Acad. Sci. Paris, LXXVII, 1474–1477.

Gorceix, M.H. (1873d), *Phénomènes volcaniques de Nisyros*, C.R. Séances Acad. Sci. Paris, LXXVIII, 444–446.

Gorceix, M.H. (1874), *Étude des fumerolles de Nisiros et de quelque-uns des produits des éruptions dont cette île a été le siege en 1872 et 1873,* Ann. Chim. Phys., Paris, 5me sér, II; 333–354.

Gut, A., Blatter, A., Fahrni, M., Lehmann, B.E., Neftel, A., and Staffelbach, T. (1998), *A new membrane tube technique (METT) for continuous gas measurements in soils*, Plant and Soil *198*, 79–88.

Hardiman, J.C. (1999), *Deep sea tephra from Nisyros Island, eastern Aegean Sea, Greece*. In (Firth, C.R. and McGuire, W.J., Eds.), *Volcanoes in the Quaternary*, Geol. Soc. London Spec. Publ. *161*, 69–88.

Hellweg, M., Seidl, D., Calvache, M., Gómez, D., Böker, F., Buttkus, B., Faber, E., Garzón, G., Greinwald, S., Morán, C., Ortega, A., Poggenburg, J., Teschner, M., and Torres, R. (2004), *The Multiparameter-Station at Galeras Volcano (Colombia): Concept and Realization*, IAVCEI General Assembly, Pucon (Chile), 14.-19.11.2004, Poster 87.

Hunziker, J.C. and Marini, L. (Eds.) (2005), *The geology, geochemistry and evolution of Nisyros volcano (Greece). Implications for the volcanic hazards,* Mémoires de Géologie, Lausanne, vol. 44, 192 pages.

Keller, J., *Mediterranean island arcs*. In (Thorpe, R.S., Ed.), *Andesites*, (Wiley and Sons, New York NY (1982)), pp 307–325.

Keller, J., Gillot, P.Y., Rehren, Th., and Stadlbauer, E. (1989), *Chronostratigraphic data for the volcanism in the eastern Hellenic arc: Nisyros and Kos*, Terra Abstr. 1, 354, OS06–26.

Koutroupis, N., *Geothermal exploration in the Island of Nisyros. Nisyros 1 geothermal well*. In (Strub, S.A. and Ungemach, P., Eds.), *European Geothermal Update*, Proc. Third International Seminar on the Results of EC Geothermal Energy Research (Reidel, Dordrecht (1983)), pp. 440-446.

Labed, V., Rannou, A., and Tymen, G. (1992), *Study of ^{222}Rn permeation through polymer membranes: Application to continuous measurement of ^{222}Rn in water,* Health Physics *63*, 172–178.

Labed, V., Robe, M.Ch., and Tymen, G. (1997), *Study of ^{222}Rn permeation through polymer membranes II: Calibration curves of a new device equipped with a polyethylene membrane, for continuous measurement of ^{222}Rn in water-saturated soils,* Health Physics *72*, 762–765.

Lee, H.F., Yang, T.F., Lan, T.F., Song, S.R., and Tsao, S. (2005), *Fumarolic gas compositions of the Tatun Volcano Group, northern Taiwan,* Terr. Atmos. Ocean. Sci. *16*, 843–864.

Le Pichon, X. and Angelier, J. (1979), *The Hellenic Arc Trench System: A key to the neotectonic evolution of the Eastern Mediterranean area,* Tectonophysics *60*, 1–42.

Marinelli, G., Marini, L., Merla, A., Sini, R., and Ungemach, P. 1983, *Geothermal exploration in the Island of Nisyros, Dodecanese, Greece.* In (Strub, S.A. and Ungemach, P., Eds.), *European Geothermal Update*, Proc. Third International Seminar on the Results of EC Geothermal Energy Research (Reidel, Dordrecht 1983)), pp. 203–205.

Marini, L., Principe, C., Chiodini, G., Cioni, R., Fytikas, M., and Marinelli, G. (1993), *Hydrothermal eruptions of Nisyros (Dodecaneses, Greece). Past events and present hazards*, J. Volcanol. Geotherm. Res. *56*, 71–94.

Marini, L. and Fiebig, J. (2005), *Fluid geochemistry of the magmatic – hydrothermal system of Nisyros (Greece).* In (Hunziker, J.C. and Marini, L., Eds.), *The Geology, Geochemistry and Evolution of Nisyros Volcano (Greece). Implications for the Volcanic Hazards*, Mémoires de Géologie, Lausanne *44*, 121–163.

Martelli, A. (1917), *Il gruppo eruttivo di Nisiro nel mare Egeo*, Societa' dei XL, Ser. 3ª, *XX*, 79–165.

Martinelli, B. (1997), *Volcanic tremor and short-term prediction of eruptions*, J. Volcanol. Geotherm. Res. *77*, 159–171.

Noguchi, K. and Kamiya, H. (1963), *Prediction of volcanic eruption by measuring the chemical composition and amounts of gases*, Bull. Volcanol. *26*, 367–378.

Oppenheimer, C. and McGonigle, A.J.S. (2004), *Exploiting ground-based optical sensing technologies for volcanic gas surveillance,* Annals of Geophysics *47/4*, 1455–1470.

Oskarsson, N. (1984), *Monitoring of fumarole discharge during the 1975–1982 rifting in Krafla volcanic center, North Iceland,* J. Volcanol. Geotherm. Res. *22*, 97–121.

Papadopoulos, G.A., Sachpazi, M., Panopoulou, G., and Stavrakakis, G. (1998), *The volcanoseismic crisis of 1996–1997 in Nisyros, SE Aegean Sea, Greece*, Terra Nova *10*, 151–154.

Pecoraino, G. and Giammanco, S. (2005), *Geochemical characterization and temporal changes in parietal gas emissions at Mt. Etna (Italy) during the period July 2000 – July 2003*, Terr. Atmos. Ocean. Sci. *16/4*, 805–841.

Poggenburg, J. and Faber, E. (2004), *Messeinrichtung mit mindestens einer an Gassensormittel anschließbaren Gasprobenentnahmevorrichtung*, Offenlegungsschrift DE 10240330A1, Deutsches Patent- und Markenamt München.

Rose, W.I., Chuan, R.L., Giggenbach, W.F., Kyle, P.R., and Symonds, R.B. (1986), *Rates of sulphur dioxide and particle emissions from White Island volcano, New Zealand, and an estimate of the total flux of major gaseous species,* Bull. Volcanol. *48*, 181–188.

Sachpazi, M., Kontoes, Ch., Voulgaris, N., Laigle, M., Vougioukalakis, G.E., Sikioti, O., Stavrakakis, G., Baskoutas, J., Kalogeras, J., and Lepine, Cl. (2002), *Seismological and SAR signature of unrest at Nisyros caldera, Greece*, J. Volcanol. Geotherm. Res. *116(1–2)*, 19–23.

Schmid, M., Fuhrer, J., and Neftel, A. (2001), *Nitrous oxide concentrations in the soil of a mown grassland: Comparison of model results with soil profile measurements*, Water, Air, and Soil Pollution: Focus *1(5/6)*, 437–446.

Seymour, K.St. and Vlassopoulos, D. (1989), *The potential for future explosive volcanism associated with dome growth at Nisyros, Aegean volcanic arc, Greece,* J. Volcanol. Geotherm. Res. *37*, 351–364.

Shimoike, Y. and Notsu, K. (2000), *Continuous chemical monitoring of volcanic gases in Izu-Oshima volcano*, Japan, J. Volcanol. Geotherm. Res. *101*, 211–221.

Smithsonian's Global Volcanism Program Bulletin (2003), *Nisyros.* Smithsonian Institution, Washington, D.C. *28*(1).

Stiros, S.C. and Vougioukalakis, G. (1996), *The 1970 Yali (SE edge of the Aegean volcanic arc) earthquake swarm: Surface faulting associated with a small earthquake,* Ann. Tecton. X, 20–30.

Symonds, R.B., Rose, W.I., Bluth, G.J.S., and Gerlach, T.M. (1994), *Volcanic-gas studies: Methods, results, and applications.* In (Carroll and Holloway, Eds.), *Volatiles in Magmas*, Rev. Mineral. *30*, 1–66.

Teschner, M., Faber, E., Poggenburg, J., Weinlich, F.H., Gómez, D.M., Silva, B., Torres, R., Garzón, G., Vougioukalakis, G.E., and Hatziyannis, G. (2004), *Development of an "on-fumarole" continuous gas monitoring system and its application in multi-parameter studies*, IAVCEI General Assembly, Pucon (Chile), 14.-19.11.2004, Poster 169.

TESCHNER, M., VOUGIOUKALAKIS, G.E., FABER, E., POGGENBURG, J., and HATZIYANNIS, G., *Real time monitoring of gas-geochemical parameters in Nisyros fumaroles*. In (FYTIKAS, M. and VOUGIOUKALAKIS, G.E., Eds.), *The South Aegean Active Volcanic Arc, Present Knowledge and Future Perspectives;* Developments in Volcanology, (Elsevier, Amsterdam, (2005)) vol. *7*, pp. 247–254.

TOUTAIN, J.P., BAUBRON, J.-C., LE BRONEC, J., ALLARD, P., BRIOLE, P., MARTY, B., MIELE, G., TEDESCO, D., and LUONGO, G. (1992), *Continuous monitoring of distal gas emanations at Vulcano, southern Italy*, Bull. Volcanol. *54*, 147–155.

WALKER, G.P.L. (1974), *Volcanic hazards and the prediction of volcanic eruptions*. In (FUNNELL, B. M., Ed.), *Prediction of Geological Hazards*, Geol. Soc. London, Miscellaneous Paper *3*, 23–41.

VOUGIOUKALAKIS, G. (1984), *Studio vulcanologica e chimico-petrografico dell'isola di Nisyros (Dodecanneso, Grecia)*, Tesi di laurea in Scienze Geologiche, Università di Pisa.

VOUGIOUKALAKIS, G. (1993), *Volcanic stratigraphy and evolution of Nisyros Island* (*in Greek with English abstract*), Bull. Geolog. Soc. Greece *28*, 239–258.

VOUGIOUKALAKIS, G., SACHPAZI, M., PERISSORATIS, C., and LYBEROPOULOU, Th. (1998), *The 1995–1997 seismic crisis and ground deformation on Nisyros volcano, Greece: A volcanic unrest?* 6th Int. Meeting on Colima Volcano, Abstract Volume.

VOUGIOUKALAKIS, G.E. (2003), *Passive fissuring in long-dormant caldera volcanoes: The Nisyros case*, *Meeting on "The South Aegean Volcanic Arc: Present knowledge and future perspectives"*, in the frame of the "Milos Conferences – Magmatism in convergent plate margins", Milos Island, Greece. Book of abstracts, 105.

VOUGIOUKALAKIS, G.E. and FYTIKAS, M., *Volcanic hazards in the Aegean area, relative risk evaluation and monitoring state of the active volcanic centers*. In (FYTIKAS, M. and VOUGIOUKALAKIS, G.E., Eds.), *The South Aegean Active Volcanic Arc, Present Knowledge and Future Perspectives*; Developments in Volcanology (Elsevier, Amsterdam, (2005)) vol. *7*, 161–183.

VROUZI, F. (1985), *Research and development of geothermal resources in Greece: Present status and future prospects,* Geothermics *14*, 213–227.

YANG, T.F., SANO, Y., and SONG, S.R. (1999), $^3He/^4He$ ratios of fumaroles and bubbling gases of hot springs in Tatun Volcano Group, North Taiwan, Nuovo Cimento *22*, 281–286.

YANG, T.F., LAN, T.F., LEE, H.F., FU, C.C., CHUANG, P.C., LO, C.H., CHEN, C.H., CHEN, C.T.A., and LEE, C.S. (2005), *Gas compositions and helium isotopic ratios of fluid samples around Kueishantao, NE offshore Taiwan and its tectonic implications*, Geochem. J. *39*, 469–480.

YANG, T.F., FU, C.-C., WALIA, V., CHEN, C.-H., CHYI, L.L., LIU, T.-K., SONG, S.-R., LEE, M., LIN, C.-W., and LIN, C.-C. (2006), *Seismo-geochemical variations in SW Taiwan: multi-parameter automatic gas monitoring results*, Pure Appl. Geophys. *163*, 693–709.

ZIMMER, M. and ERZINGER, J. (1998), *Geochemical monitoring on Merapi volcano, Indonesia*, Mitteilungen Deutsche Geophysikalische Gesellschaft e.V., DGG Special Issue III/1998, ISSN-Nr. 0947–1944, 89–92.

ZIMMER, M. and ERZINGER, J. (2003), *Continuous H_2O, CO_2, ^{222}Rn and temperature measurements on Merapi Volcano, Indonesia*, J. Volcanol. Geotherm. Res. *125(1–2)*, 25–38.

ZIMMER, M., ERZINGER, J., and SULISTIYO, Y. (2000), *Continuous chromatographic gas measurements on Merapi volcano, Indonesia*, Mitteilungen Deutsche Geophysikalische Gesellschaft e.V., DGG Special Volume IV/2000, ISSN-Nr. 0947–1944, 87–91.

To access this journal online:
www.birkhauser.ch/pageoph